UNIVERSITY OF SOUTHAMPTON

FACULTY OF ENGINEERING, SCIENCE AND MATHEMATICS

OPTOELECTRONICS RESEARCH CENTRE

Hollow optical fibers and W-type fibers for high power sources and Suppression of the stimulated Raman scattering

by

Jae Sun Kim

Thesis for the degree of Doctor of Philosophy

September 2006

UNIVERSTIY OF SOUTHAMPTON

ABSTRACT

FACULTY OF ENGINEERING, SCIENCE AND MATHEMATICS

OPTOELECTRONICS RESEARCH CENTRE

Doctor of Philosophy

Hollow optical fibers and W-type fibers for high power laser sources and Suppression of the stimulated Raman scattering

By Jae Sun Kim

In this thesis, theoretical and experimental studies on hollow optical fibers (HOFs) and depressed clad hollow optical fibers (DCHOFs) for cladding-pumped high power fiber laser sources, operating at a wavelength range 900 – 1100 nm, are reported. In addition, the suppression of the stimulated Raman scattering (SRS) in a single-mode high power fiber-based master oscillator power amplifier (MOPA) source, using W-type Yb^{3+}-doped fiber, is also studied.

The HOF consists of a ring-shaped core around an air hole in the center and a silica cladding. Such a fiber geometry can provide a relatively high pump absorption in the cladding- pump configuration due to the relatively large-ratio of the core and the cladding as compared to solid core fiber. Moreover, the core structure of HOF produces a negative dielectric volume due to the low refractive index of the air in the centre of the fiber. It provides a fundamental mode cut-off in a finite wavelength, which makes the fiber act as a distributed wavelength filter and it is thus possible to suppress the undesired emission at the longer wavelength in the fiber itself. The Er^{3+}:Yb^{3+} co-doped aluminosilicate HOF structure was investigated numerically and experimentally. It provided 2.5 W output power with 25% slope efficiency with respect to the launched pump power.

In order to realize a more efficient three (or quasi-three)-level fiber laser operating at shorter-wavelengths, the DCHOF was designed, which has an additional depressed clad around the ring-core. Its modal characteristics were investigated through a numerical method. The performance of the DCHOF with other filtering fibers such as HOFs and W-type fibers, was also investigated. Next, the Nd^{3+}-doped aluminosilicate DCHOF at 930 nm was demonstrated, which generated CW output power of 3.3 W with 41% slope efficiency with respect to the launched pump power whilst maintaining a diffraction limited beam quality (M^2 value = 1.04). Moreover, a Q-switched Nd^{3+}-doped aluminosilicate DCHOF laser provided the highest pulse energy 133 μJ at 5 kHz repetition rate at 927 nm.

Yb^{3+}-doped alumino-silicate DCHOF was also studied theoretically and experimentally for efficient 980 nm laser operation. It generated 3.1 W output power with 34% slope efficiency with respect to the launched pump power. The beam quality factor was 1.09. The power was scaled up to 7.5 W with 49% slope efficiency with respect to the launched pump power, but the beam quality factor was degraded (M^2 value = 2.7). In addition, a high power Yb^{3+}-doped alumino-silicate DCHOF operating at 1040 nm with a high slope efficiency (81% wrt the absorbed pump power) was also demonstrated.

The suppression of the stimulated Raman scattering (SRS) in a small and single-mode core becomes an issue when considering the power scaling of a fiber laser. Here a W-type fiber was designed for SRS suppression with the fundamental mode cut-off set, by design, between the signal and the 1st order Raman Stokes wavelengths. SRS suppression was demonstrated in a high peak power fiber MOPA source with a single-mode output. The maximum peak power achieved was 13 kW with a small, and single-mode, core fiber without any evidence of SRS occurring.

Contents

List of figures

List of Tables

Declaration of authorship

I, Jae Sun Kim declare that the thesis entitled **Hollow optical fibers and W-type fibers for high power laser sources and Suppression of the stimulated Raman scattering** and the work presented in it are my own. I confirm that:

- this work was done wholly or mainly while in candidature for a research degree at this University;
- where any part of this thesis has previously been submitted for a degree or any other qualification at this University or any other institution, this has been clearly stated;
- where I have consulted the published work of others, this is always clearly attributed;
- where I have quoted from the work of others, the source is always given. With the exception of such quotations, this thesis is entirely my own work;
- I have acknowledged all main sources of help;
- where the thesis is based on work done by myself jointly with others, I have made clear exactly what was done by others and what I have contributed myself;
- Parts of this work have been published as the following lists.

Signed: Jae Sun KIM .....

Date: November 2006 .....

List of publications

- The thesis is based on the following publications

■ Chapter 3

- **J. Kim** C. Codemard, J. Nilsson, and J. K. Sahu, "Erbium-Ytterbium co-doped Hollow Optical Fiber laser" *Electronics Letters*, **42**(9) p515-517 (2006).

■ Chapter 4

Journal papers

- **J. Kim**, P. Dupriez, D. B. S. Soh, J. Nilsson, and J. K. Sahu, "Core area scaling of Nd:Al-doped silica depressed clad hollow optical fiber and Q-switched laser operation at 0.9 μm" Optics Letters, 31(19) 2833-2835 (2006)

- D. B. Soh, S. Yoo, J. Nilsson, J. K. Sahu, K. Oh, S. Baek, Y. Jeong, C. Codemard, P. Dupriez, **J. Kim**, V. Philippov **"**Neodymium-doped cladding pumped aluminosilicate fiber laser tunable in the 0.9 micron wavelength range" *IEEE J. Quantum Electron.* 2004.

Conference papers

- **J. Kim**, P. Dupriez, D. B. S. Soh, J. K. Sahu, J. Nilsson, and D. Payne "Nd:Al-doped depressed clad hollow fiber laser at 930 nm" presented at ASSP 2005 Vienna.

■ Chapter 5

Journal papers

- **J. Kim**, D. B. S. Soh, J. Nilsson, and J. K .Sahu, "Fiber design for high power, low-cost Yb:Al-doped fiber laser operating at 980 nm," submitted for IEEE Journal of Selected Topics in Quantum Electronics. 1.Nov. 2006.

Conference papers

- **J. Kim**, D. B S. Soh, C. Codemard, S. Yoo, Y. Jeong, J. Nilsson, J. K. Sahu, "Yb:Al-doped depressed clad hollow optical fiber laser operating at 980 nm" *CLEO/IQEC Pacific Rim* Tokyo 11-15 Jul 2005 CTuI4-5.

- **J. Kim**, P. Dupriez, D. B. S.Soh, C. Codemard, S. Yoo, Y. Jeong, J. Nilsson, and J. K. Sahu "Depressed clad hollow optical fiber with the fundamental LP_{01} mode cut-off" presented at *Photonics West 2006* San Jose 21-26 Jan 2006.

■ Chapter 6

Journal papers

- **J. Kim**, P. Dupreiz, C. Codemard, J. Nilsson, and J. K. Sahu, "Suppression of stimulated Raman scattering in a high power Yb-doped fiber amplifier using a W-type core with fundamental mode cut-off" *Optics Express*, **14**(12) p5103-5113 (2006).

Conference papers

- **J. Kim,** C. Codemard, Y. Jeong, J. Nilsson, and J. K. Sahu "High Power Continuous-Wave Yb-Doped Fiber Laser with True Single-Mode Output Using W-Type Structure" *CLEO/QELS 2006*, Long Beach, California, USA CTuQ2 2006.

- J. K. Sahu, P. Dupriez, **J. Kim**, C. Codemard, J. Nilsson, D. N. Payne "Suppression of stimulated Raman scattering in a high-peak-power pulsed 1060 nm fiber MOPA source with purely single-mode output using W-type fiber" presented at *OFC 2006* Anaheim 5-10 Mar 2006 OWD5.

Other publications

Conference papers

- J. K. Sahu, P. Dupriez, **J. Kim,** A. J. Boyland, C. Codemard, J. Nilsson, and D. N. Payne, "New Yb:Hf-doped silica fiber for high-power fiber lasers" .*CLEO/QELS* Baltimore 22-27 May 2005 CTuK1.

- J. K. Sahu, V.Philippov, **J.Kim**, C.Codemard, P.Dupriez, J.Nilsson, A.Abdolvand, N.V,.Kuleshov, **"**Passively Q-switched thulium-doped silica fiber laser"*CLEO/IQEC 2004* San Francisco 16-21 May 2004 CThGG.

- Y. Jeong, J. Nilsson, D. B. S. Soh, C. Codemard, P. Dupriez, C. Farrell, J. K. Sahu, **J. Kim**, S. Yoo, D. J. Richardson, and D. N. Payne "High power single-frequency Yb doped fiber amplifiers" *OFC 2006* Anaheim 5-10 Mar 2006 OThJ7 (Invited).

- J. Nilsson, Y. Jeong, D. B. S. Soh, C. Codemard, P. Dupriez, C. Farrell, J. K. Sahu, **J. Kim**, S. Yoo, D. N. Payne, "High-power fiber lasers: progress and opportunities" *Proc. 14th International Laser Physics Workshop 2005 (LPHYS 2005)* Kyoto 4-8 Jul 2005 PS5 (Plenary)

- P. Dupriez, J. Nilsson, Y. Jeong, J. K. Jahu, C. Comdemard, D. B. S. Soh, C. Farrell, **J. Kim**, A. Piper, A.Malinowski, and D. J. Richardson, "Current progress in high-power fiber lasers and amplifiers" *Optical Amplifiers and their Applications (OAA)* Budapest 7-10 Aug 2005 (Invited)

- D. B. S. Soh, A. B. Grudinin, J. Nilsson, Y. Jeong, S. Yoo, **J. Kim**, C. Codemard, and P. Dupriez, "Stimulated Raman scattering effect on femtosecond pulse generation using a parabolic amplification and a pulse compressor*ONERA Scientific Day* Paris 27-28 Jun 2005

- J. Nilsson, J. K. Sahu, Y. Jeong, V. N. Philippov, D. B. S. Soh, C. Codemard, P. Dupriez, **J. Kim**, D. J. Richardson, A. Malinowski, A. N. Piper, J. H. V. Price, K. Furusawa, W. A. Clarkson, and D.N.Payne "High power fiber lasers" *OFC 2005* Anaheim 6-11 Mar 2005 OTuF1 (Invited).

- Y. Jeong, J. Nilsson, J. K. Sahu, P. Dupriez, C. Codemard, D. B. S. Soh, C. Farrell, **J. Kim**, D. J. Richardson, and D. N. Payne, ".High power fiber lasers" *CLEO/IQEC-Pacific Rim* Tokyo 11-15 Jul 2005 CWI4--1-INV (Invited)

- Y. Jeong, J. Nilsson, J. K. Sahu, D. B. S. Soh, P. Dupriez, C. Codemard, C. Farrell, **J. Kim**, D. J. Richardson, and D. N. Payne, "Beyond 1 kW, the rising power of fiber lasers" *OECC* Seoul 4-8 Jul 2005 8D1-1 (Invited).

PART I
BACKGROUND

Chapter 1. Introduction

1-1. Motivation for research

Rare-earth doped fibers based on silica materials have been the subject of a tremendous research effort over the past few decades for high power laser source applications. The main advantage of using a silica host is that it provides a low propagation loss, high gain, large bandwidth and high chemical durability [1-2]. In addition, a large surface area to volume ratio in fiber ensures excellent thermal management in a high power fiber laser compared to the conventional bulk solid state lasers [3]. Furthermore, the beam quality in a fiber laser can easily be tailored by controlling the refractive index profile of the doped core.

For scaling up the output power of fiber lasers, the cladding-pump technology [4-6], using double-clad fibers, is the obvious choice and it enables fiber lasers to reach output power levels where they can compete with conventional bulk solid state lasers, in many applications such as micro-machining, welding and materials processing. In practice, Yb^{3+}-doped double-clad fibers lasers have produced continuous wave (cw) kW output power levels at ~1.1 μm, while maintaining a nearly diffraction-limited beam quality [4-6]. Moreover, in a pulsed regime, the average power and peak power was significantly increased by a combination of cladding-pump technology and a master oscillator power amplifier (MOPA) configuration [10, 70]. However, the relatively low pump absorption in double clad fibers, compared to the core-pumping configuration, and the competition with the unwanted stimulated emissions still remains a challenge for such a technique. Specifically, the realisation of a laser and an amplifier operating at 930 nm based on Nd^{3+}-doped fiber and 980 nm for a laser based on Yb^{3+}-doped fiber requires improvements in

fiber design. Furthermore, the robust generation of a diffraction-limited beam quality in high power fiber based sources is still challenging due to fiber core area. The small core fiber causes nonlinearities e.g. stimulated Raman scattering (SRS) and stimulated Brillouin scattering (SBS) etc significantly, which prohibits further power-scaling. The research described in this thesis was targeted towards the development of a fiber waveguide structure suitable for generating high power, single-mode output fiber sources at various wavelengths.

In general, laser amplification in rare-earth doped fibers occurs at a strong emission band with a high transition strength, while at a relatively weak emission band, the stimulated emission is suppressed due to the reduced inverted population of ions. In order that the laser can be operated at the weaker emission band in the fiber, the suppression of the undesired stimulated emission is required. For this, the bulk-type filter can be used externally [7]. However, in some cases, it is ineffective because the amplified stimulated emission at the unwanted wavelength can be generated and can consume a large portion of the inverted population in the fiber itself, if the gain is high enough at the unwanted emission wavelength. On the other hand, the waveguide spectral filter can reduce the gain by preventing a build-up of the power at the unwanted wavelength, and thus it is more attractive for the laser/amplification at the weaker band. Moreover, it is then also possible to make all fiber-based, compact devices.

Nd^{3+}-doped fiber and Yb^{3+}-doped fiber normally operate at the longer wavelength (~1060 nm), where the emission cross section is much larger than the absorption cross section. It shows a four (or quasi-four) level characteristic, and in fact, very small portion of the population inversion is enough for the laser amplification [8]. However, at the shorter wavelength side, the absorption cross section, at which the laser system becomes a three (or quasi-three) level system, becomes significant [9]. It requires a much higher

population inversion state (>50%). Therefore, for the efficient cladding-pumped fiber laser operation at the shorter wavelength, a large pump absorption is also one of the important issues. Fortunately, most of the multi-mode (low brightness) pump sources consisting of laser diode stacks can reach the required power level (several or tens of watts) for such a population inversion. However, the high coupling efficiency into the fiber should be also considered.

Currently, in order to increase the coupling efficiency and pump absorption in a cladding-pump configuration, a large inner cladding and a large core are the obvious choice. However, it is difficult for the waveguide to have the required spectral filtering characteristic in the large core because the fundamental mode is guided in the fiber with a normal step index structure at all wavelengths without a modal cut-off, even though a numerical aperture (NA) is significantly reduced. The low NA and large core fiber is still useful for high power fiber lasers in terms of pump absorption and fiber nonlinearity but it is very challenging to use it for the suppression of unwanted four-level emissions in a three-level or shorter wavelength fiber lasers.

It is also a critical issue to generate a robust single mode output (a diffraction-limited beam quality) from the cladding-pumped high power fiber laser. In terms of single-mode operation, a small and single-mode core fiber is preferred. However, for such fibers, fiber nonlinearities become an important issue for very high power (kW level), cw lasers, or fiber-based master oscillator – power amplifier (MOPA) sources, to scale up the average output power in pulsed mode [10-12]. To date, most of the high power fiber sources use a large, low-NA, core and a relatively short fiber in order to mitigate nonlinear effects, such as stimulated Raman scattering (SRS) [13]. However, a single-mode core fiber still remains the obvious choice for high beam quality. In part IV, the suppression of SRS in a waveguide filter will be discussed.

In order to address the requirements, as mentioned above, the optical fiber for the high power fiber sources should have a relatively larger core, which definitely supports only a single mode through the core. If required, it should reject any unwanted emission including SRS, at a certain wavelength. For the filtering in the fiber, the waveguide should have the fundamental (LP_{01}) mode cut-off in a finite wavelength. In order to do that, the average refractive index of the core area should be less than that of the silica cladding (inner cladding), which means that the fiber has a negative dielectric volume [14]. In addition, the core should be large and be single-mode at the operating wavelength.

To achieve such characteristics a hollow structure, which consists of a ring-shaped core around an air hole in the center, is considered. The low refractive index of the air hole (n_{air} = 1) produces the negative dielectric volume which allows for a cut-off of the fundamental (LP_{01}) mode, at the desired wavelength. The ring-shaped core can improve the pump absorption, contrary to the normal step index fiber, due to the relatively large ratio of core area and cladding area [15]. In this thesis, the hollow optical fiber (HOF) and the depressed clad hollow optical fiber (DCHOF), will be mainly discussed. Their performance for fiber laser sources operating at three or quasi three-level transition will be presented.

1-2. Previous studies

1-2-1. Hollow optical fibers

The HOF consists of a ring-shaped core around an air hole, a silica cladding and a polymer coating as shown in figure 1-1. First one (fundamental mode) of guided modes in HOF has a beam profile with zero central intensity, such as a doughnut-shaped beam [16]. Such a beam is also called “dark hollow beam (DHB)”, which has various applications in optical physics, material and biological science [17]. In addition, in the dark side of the

hollow beam, atoms can experience a repulsive potential and then they can be confined into the hole in a proper condition [18]. Therefore, it is also used in atom guiding/funneling and collimating [18-19] experiments. Because of this interest the electric field distribution of the fundamental LP_{01} mode in the HOF has already been studied and the optical potential in the hollow beam has been calculated for atomic guiding [18].

Besides these, other applications of the HOF were proposed. The light is guided through the high index ring-core and so the guided ring-modes can be easily converted to a normal Gaussian mode without a significant loss, using the tapering and splicing technique of the HOF [20]. This makes possible various applications in optical communication systems. A launching condition for multimode fiber bandwidth control in gigabit ethernet [20], a mode converter for higher order mode dispersion compensation [21], and a tunable wavelength selective filter [22-23] were suggested and also experimentally demonstrated. In addition, the birefringence of the elliptical HOF and the availability for polarization maintaining (PM) fiber were also investigated [24].

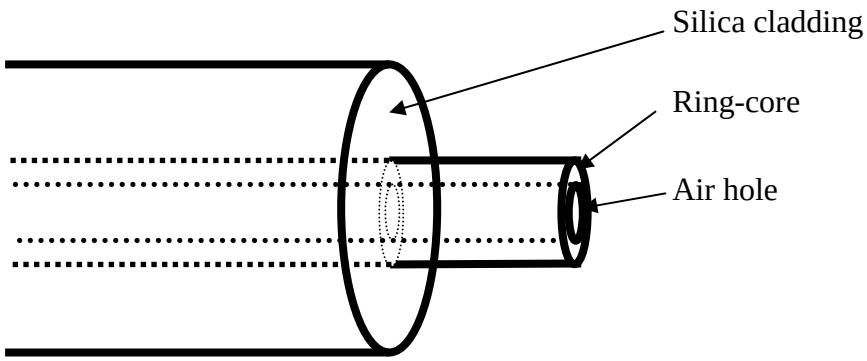

Figure 1-1. The schematic diagram of the HOF

The HOF structure is also used for the delivery of high energy-density beams, which require different materials for guiding because the high energy beam can cause damage to the silica, which is the main material in the fiber. For this, an other type of HOF

was proposed. It is composed of metal layers such as aluminum (Al) around the hollow region. The hole can be filled with air, an inert gas, or kept under vacuum [25]. In this case, the guiding mechanism is different from a normal optical fiber because the refractive index of the core (air or other gases) is much lower than that of the cladding (metal). The light is guided through the hollow core by power reflection or Bragg reflection at the single or multi-metal layers [26-27]. Using this kind of HOF, some research groups have demonstrated the delivery of laser beams covering the wavelength range from the ultraviolet (UV) to the infrared (IR) region [28-30].

All of these applications were for passive applications. Contrary to these, the HOF can produce several useful modal characteristics for active functions such as in laser and amplifier applications. First of all, the relatively large area of the ring-core, compared to the normal step index fiber, is expected to increase the pump absorption in a cladding-pump configuration. In 1997-1998, it was demonstrated that the ring-doping technique showed a higher efficiency for three-level fiber lasers than for the normal fiber [15, 31]. For the high pulse energy, the large gain volume of the ring doped region was more attractive [31]. Here, the high energy pulses are not guided through the doped region but via the air core in the center, which reduces the overlap between the pulses and the gain medium. And thus, the efficiency is degraded. In contrast, the HOF design forces light to be guided through the ring-core, which means that the modal overlap between the light and the gain medium will not be reduced and the gain efficiency will be improved.

In 1998, P. Glas investigated a Nd^{3+}-doped hollow optical fiber laser [32]. However, it was only for the requirement to generate the DHB (dark hollow beam) in order to guide atoms through the hole. In practice, the performance of the HOF itself for lasers and amplifiers was not considered.

In 2003, P. R. Chaudhuri and K. Oh numerically investigated the modal characteristics of the HOF [33]. According to this study, even though the core area is relatively large, as mentioned before, single-mode generation at a laser-operating wavelength is possible with an appropriate design. Moreover, the very low refractive index of the central air region results in the negative dielectric volume, and thus the HOF exhibits non-zero fundamental (LP_{01}) mode cut-off in the finite wavelength range, which is useful for a waveguide filtering.

1-2-2. Waveguide spectral filters

Waveguide spectral filtering is widely used in optical communication systems. Most filters are wavelength-division multiplexing (WDM) fiber couplers. Basically, they are based on tapered fiber techniques [99]. There are also twin-core fiber spectral filters [34] or anti-resonant spectral optical waveguide filters [35]. However, these devices transmit only a limited spectral band, which satisfies a certain coupling condition in a very short length of fiber (<10 cm). This is not suitable for a cladding-pumped fiber laser. In general, a relatively long length of the fiber is required for laser sources where the gain medium is uniformly doped throughout the fiber core. In order to filter out any unwanted emission from the whole fiber, the waveguide spectral filtering should be acting over the total fiber length in a distributed manner. This thesis will cover the HOF as a distributed wavelength, fiber waveguide, filter.

Several fibers were proposed for the distributed wavelength filter. K. Morishita (1989) suggested an optical fiber with different dispersive material between the core and the cladding [36]. Here the effective index of the core and the cladding can become identical at a certain wavelength because of a different variation of the effective index dependence on wavelength where, theoretically, the guided mode can be cut-off and even

the fundamental mode becomes cut-off. This feature is quite similar to the manner in which the fundamental mode becomes cut-off in the HOF. However, the fiber filter using the dispersive fiber is not practical because it is difficult to find dispersive materials for a specific wavelength pass filter. Moreover, its fabrication is also not easy using a conventional fiber fabrication system such as modified chemical vapour deposition (MCVD) [2, 100].

The W-type fiber is a well-known wavelength filter [37]. The W-type fiber consists of a depressed cladding around the raised index core and a silica outer cladding. It was originally intended for the dispersion shifted fiber [38]. Afterwards, M. Monerie (1982) found that W-type fiber can act as a waveguide filter due to the fundamental mode cut-off [37]. In such a fiber, the effective index of the guided mode in the core can vary from the refractive index of the core to that of depressed cladding. Therefore, at a certain wavelength, the effective index of the mode can be equal to the refractive index of the silica outer cladding, where the fundamental mode is allowed to be cut-off. In principle, after the fundamental mode cut-off, the light is not guided by the core anymore. Contrary to the dispersive fiber, such a W-type fiber is easy to fabricate using the conventional MCVD method and, also, the refractive index can be controlled precisely for the specific wavelength of interest. Furthermore, it is more compatible with a conventional single mode fiber, which is widely used. However, its relatively small core area can be a disadvantage at higher power, and the large core is preferred in the cladding-pumped fiber lasers and amplifiers. Other types of fiber filters such as a dual-hole assisted fiber, designed by Corning (2006) [39], continue to be studied for various applications.

1-2-3. Nd^{3+}- and Yb^{3+}-doped fibers operating at the shorter wavelength

In fiber lasers and amplifiers, the Nd^{3+} ion is one of the most important active ions and is widely used as a dopant. Laser action of such an ion in a glass material was first demonstrated in 1961 [40]. Later, a Nd^{3+}-doped single mode silica fiber laser was first realized by the Southampton group in 1985 [41]. The energy levels of Nd^{3+} ions are shown in figure 1-2. Important energy transitions for the laser and amplifier action are $^4I_{9/2} \rightarrow {}^4F_{5/2}$ (800 nm), which is the typical pumping band for Nd ions, $^4F_{3/2} \rightarrow {}^4I_{11/2}$ (1060 nm), $^4F_{3/2} \rightarrow {}^4I_{9/2}$ (900 nm) and $^4F_{3/2} \rightarrow {}^4I_{13/2}$ (1300 nm), where spontaneous emissions is observed. There have been extensive research studies on the emission at each transition for high power fiber sources.

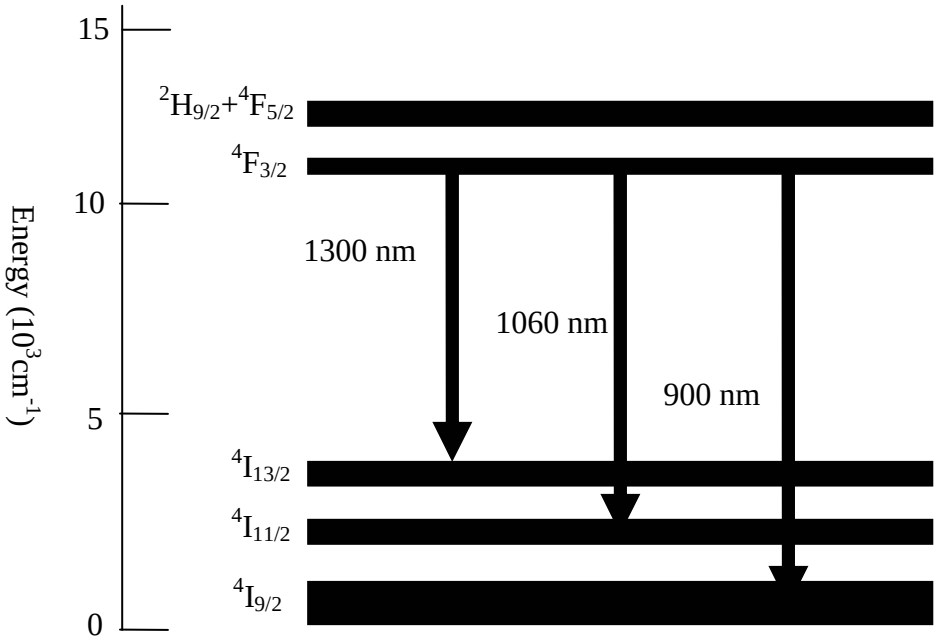

Figure 1-2. The energy diagram of Nd^{3+} ions

In particular, the energy transition ($^4F_{3/2} \rightarrow {}^4I_{11/2}$, 1060 nm) was characterized as a four-level laser transition and it is thus relatively easy to realize the laser action due to the low laser threshold and high gain efficiency. Since the cladding-pump technology was invented, the output power of the Nd^{3+}-doped fiber laser has been increased remarkably. Minelly et al. (1992) first demonstrated 1 W output power at the 1060 nm emission band

using laser-diode pumping [42]. Po et al. (1993) achieved an output power level of 5W with a 51% slope efficiency [43]. Recently, the output power at the 1060 nm emission band reached 30 W [44]. Even higher output powers are only limited by the available pump power. However, this spectral range can also be covered by Yb^{3+} ions, which are more efficient than Nd^{3+} ions in the silica host. Due to this, the research on Nd^{3+}-doped fiber lasers at 1060 nm is not of much interest.

Contrary to this, in the other spectral range, $^4F_{3/2} \rightarrow {}^4I_{9/2}$ (900 nm) for Nd^{3+} ions, the laser action is much more interesting because such a wavelength can be converted to blue light (~ 450 nm), for displays or data storage, by frequency doubling [45-46] and also used for a fiber sensor such as for water vapour sensing [47]. However, it is very challenging to design the fiber especially for power scaling using a cladding-pumped configuration because the three-level fiber laser requires much higher pump intensity in order to obtain a high level of population inversion and to overcome ground-state absorption (GSA). Also the four-level laser transition at 1060 nm, with a low threshold, competes with the 900 nm emission transition.

In such spectral ranges in Nd-doped fibers, Reekie et al. (1987) first demonstrated a fiber laser at 938 nm, for which the output power was only 3 mW with 31% slope efficiency [48]. Cook et al (1998) presented an output power of 43 mW at 925 nm and this was tunable from 896 nm-939.5 nm [49]. These previous results were demonstrated in a core-pumped laser configuration. However, such a configuration is not power-scalable because of the limited available pump power. In order to scale up the output power of a fiber laser, the cladding-pump configuration should be used.

Nd in a germano-silicate host favours the transition at 900 nm [9, 50]. However, the germano-silicate host does not permit a high Nd^{3+} ion concentration. In order to increase Nd^{3+} ion concentration, the alumino-silicate host is preferred. However, the spectroscopy

of Nd in an alumino-silicate host favours the 1060 nm transition band rather than 900 nm [9, 50]. Hence, it necessitates the use of a distributed filter to suppress the stimulated emission at 1060 nm. For this, a W-type fiber design, that has a non-zero fundamental mode (LP_{01}) cut-off, has been used [8, 46]. The LP_{01} mode cut-off can be located between the two Nd^{3+} ion emission bands, so that the fiber does not guide at 1060 nm. A good suppression of 1060 nm emission was reported [8, 46]. Recently, 10 W of cw single mode output power at 930 nm was realized with a Nd-doped alumino-silicate W-type fiber [51], in a MOPA (master oscillator power amplifier) configuration. However, the laser configuration is complicated and the core-size of the W-type fiber is relatively small, which limits the extractable energy at 930 nm from the Nd-doped fibers. Moreover, the relatively small core eventually leads to high fiber nonlinearities. Therefore, for real applications, a large core is an important design feature for the high-power cladding-pumped fiber lasers, since it allows the inner-cladding size, and thus the pump power, to be scaled whilst maintaining an acceptable pump absorption. Unfortunately, if the core size becomes bigger, the fundamental mode cut-off of a W-type fiber will be located above 1060 nm and the desired suppression can not be obtained. While it is in theory possible to reduce the refractive index step, and thus maintain 1060 nm suppression even with a larger core, this is quite challenging in practice.

To date, the Yb^{3+}-doped fiber has led to significant improvements in high power fiber laser sources. It has already reached kW power levels at ~1100 nm whilst maintaining a nearly diffraction-limited beam quality [4-6]. Figure 1-3 shows the energy level diagram of Yb^{3+} ions. There are only two levels, however, each level, $^4F_{7/2}$ and $^4F_{5/2}$, has strongly coupled Stark split sub-levels. Because of that, the laser action at 1100 nm is after considered as a quasi-four level laser transition with a low threshold and high gain efficiency.

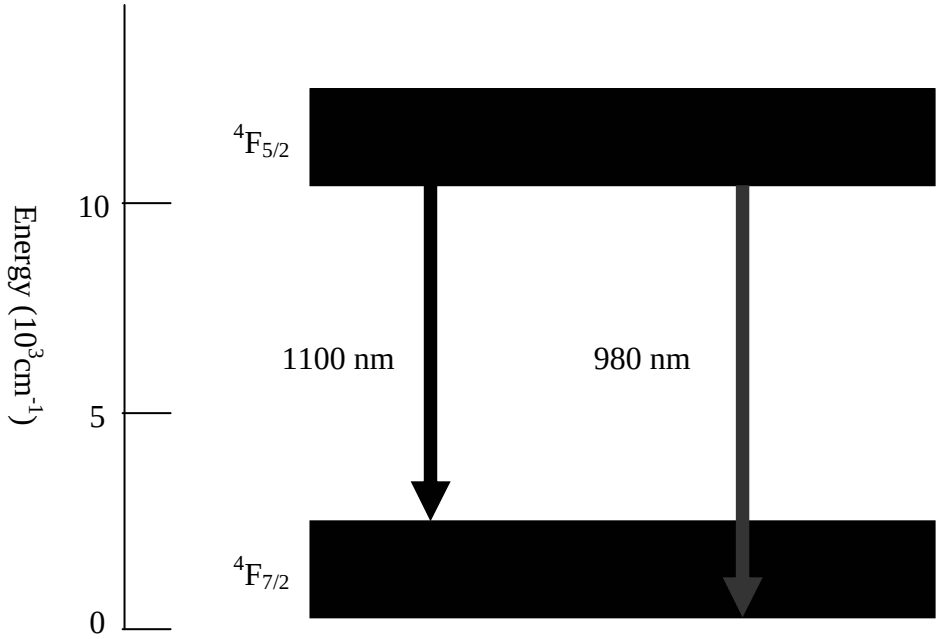

Figure 1-3. The energy diagram of Yb^{3+} ions in the fused silica

Yb^{3+}-doped fibers have a broad absorption band from 850 nm to 1070 nm and also a broad emission band from 900 nm to 1100 nm. The pumping wavelength is normally chosen at 915 nm or 980 nm because of the relatively high absorption cross section. In practice, it was pumped by a 980 nm pumping source and shows very highly efficient operation at 1100 nm. However, in the Yb^{3+}-doped fibers, laser operation at the shorter wavelength is also challenging, similar to the Nd^{3+} doped fiber operating at 900 nm. In many applications, such as for a pump source for an erbium-doped fiber amplifier and laser [52] or blue light generation by frequency doubling [53-54], high-power, single-mode 980 nm sources are of interest. Commercially available single-mode 980 nm laser diodes are not only limited by their output powers but they are expensive too. In terms of power-scaling of the fiber laser at 980 nm, the cladding-pumped concept is also available. R. Selvas *et al.* from the ORC suggested a jacketed air clad (JAC) structure [115] for the high power fiber laser at 980 nm. Using such a fiber, an output power of more than 3 W was obtained while maintaining diffraction-limited beam quality [55].

However, the JAC structure requires a small inner-cladding (~30 μm) and a short fiber length (e.g., ~40 cm in [55]). This is to suppress the Yb-emission, at around 1030 nm, along the fiber and at the same time to achieve a high level of Yb inversion (over 50%) in order to obtain gain in the 980 nm transition, because both the emission and absorption cross-sections are comparable at this wavelength. Thus, power-scaling using a JAC structure requires the use of an expensive, high-power and high-brightness multimode pump source. An alternative approach to achieve a high power 980 nm YDFL would be to design the waveguide structure such that it acts as a distributed filter along the fiber to suppress the 1030 nm ASE.

1-2-4. Suppression of stimulated Raman scattering in high power fiber lasers

The continuous wave (cw) output power of high brightness cladding-pumped ytterbium (Yb) doped fiber lasers has already reached the kW-level, as mentioned before. Moreover, fiber-based master oscillator – power amplifier (MOPA) sources show the potential to scale up the average output power of more sophisticated waveforms, such as picosecond pulses [10]. For those, fiber nonlinearities become an important issue.

One of the fiber nonlinearities, SRS, is a major obstacle for power scaling of pulsed fiber systems and even in cw single-mode, high power fiber systems. SRS can occur in the laser, or the amplifier itself, as well as in any delivery fiber. To date, most of the high power fiber sources use a large, low-NA, core and a relatively short fiber in order to mitigate SRS. Large cores, however, eventually lead to a multimode output beam, and hence to a degraded beam quality. Although, the beam quality obtained with a multimode core can be improved significantly by filtering out the higher order modes, e.g., by tapering

the fiber or coiling a low-NA fiber [56-57], these methods have their limitations and are difficult to implement in a delivery fiber. Hence, a single-mode core still remains an obvious choice for high beam quality. However, a single-mode (i.e. small) core requires a long fiber in the cladding-pumped configuration, because of the relatively low pump absorption that is due to the large area ratio between the inner cladding (pump waveguide) and the doped core. However, the resulting strong interaction of the optical field with the small core, over a long fiber length, will reduce the SRS threshold significantly [58].

Previously, in single-mode fibers, the suppression of SRS was demonstrated using several methods such as parametric suppression by the four-wave mixing (FWM) process of Raman Stokes and anti-Stokes [59-60] and polarization switching in high birefringence fiber [61]. Later on, in a dual-frequency pumping technique, the SRS suppression in the total first-order Raman Stokes was successfully achieved [62-63]. However, such techniques were not efficient in high power, cladding-pumped fiber laser systems because they allowed only one frequency component of the pump field for SRS suppression or because their suppression was only valid at a well controlled, selective parametric condition.

As an alternative method, using fiber bending loss, the stimulated Raman threshold can be increased because Raman gain is also dependent on the propagating loss at the Stokes wavelength. Kuzin et al. (1999) presented the SRS effect when bending loss was induced to the fiber [64]. Recently, Dragic et al. (2005) demonstrated, numerically, SRS suppression by the induced bending loss [65]. In practice, such a technical concept is more suitable for the cladding-pumped high power fiber lasers because it is simple and the total Raman gain band can be suppressed by the induced bending loss without any specific parametric condition in the fiber system. However, in the normal step index structure, the bending loss is detrimental over the whole wavelength range and thus it will introduce a

significant amount of loss at the signal wavelength too, because of the relatively slow dependence of bending loss on the wavelength. Therefore, in order to filter out SRS emission selectively, without any loss at a desired wavelength, a distributed fiber waveguide filter, with a modified index structure, is required. Very recently, a dual hole assisted fiber with the fundamental mode cut-off has been suggested for the suppression of Raman gain [39]. In this thesis, the suppression of SRS in W-type, Yb^{3+}-doped fibers with fundamental mode cut-off will be discussed.

1-3. Main contribution in the thesis

In the previous sub-section, the HOF and its availability for high power fiber laser sources was introduced. As mentioned before, it is very challenging to realize the fiber laser in the cladding-pumped configuration operating at the shorter wavelength, because of the relatively low pump absorption and the competition of the stimulated emission transition at longer wavelengths. In this thesis, the HOF structure is mainly considered because it has a relatively large core area and also because it provides a non-zero fundamental mode cut-off in a finite wavelength range, which yields a distributed wavelength fiber waveguide filter for the suppression of unwanted stimulated emission. I was given the project HOF to work on when I started my Ph. D. I contributed mainly to the theoretical and experimental investigation of the HOF relating to the modal characteristics, such as cut-off behavior and bend loss. The laser performance of rare-earth doped HOFs was investigated theoretically and experimentally with significant help from P. Dupriez, D. B. S. Soh and C. Codemard in the high power fiber laser group at the ORC.

1-4. Organization of this thesis

Part I contains an introduction and a brief review of fiber fabrication, waveguide theory and fiber lasers and amplifiers in the first two chapters. In chapter 1, the motivation for the research I accomplished is introduced and the previous studies in this field are presented. Chapter 2 first provides an overview of the rare-earth fiber fabrication using MCVD and, then, relevant waveguide theory is reviewed in a simple manner in order to help in the understanding of the design process of the HOF and DCHOF. The review on fiber lasers and amplifiers and SRS is basically an explanation of the important terms and equations and is given only for enabling an understanding of later chapters, because their theory has a very wide scope which goes beyond that of this thesis in many areas. In chapter 3, I described numerical simulations on the modal characteristics of step HOFs. For this, I suggested the characteristic equation for step HOFs, which is used for the analysis of cut-off characteristics, modal fields and bending loss properties, depending on fiber design. Based on numerical analysis, the cut-off behaviour of the fundamental (LP_{01}) mode was investigated experimentally. In addition, a Er:Yb co-doped, step, HOF fiber laser was investigated experimentally.

Chapter 4 deals with Nd-doped DCHOF. I derived the characteristic equation in order to analyze the modal characteristics of DCHOF. Based on the numerical analysis, I designed the DCHOF for the realization of a Nd-doped fiber laser operating at 930 nm. Laser action of the Nd-doped DCHOF was demonstrated experimentally in cw and Q-switched pulse regime and its performance was analyzed. In chapter 5, an Yb-doped DCHOF was investigated for high power fiber sources at the shorter wavelength, 980 nm. First, the optimum fiber design was found using the numerical analysis of the modal properties of DCHOF and, then, laser action of Yb-doped DCHOFs at 980 nm was

demonstrated. Next, the Yb-doped DCHOF was considered for high power fiber laser sources at the other relatively short wavelength (~1040 nm).

In chapter 6, SRS suppression was investigated in a Yb-doped W-type fiber MOPA system. For this, initially, I estimated the Raman threshold, depending on the induced loss at the Raman 1st Stokes wavelength, using a numerical approach. Using W-type fiber with the fundamental mode cut-off at the Stokes wavelength, SRS suppression was demonstrated experimentally in a fiber–based MOPA system (for pico-second and nano-second pulses), which provide high peak power. Analysis of the amplifier action was carried out in detail. In chapter 7, I summarized all the results in my thesis and present the future prospects for the DCHOF.

Chapter 2. A brief review of a fiber fabrication and design for a high power laser sources

2-1. The fabrication of rare-earth doped fibers

The requirements for rare-earth doped fibers are slightly different from those for normal long-distance communication fibers. However, their fabrication process is based on the method used for communication fibers. Communication fibers basically consist of silica (SiO_2) or silicate glasses as the main material and one or more oxides (GeO_2, P_2O_5, B_2O_3 etc) as a dopant to control the refractive index. The high purity silica fiber system is the best material for optical transmission around 1.5 μm, in terms of optical loss, physical or chemical properties and long-term reliability.

The fabrication process of the fiber is composed of two main stages: preform fabrication and fiber drawing. There are generally three techniques used to produce the fiber preform: Outer Vapour Deposition (OVD) [116], Vapour Axial Deposition (VAD) [66] and Modified Chemical Vapour Deposition (MCVD) [67]. The principal procedure is based on a vapour phase reaction, which is the oxidation of chloride or halide vapours. The MCVD process, the most versatile among these techniques, is widely used because it produces a low loss and high quality silica fiber at relatively low-cost. In this thesis, all fibers were fabricated using the MCVD process.

2-1-1. Modified Chemical Vapour Deposition (MCVD)

MCVD is basically an inner deposition process because the high purity oxides are deposited on the inside wall of a silica tube. Figure 2-1 shows the typical MCVD setup. A silica tube, which is high-purity synthesized silica is rotated on a glass-working lathe. Reactants such as $SiCl_4$, $GeCl_4$, $POCl_3$ or BBr_3 are vaporized and delivered into the silica tube by a carrier gas such as oxygen (O_2) and nitrogen (N_2) using bubbler systems. The oxy-hydrogen burner traverses along the silica tube, heating it to temperatures in the range of ~2200^{o}C. The reactants react with the oxygen and produce the oxides and chlorine gas as by-product, as shown in the following chemical reactions (2-1) and (2-2). The oxides are deposited and sintered onto the inner surface of the silica tube to produce highly dense glass layer.

$$SiCl_4\ (gas) + O_2\ (gas) \leftrightarrow SiO_2\ (solid) + 2Cl_2\ (gas) \qquad (2\text{-}1)$$

$$GeCl_4\ (gas) + O_2\ (gas) \leftrightarrow GeO_2\ (solid) + 2Cl_2\ (gas) \qquad (2\text{-}2)$$

MCVD apparatus consists of a chemical delivery system (left-side in figure 2-1) and a glass working lathe (right-side in figure 2-1). In the chemical delivery system, the chemicals for MCVD process are stored in bubblers made of glass or stainless steel, which are housed in constant-temperature baths to maintain the liquid chemicals at the desired temperature. The chemical rate at the outlet of the bubbler is determined by the partial pressure of bubbles, the vapour pressure of the chemical, and the flow rate of the carrier gas. At a constant temperature, the pressure of the bubbles and the chemical is fixed. Due to this, it is important to control the temperature of chemicals constantly to obtain the reliable chemical flow rate into the silica tube. The flow rate of the chemicals into the

silica tube is controlled by the flow rate of the carrier gas using mass flow controllers (MFCs).

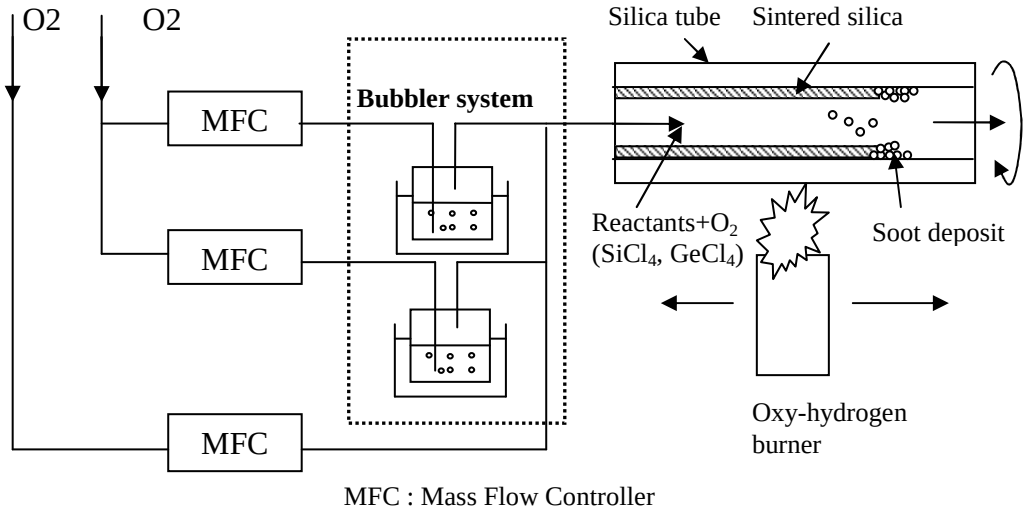

Figure 2-1. Schematic diagram of MCVD process [68].

The bubblers used in Optoelectronics Research Cetner, University of Southampton, consists of four compounds, $SiCl_4$, $GeCl_4$, BBr_3 and $POCl_3$, which is used in any combination to achieve the desired refractive index of the preform. However, the combination of BBr_3 and $POCl_3$ is avoided due to the explosive reaction. The carrier gas is oxygen except for BBr3, where the carrier gas is nitrogen gas.

The other part of MCVD apparatus, the glass working lathe, has two chucks for clamping the substrate tube. The two chucks are aligned coaxially for reducing the deformation of the silica tube during the process of deposition and collapsing. The oxi-hydrogen torch moved by a motor-driven carriage is added to the lathe, where a radiation thermometer (pyrometer) and output diameter monitor is also installed to measure the temperature and diameter of the hot zone of the tube. The temperature is controlled by the flow rate of the hydrogen and oxygen using MFC. The speed of the carriage also affects the temperature of the hot zone and thus, it should be controlled properly. One end of the

tube is put into a rotary-seal to provide the chemical into the tube and the other end has an exhaust system, which removes the reacted gas and particles.

Main MCVD process consists of the cleaning, deposition and collapsing as shown in figure 2-2. In the first step, the inner surface of the substrate tube is cleaned by etching using a flow of sulphur-hexafluoride (SF_6) and it also helps to make smooth inner wall of the tube. The processing temperature is ~2000^{o}C, and ~100 μm of silica is etched away from inside the tube. The next stage is the deposition of the cladding and core. The operating temperature is ~2050^{o}C. The deposition of the cladding generally acts as a buffer layer between the tube and the core. It reduces roughness of the inner wall of the tube and therefore reduces the scattering loss. Furthermore, it allows the fabrication of the complicated fiber structure by using index-control chemicals such as $GeCl_4$ (increases the refractive index) and BBr3 (decreases the refractive index) [101].

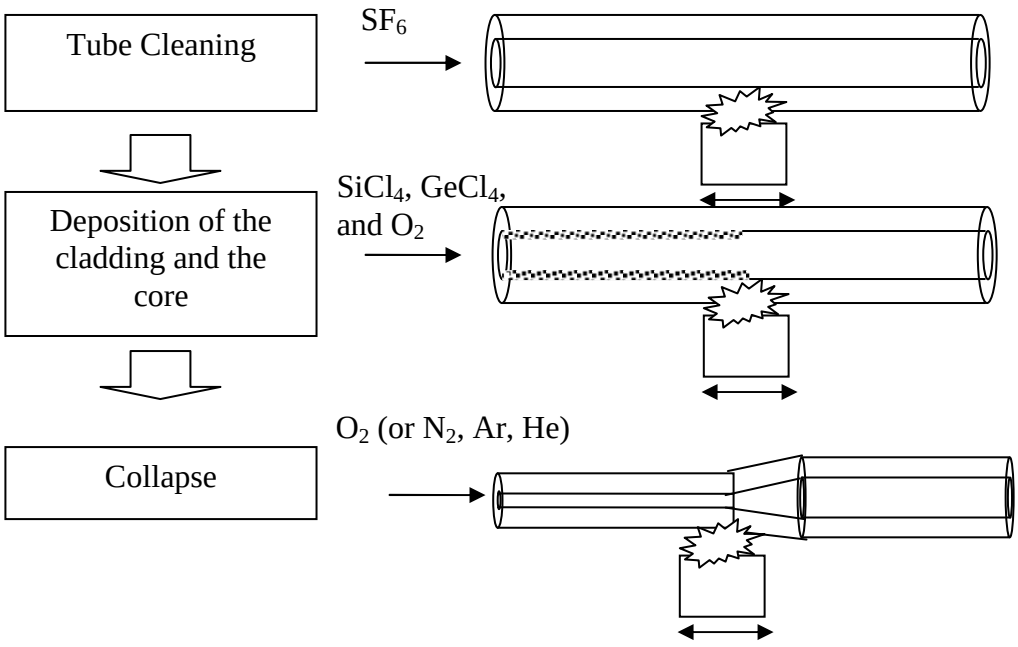

Figure 2-2. The conventional MCVD process for the fabrication of the preform

The oxy-hydrogen torch moves along the tube in the same direction as the reactant gas flow, which generate enough temperature at the reacting zone (or heat zone). There are chemical reactions which creating glass soot particles. The soot is deposited on the inner wall of the tube by thermophoresis [101, 102], which is a driving force induced by the temperature difference between the reacting zone and the deposition wall. The particles are moved in the direction of the lower temperature zone (the deposition wall) from the hot zone and set down on the wall. The deposited particle is consolidated into the silica film at the inner wall of the tube. In the core deposition, there are some differences to this process in the case of rare-earth doped fibers for amplifiers or lasers. First, contrary to normal communication fiber, where GeO_2 is mostly used, other oxides (Al_2O_3) can be used as dopants in the core in order to improve spectroscopic characteristics such as to broaden the bandwidth. Secondly, rare-earth raw materials ($ErCl_3$, $NdCl_3$ and $YbCl_3$ etc) have a much lower vapour pressure than that of other halide reactants ($SiCl_4$, $GeCl_4$) as shown in figure 2-3.

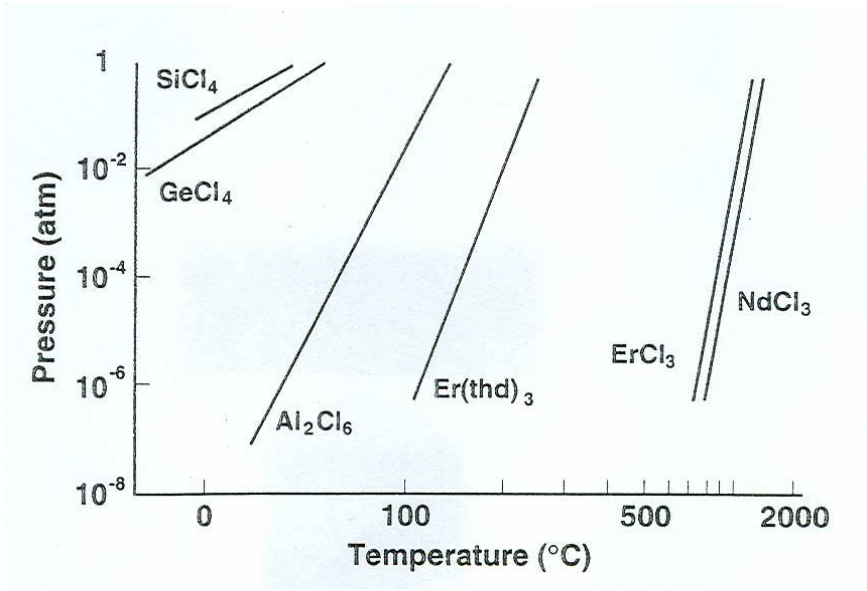

Figure 2-3. Vapour pressures of reactant halides for making rare-earth doped high silica glasses [68].

For this reason, it is very difficult to carry them into the reaction zone using bubbler systems in the MCVD process. There are several methods to add rare-earth ions into glass and the doping methods are categorized by two kinds of methods. One is the gas phase-deposition method, which means that the rare-earth ion is doped into the glass during the deposition process using vapours of rare-earth halides [2] and the other one is the after-deposition method [2], which is generally "solution doping method" [69]. The solution doping technique is widely used because of its simplicity, low cost and high uniformity of rare-earth doping. In order to do this, the operating temperature in the core (or doped region) deposition should be lower than in the cladding deposition. The temperature for the core deposition is 1500-1600^{o}C, where the soot is not sintered and maintains the high porosity for doping rare-earth materials via the solution doping process.

The final stage for the preform fabrication is the collapse of the tube. For this, a very high temperature (~2100^{o}C) is required. The tube is collapsed down to a solid rod due to the surface tension, and the reduced viscosity of the glass. At such a high temperature, tube deformation is quite easy. Therefore, this process should be carefully controlled using the properly adjusted temperature, rotation speed, and carriage speed. In addition, in this process, the diffusion of the hydroxyl (-OH) from the tube to the core can be an issue [103]. In order to reduce this, the initial preparation of the tube (ie. by using a high purity silica tube and etching the inner wall of the tube) is important. The tube I used in ORC is F300 Suprasil grade, which has the OH content less than 0.2 ppm. The cladding thickness should be carefully considered as the barrier preventing the OH diffusion. In ORC, the barrier layer is ~8 μm (measured in the final fiber) with 125 μm outer diameter. Furthermore, vaporization of the dopants at such a high temperature can occur and causes the alteration of the refractive index profile such as a central dip in the refractive index of the preform. This is especially significant in germanium doped fibers because GeO_2 has a relatively

large vapour pressure and thus, it can be easily evaporated. This can be reduced by collapsing the tube in the germanium atmosphere [101] or by etching the surface layer, where the germanium is evaporated [101].

In the case of the hollow optical fiber used in this thesis, the collapsing is not completed and the hole in the preform is maintained with a specific size. It is an important process because the size of the hole determines the thickness of the core and the cladding in the final fiber. If the hole size in the preform is too small, it may collapse in the fiber drawing process. Contrary to this, if it is too large, it becomes difficult to control the core thickness.

2-1-2. Solution doping method

As shown in figure 2-3, rare-earth materials have a low vapour pressure, which makes it difficult to directly deliver them into the reacting zone in MCVD lathe using the bubbler system. This leads to use of the solution doping technique. Solution doping is the essential process for the incorporation of rare-earth ions, which adds the rare-earth ions into silica or a silicate glass network by soaking the low density oxide (soot) in a solution containing the rare-earth compounds [69]. In the solution doping process, it is important to deposit an appropriate porous glass layer inside the tube. In addition, the doping concentration, as well as the glass structure, can be determined from the porous glass structure. This porous glass is deposited at lower temperature ($1500^{o}C$~$1600^{o}C$), which does not allow the glass to sinter. Here, the porous glass is composed of tiny glass particles (from sub micrometer to hundreds of micrometer) and pores, whose structure is determined from the temperature of the glass, where if the temperature is too low, the soot easily disassociates from the tube during the doping process and sintering process. If the

temperature is too high, the penetration of rare-earth ions is not enough and their doping uniformity is impaired.

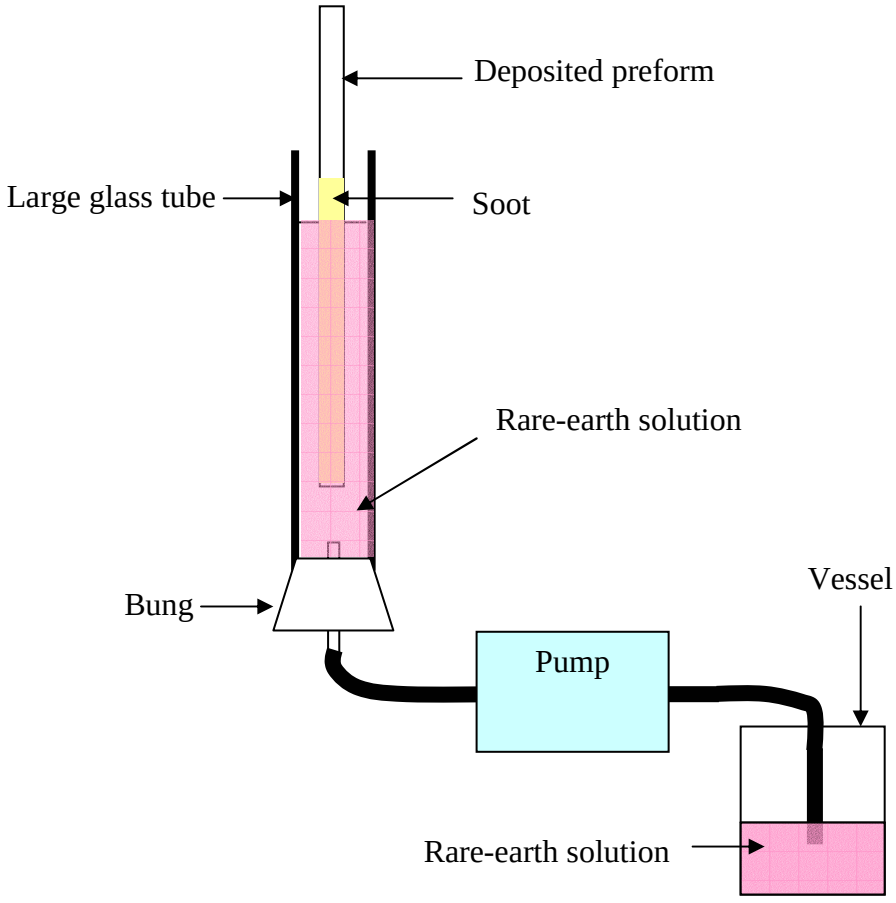

Figure 2-4. The schematic diagram of the apparatus for solution doping.

Figure 2-4 shows the schematic diagram of the apparatus used for the solution doping. A rare-earth solution made of methanol (or water, alcohol) and rare-earth raw materials is directly introduced into a deposited porous glass and soaked in their pores. In general, in order to improve the solubility of rare-earth ions, $AlCl_3$ is used in the combination of rare-earth chlorides. This solution should be pumped in the tube with a slow speed for preventing any dislodging of soot particles. In order to control the concentration of rare-earth ions in the silica, the concentration of the solution is properly adjusted. The soaking time is ~1 hr, which is enough for the complete diffusion of rare-

earth ions into the soot. After soaking, the solution is expelled from the tube and the porous glass is dried. At first, the soot is dried in the air for several hours and this time should ensure complete drying. In some cases, He, N_2 or O_2 gas can be used in the lathe to make the drying process faster. Then, this rare-earth doped porous glass is sintered in the MCVD lathe. The sintering temperature is ~1850^{o}C, which should make the soot glass transparent. In this process, the temperature is controlled very carefully in order to prevent the evaporation of the rare-earth chlorides and aluminium chlorides ($AlCl_3$) before the oxidation reaction occurs. After consolidating the soot, the tube is collapsed in the usual way at high temperature. In the sintering or collapsing process Cl_2 gas, which is the drying gas, can be used to reduce the water content. The preform made with this process is drawn into the fiber *via* the drawing process.

The main disadvantage of the solution doping process is that it is very difficult to employ for multiple core layers. For this, the whole process as mentioned before should be repeated for every single core layer. However, it is not practical and is very time-consuming job. It can also cause significant tube deformation. Therefore, it is challenging to obtain large core fibers. In order to solve this, an alternative preform processing stage is required. After completing MCVD process, the preform is etched to give the desired ratio of the core and cladding in hydrofluoric acid solution. In addition, in order to improve the pump absorption, a non-circular symmetry of the preform is necessary [104, 105]. For this, the preform is milled into a D-shape or a rectangular shape [106, 107].

2-1-3. Fiber drawing process

Figure 2-5 shows a schematic diagram of the drawing apparatus, which is mainly composed of the preform feed controller, a high temperature (>2000 ^{o}C) furnace, diameter

gauge, the polymer coating assembly including a ultraviolet (UV) curing furnace, and a fiber take-up assembly. The preform is mounted in a chuck with x-y stage in order to align the prefrom in the center of the furnace. It is fed into the high temperature furnace with a controlled constant speed. In general, the heating element of the furnace is high purity carbon, which can be easily oxidized when it meets air at high temperature. In order to protect the graphite element, an inert gas, such as argon (Ar), is introduced into the furnace. If the temperature is fixed to a point where it softens the preform, the fiber diameter is controlled by adjusting the preform feeding speed and draw speed. Their relation is presented in the following simple equation according to the conservation of mass:

$$\frac{v_p}{v_f} = \frac{d_f^2}{d_p^2} \tag{2-3}$$

where, v_p and v_f are the feed and draw speeds respectively, and d_p and d_f indicate the preform and fiber diameters respectively. The take-up speed of the fiber is controlled by a signal from the output diameter gauge located below the furnace. The feedback loop system helps to maintain the outer diameter at a constant value. In principle, a fluctuation of the fiber diameter eventually causes a variation of the fiber geometry, which can produce detrimental effects on waveguide properties. Therefore, precise control is important. Fluctuation of the diameter comes from two major origins. One is that it is caused by the temperature fluctuation, which results in ±0.5 μm variation of the fiber diameter when the temperature fluctuation is in ±0.2^{o}C in a length period of 100 cm [2]. In order to minimize this, the flow rate of the inert gas and the ratio of the preform diameter to the heater diameter should be optimized [117]. The other is the variation of the take-up speed, which causes the long-term fluctuation. Its periodic length is longer than 100 cm. This fluctuation is minimized by controlling the take-up speed constantly and precisely via monitoring the signal from the diameter gauge.

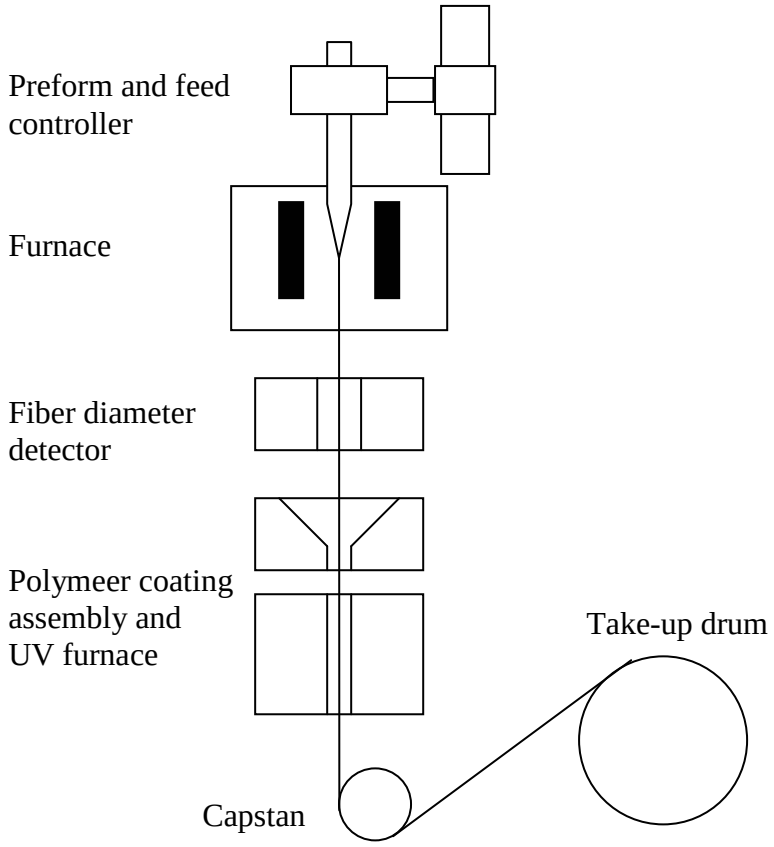

Figure 2-5. Schematic diagram of the fiber drawing apparatus

The fiber enters a coating cup in the polymer coating assembly, which contains a viscous acrylate fluid. The hole size in the bottom of the cup (coating die) is selected depending on the fiber diameter and the desired coating thickness. The coating material is cured in the UV furnace. The consolidation strength of the coating is highly dependent on the curing temperature (or UV power) and it should be high enough to protect the fiber breakage during fiber bending and handling. In addition, the coating thickness should be also optimized. For a commercial single-mode fiber, the coating diameter is ~250 μm. However, it may be different for other applications. There are two coating methods. One is the gravity-force coating, which is generally used in ORC in the case of the low drawing speed (5 ~ 20 m/min) and small coating diameter (≤250 μm). Here, the coating material is stored in the coating cup and sticks onto the fiber, when the fiber passes through the

coating material. The coating thickness depends on the hole size in the coating die and drawing speed. This process is quite simple. However, it is difficult to use at the high drawing speeds and for large fiber diameters. The other method is the pressurized coating system [108], which is useful for very high drawing speeds and large fiber diameters. In the pressurized system, the coating material is injected to the surface of the fiber by carefully controlling the pressure with an inert gas (in general, N_2). In order to do this, the coating cup is specially designed [109]. In some cases, in order to control the injection speed of the coating material, its viscosity is controlled and thus, the coating unit contains the thermal apparatus [110]. For most commercial manufacturers of fibers industries, the pressurized coating method is used.

The fiber then passes round the capstan, whose speed generally corresponds to the take-up speed, and it is wrapped onto a take-up drum. The important thing in the drawing process is to maintain the mechanical strength of the fiber. However, in the drawing process, the scattering loss of the fiber can be varied depending on the temperature and take-up speed [111]. This is due to the induced stress in the fiber by the drawing tension during the drawing process [111]. Therefore, for optimizing the optical and mechanical properties of the fiber, the temperature and the take-up speed should be carefully considered.

2-2. Review of waveguide theory

In this section, the basic theory of a waveguide in a simple step index fiber is reviewed using electromagnetic theory. In principle, the electric and magnetic fields of a guided wave satisfy Maxell's equations and the boundary conditions imposed by the cylindrical dielectric core and cladding. There are certain solutions, which are called modes, each of which has a distinct propagation constant (or effective refractive index),

which represent the modal characteristics in a fiber waveguide. Therefore, it helps to understand the design process of more complicated fiber waveguides.

An electromagnetic field in a medium is composed of two related vector fields, which satisfy the following partial differential equations, known as Maxwell's equations [71].

$$\nabla \times \mathbf{E} = -\frac{\partial \mathbf{B}}{\partial t} \tag{2-4}$$

$$\nabla \times \mathbf{H} = \frac{\partial \mathbf{D}}{\partial t} \tag{2-5}$$

$$\nabla \cdot \mathbf{D} = 0 \tag{2-6}$$

$$\nabla \cdot \mathbf{B} = 0 . \tag{2-7}$$

where, the medium is linear, non-dispersive, homogeneous, and isotropic, which indicates that physical properties are the same in all directions at a given point in the medium. It is also assumed that the medium is source-free. $\mathbf{H}$ and $\mathbf{E}$ are the magnetic field (A/m) and electric field (V/m) respectively. $\mathbf{D}$ and $\mathbf{B}$ are the electric flux density (or the electric displacement; C/m^2) and the magnetic flux density (Tesla) respectively. t is the time variable. $\nabla \times$ and $\nabla \cdot$ are the curl and the divergence operations respectively. The relation between $\mathbf{E}$ and $\mathbf{D}$ depends on the electric properties of the medium. Similarly, The relation between $\mathbf{H}$ and $\mathbf{B}$ depends on the magnetic properties of the medium. Such relations are defined as;

$$\mathbf{D} = \varepsilon_0 \mathbf{E} + \mathbf{P} \tag{2-8}$$

$$\mathbf{B} = \mu_0 \mathbf{H} + \mu_0 \mathbf{M} \tag{2-9}$$

where, $\mathbf{P}$ is the polarization density, which is the macroscopic sum of the electric dipole moments and $\mathbf{M}$ is the magnetization density, which is also defined in the same way with the polarization density. Most dielectric mediums, including pure silica, are nonmagnetic and thus, it can be assumed that $\mathbf{M} = \mathbf{0}$, which is always valid throughout this thesis. ε_0 is

the electric permittivity of free space and μ_0 is the magnetic permeability of free space. For a linear, non-dispersive, homogeneous, and isotropic medium, **P** and **E** at any position and time are parallel and proportional, so that their relation is defined as

$$\mathbf{P} = \varepsilon_0 \chi \mathbf{E}. \tag{2-10}$$

Where, χ is electric susceptibility, which is a scalar constant. Substituting (2-10) in (2-8), the relation between **E** and **D** can be found as

$$\mathrm{D} = \varepsilon \mathbf{E} \tag{2-11}$$

where, $\varepsilon = \varepsilon_0(1+\chi)$, which is the electric permittivity of the medium and the ratio $\varepsilon / \varepsilon_0$ is the dielectric constant. Using these relations, Maxwell equations (2-4) – (2-7) can be presented as

$$\nabla \times \mathbf{E} = -\mu_0 \frac{\partial \mathbf{H}}{\partial t} \tag{2-12}$$

$$\nabla \times \mathbf{H} = \varepsilon \frac{\partial \mathbf{E}}{\partial t} \tag{2-13}$$

$$\nabla \cdot \mathbf{E} = 0 \tag{2-14}$$

$$\nabla \cdot \mathbf{H} = 0 \tag{2-15}$$

Using the vector identity $\nabla \times \nabla \times A = -\nabla^2 A + \nabla(\nabla \cdot A)$, where ∇^2 is the Laplacian and ∇A indicates the gradient of a scalar function A, components of **E** and **H** satisfy the wave equation as follows

$$\nabla^2 \mathbf{E} - \frac{1}{c^2}\frac{\partial^2 \mathbf{E}}{\partial t^2} = -\nabla\left(\frac{1}{\varepsilon}\nabla\varepsilon \cdot \mathbf{E}\right) \tag{2-16}$$

$$\nabla^2 \mathbf{H} - \frac{1}{c^2}\frac{\partial^2 \mathbf{H}}{\partial t^2} = 0 \tag{2-17}$$

Here, c is the speed of light in a medium. From relations above, $c = 1/(\varepsilon\mu_0)^{1/2}$. In a medium, the speed of light is again

$$c = \frac{c_0}{n} \tag{2-18}$$

where, $n = (\varepsilon / \varepsilon_0)^{1/2} = (1+\chi)^{1/2}$, which is the refractive index of the medium. c_0 is the light velocity in vacuum. If ε is not varied in space significantly compared to $\mathbf{E}$, ε does not change within a wavelength distance and thus in equation (2-16), the right term $-\nabla(\frac{1}{\varepsilon}\nabla\varepsilon\cdot\mathbf{E}) = 0$. Finally, the wave equations can be expressed as follows

$$\nabla^2\mathbf{E} - \frac{1}{c^2}\frac{\partial^2\mathbf{E}}{\partial t^2} = 0 \tag{2-19}$$

$$\nabla^2\mathbf{H} - \frac{1}{c^2}\frac{\partial^2\mathbf{H}}{\partial t^2} = 0\,. \tag{2-20}$$

For a step index fiber, equation (2-19) and (2-20) is solved for the core and the cladding separately, and the boundary conditions are used to match the solutions. The electric field and the magnetic field are a function of a time and a space. If the electromagnetic wave is monochromatic, the electric field and the magnetic field are harmonic functions of time at the same frequency. Therefore, they can be expressed in terms of their complex amplitudes as follows

$$\mathbf{E}(r,t) = \mathrm{Re}\{\mathrm{E}(r)\exp(j\omega t)\}\,, \tag{2-21}$$

$$\mathbf{H}(r,t) = \mathrm{Re}\{\mathrm{H}(r)\exp(j\omega t)\}\,, \tag{2-22}$$

where $\mathrm{E}(r)$ and $\mathrm{H}(r)$ are the complex amplitudes of the electric and magnetic fields respectively. $\omega = 2\pi\nu$ is the angular frequency, and ν is the frequency. Using equation (2-21) and (2-22), the wave equations (2-19) and (2-20) are reduced to

$$\nabla^2\mathrm{E} + k^2\mathrm{E} = 0\,, \tag{2-23}$$

$$\nabla^2\mathrm{H} + k^2\mathrm{H} = 0\,, \tag{2-24}$$

where $k = \omega(\varepsilon\mu_0)^{1/2} = nk_0$ is the wave number, and k_0 is the wave number in free-space. Assuming the monochromatic light is propagated through a step-index fiber, the electric field and the magnetic field of light must satisfy wave equations (2-23) and (2-24), where $n = n_{co}$ in the core ($r < a$) and $n = n_{clad}$ in the cladding ($r > a$). In a cylindrical coordinate system, the wave equation becomes

$$\frac{\partial^2 U}{\partial r^2} + \frac{1}{r}\frac{\partial U}{\partial r} + \frac{1}{r^2}\frac{\partial^2 U}{\partial \phi^2} + \frac{\partial^2 U}{\partial z^2} + n^2 k_0^2 U = 0, \qquad (2\text{-}25)$$

where the complex amplitude $U = U(r, \phi, z)$ represents E or H. Taking waves travelling in the z direction, the z dependence of U is of the from $e^{-j\beta z}$, where β is the propagation constant. Because U is a periodic function of the angle ϕ with period 2π, it can be assumed that the dependence on ϕ is harmonic, $e^{-jl\phi}$, where l is an integer ($l = 0, \pm 1, \pm 2 \ldots$). Substituting $U(r, \phi, z) = u(r)e^{-jl\phi}e^{-j\beta z}$ into equation (2-25), the ordinary differential equation for $u(r)$ can be obtained.

$$\frac{d^2 u}{dr^2} + \frac{1}{r}\frac{du}{dr} + (n^2 k_0^2 - \beta^2 - \frac{l^2}{r^2})u = 0. \qquad (2\text{-}26)$$

The wave is guided if the propagation constant (β) is smaller than the wavenumber in the core ($n_{co}k_0$) and larger than the wavenumber in the cladding ($n_{clad}k_0$). Each mode parameter is defined as follows

$$v^2 = n_{co}^2 k_0^2 - \beta^2, \qquad \beta < n_{co}k_0 \qquad (2\text{-}27)$$

$$\gamma^2 = \beta^2 - n_{clad}^2 k_0^2, \qquad \beta > n_{co}k_0 \qquad (2\text{-}28)$$

Equation (2-26) can be written in the core and cladding respectively as follows

$$\frac{d^2 u}{dr^2} + \frac{1}{r}\frac{du}{dr} + (v^2 - \frac{l^2}{r^2})u = 0, \qquad r < a \text{ (core)} \qquad (2\text{-}29)$$

$$\frac{d^2u}{dr^2}+\frac{1}{r}\frac{du}{dr}-(\gamma^2+\frac{l^2}{r^2})u=0, \qquad r>a \text{ (cladding)} \qquad (2\text{-}30)$$

The solutions of differential equation (2-29) and (2-30) can be expressed as the family of Bessel functions in a cylindrical coordinate system [118]. The related solutions using Bessel functions are

$$u(r)\propto\begin{cases}J_l(vr), & r<a \quad (core)\\ K_l(\gamma r), & r>a \quad (cladding)\end{cases} \qquad (2\text{-}31)$$

where, $J_l(x)$ is the Bessel function of the first kind and order l, and $K_l(x)$ is the modified Bessel function of the second kind and order l. The mode parameters v and γ determine the variation of $u(r)$ in the core and cladding respectively. It is convenient to normalize v and γ by defining

$$X=va, \qquad Y=\gamma a \qquad (2\text{-}32)$$

Using (2-32), $X^2+Y^2=V^2$ is defined, where $V=NA\cdot k_0\cdot a$ ($NA=\sqrt{n_{co}^2-n_{clad}^2}$) is V-number (normalized frequency), which is important parameter that determines the number of modes of the fiber.

Most fibers are weakly guiding, which means $n_{co}\approx n_{clad}$ or the refractive index difference (Δn) between n_{co} and n_{clad} is much less than 1. In this case, the longitudinal components of the electric and magnetic fields are much weaker than the transverse components. And thus, the guided wave can be assumed to be a transverse electromagnetic (TEM) wave. A β satisfying the boundary condition between the core and the cladding, can be found from equation (2-31). The equation for obtaining β is expressed to the characteristic equation. For each Bessel order l, the characteristic equation has multiple solutions yielding discrete propagation constant β_{lm}, $m=1,2,\ldots$. Each solution indicates a mode. The linear polarization in the x and y directions form orthogonal states of

polarization and this linearly polarized (l, m) mode is denoted as a LP_{lm} mode. The two polarized modes propagate in the same direction with a same propagation constant β. In this thesis, this assumption is always valid. For a weakly guiding step-index fiber, the characteristic equation can be obtained by applying the boundary condition in equation (2-31). The condition is that the function $u(r)$ is continuous at $r = a$ and also, its derivative at $r = a$ must be continuous. These two conditions yield the characteristic equation for such a fiber.

$$\frac{(va)J_l^{'}(va)}{J_l(va)} = \frac{(\gamma a)K_l^{'}(\gamma a)}{K_l(\gamma a)} \tag{2-33}$$

Here, $J_l^{'}$ and $K_l^{'}$ are derivatives of the Bessel function of the first kind and order l and the modified Bessel function of the second kind and order l. Using the relation as follows [118]

$$J_l^{'}(x) = \pm J_{l\mp1}(x) \mp l\frac{J_l(x)}{x} \tag{2-34}$$

$$K_l^{'}(x) = -K_{l\mp1}(x) \mp l\frac{K_l(x)}{x}, \tag{2-35}$$

Equation (2-33) can be rewritten as

$$\frac{(va)J_{l\pm1}(va)}{J_l(va)} = \frac{(\gamma a)K_{l\pm1}(\gamma a)}{K_l(\gamma a)} \tag{2-36}$$

Solutions, mode parameters v_{lm} and γ_{lm}, must satisfy the characteristic equation (2-36) (m = 1,2,3,…) and in this case, the propagation constant β_{lm} is also determined by equation (2-27) and (2-28), which determines all modal properties, including modal field, modal dispersion, and induced bending loss. In order to analyze modal characteristics of the fiber waveguide, it is very important to derive and solve the characteristic equation for the designed fiber to obtain the propagation constant β_{lm}. However, in the more

complicated fiber waveguide structure, it is not easy to achieve the analytical solution as simple as equation (2-31) although the derivation process is similar to what was shown through this section. In this thesis, in order to solve this problem, a simple numerical approach (e.g. basically a Newtonian method) was used.

2-3. Stimulated Raman scattering in optical fibers

Stimulated Raman Scattering (SRS) is a nonlinear process that can be a serious obstacle for power-scaling in fiber laser sources [58]. In this section, a simple approach to SRS in optical fibers will be presented.

In a molecular medium, light at a frequency (ω_P) can be converted to a frequency-shifted light (ω_S), which is determined by the vibrational modes of the medium. This process is called the Raman effect [72]. In optical fibers, incident light acts as a pump for generating the frequency shifted radiation (e.g. Stokes wave), where the strength of the Stokes wave is dependent on the light intensity. Similarly, the original signal in an amplifier or laser system can act as a pump for SRS generation. If the pump reaches an intensity level where Raman effects begin, energy is transferred to other frequencies and the energy at the original frequency is decreased. Therefore, in high power fiber sources, the signal is easily amplified to such a level where it transfers to Raman. The conversion from the signal to the Raman prevents the scaling-up of the output power of the signal. In general, in fused silica, the frequency is shifted from the original frequency by ~13.2 THz (440 cm^{-1}) when it is pumped by the pump wavelength of 1.0 μm; this shift is slightly different depending on the composition of the fiber core. In cw and quasi-cw systems, the evolution of the Stokes wave is presented for simplicity as follows [72];

$$dI_S / dz = g_R I_P I_S \tag{2-37}$$

where I_S and I_P are the Stokes wave intensity and the pump intensity respectively. g_R is the Raman gain coefficient, which is related to the cross section of spontaneous Raman scattering. Spontaneous Raman scattering generated by the incident pump beam acts as a seed source and is amplified with propagation in the fiber within the bandwidth of the Raman gain spectrum $g_R(\Omega)$ (Ω represents the frequency difference between the pump and Stokes wave, which is slightly different depending on the material and the pump frequency). If the pump intensity reaches a certain threshold value, the Stokes wave is increased exponentially [72, 73].

In order to estimate Raman threshold, the interaction between the pump and Raman Stokes waves in the optical fiber is considered next. For simplicity, the two coupled wave equations are defined as

$$dI_S / dz = g_R I_P I_S - \alpha_S I_S \tag{2-38}$$

$$dI_P / dz = -\frac{\omega_P}{\omega_S} g_R I_P I_S - \alpha_P I_P . \tag{2-39}$$

where α_S and α_P indicate fiber losses at the Stokes and pump wavelength respectively. ω_S and ω_P are the frequencies of Stokes and pump beam respectively. Here, light is assumed to be cw or quasi-cw. In an ideal condition (no loss), the total number of photons in the pump and Stokes wave is constant through the fiber during SRS.

$$\frac{d}{dz}\left(\frac{I_S}{\omega_S} + \frac{I_P}{\omega_P}\right) = 0 \tag{2-40}$$

From equations (2-38) and (2-39), based on the assumption that there is no pump depletion, the analytical solution for the evolution of the Stokes wave can be obtained as follows:

$$dI_S / dz = g_R I_0 \exp(-\alpha_P z) I_S - \alpha_S I_S , \tag{2-41}$$

where I_0 is the incident pump intensity at $z = 0$. Equation (2-41) can be solved and thus, the Stokes wave evolution is presented as

$$I_S(L) = I_S(0)\exp(g_R I_0 L_{eff} - \alpha_S L), \tag{2-42}$$

here, L is the fiber length and effective length $L_{eff} = (1 - \exp(-\alpha_P L))/\alpha_P$, which is reduced due to the pump loss. $I_S(0)$ is the input intensity of the Stokes wave. SRS is initiated from spontaneous Raman scattering, as mentioned before, and thus, by estimating the power of the spontaneous Raman scattering, the input intensity of the Stokes wave can be determined. The spontaneous Raman scattering generates photons within the entire bandwidth of the Raman gain spectrum and its power is determined by the number of photons. The Raman power is defined as [72]

$$P_S(L) = P_{S0}^{eff}\ \exp(g_R I_0 L_{eff} - \alpha_S L), \tag{2-43}$$

where, the effective input power $P_{S0}^{eff} = h\omega_S B_{eff}$, where $B_{eff} = (\frac{2\pi}{I_0 L_{eff}})^{1/2} \left| \frac{\partial^2 g_R}{\partial \omega^2} \right|_{\omega=\omega_S}^{-1/2}$ is the effective bandwidth of the Stokes wave centred near the gain peak [72]. Although B_{eff} depends on the pump intensity and the fiber length, the spectral width of the dominant peak provides an order-of-magnitude estimate for it.

Raman threshold is usually defined as the input pump power at which the Stokes power becomes equal to the pump power at the fiber output [72].

$$P_S(L) = P_P(L) \equiv P_0\ \exp(-\alpha_P L). \tag{2-44}$$

From equations (2-43) and (2-44), if the assumption $\alpha_P \approx \alpha_S$ should be valid, the Raman threshold condition can be represented as follows

$$P_{S0}^{eff}\ \exp(g_R P_0 L_{eff}\ /\ A_{eff}) = P_0, \tag{2-45}$$

where $P_0 = I_0 A_{eff}$ is the input pump power and A_{eff} is the effective area of the core. Assuming a Lorenzian shape for the Raman gain spectrum, the critical pump power satisfying equation (2-45) is approximately given by

$$\frac{g_R P_0^{cr} L_{eff}}{A_{eff}} \approx 16 \qquad (2\text{-}46)$$

In practice, if polarization is not preserved, the Raman threshold is increased by a factor of ~2.

The solution, equation (2-46) for the Raman threshold, is so simplified that it cannot be applied to many real cases. For example, in an amplifier system, the rare-earth doped fiber act as a gain medium for a signal. The signal power (or intensity) is increased throughout the fiber. When the signal power reached to a critical power at a certain position in the fiber, SRS can be generated and the signal power is degraded. On the other hand, if the signal power is degraded by the Raman conversion, the Raman is also decreased because of the depletion of the signal. Considering this effect, it is difficult to define the Raman threshold. Moreover, it is important to find how much fraction of the Raman conversion makes a significant effect on the signal in order to determine the Raman threshold in the laser/amplifier system.

The discussion of all of these will be presented in Chapter 6, where the evolution of the signal and Stokes wave in a real amplifier system will be numerically investigated. From this, the Raman threshold will be re-considered and the fiber structure for suppression of SRS in a high power fiber source will be suggested.

PART II.

STEP HOLLOW OPTICAL FIBERS

Chapter 3. Er:Yb co-doped step hollow optical fiber

3-1. Waveguide property of step HOFs

3-1-1. Effective index in step HOFs

A step hollow optical fiber consists of air surrounding the raised index core and a silica cladding as shown in figure 3-1.

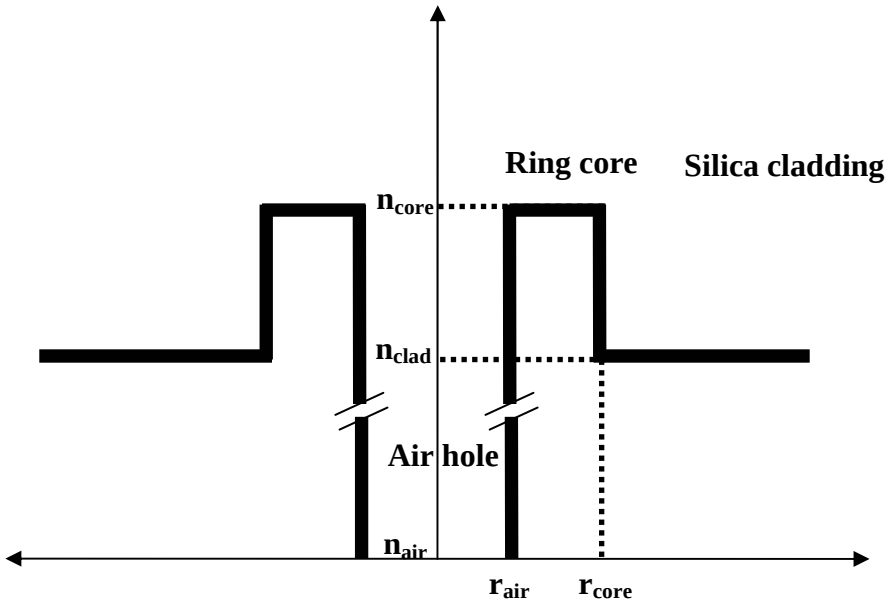

Figure 3-1. The schematic diagram of a step HOF

The numerical analysis of HOFs should be done by a full vectorial calculation rather than a weakly guiding assumption because of the large index difference between an air hole and ring core. However, as far as mode cut-off was concerned, the linearly-

polarized, weakly guiding approximation is still valid. To confirm this, the results using the LP mode assumption and commercial software (Femlab) that uses a full vectorial simulation were compared. The error in the calculated effective indices of modes was within 1% in most cases. Therefore, in this thesis, the weakly guiding approximation and the linearly polarized (*LP*) modes were considered for simplicity. This assumption will also be applied to the numerical approach to the modal properties of the DCHOF, which will be discussed in later chapters.

The refractive indices of the core, cladding and the air-hole sections are n_{core}, n_{clad} (=1.457 or 1.45) and n_{air} (=1) respectively, and the air-hole, the core and the cladding radii are r_{air}, r_{core} and r_{clad} respectively. Here, the core thickness (t) is defined as $t = r_{core} - r_{air}$. The electric field component of guided modes is defined as $E(r,\phi,z) = e(r)\exp(-jl\phi)\exp(-j\beta z)$, l =0, ±1, ±2, … where r,ϕ are the radial and tangential co-ordinates in the plane perpendicular to the fiber axis and z is the length axis of the fiber. $e(r)$ is an eigensolution of the Helmholtz equation, which means the radial dependence of the electric field component. It can be written as follows [33];

$$e(r) = \begin{cases} AI_l(vr) & r < r_{air} \\ BJ_l(ur) + CY_l(ur) & r_{air} \le r \le r_{core} \\ DK_l(wr) & r > r_{core} \end{cases} . \qquad (3\text{-}1)$$

Here, r is the radial position and A, B, C *and* D are constants. I_l (K_l) is the l th order modified Bessel function of the first (second) kind and J_l (Y_l) is the l th order Bessel function of the first (second) kind. v, u and w are the mode parameters and they are defined as $v = \sqrt{\beta^2 - {n_{air}}^2 {k_0}^2}$, $u = \sqrt{{n_{core}}^2 {k_0}^2 - \beta^2}$ and $w = \sqrt{\beta^2 - {n_{clad}}^2 {k_0}^2}$. Here, the

eigenvalue of β is the propagation constant of each mode and k_0 is the wave number. By applying the continuity of electric field at two boundaries $r = r_{air}$ and r_{core}, the following 4x4 matrix type characteristic equation can be obtained [33, 74].

$$\begin{vmatrix} I_l(vr_{air}) & -J_l(ur_{air}) & -Y_l(ur_{air}) & 0 \\ vI_l'(vr_{air}) & -uJ_l'(ur_{air}) & -uY_l'(ur_{air}) & 0 \\ 0 & J_l(ur_{core}) & Y_l(ur_{core}) & -K_l(wr_{core}) \\ 0 & uJ_l'(ur_{core}) & uY_l'(ur_{core}) & -wK_l'(wr_{core}) \end{vmatrix} = 0 \qquad (3\text{-}2)$$

The propagation constant (β) can be obtained from equation (3-2) numerically and for each azimuthal index l, the characteristic equation has multiple solutions yielding discrete propagation constants β_{lm} (m =1, 2,…), which represents a guided mode. The transverse field distribution of each mode can be computed from equation (3-1) after determining the constants $A, B, C \text{ and } D$ from the achieved propagation constant (β) value.

This thesis primarily targets the HOF as a distributed fiber waveguide filter for high power fiber laser sources operating at short wavelengths. Therefore, calculating fiber parameters for the fundamental mode cut-off are the main objective. In order to obtain the fundamental mode cut-off wavelength, the propagation constant of the LP_{01} mode at several core thicknesses was calculated depending on wavelength and then it was converted to the effective index, which is defined as $n_{eff} = \beta / k_0$. Figure 3-2 shows the variation of the effective indices of the LP_{01} mode depending on core thickness and wavelength at a fixed NA_{co} (NA_{co} = 0.09, $NA_{co} = \sqrt{{n_{co}}^2 - {n_{clad}}^2}$) and hole diameter of 4 μm. Here, the refractive index of silica at 1.0 μm was 1.4571. In general, the modal cut-off takes place when the effective index of the guided mode becomes equal to the silica

cladding index. After cut-off wavelength, the mode does not guide through the core any more. In figure 3-2, it is noted that HOF shows a fundamental (LP_{01}) mode cut-off wavelength where the effective index (n_{eff}) of the LP_{01} mode becomes equal to the silica cladding index (n_{clad}). Beyond this wavelength, the fundamental mode does not exist in the core. This property is similar to that of W-type fiber, which exhibits the waveguide filter characteristics [75]. The appearance of the fundamental mode cut-off in a HOF is due to the negative value of the volume integration of relative refractive index in a hollow structure (because of its central air hole section) [76]. However, in the HOF, the decay rate of effective index was not steep at the LP_{01} mode cut-off range, which is detrimental to obtaining sharp filtering characteristics. This is also verified in figure 3-3.

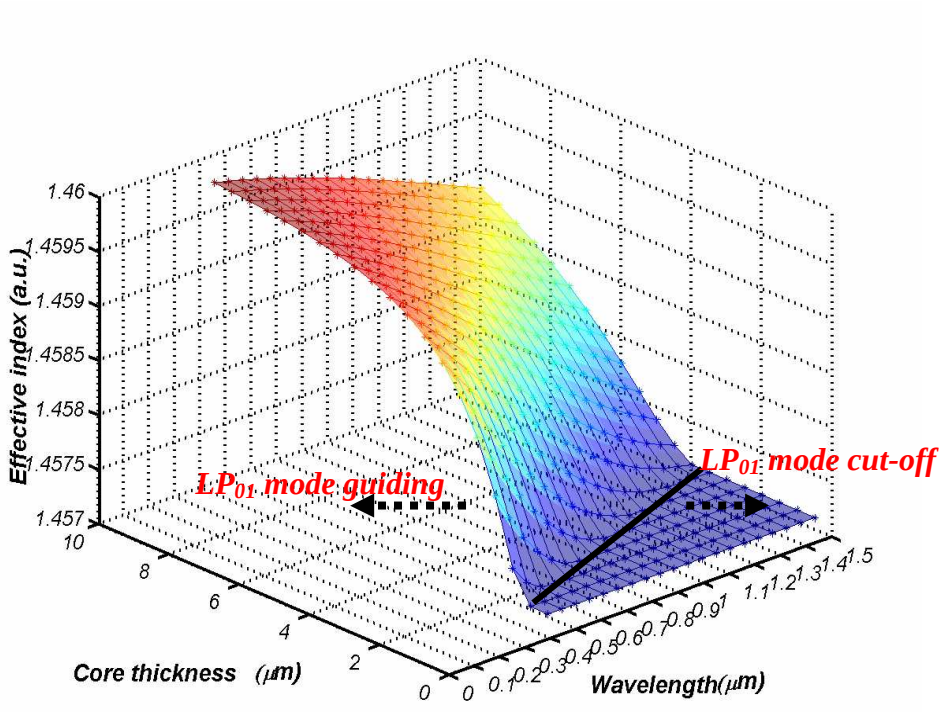

Figure 3-2. The variations of effective indices depending on the wavelength and the core thickness (calculated at a fixed NA of 0.09 and hole size of 4 μm diameter)

In the HOF, the air hole effects the modal characteristics. In figure 3-3, the effective index changes of LP_{01} and LP_{11} mode were calculated at a fixed core thickness of

4μm and the core NA of 0.09. Here, the refractive index of silica cladding was 1.45. The cut-off wavelength of the LP_{01} mode was not significantly changed in all three cases as shown in figure 3-3, which indicates that the dependence on the air hole size in the cut-off wavelength of the LP_{01} mode is small. However, the effective indices of the LP_{01} mode at shorter wavelengths were different, depending on the hole size, which in fact will affect the modal properties of bending loss of HOF. For example, the low effective index of LP_{01} at a given wavelength could be detrimental to the bending performances of the LP_{01} mode in the fiber. In terms of the fiber waveguide filter, the bending loss is highly related to the sharpness of the filter and it will be described in the following section 3-1-3.

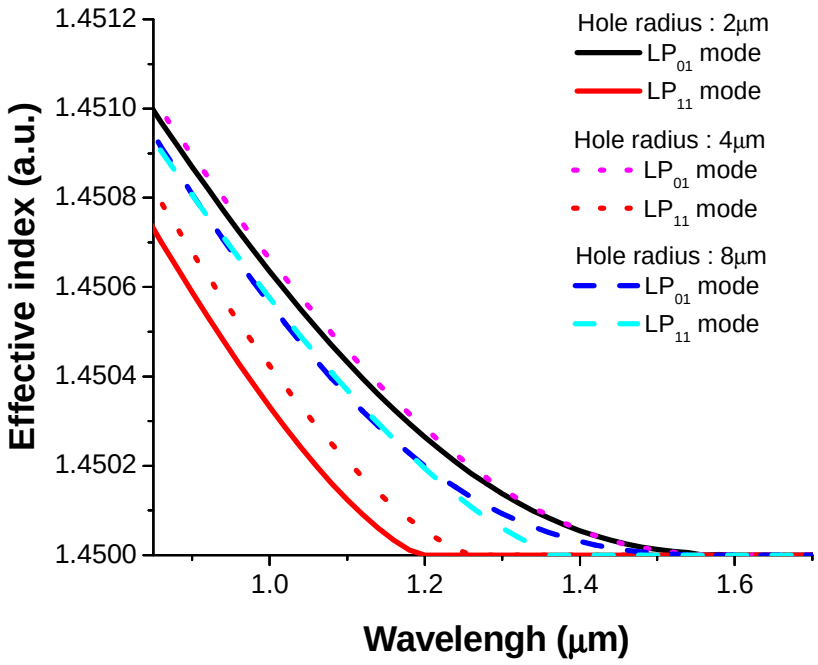

Figure 3-3. Effective index changes of fibers with different hole size as a function of wavelength (solid line : 2 μm hole radius, dot line : 4 μm hole radius and dashed line : 8 μm hole radius).

For the higher order mode, LP_{11}, the cut-off wavelength shifted to longer wavelength side when the hole size is increased. In the case of HOF with the hole radius of 8 μm, the effective index of the LP_{11} mode significantly close to that of the LP_{01} mode,

which means that the fiber with the larger hole size can easily be multimoded and it is difficult to separate the higher order modes from the fundamental (LP_{01}) mode. Therefore, for the gain medium, if the hole size becomes bigger, the core area can be relatively increased and this improves the pump absorption in cladding pump configuration, while the single-mode operation at a desired wavelength will become more challenging.

3-1-2. Modal field distribution in step HOFs

The propagation constants (β) and the parameters v, u *and* w are calculated from the characteristic equation (3-2). Also, by applying the boundary conditions (field continuity at $r = r_{air}$ and r_{core}), the constants A, B, C *and* D can be calculated numerically from equation (3-1). After obtaining all these parameters, the modal field distribution of LP modes supported by the ring-core can be obtained.

Figure 3-4 shows the modal field distributions of different modes (LP_{01}, LP_{11}, LP_{21} and LP_{31}) in a HOF with a 5 μm hole radius and a 3 μm core thickness. In order to see other higher order modes, the core index was increased to NA_{co} = 0.19 ($\Delta n \sim 0.012$) and the wavelength was considered as 1.55 μm. The modal field distribution of the LP_{01} mode was doughnut-shaped and the optical field is well confined in the ring-core as shown in figure 3-4 (a). However, the field component in the central air region is very weak, while it is relatively strong in the ring core and the field is broadened from the ring-core to the silica cladding, which causes the increase of the mode field diameter (MFD). The higher order mode fields are also formed in the ring core, whose cut-off characteristics are significantly dependent on the hole size as mentioned in the previous section 3-1-1.

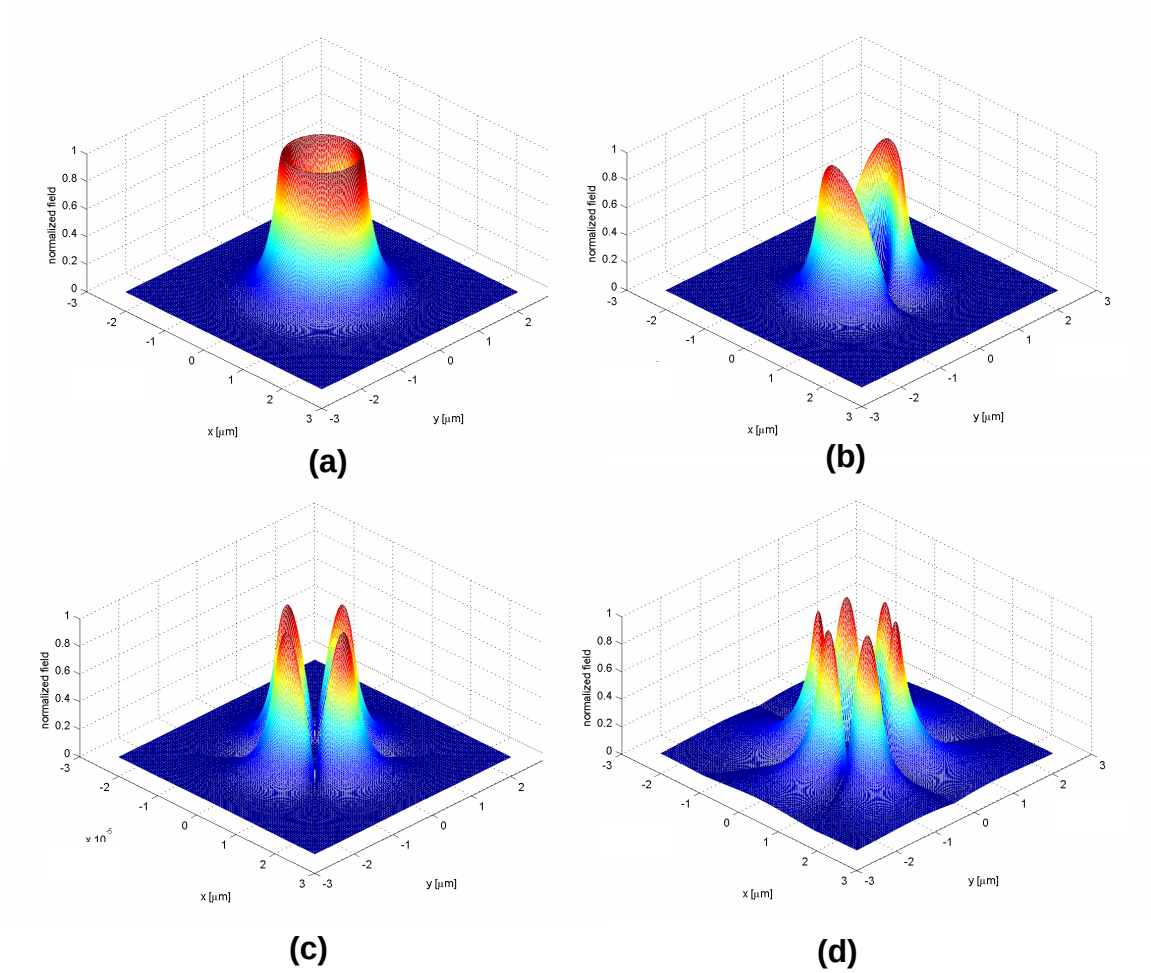

Figure 3-4. Modal field distribution of HOFs; Wavelength : 1.55 μm, Hole Radius : 5 μm, core thickness : 3μm, NA_{co} : 0.19, (a) LP_{01}, (b) LP_{11}, (c) LP_{21}, (d) LP_{31}

For a fiber laser, the mode confinement factor (overlap factor with a doped core) of the signal is one of the important parameters, because the signal gain linearly increases depending on the mode confinement factor [77, 78]. When the effective index (n_{eff}) is close to the refractive index (n_{clad}) of the silica cladding, the modal parameter u is increases and w decreases, and the field penetrates deeper into the silica cladding. In figure 3-5, the normalized radial field distributions of the LP_{01} mode were calculated at several core thicknesses. Here, the core NA_{co} of 0.19 and hole radius of 5 μm was fixed. With the smaller core thickness (e.g. see the normalized field in the case of 2 μm core thickness in figure 5-5) as the wavelength of the light approaches the fundamental mode cut-off of the fiber, the modal confinement factor is significantly reduced and the field

gets broad. Beyond the fundamental mode cut-off where $n_{eff} = n_{clad}$, the modal field does not exist in the ring-core any more. This makes the HOF suitable for a distributed wavelength filter.

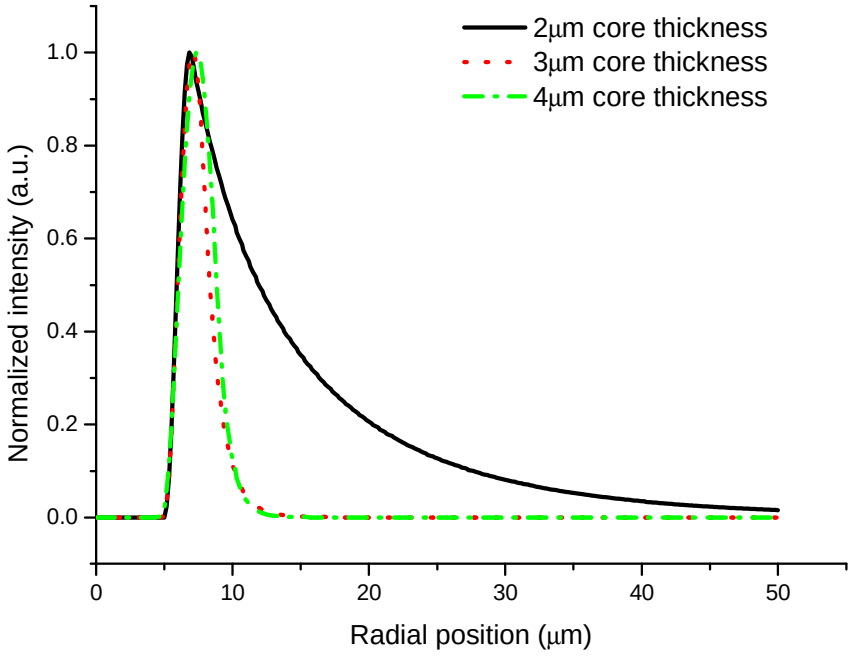

Figure 3-5. Radial intensity distribution of LP_{01} mode in HOFs; Wavelength : 1.55 μm, Hole Radius : 5 μm, NA_{co} : 0.19.

3-1-3. Numerical approach to the bending loss of step HOFs

Bending loss in the fiber is one of the important issues for high power fiber laser sources. A high bending loss at the signal wavelength degrades amplifier performance by reducing the gain. In addition, for compact devices, a bend-resistant fiber is may be needed. In a cladding-pumped configuration, the signal that escapes from the core caused by bending can become a noise source which may cause cladding mode lasing or amplified stimulated emission (ASE) noise due to mode-mixing or mode-coupling between the fundamental mode and other higher modes.

In order to study the bending loss property of HOFs, the uniform bending loss ($\alpha_{bending}$) formula for an arbitrary index profile single mode fiber derived by Sakai and Kimura [81] is used.

$$\alpha_{bending} = \frac{\sqrt{\pi} A_{cl}^2 \exp\left\{-\frac{\sqrt{2}}{3}\frac{\lambda^2 R}{\pi^2 n_{core}^2 W_\infty^3}\right\}}{2P_t\left\{\frac{\sqrt{2}}{W_\infty}\right\}^{3/2}\left\{R+\frac{2\pi^2 n_{core}^2 W_\infty^2 r_{core}}{\lambda^2}\right\}^{1/2}} \tag{3-3}$$

where R is bending radius, n_{core} is the refractive index of the core, r_{core} is the core radius, λ is the operating wavelength. W_∞ is the new mode field radius representing the bend sensitivity. This is defined by the propagation constant β of the LP_{01} mode and the wavenumber in the cladding k_{clad} as follows [119];

$$W_\infty^2 = \frac{2}{\beta^2 - k_{clad}^2} \tag{3-4}$$

The bend sensitivity is determined by the propagation constant (β), which is varied by the core size, refractive index difference between core and cladding, and the wavelength. When β approaches the wavenumber in the cladding k_{clad}, the bend sensitivity is significantly increased. It means that the index difference between effective core index (n_{eff}) and silica cladding is related to the bending loss. The smaller it is, the higher the bending loss becomes [80]. In equation (3-3), A_{cl}^2 / P_t is another important parameter, which represents the normalized field intensity coefficient in the cladding region. This parameter can be obtained from the following relations;

$$e(r) = A_{cl} K_0\left(\frac{\sqrt{2}}{W_\infty} r\right), \qquad r > r_{core} \tag{3-5}$$

$$P_t = \int_0^{\infty} e^2(r) r dr \tag{3-6}$$

where $e(r)$ is the radial field function in the cladding, A_{cl} is the coefficient of the field function, and K_0 is the modified Bessel function of the first order. P_t is the integrated field intensity, which is determined by the radial field distribution $e(r)$ in the cladding.

For the distributed wavelength waveguide filter, the bend sensitivity is very high around the fundamental mode cut-off wavelength range, because the effective index (n_{eff}) of the fundamental mode is close to the refractive index of the silica cladding (n_{clad}). In the case of a HOF, the bending loss is significantly increased just before reaching the fundamental mode cut-off wavelength, while the bending loss is maintained at a low value far from the fundamental mode cut-off wavelength to the shorter wavelength side. Although the fundamental mode cut-off in the HOF is well-defined in theory ($n_{eff} = n_{clad}$), the mode cut-off wavelength is difficult to define in a real case because of the very high bend-sensitivity near the theoretical fundamental mode cut-off wavelength.

The bending loss and effective indices as a function of the wavelength were calculated in the HOF at several bending radii using equations (3-3)-(3-6) based on the J Sakai paper [81]. The calculated result is presented in figure 3-6. Here, the HOF is composed of the 4 μm core thickness, 5 μm hole radius, and 0.09 NA_{co}. The theoretical fundamental mode cut-off wavelength was 1.53 μm. At this wavelength, the bending loss of the LP_{01} mode is significantly high (>500 dB/m), which indicates that the light cannot be confined any more in the ring-core. Further coiling causes huge bending loss at the shorter wavelength side and it effectively makes the fundamental mode cut-off wavelength shift to shorter wavelengths. In practice, the induced loss of 5 dB/m (~70% loss of the power per unit length) is large enough for the fiber to be considered as ‘non-guiding’ [82].

Based on this, the fundamental mode cut-off wavelength can be defined practically, which is called as the effective fundamental mode cut-off wavelength. In figure 3-6, the effective fundamental mode cut-off wavelength is 1.2 μm, when the fiber was coiled with a bending radius of 20 cm and it is shifted to the shorter wavelength by bending, 1.13 μm for a bending radius of 10 cm and 1.05 μm for a bending radius of 5 cm. A significant discrepancy exists between the effective and theoretical fundamental mode cut-off wavelength. As presented in figure 3-6, the wavelength space between the theoretical and the effective fundamental mode cut-off is ~ 0.3 μm for 20 cm bending radius, which is, in fact, too broad. This should be considered when the fiber waveguide is designed.

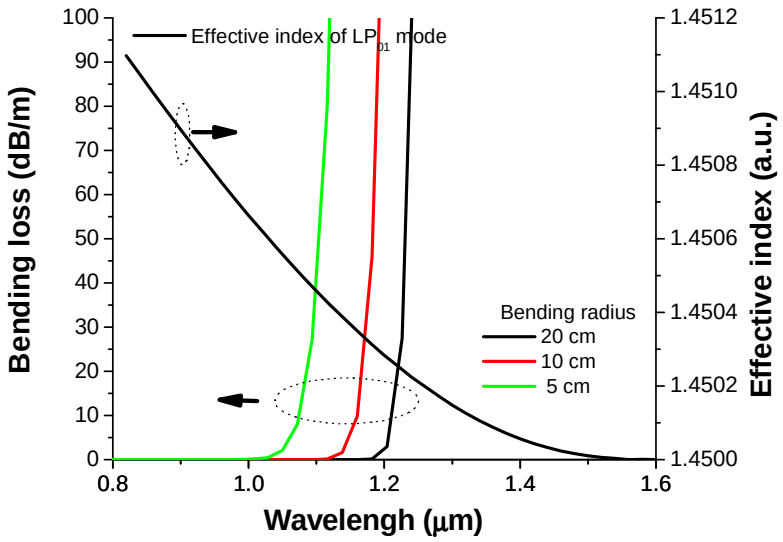

Figure 3-6. Bending loss at different bending radii (20 cm, 10 cm and 5 cm) and effective indices of LP_{01} mode

For fiber lasers, the bending loss at unwanted wavelengths should be high, while it should be maintained at a low value at the operating wavelength. For example, in figure 3-6, the operating wavelength for the fiber laser should be less than 1 μm at a bending radius of 5 cm, where the bending loss in the fiber is maintained at a low value. Over 1 μm, the bending loss is too high to be used as a fiber laser.

3-2. Experimental investigation of Er:Yb co-doped step HOFs

3-2-1. Fundamental mode cut-off characteristics of Er:Yb co-doped step HOFs

The preform for Er:Yb co-doped step HOFs (LF202) was fabricated using the standard MCVD technique and solution doping technique. During HOF preform fabrication process, a hole was left at the final collapsing stage of the preform. It was then drawn into fibers having different outer diameters (ODs). Each fiber was coated with a high refractive index polymer (DSM314 : n~1.46). Depending on ODs, the core thickness and hole size is changed. Table 3-1 summarizes the fiber dimensions for each fiber and figure 3-7 shows the optical microscope image of a fabricated HOF. These fibers have a relatively large air hole. Due to this, higher order modes can be easily excited as mentioned in the previous section 3-1-1. This was verified in the numerical simulation, as shown in figure 3-8. All fibers have a very narrow single mode range, which makes it difficult to obtain single mode operation at the desired wavelength.

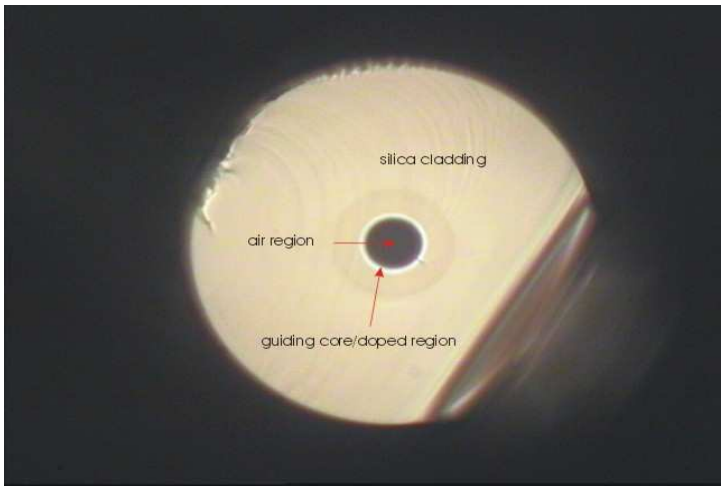

Figure 3-7. Cross sectional image of fabricated Er:Yb-doped step HOFs (F512-LF202)

Table 3-1. The index structure of fabricated Er:Yb co-doped step HOFs

Er/Yb codoped HOF	Outer diameter (μm)	Hole diameter (μm)	Core thickness (μm)	Δn (NA)
F512_LF202_1	125	10.5	1.9	0.012 (0.19)
F512_LF202_2	110	9.2	1.7	0.012 (0.19)
F512_LF202_3	85	7.1	1.3	0.012 (0.19)

Figure 3-8 presents the changes of effective indices of three different modes (LP_{01}, LP_{11}, and LP_{21}) as a function of the wavelength for different HOFs as listed in table 3-1. It is observed that for a fixed NA, depending on the core thickness, the LP_{01} mode cut-off wavelength changes significantly. Moreover, such fibers were multi-moded at most wavelengths, where light can be guided. The wavelength range for single mode guidance is not clearly seen, as presented in figures (a) - (c) and the higher order (LP_{11}) mode is still maintained around the LP_{01} mode cut-off wavelength. According to these calculations, the higher order (LP_{11}) mode can be fundamentally guided in these HOFs, which have a relatively large hole size. In order to produce single mode output beam quality in a fiber-based laser system, it is preferred that the core structure supports only the fundamental mode at a laser operating wavelength. In terms of this, it is difficult to generate a single mode output in a HOF. In the HOF, the dominant factor for determining a single mode operation at desired wavelengths, is the hole size as mentioned in the previous section 3-1-1 and a small hole size will be preferred for a robust single mode output.

In figure 3-8, the separation between LP_{01} mode and LP_{11} mode cut-off wavelength is too narrow to separate them and their cut-off wavelengths are located very closely. In this case, it is difficult to define where the fundamental mode cut-off is. However, it is very clear that both LP_{01} and LP_{11} mode are cut-off from the ring-core of the HOF, and it produces the filtering characteristic in the HOF. In order to prove this cut-off filtering in HOFs, white light (400 nm-1700 nm) was transmitted through the fiber and the transmission spectrum was monitored using an optical spectrum analyzer (OSA).

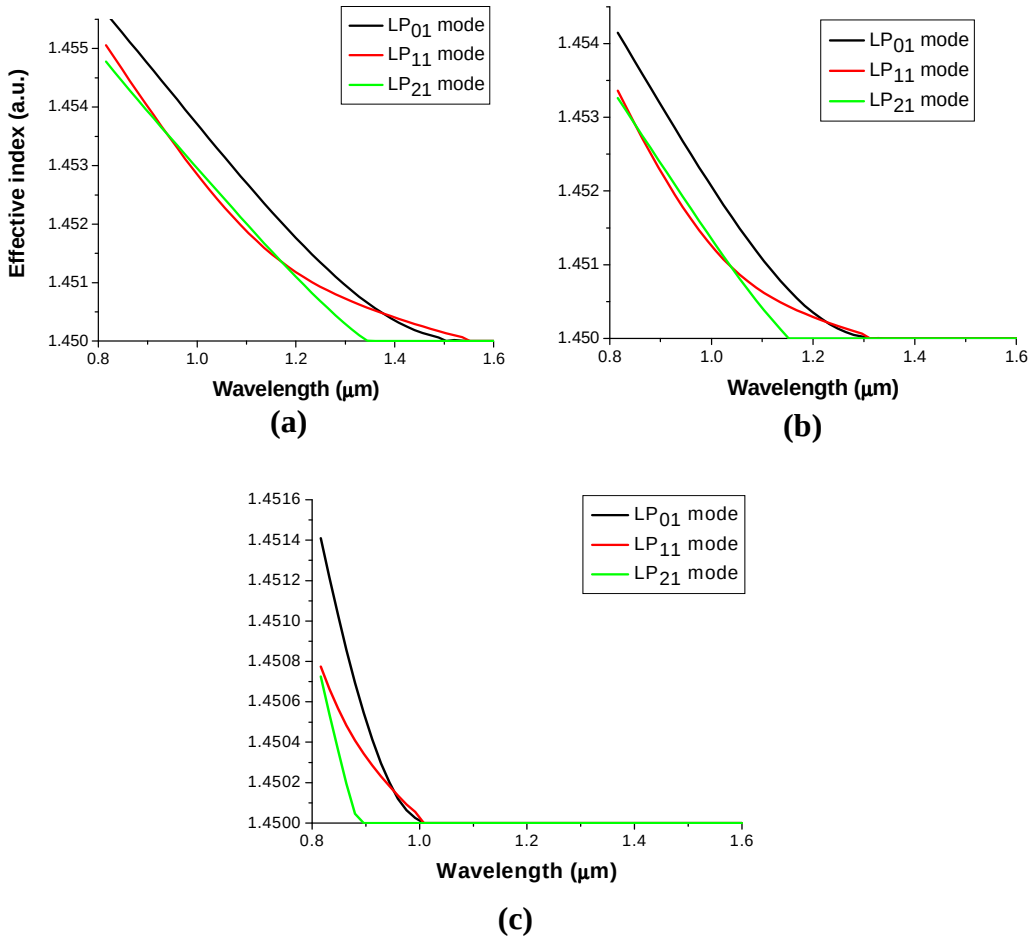

Figure 3-8. The changes of effective indices of fabricated fibers. (a) OD 125 μm, (b) OD 110 μm, (c) OD 85 μm.

Figure 3-9 shows the experimental transmission characteristics of such fibers. The modal cut-off wavelengths were checked by bending the fibers at different curvatures. Generally, the modal loss occurred beyond the cut-off wavelength of the mode. This is called a modal leakage loss, and it can be shifted to the shorter wavelengths by bending the fiber. In practice, the fundamental mode contains the highest portion of the power compared to the other modes and its cut-off generates a significant propagation loss, which can be measured in the simple white-light transmission measurement. Figure 3-9 exhibits the white light transmission spectra through the fabricated step HOFs presented at table 3-1.

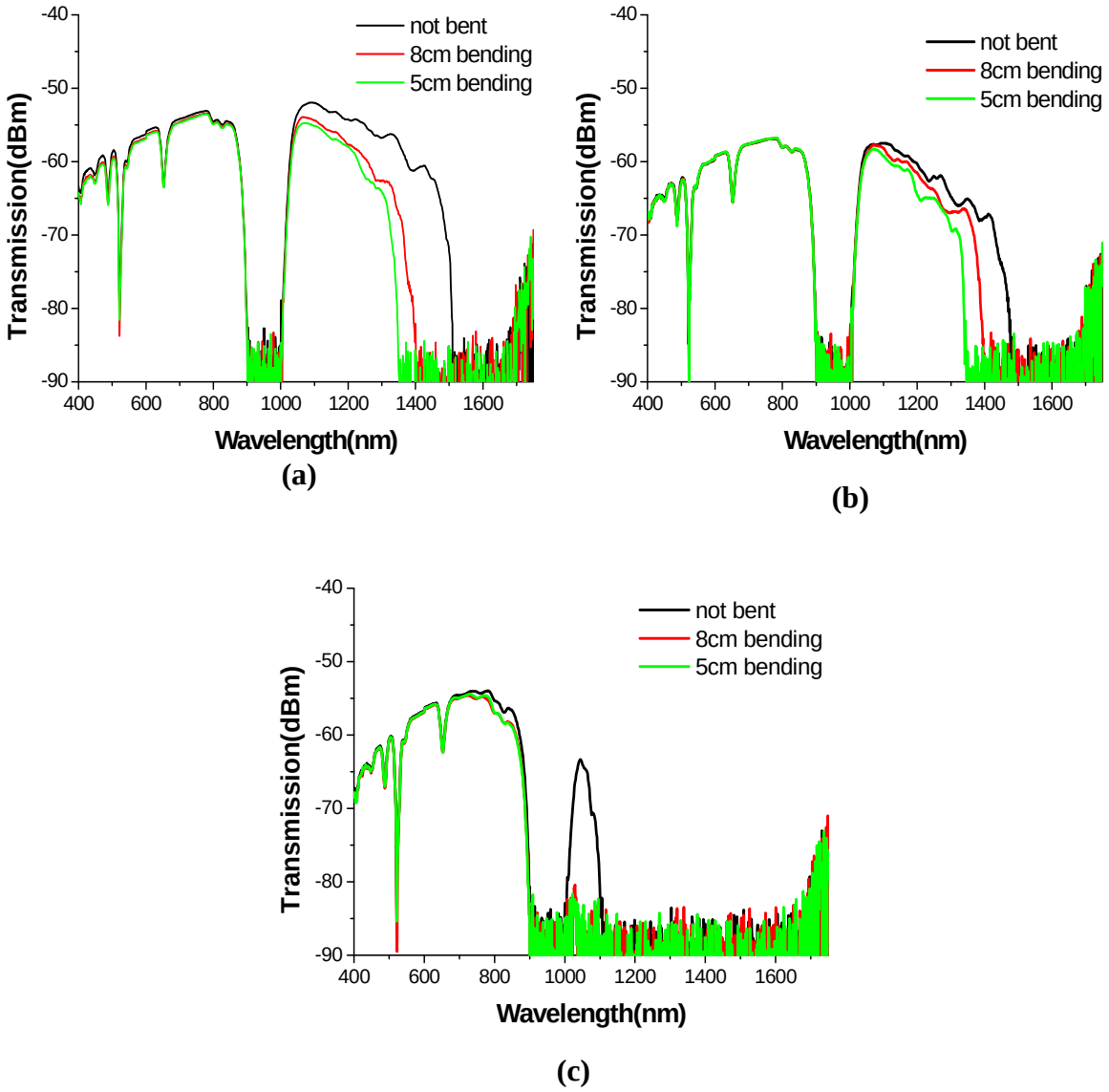

Figure 3-9. Transmission spectra of Er:Yb co-doped step HOFs (a) OD 125 μm, (b) OD 110 μm, and (c) OD 85 μm.

In figure 3-9, HOFs clearly exhibit the fundamental mode cut-off, which depends on the core thickness of such fibers. The fiber with OD of 125 μm has the fundamental mode cut-off at ~1500 nm and when the OD was reduced to 110 μm and 85 μm, the fundamental mode cut-off wavelength shifted to the shorter wavelength, ~1480 nm and ~1100 nm respectively. After the fundamental mode cut-off wavelength, light is not

confined anymore in the core. In addition, coiling of the fiber makes the fundamental mode cut-off wavelength shift to the shorter wavelength side. This property of the HOF indicates that it could be used for a distributed wavelength filter. This is a similar kind of behaviour as observed in the W-type fiber structure [37]. Such characteristics of HOF could be useful to realise fiber lasers and amplifiers at shorter wavelength, for example, a 930 nm laser from a Nd-doped fiber by suppressing the four-level transition at 1060 nm, an S-band amplifier/laser from an Er-doped fiber by suppressing the distributed ASE in the C-band. In addition, if the hole size is properly controlled, the single mode operation wavelength range in the HOF can also be increased.

3-2-2. Er:Yb co-doped step HOF laser operating at 1544 nm

HOF has advantages over conventional solid core fiber in laser applications, such as a relatively larger effective core area due to the ring-core structure. As a result, high pump absorption is possible in a double-clad configuration, and thus allows the use of short fibers with reduced nonlinear effects. Therefore, such a structure could be useful for power scaling from fiber lasers. In the following section, the lasing performance of cladding pumped Er:Yb co-doped HOF (EYDHOF) in the 1550 nm spectral region is presented.

Laser operation in the eye safe 1550 nm region from Er is important for many applications such as remote sensing and satellite optical communication, range finding, spectroscopy, and high capacity optical communications. Sensitising Er doped fiber with Yb is a well-known technique to broaden the pump absorption band. In addition, the pump absorption in Er:Yb co-doped fiber (EYDF) increases by an order of magnitude compared to Yb free Er doped fiber, and thus makes it attractive to construct a high power fiber laser in the 1550 nm band. In fact, an Er:Yb co-doped fiber laser (EYDFL) with an output power

of greater than 100 W has been reported recently [86]. However, significant Yb co-lasing at 1060 nm was observed at high pump powers, which in fact degrades the 1550 nm output performance. In an Er:Yb system, the Er ions are pumped indirectly via energy transfer from Yb ions. As the pump power increases, more and more Yb ions are excited, and at some point the Yb-excitation reaches a level where it starts to lase at 1060 nm, and finally the energy transfer between Yb and Er ions becomes 'bottle-necked'. Therefore, in order to improve the performance of EYDF at high pump powers, it is important to control either the fiber geometry or the composition that will suppress the Yb co-lasing at 1060 nm. For example, a phosphosilicate host is now considered to be the best for efficient energy transfer from Yb to Er by preventing the backflow of energy, and thus increasing the Yb co-lasing threshold [87]. However, the effect of fiber geometry for efficient operation of the Er:Yb system has not been fully explored. Here, the performance of a cladding pumped EYDHOF laser for operation in the 1550 nm band is presented.

For the fiber laser in the 1550 nm range, the Er:Yb co-doped preform, which was same as that used in the previous section 3-2-1, was employed. Additionally, in order to improve the pump absorption in a cladding-pumped configuration, the preform was milled to make a D-shaped and, as a result, the preform had a diameter of 12.2/11 mm along the long/short axes. Fibers were then drawn from the preform with different ODs: 125 μm (F507-LF202-1), 150 μm (F507-LF202-2) and 250 μm (F504-LF202) respectively. They were coated with a low index polymer outer cladding, which provided a nominal inner-cladding NA of 0.48 for the cladding-pumped configuration. Here, fiber diameters (based on the long-axis) were larger than that used in the previous section, 3-2-1, because the fiber with small OD does not allow the guidance of the signal at 1550 nm, as shown in figure 3-8, due to the loss caused by the fundamental mode cut-off. The dimensions of each fiber were shown in table 3-2.

Table 3-2. Fiber parameters and calculated guided mode number in the core layer

Fiber diameter (μm)	Core thickness (μm)	Hole diameter (μm)	Mode number* (@1550nm)
125	~2.0	11	2
150	~2.4	12	3
250	~3.2	27	8

* calculated guided mode number

The guided fundamental mode in HOF is ring-shaped and the higher order modes, such as LP_{02}, LP_{03} etc, can easily be suppressed depending on the core thickness. However, the other higher order modes such as LP_{11} and LP_{21}, can be supported and excited easily in the hollow structure. According to the modal analysis, the current fibers are multi-moded. This is due to the large hole size and the high NA in the fiber. The calculated guided mode numbers at 1550 nm for three different fibers (125, 150, and 250 μm fibers) are 2, 3 and 8 respectively. Although the current fibers are multi-moded, single-mode operation is possible by controlling the NA, hole size and the core thickness in the fiber.

The laser configuration is shown in figure 3-10. It consists of a 6 m long double clad EYDHOF (bending radius : 20 cm), pumped by a 915 nm (or 975 nm) fiber-coupled multimode laser diode through a combination of collimating lenses, such that as much as 80% of the pump could be launched into the fiber. The laser cavity was formed between perpendicularly cleaved end facets of the fiber (4% Fresnel reflections). Two types of dichroic mirrors (as shown in figure 3-10) were used in the set up; one for separating the pump from the signals (high reflectivity @ 915-980 nm and high transmission both @ 1060 and 1550 nm), and the other one for separating the Er signal from the Yb signal (high reflectivity @ 1060 nm and high transmission @ 1550 nm). The small-signal absorption at the pump wavelength (915 nm) was ~ 1dB/m.

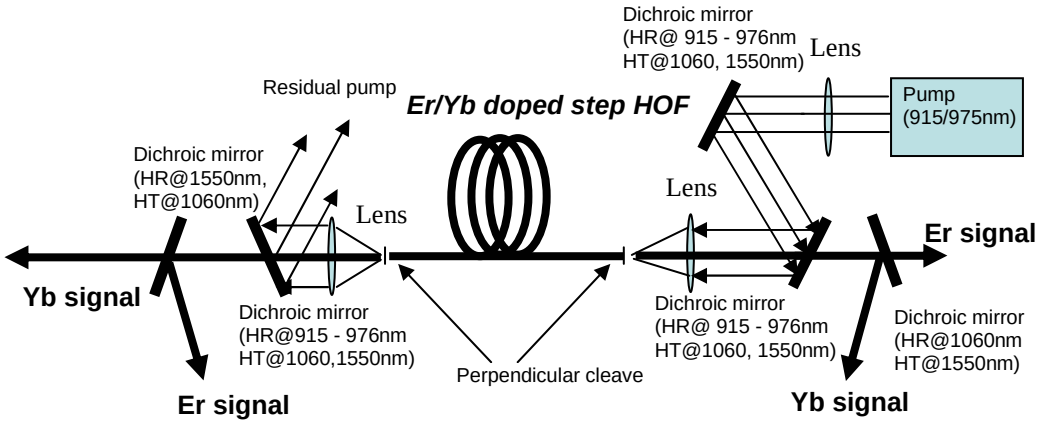

Figure 3-10. The laser arrangement for Er/Yb co-doped HOF. HR: high reflectivity, HT: high transmission

Figure 3-11 shows the laser output characteristics. The lasing wavelength was 1535 nm in the case of both the 125 and 150 μm diameter fibers and 1544 nm for 250 μm fiber. The slope efficiency (η) improved significantly with increasing fiber diameter, and it was 8%, 10% and 25% respectively (with respect to launched pump power) for 125, 150 and 250 μm fibers. The smaller core thickness fibers showed relatively low slope efficiencies because the loss at the signal (~1550 nm) is increased and the induced modal loss is caused by the fundamental mode cut-off. As shown in figure 3-9 in the previous section 3-2-1, the fundamental mode cut-off wavelength of the fiber with 125 μm cladding diameter was measured, which was ~1570 nm when the fiber was not bent. The leakage loss of the fundamental mode start to occur from ~1400 nm and increases rapidly as the wavelength increases. This reduces the gain at the signal wavelength (1544 nm). Otherwise, the light at 1060 nm is well-guided and has a relatively low loss. As the pump power increases, the Yb gain at 1060 nm is growing enough to overcome the total cavity loss and co-lasing at 1060 nm is occurring. Furthermore, according to the bending loss calculation in the previous section 3-1-3, the induced bending loss near the fundamental mode cut-off wavelength, is very significant. In the laser configuration, the 6 m fiber length was used and it is not

practically possible to keep the fiber straight the fiber in order to reduce bending loss. Hence, it might also cause the significant bending loss at the signal wavelength (~1544 nm) at a relatively large bending radius (~20 cm) and degrade the efficiency contributed by Er-ions.

On the other hand, as the diameter increased the Yb co-lasing at 1060 nm became less and less pronounced because the loss at 1550 nm is significantly reduced and the energy transition between Yb and Er becomes more effective. In fact, for 250 μm diameter fiber we did not observe any 1060 nm lasing at the maximum pump power.

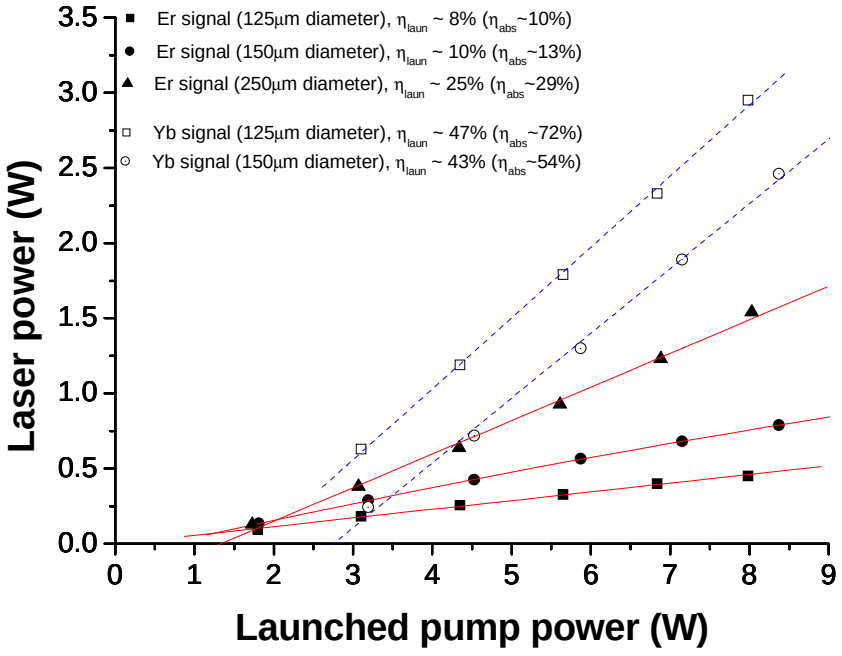

Figure 3-11. Laser output characteristics of Er/Yb co-doped HOF both at ~1.55 μm and 1.0 μm depending on the fiber diameter, η_{laun} : slope efficiency with respect to the launched pump power, η_{abs} : slope efficiency with respect to the absorbed pump power.

Figure 3-12 shows the laser thresholds, both at Er and Yb wavelengths, as a function of the fiber diameter. The Yb threshold at 1060 nm was increasing rapidly as fiber diameter increased. The laser performance of 250 μm diameter fiber was also measured using a 975 nm pump source with a similar fiber laser setup, as shown in figure 3-13. The

3 m fiber length was used. 2.5 W of output power at 1544 nm was obtained when 12.6 W of pump was launched, with a 26% slope efficiency with respect to the launched power (29% with respect to the absorbed pump power), as shown in figure 3-11. No indications of Yb-lasing even at maximum output power were observed.

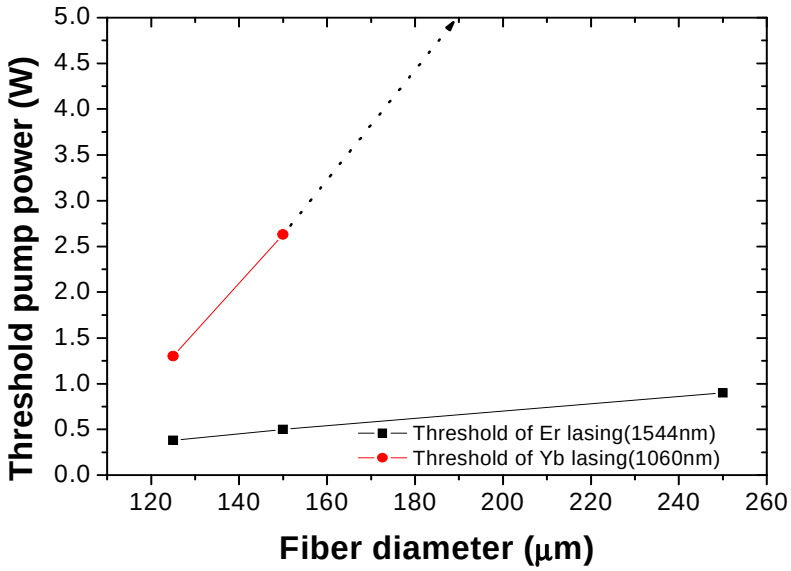

Figure 3-12. The laser threshold as a function of the fiber diameter.

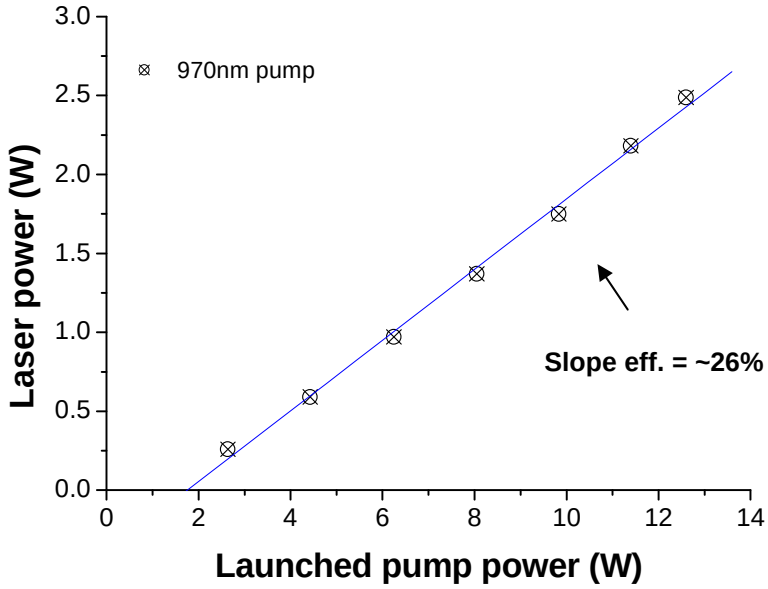

Figure 3-13. Laser output characteristics of 250μm diameter Er:Yb doped HOF when pumped by 970 nm laser diode.

The differences between the Yb and Er threshold, and its dependence on fiber diameter, can be attributed to the differences in signal overlap factors (Γ_s) and the leakage loss as mentioned before between the larger and the smaller core thickness (t_{core}) fibers. Here, the signal overlap factor is defined as a fraction of a modal intensity in the doped-core. Normally, the intensity distribution in a fiber at longer wavelength is broader than that at the shorter wavelength. In the case of EYDHOFs, the overlap factors at each wavelength are highly dependent on the fiber geometry, in contrast to the normal solid core fiber. According to the calculations, the overlap factor for t_{core} of 3.2 μm (OD:250 μm) EYDHOF is 7.6 times larger than t_{core} of 2.0 μm (OD:125 μm) at 1550 nm (Er lasing wavelength). Whereas, the overlap factor at 1060 nm (Yb-lasing wavelength) is just 1.4 times larger in the case of 3.2 μm core fiber compared to the small core one. Therefore, the small core fiber has a much broader intensity distribution and is more attenuated at longer wavelengths. On the other hand, the thicker core would have the better overlap factor at longer wavelengths, causing both high gain at the 1550 nm band and a high threshold at 1060 nm.

The measured beam quality (M^2) factors of 125, 150 and 250 μm fibers were 1.5, 2.4 and 5.2 respectively, and were found to be very much dependent on the number of guided modes in the core. The guided mode numbers at 1550nm for different fibers are 2, 3 and 8 for 125, 150 and 250 μm fibers respectively (Table 3-2). Although the current large OD fiber has a beam quality of 5.2, it is possible to improve the beam quality by controlling the NA and the core thickness in the fiber, and thus it is possible to achieve a single-mode operation in the 1550 nm wavelength range.

The beam quality factor (M^2 value) of the fundamental mode (ring-shaped mode) in the HOF is not defined theoretically. This may be different from M^2 value = 1 of a purely single mode (LP_{01}) in a conventional step index fiber. According to a simple calculation

using an existing method [84], the calculated M^2 value HOF with small hole (2 μm hole radius) was 1.27. However, when the hole size was increased (>8 μm hole radius), calculated results showed unreasonable value, less than 1. This means that the calculation method cannot be used for the HOF. Therefore, in order to reach a theoretically acceptable M^2 value of the fundamental ring-shaped mode in the HOF, more serious theoretical and mathematical research is required and this is out of scope of this thesis. Throughout the thesis, the measured M^2 value will only be considered, and for the reasonable expectation on M^2 value of the HOF, the M^2 value is measured after the hole in the HOF is collapsed.

3-3. Summary

In this chapter, the modal properties of the step HOF and the laser performance of Er:Yb co-doped step HOF were investigated. The main property of the step HOF is that it exhibits the fundamental mode cut-off at a finite wavelength depending on the ring-core structure. This can be used for the distributed wavelength filter to suppress unwanted emission in rare-earth doped fiber lasers and amplifiers. Furthermore, the ring-core provides the relatively larger core area compared to the normal step index fiber and it can improve the pump absorption in the cladding-pumped configuration. However for many applications, the sharpness of the fundamental mode cut-off needs to be improved in order to use such a fiber as a distributed wavelength filter. For example, the laser wavelength in Er:Yb co-doped step HOFs was 1544 nm, which could not be shifted to the shorter wavelength (S-band). This was due to the slow dependence on the wavelength of the fundamental mode filtering, which means that the modal leakage loss at the shorter wavelength is also high and it prevents the gain from overcoming the ground state absorption (GSA) at the shorter wavelength (<1530 nm).

Laser performance of double clad Er:Yb co-doped HOF was also presented. The maximum output power was 2.5 W at a slope efficiency of 26% with respect to the launched pump power (29% with respect to the absorbed pump power) when the core thickness was 3.2 μm (OD:250 μm). In this fiber, the fundamental mode cut-off was located at a longer wavelength (~2000 nm), which is beyond the range of the optical spectrum analyzer (OSA). As the core thickness becomes smaller, the fundamental mode cut-off shifts to the shorter wavelength side. In the case of the 2.0 μm core thickness (OD : 125 μm), the fundamental mode cut-off wavelength was ~ 1570 nm. The slope efficiency was only 8 % with respect to the launched pump power. The degradation of the slope efficiency was due to the modal leakage loss and poor overlap factor with the doped core at the signal wavelength (1544 nm) induced by the fundamental mode cut-off in the step HOF. This was related to the threshold of Yb co-lasing at 1060 nm, which was dependent on the core thickness. In the step HOF with the larger core thickness (the low loss and high overlap factor at the signal wavelength), the energy transfer from Yb to Er was more efficient, which increase the threshold of Yb co-lasing. Otherwise, the threshold of Yb-co lasing at 1060 nm was decreased in the step HOF with the smaller core thickness (the large loss and low overlap factor at the signal wavelength). The current result indicates that the prospect for significant improvement in the output power from a hollow fiber laser at an eye safe wavelength is promising.

PART III.

DEPRESSED CLAD HOLLOW OPTICAL FIBERS

Chapter 4. Nd:Al-doped Depressed clad hollow optical fiber

The hollow structure exhibits the fundamental (LP_{01}) mode cut-off in a finite wavelength as mentioned in chapter 3. Such a property of the HOF allows it to act as a distributed wavelength waveguide filter. It is normally employed to suppress the unwanted stimulated emissions in rare-earth doped fibers. For example, a Nd-doped fiber laser (NDFL) operating at 930 nm (quasi-three level) requires the suppression of the stimulated emission at 1060 nm (four-level). For the effective suppression of undesired emissions in a fiber itself, the fundamental (LP_{01}) mode at that wavelength should escape the core rapidly. Otherwise, the desired signal could be affected by the loss induced by the LP_{01} mode cut-off. In the previous chapter, the fundamental mode cut-off characteristics of step HOFs were reviewed. It was noted that the fundamental mode cut-off characteristic of the step HOF was not sharp. In practice, the induced loss caused by the cut-off affected a broad wavelength range (~ 300 nm below the fundamental mode cut-off). In addition, around the fundamental mode cut-off, the fiber becomes highly bend sensitive, which induces significant loss around the operating wavelength in the fiber.. Therefore, the step HOF was not the best solution for the distributed wavelength filter.

Considering the pump absorption in the cladding-pump configuration, the ring-core structure is still superior to the normal step-index core fiber because of the relatively large core area [15]. Therefore, in order to meet the sharp filtering chactacteristic and also to maintain the ring-core structure of step HOFs, the modified hollow structure is required. In this chapter, the depressed clad hollow optical fiber (DCHOF) is proposed and its waveguide properties and filtering characteristics is presented theoretically and

experimentally. Using such properties, Nd-doped DCHOF operating at 930 nm is demonstrated.

4-1. Waveguide properties of the DCHOF

4-1-1. Characteristic equation for the DCHOF

Figure 4-1 shows a depressed clad hollow index structure with an air hole at the center of the fiber, a ring-shaped core (n_{co}) surrounding the central air hole, a depressed refractive index of the first cladding (n_{dip}) and a second cladding ($n_{clad} = 1.4571$(silica)).

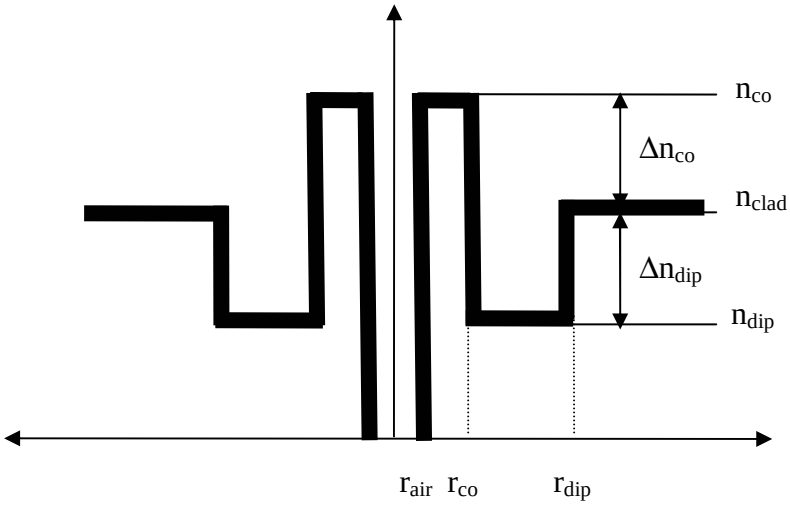

Figure 4-1. Schematic refractive index structure of DCHOF

The air hole radius, the outer radius of the core and the outer radius of the depressed clad are r_{air}, r_{co} and r_{dip} respectively . In the same way as with the step HOF in chapter 3, the weakly guiding condition and the linearly polarized (LP) modes were assumed for the numerical simulation. The radial dependence of the transverse field component can be written as,

$$e(r)=\begin{cases} A_0 I_m(vr) & r < r_{air} \\ A_1 J_m(ur) + A_2 Y_m(ur) & r_{air} < r < r_{co} \\ A_3 I_m(wr) + A_4 K_m(wr) & r_{co} < r < r_{dip} \\ A_5 K_m(sr) & r > r_{dip} \end{cases} \quad (4\text{-}1)$$

Here, r is the radial position, $A_i\,(i=0,1,2,3,4,5)$ is constant, and $J_m(Y_m), I_m(K_m)$ are Bessel functions of first (second) kind and modified Bessel functions of first (second) kind respectively. The mode parameters are defined as $v=\sqrt{\beta^2-k_0^2}$, $u=\sqrt{n_{co}^2k_0^2-\beta^2}$, $w=\sqrt{\beta^2-n_{dip}^2k_0^2}$, and $s=\sqrt{\beta^2-n_{clad}^2k_0^2}$, where β is the propagation constant of the mode and k_0 is the vacuum wave number. We can define a modal effective index (n_{eff}) as $n_{eff}=\beta/k_0$. The field and its radial derivative must be continuous at the three boundaries ($r=r_{air}$, $r=r_{co}$ and $r=r_{dip}$) and can be written as,

$$\begin{aligned} &e(r_{air}-)=e(r_{air}+) \\ &de(r_{air}-)/dr=de(r_{air}+)/dr \\ &e(r_{co}-)=e(r_{co}+) \\ &de(r_{co}-)/dr=de(r_{co}+)/dr \\ &e(r_{dip}-)=e(r_{dip}+) \\ &de(r_{dip}-)/dr=de(r_{dip}+)/dr \end{aligned} \quad (4\text{-}2)$$

From these conditions, the characteristic equation is obtained as follows:

$$\begin{vmatrix} I_m(vr_{air}) & -J_m(ur_{air}) & -Y_m(ur_{air}) & 0 & 0 & 0 \\ vI_m'(vr_{air}) & -uJ_m'(ur_{air}) & -uY_m'(ur_{air}) & 0 & 0 & 0 \\ 0 & J_m(ur_{co}) & Y_m(ur_{co}) & -I_m(wr_{co}) & -K_m(wr_{co}) & 0 \\ 0 & -uJ_m'(ur_{co}) & -uY_m'(ur_{co}) & -wI_m'(wr_{co}) & -wK_m'(wr_{co}) & 0 \\ 0 & 0 & 0 & I_m(wr_{dip}) & K_m(wr_{dip}) & -K_m(sr_{dip}) \\ 0 & 0 & 0 & wI_m'(wr_{dip}) & wK_m'(wr_{dip}) & -sK_m'(sr_{dip}) \end{vmatrix} = 0 \quad (4\text{-}3)$$

* $J_m'(Y_m'), I_m'(K_m')$: derivatives of $J_m(Y_m), I_m(K_m)$

All mode properties such as mode field or guiding properties are functions of the propagation constant β. The characteristic equation (4-3) can be solved numerically for the quantized propagation constant β. Once β is known, each mode parameter, v, u, w and s, can be obtained and also the mode profile and the cut-off wavelength of each mode can be estimated.

The DCHOF was designed for a NDFL operating at 930 nm. In the case of the NDFL, there are two strong emission bands, 930nm emission band ($^4F_{3/2} \rightarrow {}^4I_{9/2}$) and 1060nm ($^4F_{3/2} \rightarrow {}^4I_{11/2}$). In order to improve the laser preformance at the 930 nm emission band, the suppression of the strong four-level ($^4F_{3/2} \rightarrow {}^4I_{11/2}$) transition in the 1060 nm wavelength range, is required because the stimulated emission at 1060 nm strongly competes with the 930 nm emission. For this suppression, the distributed wavelength filtering is one option.

4-1-2. Effective indices of guided modes in DCHOFs

In order to investigate the fundamental mode cut-off of the DCHOF, the effective index of the LP_{01} mode was calculated, based on the characteristic equation which was shown in the previous chapter. For this, both the refractive indices (n_{co} and n_{dip}) of the ring-core and the depressed clad were fixed, which provides a NA_{co} of 0.09 (Δn_{co} = ~ 0.0027) and a NA_{dip} of 0.08 (Δn_{dip} ~ 0.002) in the core and the depressed clad respectively. This is with respect to the silica outer cladding. In general, the refractive index of the core and the depressed cladding was mainly determined by the composition of materials deposited during the MCVD process.

Other variable parameters in the DCHOF are the air hole size, the depressed clad width and the core thickness. For simplicity of the numerical simulation, both the air hole

and the depressed clad size were fixed at 2 μm for the radius and 8 μm for the width. If the refractive index of the core is fixed, the fundamental mode cut-off wavelength is mainly determined by the core thickness rather than by other parameters. In order to get the propagation constants of each mode, the characteristic equation (4-2) was solved numerically. Figure 4-2 shows the effective index changes of the fundamental (LP_{01}) mode as a function of core thickness and wavelength, where the bold line indicates the fundamental mode cut-off wavelengths at different core thicknesses.

For the NDFL operating at 930 nm, the fundamental mode cut-off should be located between the four-level emission band at 1060 nm and the quasi-three level emission band at 930 nm. In order to meet this condition, the core thickness will be ~ 3.9 μm in figure 4-2 (dotted line). If the core thickness is increased, the fundamental mode cut-off wavelength shifts towards longer wavelengths. The fundamental mode cut-off wavelength also depends on both the hole size and the width of the depressed clad. However, their effects are not significant compared to the variation of the core thickness.

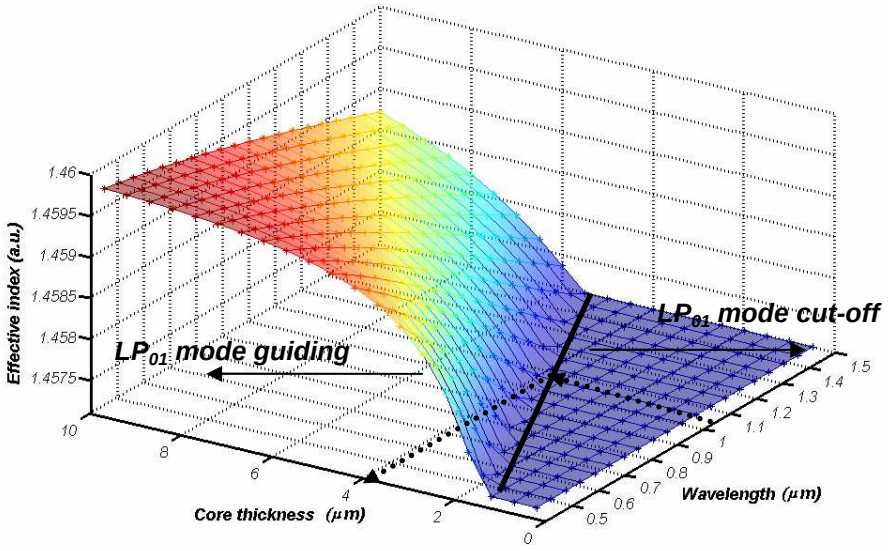

Figure 4-2. The variation of effective indices of LP_{01} mode depending on wavelength and core thickness; the NA_{co} and NA_{dip} are 0.09 and 0.08 respectively, the width of depressed clad is 8 μm and hole radius is 2 μm.

Figure 4-3 shows the variation of effective indices of the LP_{01} mode at 1060 nm as a function of the width of the depressed clad at different hole radii. Here, the NA_{co} of the ring-core and NA_{dip} of the depressed clad were fixed as 0.09 and 0.08 respectively. The core thickness was also maintained at the same value of 3.8 μm and the operating wavelength was 1060 nm. As shown in figure 4-3, in the case of 1 μm hole radius, at a range of < 3.8 μm, if the width of the depressed clad becomes smaller, the effective index of the fundamental mode is increased and becomes higher than the refractive index of the silica cladding, which indicates that the LP_{01} mode is guided through the ring-core at 1060 nm. On the other hand, when the width of the depressed clad is higher than 3.8 μm, there is no eigensolution for that case, which means that there is no guided mode through the core. In addition, the hole size also affects the fundamental mode cut-off wavelength. The large hole size compensates for the small width of the depressed clad.

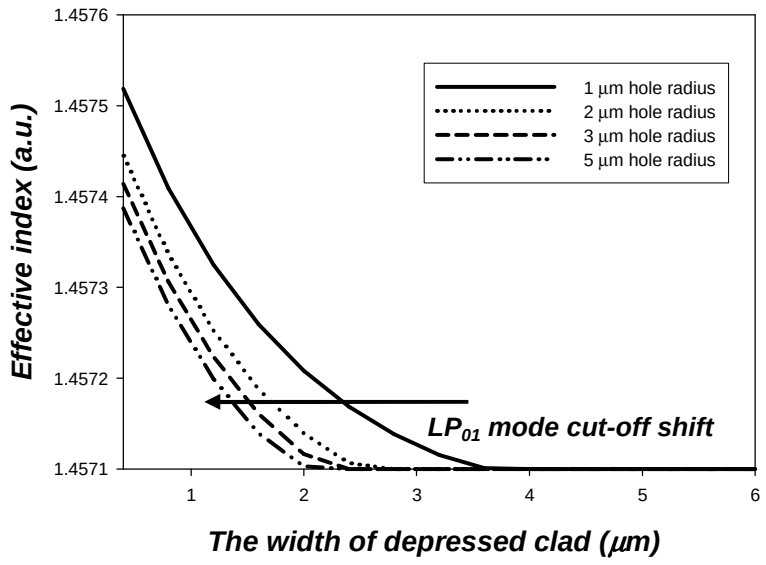

Figure 4-3. The variation of effective indices of LP_{01} mode depending on the hole radius and the width of depressed clad; the NA of ring core and depressed clad are 0.09 and 0.08, core thickness is 3.8 μm and the operating wavelength is 1060 nm.

Table 4-1 shows the variation of the fundamental mode cut-off wavelength around 1060 nm when each fiber design parameter is varied. The variation of the core thickness and the NA_{co} results in the large movement of the fundamental mode cut-off, while the width, NA_{dip} of the depressed clad and hole diameter makes a relatively small effect on that. Therefore, critical fiber parameters are both the thickness and NA_{co} of the core. In general, the NA_{co} of the fiber is determined by the composition of the fiber core material in the MCVD and solution doping process (eg. solution concentration). The fiber drawing process determines the fiber core size. For a proper cut-off wavelength, the core NA should be initially designed and controlled through the preform fabrication process and later, by varying the fiber diameter in drawing process, the required core thickness is achieved.

Table 4-1. The variation of the fundamental mode cut-off wavelength depending on the tolerance of each fiber parameter.

Fiber parameter	Core thickness	The width of depressed clad	Hole diameter	NA_{co}	NA_{dip}
Tolerance	±1 μm	±1 μm	±1 μm	±0.01	±0.01
LP_{01} mode cut-off shift	±0.31 μm	±0.01 μm	±0.04 μm	±0.16 μm	±0.04 μm

Depending on the hole size, the DCHOF can be multi-moded at a certain wavelength, similar to the behaviour of the step HOF, shown in the previous chapter 3. Figure 4-4 shows the effect of the hole size on effective indices of LP_{01}, LP_{11}, and LP_{21} mode at 930 nm as a function of the hole radius. Here, the core thickness was 4 μm and the width of the depressed clad was 8 μm. The NAs of the core and the depressed cladding were 0.09 and 0.08 respectively. This corresponds to the LP_{01} mode cut-off wavelength of 1060 nm in the fiber. The operating wavelength was 930 nm. Here, the LP_{11} mode at 930

nm appears above 5 μm of the hole radius and then, above 13 μm of the hole radius, the other higher order mode, LP_{21} mode, is excited in the core. The larger hole size easily causes a multi-mode guided core at 930 nm. Therefore, in order to maintain a single-mode guiding in the core, the small hole radius is preferred. The hole radius should be less than 5 μm. In figure 4-4, with the small hole size, the effective index of the LP_{01} mode is increased, which means that such a mode can be confined more strongly in the core and becomes more resistant to the bending loss. Thus, the small hole size in DCHOF is better than the large hole size. However, the small hole size accompanies the small core area in the DCHOF and thus, it is not the best choice in terms of the pump absorption in the cladding-pump configuration. Therefore, when the DCHOF is designed, both hole size and core thickness should be considered properly. Hole size is initially determined in the preform in the MCVD process by controlling the preform diameter in final collapsing process. This is done by controlling the collapsing temperature and maintaining the gas flow (or pressure) in the tube. ~1 mm of the final hole size and ~12 mm of the final prefrom diameter is regularly obtained in the perform. The refractive index profile is measured by the preform analyzer (P104, York Technology). It is a critical part of the fabrication process to provide a desired hole size and it also determines the core thickness in the preform. However, during the fiber drawing process, the hole size is varied depending on the drawing conditions such as furnace temperature and drawing speed. For a desired DCHOF, all the fiber fabrication process should be carefully managed.

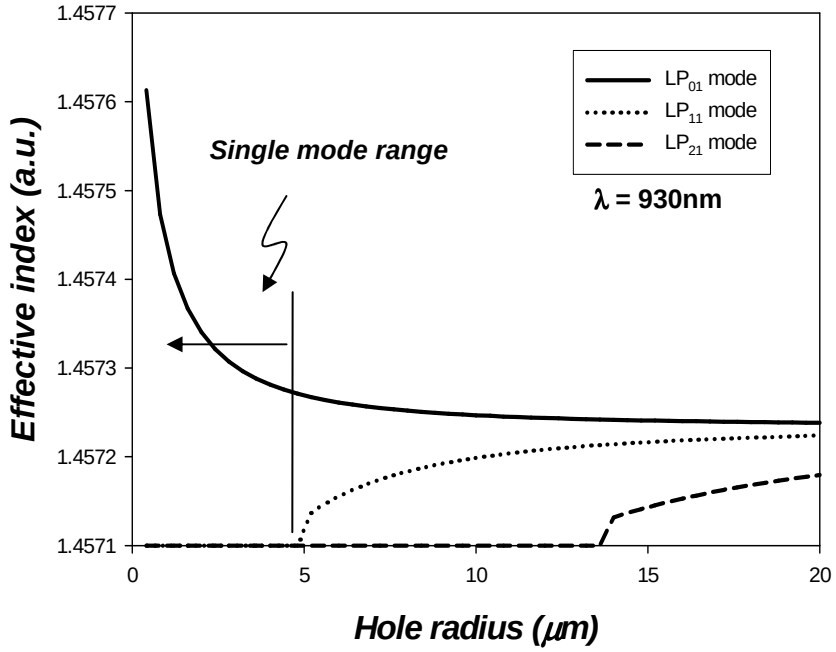

Figure 4-4. The effects of hole size on core guiding characteristics of Nd/Al-doped DCHOF; λ : 930nm, core thickness : 4 μm, the width of depressed clad : 8 μm, core NA and depressed clad NA : 0.09 and 0.08 respectively

4-1-3. Modal field distribution in DCHOFs

It is important to investigate the modal field distribution in the fiber because it determines the overlap factor with the doped core, which is one of the important factors for the estimation of the gain in rare-earth doped fibers. In this section, the mode field shape and overlap factor with the doped core in the DCHOF is presented.

From the characteristic equation (Equation 4-3), the propagation constants (β) and the parameters $v, u, w, and\ s$ are calculated in the same manner as with the step HOF in previous chapter. Figure 4-5 shows normalized modal field distributions of different guided modes (LP_{01} and LP_{11}) in a DCHOF with a hole radius of 4 μm and a core thickness of 4 μm.. The width of the depressed clad was 8 μm. The corresponding NAs of

the core and the depressed clad were 0.09 and 0.08 respectively. The operating wavelength was 850 nm, which was chosen to investigate the field shape of the LP_{11} mode. At this wavelength, other higher order modes (LP_{21}, LP_{31} and LP_{02} etc.) do not exist in such a core structure.

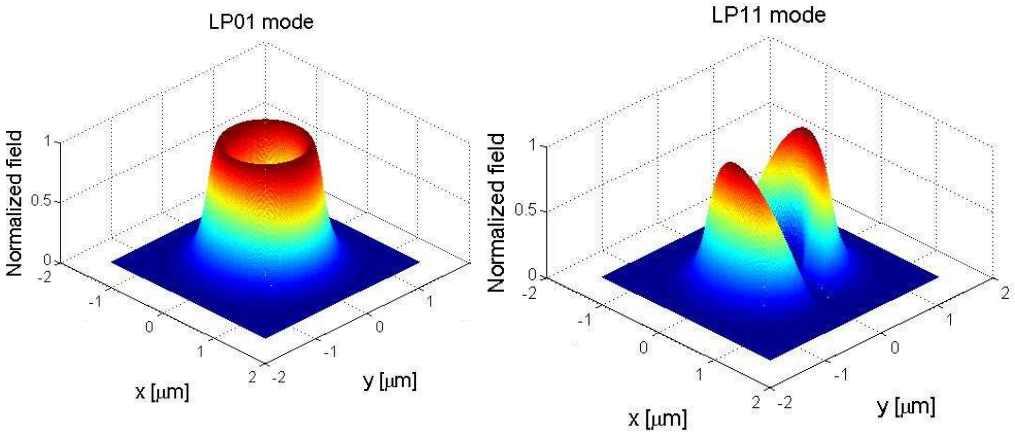

Figure 4-5. Normalized modal field distribution of (a) LP_{01} mode and (b) LP_{11} mode at 850 nm in the DCHOF; core thickness: 4 μm, the width of the depressed clad : 8 μm, hole radius : 4 μm, NA_{co} : 0.09 and NA_{dip}: 0.08.

Using a modal field distribution, the modal overlap factor of the signal in the fiber useful for an estimation of the gain in rare-earth doped fiber, can be obtained. In general, a large overlap factor gives the large gain. In the step HOF, as presented in the previous chapter, the overlap factor of a signal was significantly reduced near the fundamental mode cut-off wavelength and the mode field diameter (MFD) of the signal was increased, which indicates that the modal power easily leaks out from the core to the cladding (modal leakage loss). This was experimentally demonstrated in the Er:Yb co-doped step HOF. The laser efficiency was significantly decreased due to the reduction of the overlap factor. Contrary to this, for the DCHOF, the optical field does not get broadened even near the fundamental mode cut-off and is much less attenuated, which means that it has a more distinct fundamental mode cut-off characteristic. Figure 4-6 shows normalized modal field

distributions in the DCHOF with several different core thicknesses at 900 nm. Other fiber parameters were same as used in figure 4-5. This indicates that the signal overlap factor with a ring-core will not be significantly changed at different core thicknesses.

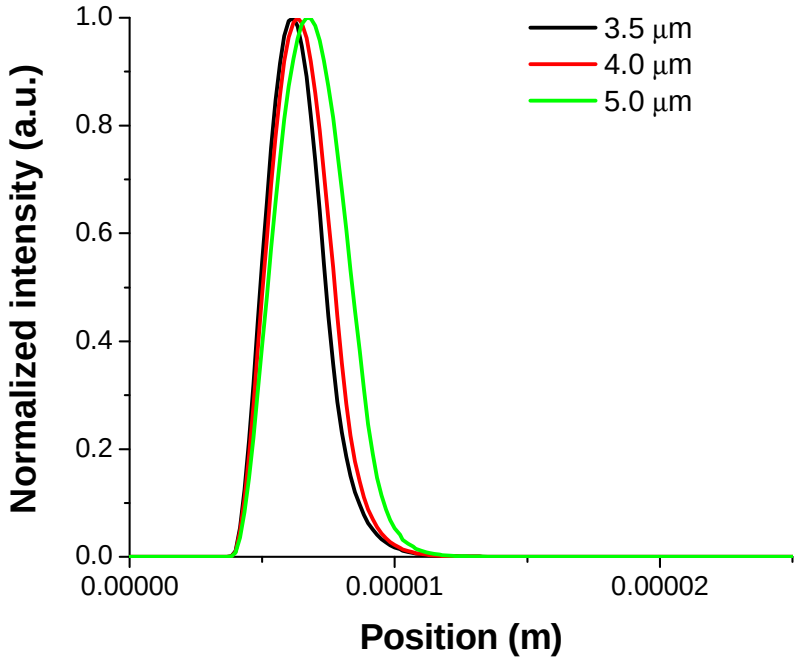

Figure 4-6. Normalized modal intensity distribution of LP_{01} mode in the DCHOF at 900 nm for different core thicknesses (3.5 μm, 4.0 μm, and 5.0 μm

In order to verify this, the change in overlap factor with the ring-core as a function of the wavelength at two different core thickness were calculated, as shown in figure 4-7. Even at the wavelength close to the fundamental mode cut-off, the overlap factor with the ring-core is well-maintained at more than 70%, which enables very effective practical separation of the desired wavelength from the undesired band.

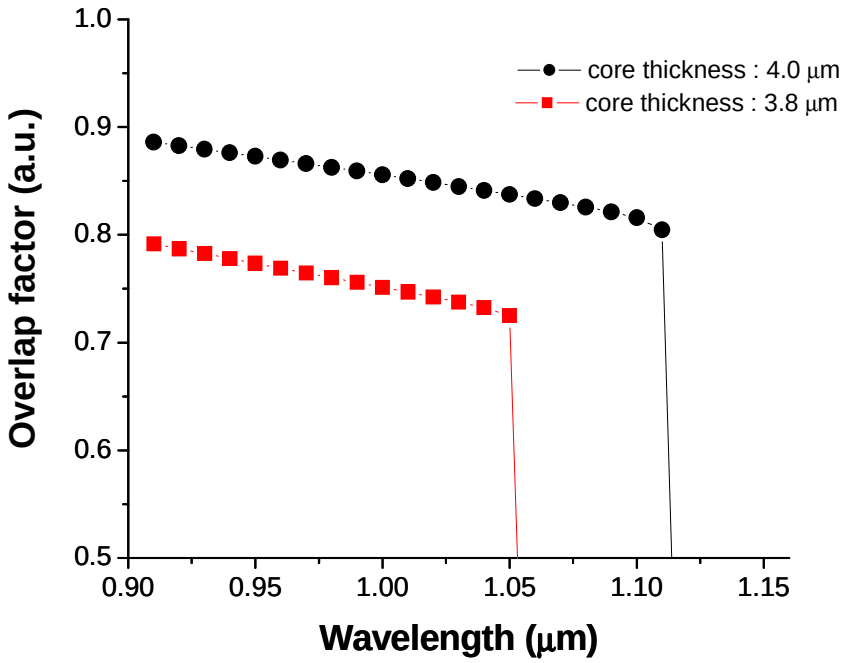

Figure 4-7. Overlap factor changes of a signal at 900 nm as the function of wavelength at different core thicknesses (3.8 and 4.0 μm)

4-1-3. Bending loss properties in DCHOFs

In the previous chapter, the step HOF shows very high bending sensitivity near the fundamental mode cut-off wavelength. The bending loss was significant on a broad operating range (~ 300 nm) and was increased by the additional coiling of the fiber. The bending loss is detrimental in order to obtain a sharp filtering between desired emissions and undesired emissions. On the other hand, the DCHOF shows improved performance in the slope of the filtering characteristic compared to the step HOF. Figure 4-8 shows effective indices and bending loss of the LP_{01} mode as a function of wavelength at different bending radii. Here, the core thickness was 4 μm and the width of depressed clad was 8 μm. The NA of the ring-core and NA of the depressed cladding were 0.09 and 0.08 respectively. The bending loss was confined to the relatively narrow range, only ~ 60 nm

compared to the step HOF, which is good for the sharp filtering of the unwanted emission as well as to maintain low loss at the operating at the desired wavelength e.g. 930 nm for Nd-doped fiber. In addition, the fundamental mode cut-off wavelength shifts effectively to shorter wavelengths by bending of the fiber.

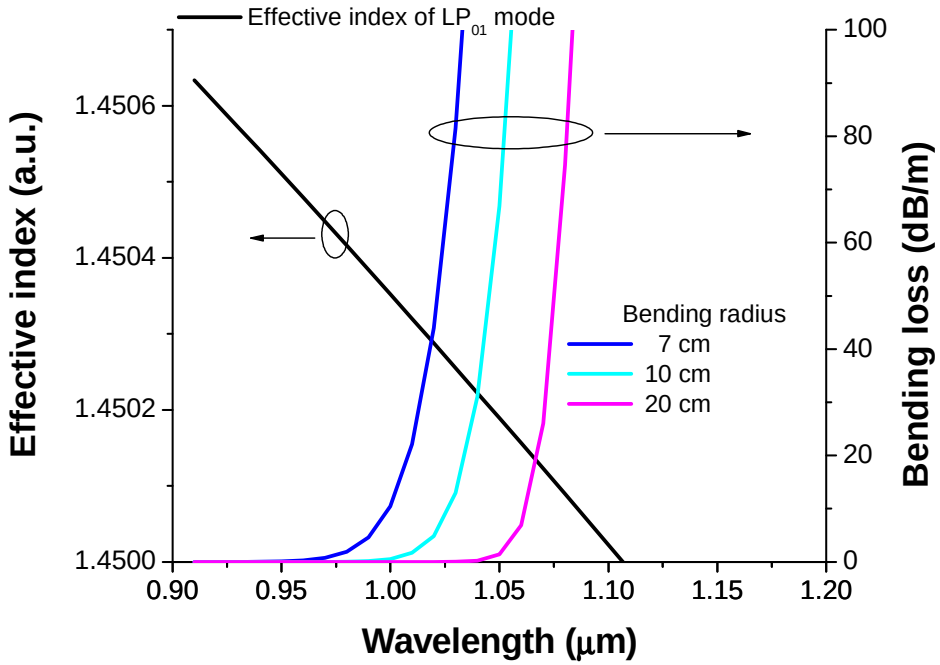

Figure 4-8. Effective indices and bending losses as function of wavelength. The core thickness : 4 μm, the core NA : 0.09, the depressed clad width : 8 μm, the dip NA : 0.08, and the Hole radius : 4 μm.

4-2. Nd:Al-doped DCHOF laser operating at 930 nm

To date, the output power of fiber lasers and amplifiers has been significantly increased. In particular, the cladding-pumped Yb-doped fiber lasers have already beem achieved kW level output power [5, 6] at 1.1 μm (four-level system), which can compete

with solid-state lasers in many applications such as material processing. However, a relatively low pump absorption in the cladding-pump configuration, compared to the core pumping configuration, still remains challenge in realizing three (or quasi three)- level fiber lasers and amplifiers such as the 930 nm laser based on Nd-doped fiber. This is due to the unwanted four or quasi-four level laser transition that competes with the three level laser transition which has the high threshold due to the ground state absorption (GSA). Therefore, in order to realize the high efficiency and high power of the three-level fiber laser, the high pump absorption and the suppression of the unwanted four (quasi-four)-level transition are essential.

There are several approaches to realize NDFL operating at 930 nm. One of the options is to reduce the GSA. At very low temperatures, Nd ions in the silica glass host act as a four-level transition system at 930 nm, which enables the reduction of the laser threshold. Using this, a cladding-pumped, nitrogen-cooled, high power 938 nm amplifier was demonstrated [88]. However, this is not practical in real applications. Another option is to use a host material with favourable spectroscopy at 930 nm such as germano-silicate [50]. However, in the case of the germano-silicate, the solubility of Nd-ions in such a host is so low that it makes the 930 nm laser inefficient because of the longer device length and hence the increase in the background loss [121]. Contrary to this, the alumino-silicate host has the improved solubility of Nd-ions without a serious concentration quenching [112]. Finally, a distributed wavelength filter that suppress the four-level emission at 1060 nm can be used. For this, the filter should be distributed along the fiber. Otherwise, the gain at 1060 nm is so high that the strong emission at such a wavelength would prevent the amplified emission at 930 nm and degrade the laser efficiency in this wavelength.

Several types of the fiber have been suggested. One of these is W-type fibre and the other is DCHOF which is considered here. As described in the previous section, DCHOF

also has the fundamental (LP_{01}) mode cut-off at a certain wavelength. It provides the distributed wavelength filter characteristic. Previously, using W-type fiber, a high power, high beam quality 930 nm Nd-doped fiber laser was demonstrated [8, 51]. However, it is difficult to scale to large core areas because if the core area becomes bigger, the fundamental cut-off cannot be maintained at the desired wavelength. By reducing the core NA, the core area can be increased but, the low NA fiber makes the cut-off less distinct. In order to solve this, the DCHOF is suggested in this thesis.

4-2-1. Comparisons among W-type fiber, step HOF and DCHOF

As mentioned before, the stimulated emission at 1060 nm should be suppressed for an efficient NDFL operating at 930 nm. In order to do this, the distributed wavelength filter can be used. There are several types of such fiber; W-type fiber, step HOF and DCHOF, which was presented in the earlier chapter. Generally, such fibers have a common feature in a refractive index structure, which is a negative dielectric volume. It means that an average refractive index at the core area is less than that of the cladding [14]. In that case, the effective index of the fundamental mode can be lower than that of the cladding, where the fundamental mode is leaking from the core.

For W-type fiber, the refractive index structure consists of an index-raised core, a depressed clad around the core and a cladding. The depressed clad around the core decreases the average refractive index of the core. Therefore, in W-type fiber, the design of the depressed clad is critical to obtain the fundamental mode cut-off at the required wavelength. Both step HOF and DCHOF have the same feature as W-type fiber, where the hole plays a key role in reducing the average refractive index of the core. In this section, in

order to find out the appropriate fiber structure for the NDFL at 930 nm, three types of fibers; W-type fiber, step HOF, and DCHOF, are compared.

Figure 4-9 shows the variation of the effective index of LP_{01} and LP_{11} mode for different fibers. Here, the fundamental mode cut-off was set at 1100 nm for all fibers. In order to do this, the NA of the core was fixed at 0.09 for all fibers. The NA of the depressed clad in both DCHOF and W-type fiber was 0.08. The hole radius was 4 μm for both DCHOF and step HOF. The core size was only varied in order to set a similar fundamental mode cut-off wavelength. In order to find effective indices at each wavelength, the characteristic equation of each fiber structure was solved, which was shown in chapter 3. As mentioned before, the effective index determines most of the modal characteristics such as, a modal leakage loss, bending loss, and modal dispersion. In addition, the decay slope of effective indices determines the sharpness of the modal cut-off.

In figure 4-9, in the case of the DCHOF, a relatively faster decay of effective index of the fundamental mode compared to other fibers was obtained. On the other hand, in the step HOF, the decay rate of the fundamental mode effective index is very slow and the effective index at each wavelength compared to other fibers is small. It means that the mode is poorly-guided and it experiences a high bending loss. W-type fiber shows a similar decay rate of the fundamental mode with DCHOF. Therefore, DCHOF and W-type fiber show the similar steepness of the fundamental mode cut-off.

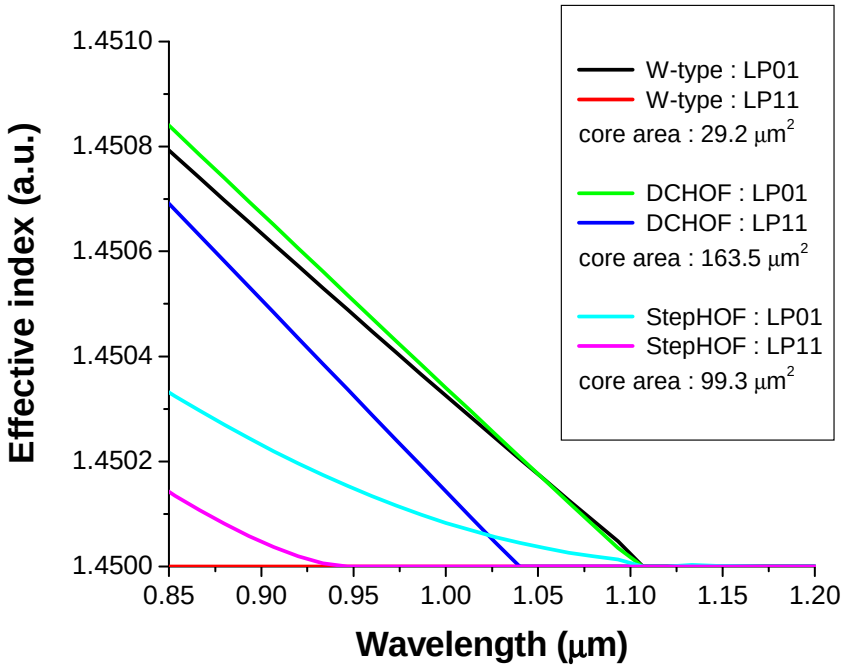

Figure 4-9. Effective index changes of LP_{01} and LP_{11} mode as a function of wavelength for three different fibers; W-type fiber, DCHOF and Step HOF. The silica cladding index : 1.45.

However, there are big differences in the core area of such fibers. As shown in figure 4-9, the core area of the DCHOF is 5.5 times larger than that of the W-type fiber, which is an advantage of the DCHOF over W-type fiber in the cladding-pumping configuration. Large core area fiber can normally provide the large pump absorption and also mitigate fiber nonlinearity. Moreover, it guarantees relatively high extractable energy in a gain medium. These are, in practice, the main fiber design features for high power fiber sources. In addition, a single mode operation at a wanted wavelength is also preferred in most applications. As mentioned in the previous chapter, the higher order mode (LP_{11} mode) is more easily excited in the hollow structure. As shown in figure 4-9, for both of the DCHOF and the step HOF, the higher order mode is more easily excited, contrary to the W-type fiber, and the single mode range is relatively narrow. The single mode range

can be widened by reducing the hole size, as it causes the reduction of the core area. If the hole size is properly controlled, the core area in the DCHOF can be increased by a factor of 4 ~ 5 compared to the W-type fiber, whilst still maintaining a single mode output at a desired wavelength.

The low effective index of the fundamental mode near cut-off wavelength causes a high bending loss, which is an important property for investigating the modal cut-off behaviour. Figure 4-10 shows bending loss for three types of fibers, which have the cut-off wavelength of the fundamental mode as shown in figure 4-9. Here, the bending radius was 10 cm. In the case of the step HOF, the bending loss of the LP_{01} mode, is rapidly growing over 50 dB/m at 930 nm although the theoretical LP_{01} mode cut-off wavelength was same as with other fibers. This is due to much lower effective index at 930 nm compared to other fibers. If the fiber is straight, the bending loss is not induced at 930 nm. However, if the relatively long length of the fiber is used, it is not practical in real fiber devices. Otherwise, both the DCHOF and W-type fiber show significantly low loss at 930 nm, while the bending loss near the cut-off wavelength of the fundamental mode is extremely high, which prevents the effective separation between two emissions at 930 nm and 1060 nm in the Nd-doped silica fiber system. The high loss at 1060 nm is good for suppression of the stimulated emission at 1060 nm in Nd-doped fiber (NDF).In the DCHOF, the induced loss by coiling the fiber is much higher than the loss in the W-type fiber. In figure 4-10, the loss difference between 930 nm and 1060 nm is ~ 50 dB/m for DCHOF and ~ 1.6 dB/m for W-type fiber respectively at the same bending radius. From this, DCHOF represents sharper cut-off characteristisc than W-type fiber and thus, it will provide more effective suppression of the unwanted suppression at the longer wavelength.

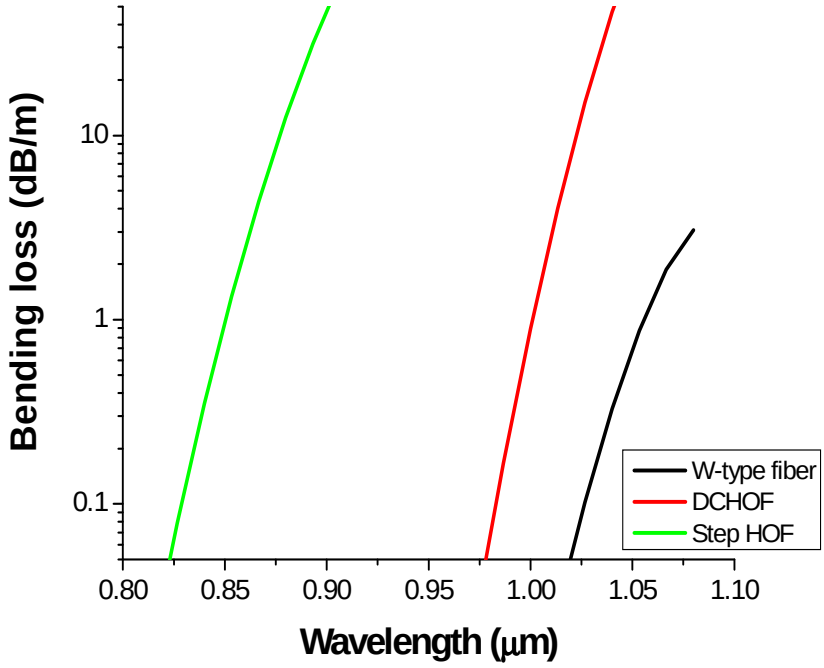

Figure 4-10. Bending loss of LP_{01} mode as a function of wavelength for three different fibers; W-type fiber, DCHOF, and Step HOF; bending radius : 10 cm

Figure 4-11 presents the variation of the overlap factor of the fundamental mode as a function of the wavelength. The overlap factor is important because it is one of the parameters determining the signal gain [78]. In theory, after the fundamental mode cut-off, no modes can be guided through the core, at which point the overlap factor will become close to zero, which means that the mode cannot obtain the gain. In practice, in the double-cladding fibers, the escaped beam from the core still exists in the inner cladding (cladding modes), which will then overlap with a small portion of the doped core, which can experience the gain. However, due to the large ratio of the cladding to the core in normal double clad fibers, the portion of the overlap of the cladding modes is so low that it can be neglected. In figure 4-11, for the DCHOF and W-type fiber, the overlap factor of the fundamental mode, depending on the wavelength, is well-maintained with a large value (> 80%), while after the cut-off wavelength of 1100 nm, it could not be calculated. On the

other hand, for the step HOF, the overlap factor of the fundamental mode gradually decreased, contrary to the other fibers. Moreover, the overlap factor becomes as low as 10% just near the fundamental mode cut-off wavelength.

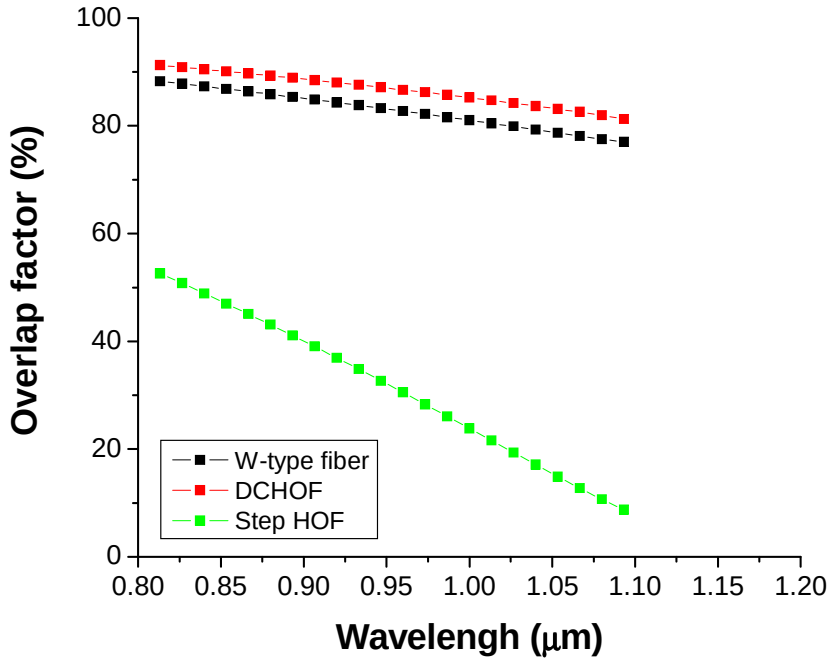

Figure 4-11. The overlap factor of the LP_{01} mode as a function of wavelength for three different fibers; W-type fiber, DCHOF, and Step HOF

Based on the above simulation, both the DCHOF and W-type fiber is suitable for a NDFL at 930 nm. However, in the cladding-pump configuration, the large core area (the large doped area) is generally preferred. By reducing the NA of the core, the core size can be increased. In DCHOF and W-type fiber, how large the core can be scaled up to is investigated. Figure 4-12 shows the available core area as a function of the NA of the core, where the fundamental mode cut-off was set at 1100 nm for both the DCHOF and W-type fiber. In addition, the width and NA of the depressed clad was also same, at 8 μm and 0.08 respectively. The core area in the DCHOF is 3-5.5 times larger than that in the W-type fiber, depending on the core NA, and thus the DCHOF shows a more scalable core area

than the W-type fiber. Therefore, DCHOF can provide the larger pump absorption, the larger extractable energy, and relatively low fiber nonlinearity. Due to these benefits, the DCHOF was chosen for the NDFL operating at 930 nm.

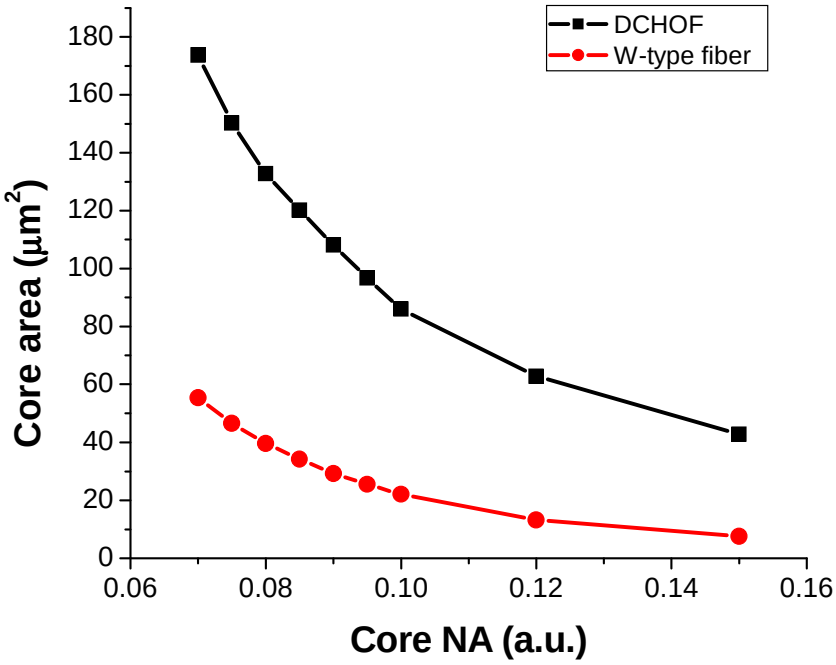

Figure 4-12. The variation of the core area as a function of the core NA for the DCHOF and W-type fiber; Hole radius of DCHOF : 2 μm, The width and NA of the depressed clad : 8 μm and 0.08 respectively .

4-2-2. Experimental investigation of continuous wave (CW) Nd-doped DCHOF laser operating at 930 nm

A Nd:Al-doped DCHOF was fabricated using standard MCVD and solution doping techniques. A depressed clad is formed by adding the correct level of boron into silica matrix and a hole was left in the centre of preform at the final collapsing process. The hole diameter was ~ 0.8 mm. Fabricated preform (LF227) was milled to a double D-shape in order to improve the pump absorption in the doped core. The flat side (D-shaped) was

formed asymmetrically. The NA of the ring shaped core and the depressed clad was ~0.09 and ~0.078 respectively. The core thickness ($t = r_{co} - r_{air}$) was ~ 0.2 mm and the width of the depressed clad was ~0.55 mm. The index structure of the fabricated preform is shown in figure 4-13 (a), which was measured by the preform analyzer (P104, York Technology). Due to the very low refractive index of the air hole, the hole size and the core thickness may not be accurate and thus, it was used for the rough estimation of the preform structure.

The preform was drawn to a fiber (F574-LF227) with 140 μm inner-cladding diameter and coated with a low-index polymer (UVF-375 from LUVANTIX) outer cladding, which provided a nominal inner-cladding NA of 0.48. The core comprised of a ~ 4 μm Nd-doped ring around an air hole of 3.63 μm diameter, and the width of the depressed cladding is 7.8 μm. The pulled fiber cross section is shown in Figure 4-13 (b).

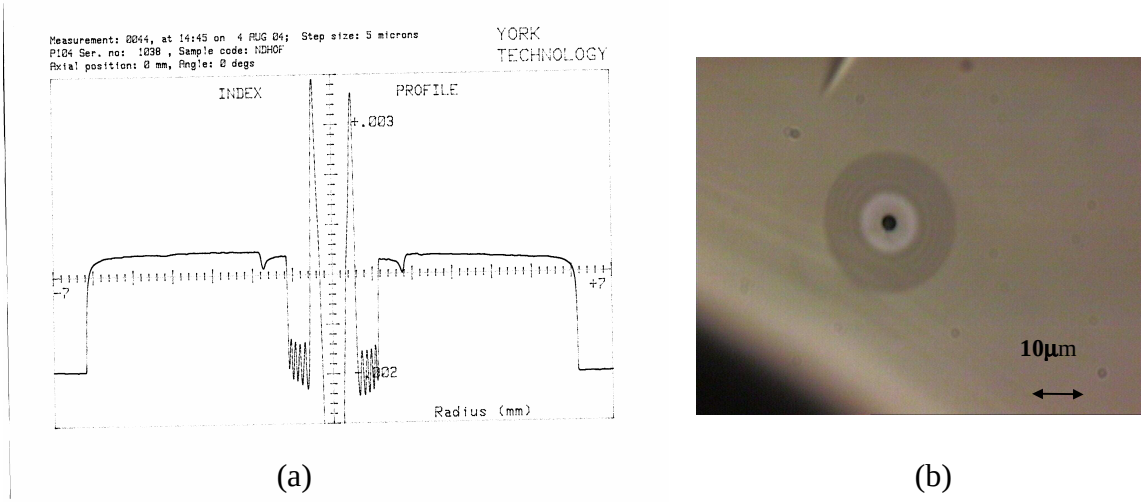

Figure 4-13. (a) Measured refractive index structure of the fabricated preform (LF227) and (b) the microscope cross-section image of pulled Nd-doped DCHOF.

Using the structure of the fabricated fiber, the modal characteristics of such a fiber geometry were calculated. Figure 4-14 (a) shows the effective indices of the fabricated fiber for different modes. Here, two important things are noticed. Firstly, the fundamental mode cut-off is ~1000nm as expected. As shown in Figure 4-14 (b) and (c), the modal field

is confined in the core at 930nm but this ring core does not guide any light at 1060nm. Secondly, the cut-off wavelength of the LP_{11} mode is 0.9 μm. Figure 4-14 suggests that the single mode operation range in the DCHOF is narrower than W-type fiber as mentioned in the previous section (figure 4-9). Also, the other higher order ring modes such as LP_{02} and LP_{03} are not supported in this structure

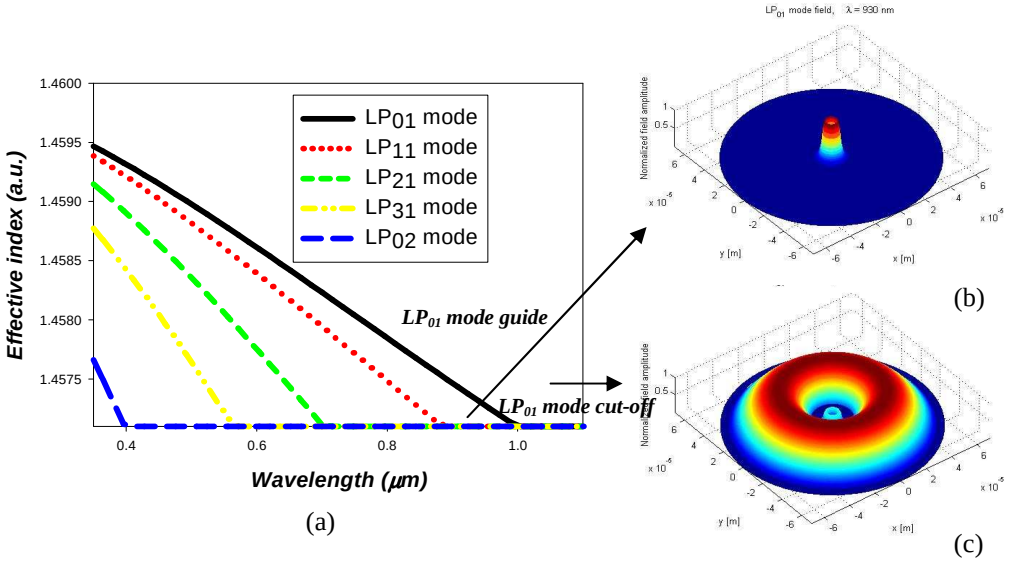

Figure 4-14. (a) Effective index change of different modes of the DCHOF (b) the guided LP_{01} mode field at 0.93μm (c) the LP_{01} (cladding) mode field at 1.06μm filtered out from the core.

The fundamental mode cut-off wavelength of the fabricated Nd:Al-doped DCHOF was ~1030 nm as shown in figure 4-14 (a). This fitted well with the measured cut-off wavelength, which is deduced from the white-light transmission measurement shown in figure 4-15. Moreover, the loss difference between 930 nm and 1060 nm is around 15 dB/m. With additional bending, the loss at the shorter wavelength is increased, which means that the fundamental mode cut-off is effectively shifted to the shorter wavelength with bending. The excessive coiling of the fiber causes a significant loss at 930 nm as well. Thus, the bending radius of the fiber is properly controlled to achieve the maximum output

power at 930 nm. The cladding absorption from the white light measurement was 0.48 dB/m at 808 nm.

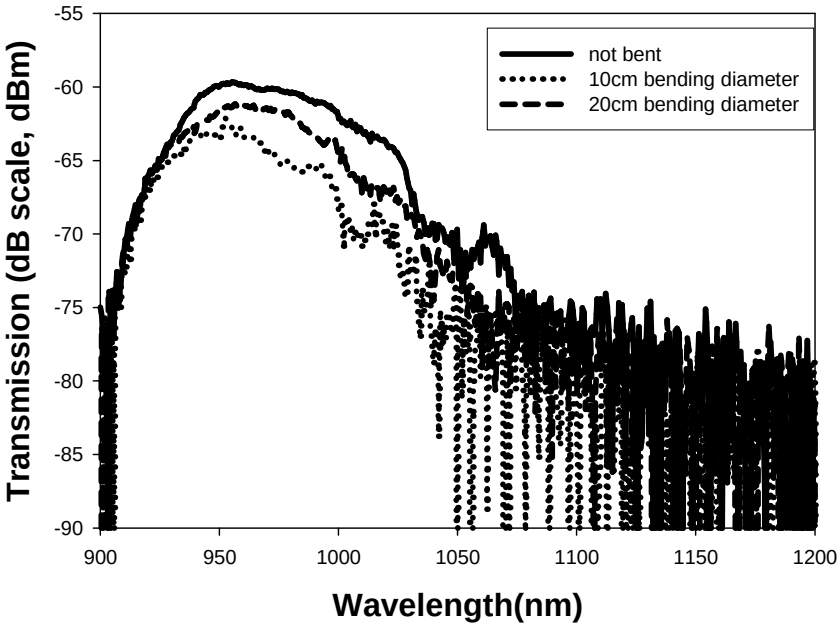

Figure 4-15. Spectrum of transmitted light from a tungsten filament lamp (fiber length : 1 m, OSA resolution : 1 nm)

The Nd:Al-doped DCHOF was pumped by a 808 nm multimode laser diode through a combination of collimating lenses and dichroic mirrors. As much as 60% of the pump power could be launched into the fiber. First, a simple laser cavity was formed between perpendicularly cleaved end facets of the fiber, providing 4% Fresnel reflections as shown in figure 4-16. Dichroic mirrors (high reflection at 930 nm, high transmission at 808 nm) were used to separate signal and pump beams. The efficiency of the NDFL with different lengths was measured in order to find an optimum length. The bending radius of the fiber was 20 cm. In figure 4-17, for a 12 m long fiber, the output power reached 2.4 W with a slope efficiency of 45% with respect to the absorbed pump power. The threshold was 2.2 W of absorbed pump power. The variation in slope efficiency depending on fiber length is related with the propagation loss including ground state absorption (GSA) and

induced bending loss at 930 nm. In addition, the signal that leaked out from the core still existed in the inner cladding, which also experiences the gain. It causes a loss as well and degrades the efficiency of the fundamental mode lasing in the core.

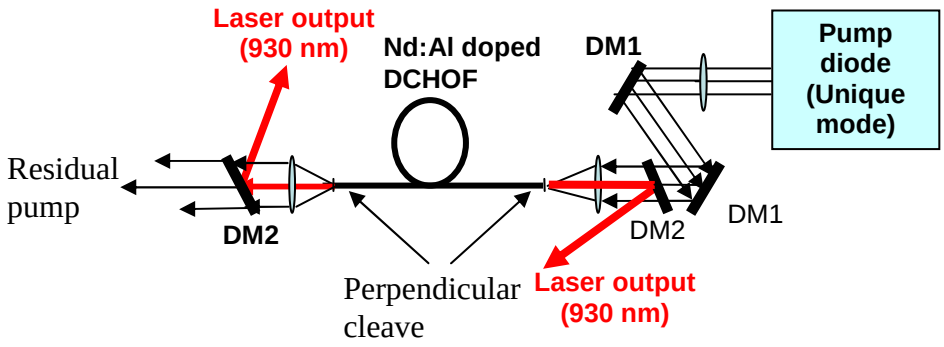

Figure 4-16. Laser configuration (4% Fresnel reflections) of Nd:Al-doped DCHOF. DM1 : HR@808nm HT@930nm, DM2 : HR@930nm&@1060nm HT@808nm *DM : Dichroic Mirror *HT : High Transmission *HR : High Reflection. Bending radius : 20 cm

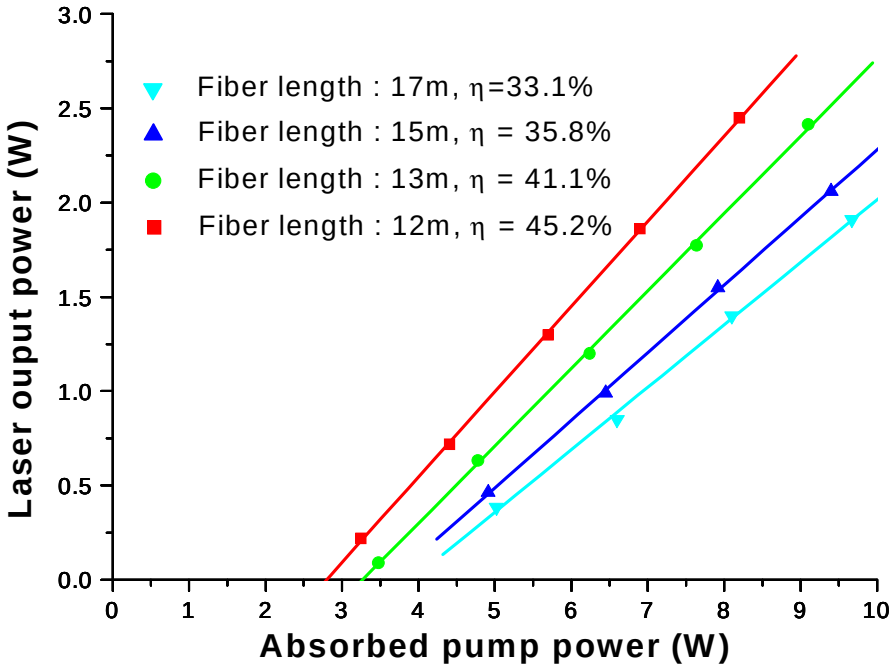

Figure 4-17. Laser output characteristics of Nd:Al-doped DCHOF at different fiber lengths, η=slope efficiency with respect to the absorbed pump power

Next, the laser configuration using an external grating was constructed in order to check the tuning range of Nd-doped DCHOF at 930 nm as shown in figure 4-18. Here, one end of the fiber was perpendicularly cleaved (4% Fresnel reflection) and the other end was angle cleaved to suppress wavelength-independent feedback. The laser cavity was formed between the 4%-reflecting perpendicular cleave and a lens-coupled diffraction grating in a Littrow configuration. The first-order diffraction-efficiency was 60%. The single-pass pump absorption was 6.8dB.

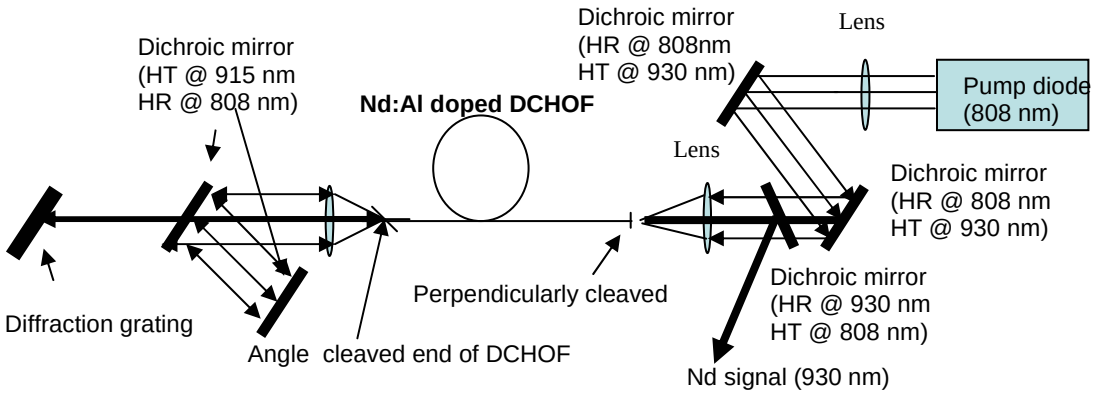

Figure 4-18. Laser configuration with an external grating in Littow configuration and single ended output for Nd:Al doped DCHOF at 930 nm.

The residual pump was re-launched into the fiber via a mirror with high reflectivity at 808 nm. Figure 4-19 shows the laser output characteristics for a fixed grating position. The induced bending radius was 20 cm. The slope efficiency was 41% with respect to the launched pump power with a maximum output power of 3.3 W at 929 nm, and the threshold was 2.5 W of launched pump power. The inset in figure 4-19 shows the laser output spectrum at maximum pump power.

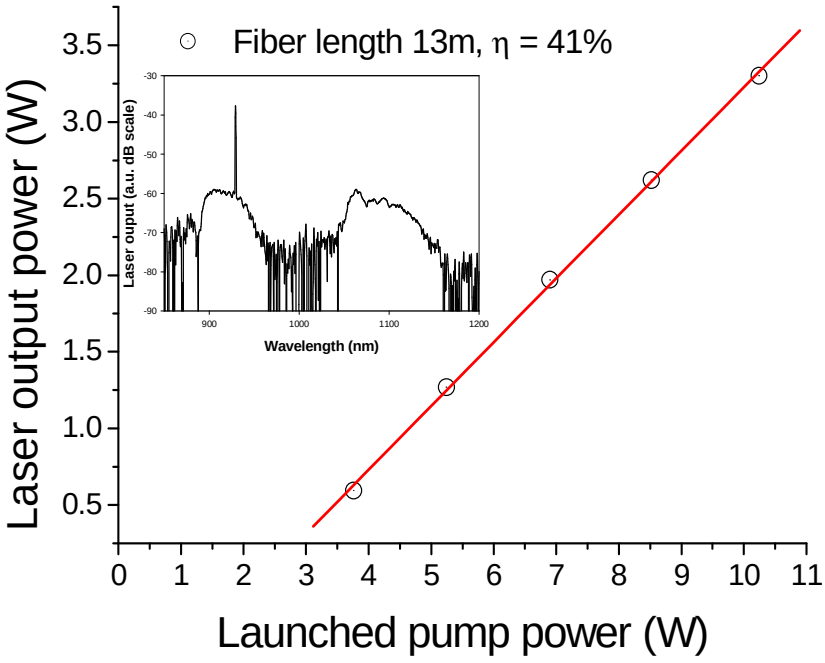

Figure 4-19. Laser output characteristics of tunable fiber laser. 929 nm. Inset: laser spectrum. OSA resolution : 1 nm

Figure 4-20 shows the tuning characteristics of a NDFL when the output power at 929 nm was 2.2W. The laser was tunable from 917 nm to 936 nm.

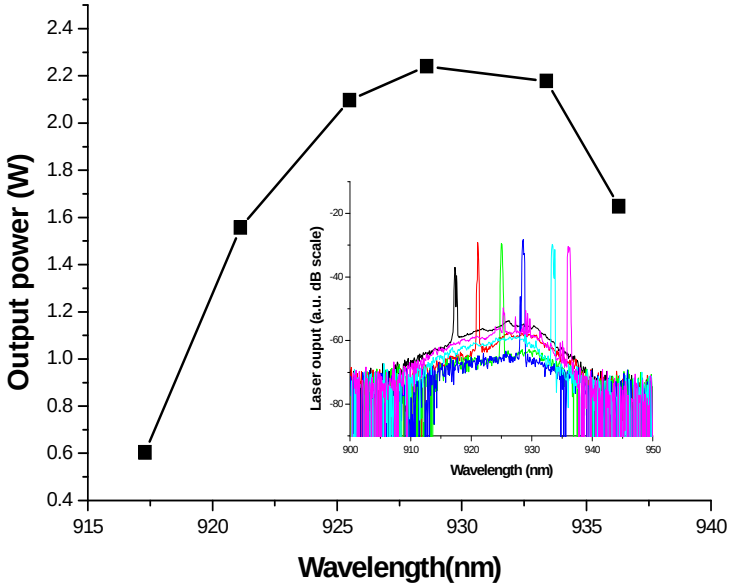

Figure 4-20. Laser tuning characteristics of 930nm Nd:Al-doped DCHOF at 2.2W output power. Inset : tuning spectra

The beam quality factor, M^2, at 929 nm was measured using the beam profiler (DataRay Inc.). According to the calculation, this fiber will support only the fundamental mode (LP_{01}) at 930 nm. Since the fiber has a ring shaped core, the fundamental mode (LP_{01} mode) is expected to have a ring shaped field distribution, which is different from the normal Gaussian mode, and thus the M^2 value would be higher than unity. We measured $M^2 = 1.3$, which is quite similar with the calculated M^2 value of the ring-shape mode in the previous chapter. Next, we measured the M^2 value after collapsing the hole in the output end of the fiber in order to obtain the Gaussian beam. The measured M^2 value was 1.05, which means that this fiber laser is truly single mode, in agreement with our modelling. The power penalty after collapsing the end of fiber was around 5%, which shows that the collapsing process does not have significant impact on the output power.

4-3. Q-switched laser operation at 930 nm using Nd:Al-doped DCHOF

4-3-1. Introduction to Q-switched NDFL operating at 930 nm

Q-switched fiber lasers can generate energetic nanosecond pulses in a compact, simple, and robust way [89], and are of interest for applications in industry, sensing and medicine. Recently, a Q-switched cladding pumped Yb-doped fiber laser that could generate pulses in the mJ regime operating at ~1.1 μm was reported [90]. While the highest pulse energies have been reached with Yb-doped fiber lasers in this wavelength regime, other applications require other wavelengths. For example, a Nd-doped fiber laser (NDFL) at 0.9 μm can be

frequency-doubled to generate blue light for display applications. However, operation of this three-level laser around 930 nm, from the level $^4F_{3/2}$ to the ground state ($^4I_{9/2}$), is much more challenging because of the competing unwanted four-level laser transition ($^4F_{3/2} \rightarrow {}^4I_{11/2}$) at ~ 1060 nm with lower threshold. This is particularly so with high-energy pulses and cladding-pumping. With cladding-pumping, the obtainable Nd excitation levels are relatively low. Re-absorption reduces the gain at 930 nm relative to that at 1060 nm in this regime. The extractable energy from a fiber laser is proportional to the achievable gain at the operating wavelength (930 nm), but normally this is restricted to a relatively low value because of the higher gain at 1060 nm. Thus, for efficient high-energy pulse generation at 930 nm, it is necessary to suppress the 1060 nm gain so that a high 930 nm gain can be achieved. In addition, for high peak powers, an aluminosilicate host is attractive due to the relatively high permissible Nd-concentration. This helps to keep the fiber short and thus to suppress nonlinear scattering (e.g., stimulated Raman scattering). This is important with the high peak powers often reached in the pulsed regime. However, the Nd-spectroscopy in aluminosilicate is particularly unfavorable with regard to the relation between the 930 nm and 1060 nm gain, as mentioned before [9]. Therefore, distributed filters have been used to suppress stimulated emission at ~ 1060 nm and thus enable operation at ~ 930 nm. Previously, a W-type fiber that exhibits a non-zero fundamental mode (LP_{01}) cut-off have been used for this [37]. With proper design, the W-type fiber can have a cut-off for the fundamental mode between the two neodymium emission bands, so that the fiber does not guide at 1060 nm. By contrast, a conventional step-index fiber in theory guides the fundamental mode for all wavelengths. Recently, several watts of output power at ~ 930 nm was reported from a single-mode Nd-doped aluminosilicate W-type fiber [8, 46], but that was in the continuous-wave regime or with pulses of relatively low pulse energy (up to ~ 10 μJ). A reason for this is that W-type fibers

are difficult to scale to large core areas. A large core allows more energy to be stored in the fiber. Moreover, with cladding-pumping, since the pump absorption length is proportional to the inner cladding / core area ratio (if the fiber is doped throughout the core), it allows also the inner cladding size to be increased whilst maintaining an adequate pump absorption. Thus higher pump powers in larger-diameter pump beams can be used. A larger core also counteracts the nonlinear interaction as well as optical damage. However, in order to maintain the cut-off wavelength between 930 and 1060 nm as the core size is increased, the numerical aperture (NA) must be reduced. Unfortunately, this makes the cut-off less distinct, and the difference between propagation loss between the two emission bands decreases. As a result, the gain that can be achieved at 930 nm decreases. An additional limitation is that guidance becomes poor at too low NAs. It is therefore of considerable interest to find alternative fiber designs, which allow for a larger core size than the conventional W-type fiber does, with a maintained cut-off behavior. One solution is to use a DCHOF presented in this thesis. In this section, a Nd:Al-doped DCHOF structure is used to demonstrate a Q-switched 930 nm NDFL.

4-3-2. Experimental investigation of the Q-switched Nd:Al-doped DCHOF laser at 930 nm

For generating 930 nm lasing in the NDFL, Both W-type fiber and DCHOF are used as mentioned before. In the previous section, the cw Nd:Al-doped DCHOF laser operating at 930 nm was experimentally demonstrated. In order to investigate the core-scalability and hence the better extractable energy from a Nd:Al-doped DCHOF a theoretical comparison between W-type fibers and DCHOF is again studied in detail in the following section.

Figure 4-21 shows the result of numerical calculations of the effective index and bending loss of the fundamental mode for different DCHOF and W-type fibers. Although the fiber parameters are different, they all have a cut-off wavelength of ~ 1060 nm, which is suitable for 930 nm NDFLs. Here, the DCHOF structure is the same as that used in the previous section.

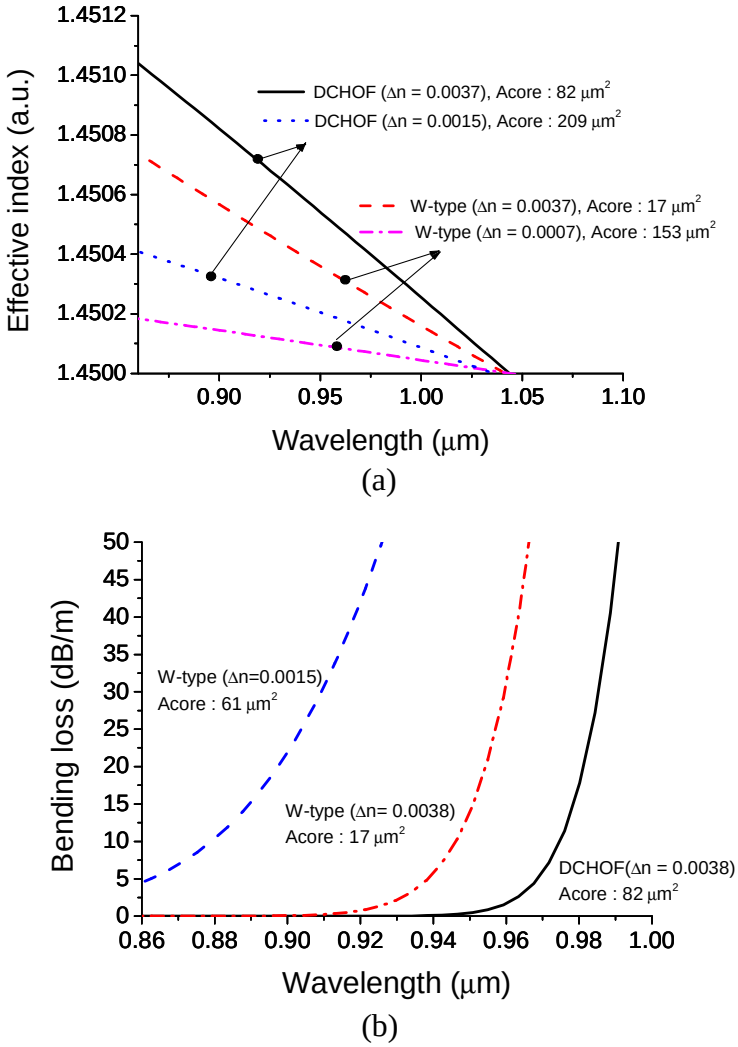

Figure 4-21. (a) Theoretical effective index *vs*. wavelength for different DCHOFs and W-type fibers. Acore: core area, Δn: refractive index difference between core and silica cladding; (b) Theoretical bending loss of DCHOF and W-type fiber at 5 cm bending radius.

As shown in figure 4-21 (a), larger-area cores have a weaker dependence of the effective index on the wavelength, i.e., a less distinct cut-off. This compromises the ability to scale up the core area whilst maintaining adequate wavelength filtering. Furthermore, the DCHOF shows a stronger dependence than the W-type fiber does.

The sharper cut-off of the DCHOF can be traded for a larger core, making it possible to increase the doped area significantly whilst maintaining adequate suppression of the 1060 nm emission. For the same refractive index of the core, the core area in a DCHOF is found to be ~ 5 times larger than for a W-type fiber maintaining the same fundamental mode cut-off characteristics as shown in figure 4-21 (a). Therefore, intrinsically, the DCHOF can have ~ 5 times larger energy storage than W-type fiber because the stored energy is proportional to the core area if all other factors remain identical. Obviously, by reducing the core NA, the core area of the W-type fiber can also be increased. However, as shown in Figure 4-21 (b), the low NA W-type fiber (dashed line) shows much higher bending loss at 930 nm and the sharpness of the fundamental mode cut-off is considerably degraded. The degradation of the sharpness remains also at larger bend radii with more appropriate, but still inadequate, loss spectra. Furthermore, the core area is still less than the DCHOF with the higher NA. The DCHOF is therefore promising for fiber lasers that require a short-pass filter and a large core such as cladding-pumped high energy NDFLs at 930 nm.

Figure 4-22 shows the laser setup used for the Q-switching experiment. A 13 m long Nd-doped DCHOF was end-pumped by a beam-shaped 808 nm laser diode bar, via a combination of collimating lenses and dichroic mirrors. Up to 8.5 W (60%) of the pump light was launched into the fiber. Of this, 5.1 W was absorbed in a single pass. Both ends of the fiber were collapsed to convert the ring-shaped mode of the DCHOF to a nearly Gaussian-shaped mode in the fiber ends. According to our calculations, the DCHOF will

support only the fundamental mode at 930 nm and this was demonstrated in the earlier section by obtaining 1.04 of M^2 value . This facilitates low-loss adiabatic conversion from the ring-mode to a nearly diffraction-limited Gaussian mode. In the pump launch end, the fiber was perpendicularly cleaved to provide 4% Fresnel feedback for the laser cavity. At the other end, a lens-coupled free-space diffraction grating in a Littrow configuration closed the laser cavity, while that fiber end was angle-cleaved to suppress broadband feedback. The first-order diffraction-efficiency of the grating was 60%. The laser cavity was switched by 'on-off' of an acousto-optic modulator (AOM) between the fiber and the diffraction grating. The transmission of the AOM was ~70% in its deflecting "on" state. The laser output was taken from the pump launch end of the fiber. The fiber was coiled with a radius of 20 cm.

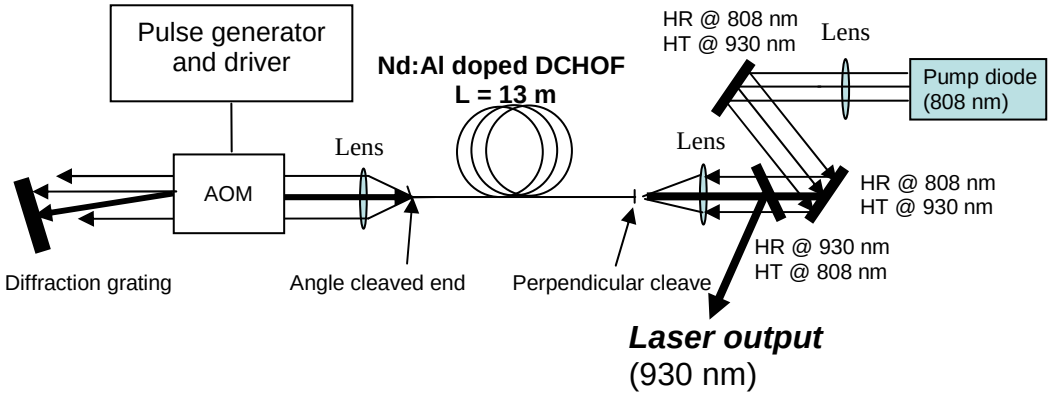

Figure 4-22. Experimental set-up of the Q-switched Nd:Al doped DCHOF laser. HR: High reflectivity; HT: High transmission; AOM: Acoustic optic modulator.

The output pulse energy was measured with an energy meter and the pulse shapes was measured with a 1 GHz bandwidth detector and a 500 MHz oscilloscope. At low repetition rates (< 5 kHz), the energy meter was used to determine the average output

power (in the pulses). This average power does not include the relatively high power amplified spontaneous emission (ASE) present in this regime. At higher repetition rates, where the ASE was negligible, the average output power was measured with a thermal power meter.

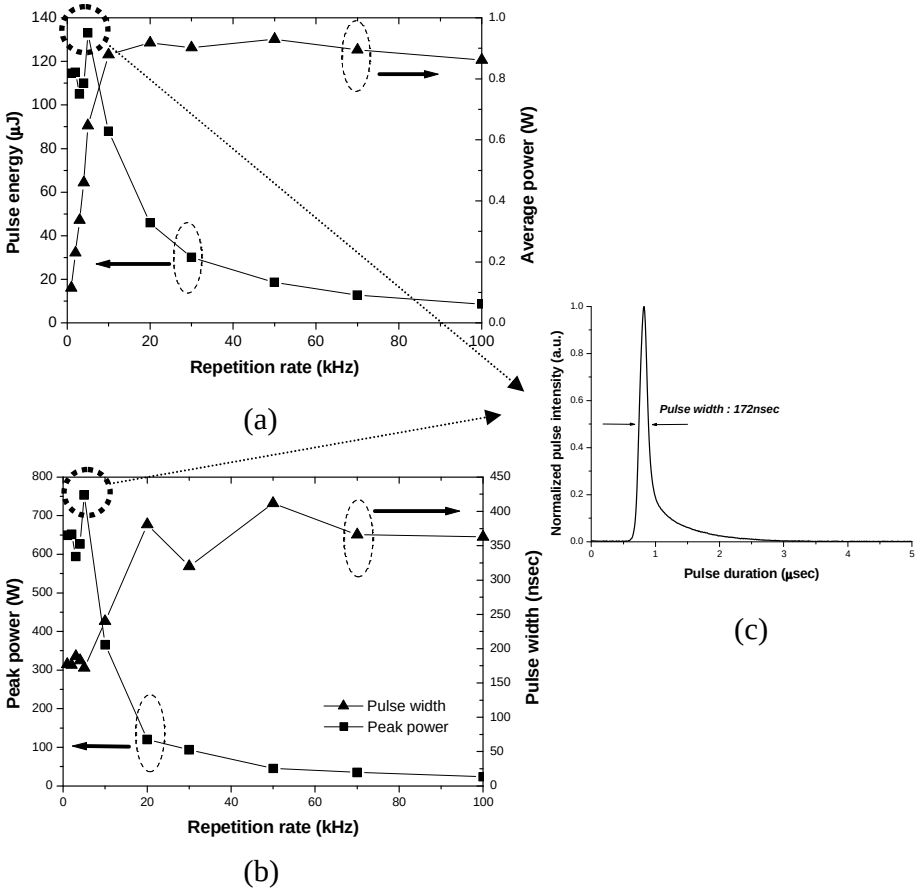

Figure 4-23. The characteristics of Actively Q-switched, clad pumped Nd-DCHOF laser. (a) Pulse energy and average power, (b) Peak power and pulse width depending on repetition rates, (c) pulse spectrum at maximum pulse energy.

Figure 4-23 (a) shows the pulse energy and average power at different repetition rates. The maximum pulse energy, 133 μJ, was reached at a 5 kHz repetition rate at a wavelength of 927 nm. The average power was 647 mW. The second moment of the pulse

shapes were calculated and used for determining the pulse width. At the maximum pulse energy, the pulse width was 172 ns in figure 4-23 (c). This corresponds to more than 750 W of peak power. The width increased to 350 ns at a repetition rate of over 20 kHz.

For comparison, the W-type fiber used for the 0.9 μm NDFL, reported in reference [8], was also tried in our Q-switched configuration. This fiber has a similar fundamental mode cut-off wavelength and Nd^{3+} ion concentration as the DCHOF reported here. The maximum pulse energy was ~ 30 μJ, i.e., smaller by ~ 4.5 times than the energy obtained with the DCHOF. This matched well with our expectation, and was due to the difference in the core area between the DCHOF and the W-type fiber.

The output of the DCHOF was tunable from 919 to 935 nm, as shown in figure 4-24. We obtained more than 100 μJ of pulse energy over a broad wavelength range of 921 – 931 nm. We measured the M^2 value to be 1.08, which is in agreement with our modeling.

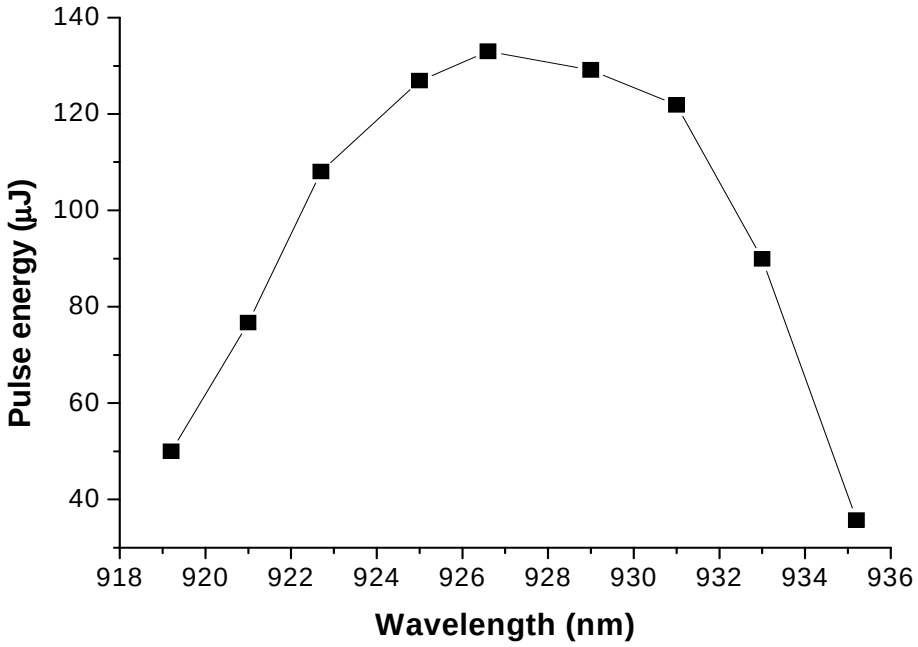

Figure 4-24. Q-switched laser tuning characteristics of 927nm Nd/Al-doped DCHOF at 133μJ pulse energy

The use of a DCHOF as a way of overcoming the limitations in core area of W-type fibers was investigated in this section. Both the DCHOF and the W-type fiber have a cut-off for the fundamental mode, which make them attractive for 0.9 μm NDFLs and other fiber lasers that require the suppression of unwanted long-wavelength emission. It is found that a DCHOF can obtain similar cut-off characteristics with a core area that is ~ 5 times larger than that of a W-type fiber. This is important, as a large core is the most important design feature of high-power cladding-pumped fiber lasers, and is particularly important in the pulsed regime. Experimentally, for the first time, an actively Q-switched cladding pumped Nd:Al-doped DCHOF laser operating at 920 – 930 nm was demonstrated. The laser generated single mode output with 133 μJ pulse energy at 5 kHz repetition rate. The pulse width was 172 ns and the average power was 647 mW, which corresponds to a peak power of 750 W. This initial result opens up possibilities for high power blue source generation by frequency doubling of a simple Nd-doped fiber laser.

4-3-3. Frequency doubling of the Q-switched Nd:Al-doped DCHOF laser source at 930 nm

A Q-switched Nd:Al-doped fiber laser operating at 930 nm provided high pulse energy and peak power. It can allow relatively high conversion efficiency in frequency doubling. Figure 4-25 shows the setup for the frequency doubling of the Q-switched Nd:Al-doped DCHOF laser at 930 nm. The fiber was perpendicularly cleaved in the launch end to provide 4% Fresnel feedback for the laser cavity. At the other end, instead of a free-space diffraction grating, a high reflectivity mirror (100% @ 930 nm) was used in a Littrow configuration and closed the laser cavity, while the fiber end was angle-cleaved to suppress broadband feedback. Single-pass pump was only absorbed in the fiber. The pump

absorption was 0.48 dB/m at 808 nm. The laser cavity was switched by an acousto-optic modulator (AOM) between the fiber and the 100% high reflectivity mirror. The transmission of the AOM was ~70% in its deflecting "on" state. The laser output was taken from the pump launch end of the fiber. Here, in order to reduce a pulse broadening by the fiber dispersion, the relatively short fiber length (8 m) was used contrary to the previous experiment when 13 m long fiber was used. The fiber was coiled with 20 cm of bending radius. Based on earlier results, the repetition rate was fixed at 5 kHz, where the maximum pulse energy and peak power have been obtained.

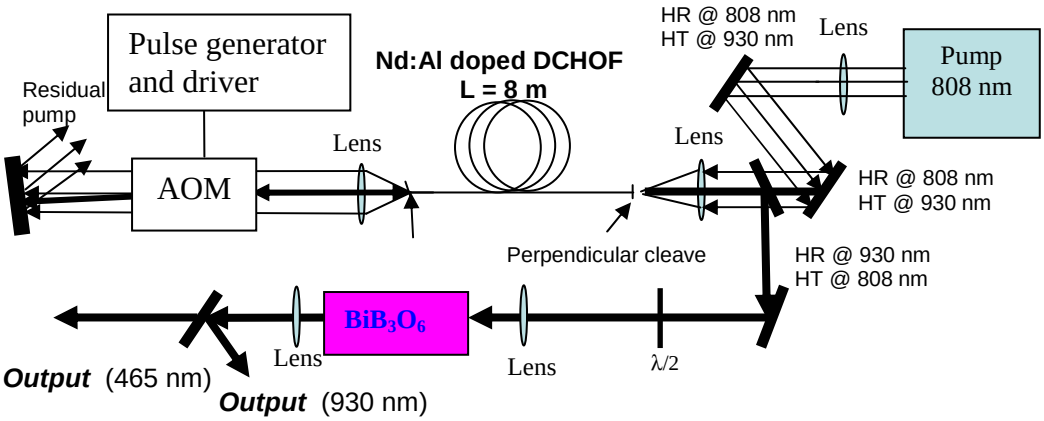

Figure 4-25. Experimental set-up of the Q-switched Nd:Al doped DCHOF laser for frequency doubling. HR: High reflectivity; HT: High transmission; AOM: Acoustic optic modulator.

As shown in figure 4-26, the maximum average output power was 902 mW at a 5 kHz repetition rate at a wavelength 927 nm and pulse energy was 176 μJ, where the pulse width was 140 nsec. The corresponding peak power was 1.3 kW. This output characteristic was improved in comparison with the earlier results because the total cavity loss was reduced by using the 100% reflection mirror and a short length fiber. Moreover, the angle-cleaved state of the fiber end could be further improved and thus one could launch more

pump power without any spurious lasing. The output beam was transmitted through a half wave-plate, which is used to adjust the polarization of the beam. The output beam was focused to an optimum e^{-2} intensity of radius of ~10 μm into the nonlinear crystal (e.g. BiB_3O_6 (bismuth borate)), which is estimated. In fact, the beam radius in the nonlinear crystal was optimized by the maximum power of the blue by tuning the focal point of lens.

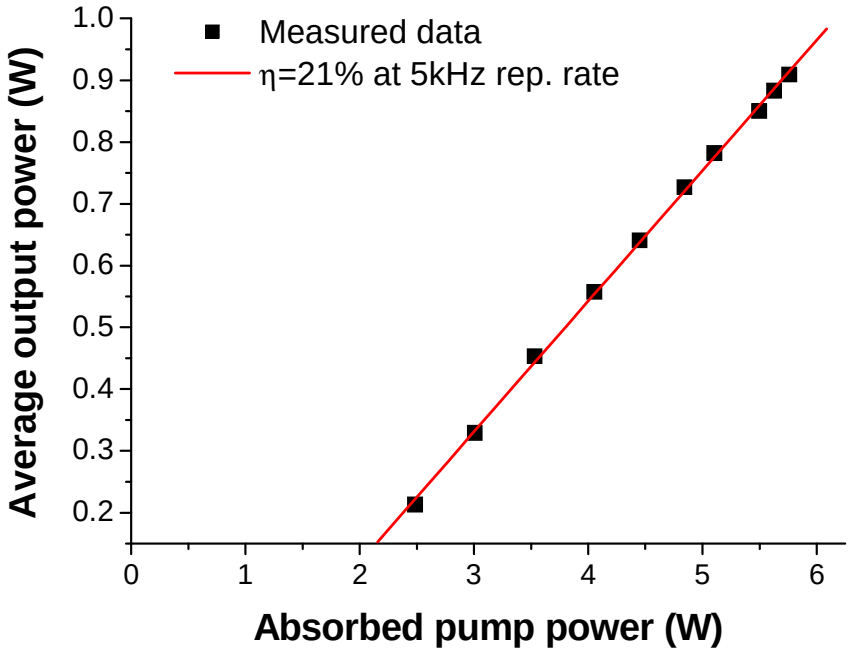

Figure 4-26. Laser output characteristics in Q-switched Nd:Al-doped DCHOF operating at 927 nm. Repetition rate : 5 kHz.

Here, BiB_3O_6 crystal was used for the frequency doubling of the output beam at 927 nm from the Q-switched Nd:Al-doped DCHOF laser. Both ends of it were anti-refection (AR)-coated. The crystal was 20 mm long with a cross-section of 3 mm × 3 mm. The crystal operated at room temperature (~27 °C).

The blue power and wavelength of this frequency doubling process is shown in figure 4-27. The maximum blue average power was 50 mW at 463.5 nm. In order to assess the efficiency of the crystal, the actual incident power should be considered. In fact, the

infrared output beam at 927 nm from the fiber is mixed-polarized. If considering just two perpendicularly linearly polarized beam, the actual incident power is half of the maximum output power and it thus becomes ~ 450 mW. Using this value, the conversion efficiency is is estimated as 10.8%. However, in this experiment, the polarization-state of the infrared output beam from DCHOF has not be looked into. Therefore, this conversion efficiency at 463.5 nm will not be accurate. In spite of this, it provided a relatively high efficient blue light via simple frequency doubling process due to the high peak power of the laser output at 927 nm. The study on DCHOF for the polarization-maintaining fiber is another issue and it will be considered for one of future works.

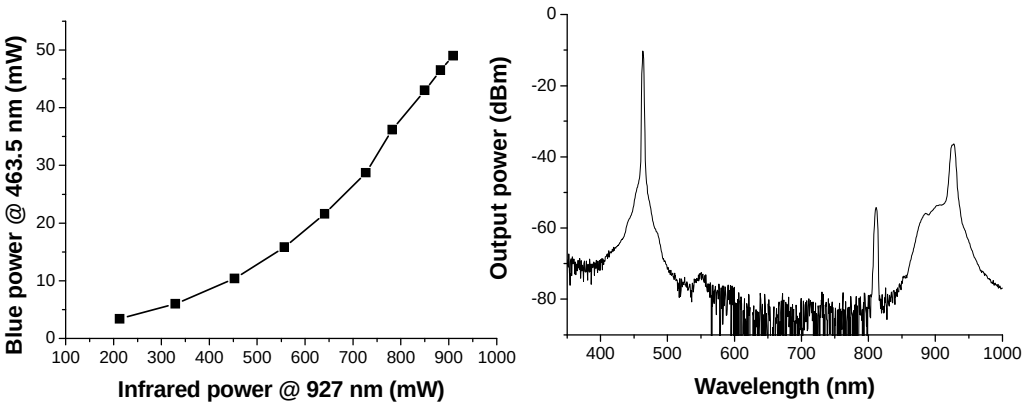

Figure 4-27. 463.5 nm blue light output characteristic and spectrum (OSA resolution : 2 nm). The maximum blue power was 49 mW.

4-4. Summary

In this chapter, the DCHOF, which is suitable for three-level fiber lasers is proposed and its modal characteristics was investigated theoretically. Comparing it with the other fiber waveguide filters such as step HOF and W-type fiber, the DCHOF shows the better performance in terms of the sharpness of the fundamental mode cut-off and the

scalability of the core area, which were demonstrated experimentally using the Nd:Al-doped DCHOF.

In the cw experiment, the laser output at 929nm in the Nd:Al-doped DCHOF was realized easily using 4%-4% Fresnel reflection cavity without any other treatments such as signal feedback or cooling. This means that the suppression of 1060nm emission by the fundamental mode cut-off was efficient. The slope efficiency was 41% with respect to the launched pump power and maximum output power was 3.3 W at 929 nm. Tuning range was from 917 nm to 936 nm and the output was a diffraction-limited beam (single mode) with 1.05 of M^2 value at 929nm.

Furthermore, the DCHOF was demonstrated as a way of overcoming the limitations in core area of W-type fibers and used to demonstrate the Q-switched Nd:Al-doped DCHOF operating at 927 nm. The laser generated single mode output (M^2 value : 1.09) with 133 μJ pulse energy at 5 kHz repetition rate. The pulse width was 172 ns and the average power was 647 mW, which corresponds to a peak power of 750 W. From the later experiment for the frequency doubling, the maximum average output power of the Q-switched laser source was increased to 902 mW at a 5 kHz repetition rate at a wavelength of 927 nm. The pulse energy was 176 μJ and the pulse width was 140 nsec. The peak power was increased to1.3 kW. This source was frequency-doubled to the generate the blue light at 463.5 nm. The maximum blue output power was 50 mW, and the conversion efficiency of bismuth borate (BiB_3O_6) crystal, used for the frequency doubling, was ~10.8%.

The DCHOF is promising for the suppression of the undesired emissions by the fundamental mode cut-off. In addition, the core area scalability in DCHOF over W-type fiber would allow the generation of the high energy pulsed laser source at the three (or quasi-three) level emission band.

Chapter 5. Yb:Al - doped depressed clad hollow optical fiber

In the previous chapter 4, the modal characteristics and the bending loss properties of the DCHOF were reviewed. The DCHOF shows better performance in terms of the sharpness of the fundamental mode cut-off and the scalability of the core area, whilst maintaining the cut-off wavelength of the fundamental mode at the correct location in order to suppress the unwanted emissions. Through the characterization of the Nd:Al-doped DCHOF lasers, operating at 930 nm, in cw and in a pulsed system, the high efficiency and high extractable energy of the DCHOF was experimentally demonstrated.

Yb:Al-doped DCHOFs will be investigated in this chapter. The Yb-doped fiber has a broad absorption band (860 nm – 1060 nm), which leads to a wide range of pumping wavelengths and its broad emission band (960 nm - 1100 nm) allows the realization of laser sources operating at various wavelengths. However, while the high power and high efficiency of the cladding-pumped YDFL at the longer wavelength side of the emission band (~1.1 μm) has been already demonstrated, laser operation at the shorter wavelengths has not so far been widely reported. This is due to the relatively low pump absorption in the cladding-pumped configuration. In order to operate efficiently at the shorter wavelength in the Yb-doped fiber, a large pump absorption is required as well as the suppression of the longer wavelength emission (1030 -1080 nm) is important. The use of the DCHOF for the realization of the Yb-doped fiber laser operating at the shorter wavelength is considered here.

Firstly, the generation of the YDFL at 980 nm will be investigated, which is very challenging due to the very large GSA at 980 nm and the high gain at 1030 nm and 1060

nm. According to the previous results, the DCHOF allows the sharp filtering characteristic, which helps the effective suppression of the high gain at 1030 nm and 1060 nm by means of the fundamental mode cut-off. The relatively large core leads to a large enough pump absorption that is required to overcome the GSA at 980 nm.

Secondly, the other issue is the possibility of the power-scaling at the shorter wavelengths. In practice, it is not easy to scale up the output power at the shorter wavelength (1030 nm - 1060 nm) due to the competing emissions at ~1100 nm with low GSA. However, the laser at the shorter wavelength can be practically required in many applications. Furthermore, the laser operating at the shorter wavelength has a relatively low quantum defect, which theoretically allows the higher conversion efficiency. This can reduce any other detrimental effects due to the low quantum defect, such as thermal problems in the kW power level.

5-1. Yb:Al - doped depressed clad hollow optical fiber laser operating at 980 nm

High-power, single-mode 980 nm sources are required in many applications, such as for pump sources for erbium-doped fiber amplifiers and lasers [52] or for blue light generation by frequency doubling [53, 54]. Commercially available, single-mode, 980 nm laser diodes are not only limited by their output powers but they are expensive too. As an alternative, high power cladding-pumped Yb-doped fiber sources operating at 980 nm have been demonstrated using a jacketed air clad (JAC) structure [55]. However, the JAC structure requires a small inner-cladding (~30 μm) and short fiber length (e.g., ~40 cm in [55]). This is to suppress the Yb-emission at around 1030 nm along the fiber and at the same time to achieve a high level of Yb inversion (over 50%) in order to obtain gain in the

980 nm transition because both the emission and absorption cross-sections are comparable at this wavelength. Thus, power-scaling using a JAC structure requires the use of an expensive, high-power and high-brightness multimode pump source. An alternative approach for achieving a high power 980 nm YDFL would be to design the waveguide structure such that it acts as a distributed filter along the fiber optimised to suppress the 1030 nm ASE. The solution described here is to use a DCHOF.

In this section, the DCHOF structure for generating laser output at 980 nm in YDF will be investigated. The non-zero fundamental mode cut-off characteristic in such a waveguide structure was used here to suppress the undesired 1030 – 1090 nm Yb ASE along the fiber. While DCHOF has been used for a cladding-pumped Nd-doped fiber laser operating at 930 nm, as shown in the previous chapter 4, in which competing 1060 nm emission needs to be suppressed, the much smaller wavelength spacing between the desired laser emission (980 nm) and the competing emission (1030 nm-1100 nm) makes this much more difficult in case of the 980 nm YDFL. Therefore, in this section, the modal characteristics of the DCHOF will be more carefully analyzed to determine the fiber parameters suitable for 980 nm laser operation.

5-1-1. Requirements for the Yb:Al-doped fiber laser at 980 nm

In order to realize an YDFL operating at 980 nm, the competing stimulated emissions at the longer wavelength (1030 nm-1060 nm) in Yb-doped fiber (YDF) should be suppressed. In order to design the fiber properly, it is important to estimate the gain at the competing wavelengths, especially at 1030 nm, because the gain peaks there and it is close to 980 nm as well. The gain calculation at 1030 nm in YDF was well-described in the reference [15]. From the reference [15], the undesired gain at 1030 nm, in logarithmic units, is given by

$$G_{1030} \approx 0.25 G_{980} + 0.72 \eta \alpha_p \quad (5\text{-}1)$$

where G_{1030} and G_{980} are the gain at 1030 nm and 980 nm respectively. $\eta = A_{clad} / A_{co}$, which is the cladding to core area ratio and α_p is the operating pump absorption in dB. It is here assumed that each pump mode sees the same absorption, given by the core absorption and divided by the area ratio. Although each cladding mode experiences a different characteristic absorption, a practical, well-designed cladding-pumped fiber should exhibit uniform absorption along its length owing to a combination of mode scrambling techniques and special geometric fiber designs. The constants at the right side in the equation (5-1) can be varied depending on the emission and absorption cross-sections at each wavelength, and can be considered typical for Yb-doped fibers at these wavelengths. For these constants in equation (5-1), the absorption and emission cross sections were 25.7×10^{-25} and 25.8×10^{-25} m^{-2} at 980 nm respectively. They were 8.25×10^{-25} m^2 and 0.25×10^{-25} m^2 at 915 nm, and, at 1030 nm, 0.45×10^{-25} m^2 and 6.25×10^{-25} m^2 respectively, as shown in the reference [15]. If the laser oscillator with a 100% reflectivity at 980 nm at one end and a 4% reflectivity at the other end is considered, the total round-trip cavity losses for 980 nm are ~14dB, therefore, the laser operating gain (G_{980}) is ~7dB, where the background loss of the fiber is neglected for simplicity. For example, consider the fiber with 120 μm cladding diameter (the cladding area : 11300 μm^2). The ratio η is varied depending on the core area. If 300 μm^2 core area is considered, η = 37.6. Then, the gain at 1030 nm is ($1.75 + 27.2\alpha_p$)dB, where the contribution of 980 nm gain (0.25×7=1.75 dB) is relatively low. Otherwise, approximately, every decibel of the pump absorption contributes 27.2 dB gain at 1030 nm in this case. In practice, this would restrict the operating pump absorption to 1 – 2 dB, which is insufficient for efficient operation. By contrast, the contribution of the 980 nm gain (the first term in equation 5-1) is unimportant.

Figure 5-1 shows the required suppression to achieve 0 dB net gain at 1030 nm depending on the core area for an inner cladding area of 11300 μm^2. The 980 nm gain is assumed to be 1.2 dB/m, or 7 dB in a 6 m long fiber. From this, the large core is preferred (or the cladding size should be significantly reduced). However, the large core eventually leads to the multimode output beam quality and the small inner cladding requires a pump source with the high beam quality, which is very expensive. Although up to ~ 40 dB of gain at 1030 nm can be accepted, it is still clear that for acceptable single-mode core areas of up to, say, 300 μm^2, the 1030 nm gain would have to be suppressed along the fiber. It is emphasized that these values depend strongly on the spectroscopic cross-sections, and that these may be different in fibers of different composition than what assumed in reference [15].

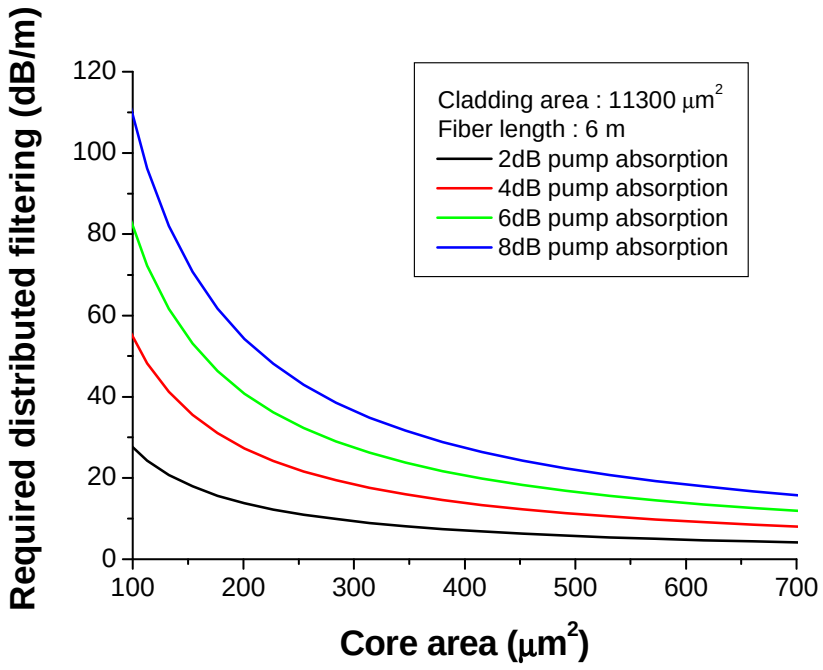

Figure 5-1. Required distributed filtering for complete suppression of the gain at 1030 nm as a function of the core area at several operating pump absroptions. Cladding area : 11300 μm^2 (120 mm diameter) and fiber length 6 m

In addition, the required distributed loss at 1030 nm is increased with increasing the pump absorption. In figure 5-1, if the fiber length is 6 m and 4 dB absorption is presented there, the ~17 dB/m filtering loss at 1030 nm is required at a 300 μm^2 core area. The required filtering loss can be reduced by increasing the fiber length and the core area. However, the short fiber length is preferred to achieve the high level of Yb-ion excitation through the whole fiber length. For this, it is essential to increase the core area, whilst maintaining the fundamental mode cut-off at the correct wavelength

In order to fix the fiber length to 6 m, as in figure 5-1, the Yb-concentration of the fiber has to be changed to obtain the different core absorptions. As already noted, the Yb-excitation level will be close to 50% in a 980 nm YDFL, and the operating pump absorption per unit length will be slightly less than half of the un-pumped (low-power) absorption, with all the ions in the ground state, and measured, e.g., with a low pump power. Thus, an operating absorption of 8 dB in a 6 m long fiber implies that the un-pumped pump absorption should be ~2.7 dB/m. This also fixes the Yb-concentration of the fiber. The fiber which is fabricated and used in the experiments had a Yb-concentration of 1500 ppm by weight, which is 40% higher.

Given a specific Yb-concentration and cross-section data, it is also straightforward to calculate the unwanted gain at 1030 nm at 50% Yb-excitation. For example, at a Yb concentration of 3000 ppm by weight, it becomes 34 dB/m, using the cross-sections of ref. [15]. It follows that points in figure 5-1 with the same required distributed filtering correspond to fiber designs with similar Yb concentrations, with slight differences resulting from slight differences in the Yb-excitation. The tolerable loss at 980 nm can be also assessed. In order to keep the efficiency close to the theoretical maximum, the loss should be less than 1 dB, or so less than 0.2 dB/m in a 5 – 6 m long fiber.

If the Yb-concentration is reduced with a fixed area ratio, the required 1030 nm filtering loss per unit length becomes lower. To obtain a given operating pump absorption, it is then necessary to use a longer fiber. The total 1030 nm filtering loss will be same, As the total tolerable loss at 980 nm also stays the same, the acceptable loss per unit length is becomes smaller. If on the other hand, the area ratio is reduced with a fixed Yb-concentration, the pump absorption increases so that a shorter fiber can be used and a higher loss at 980 nm can be tolerated. This relaxes the differences in loss between 980 nm and 1030 nm that a filter must provide, i.e., it relaxes the requirements on the filter sharpness. Thus, different Yb-concentrations, area-ratios, and operating pump absorptions lead to different requirements on the 1030 nm suppression and the tolerable 980 nm loss, as it comes to total values (over the whole fiber) as well as per unit length. It also affects the relation between the acceptable 980 nm fiber loss and required 1030 nm loss, i.e., the filter sharpness. Key is to find a fiber design that satisfy the filter requirements in a fiber with a sufficiently large inner cladding for scaling to high powers and a pump absorption sufficiently large for a high efficiency. Both the fiber requirements and the filter characteristics depend on the fiber design.

Next, the threshold at 980 nm should be considered for efficient operation. A 980 nm YDFL requires that ~50% of the ions are excited to reach gain. In order to obtain the threshold in terms of absorbed pump power, it is necessary to define the small signal absorption (α_{ss}^{s}) and the saturated signal power (P_{sat}^{s}) [78].

$$\alpha_{ss}^{s} = N_0 L \sigma_a^p \tag{5-2}$$

$$P_{sat}^{s} = \frac{h\nu_s A_{core}}{\tau(\sigma_a^s + \sigma_e^s)} \tag{5-3}$$

where, N_0 is the total Yb ion concentration, L is the fiber length, and σ_a^p is the absorption cross-section at pump wavelength. $h\nu_s$ is the signal photon energy and A_{core} is the core

area. In practical, it is supposed to be effective area, but here, it is assumed that the effective area is closed to the core area. τ = 0.76 ms is the fluorescence lifetime. σ_e^s and σ_a^s are the emission and absorption cross-sections at the signal wavelength.

In the cladding-pump configuration, total Yb ion concentration in the whole fiber length is defined as

$$N_0 L = \frac{A_{clad}}{A_{core}} \frac{\alpha_{ss}^p}{\sigma_a^p} \tag{5-4}$$

where α_{ss}^p is the pump absorption in nepers with all the Yb-ions in the ground state. A_{clad} is the inner-cladding area (11300 μm^2). The threshold in terms of the absorbed pump power is defined as [78]

$$P_{abs}^{th} = \alpha_{ss}^s P_{sat}^s \frac{\nu_p}{\nu_s} \tag{5-5}$$

where, ν_p and ν_s are pump and signal frequency respectively. Substituting equations (5-2)-(5-4) into equation (5-5), The threshold in terms of the absorbed pump power is given by

$$P_{abs}^{th} = \frac{h\nu_p \sigma_a^s}{\tau \sigma_a^p (\sigma_e^s + \sigma_a^s)} A_{clad} \alpha_{ss}^p = (0.178 mW/\mu m^2) A_{clad} \alpha_{ss}^p \tag{5-2}$$

If α_{ss}^p = 3.8 Np or 16.5 dB, the operating pump absorption becomes 8 dB, which is a reasonable value. Thus, with an inner-cladding area A_{clad} of 11300 μm^2, P_{abs}^{th} becomes 7.65 W. This is actually the absorbed pump power required to bleach the 980 nm absorption, whereas a marginally higher pump power will be needed to create the gain needed for lasing. Furthermore, a pump absorption of 8 dB implies a pump leakage of 16%. Even with these minor adjustments, the laser threshold would be less than 10 W of

launched pump power. This is reasonable, given that 915 nm diode pump sources with 30 – 40 W of power from a 0.22 NA, 100 μm core diameter, fiber pigtail are currently commercially available. Thus, even with an inner cladding diameter of 120 μm, the threshold of a 980 nm YDFL is not prohibitively large. The challenge is rather to implement a filter that provides a high loss at 1030 nm without inducing excessive loss at 980 nm.

It is worth pointing out that the very low saturation power of 980 nm YDFLs makes it very easy to overcome (excess) losses at 980 nm, e.g. from bending, or any other cavity losses. It only takes 3.8 mW of absorbed pump power to increase the gain by 1 dB with a core area of 300 μm^2. This is much smaller than the laser threshold. It is also possible to create gain for cladding modes. The gain slope becomes 6.9 dB/W on average with an inner-cladding area of 11300 μm^2, but it will be significantly higher for cladding modes with high overlap with the core.

5-1-2. Yb:Al-doped DCHOF design consideration for the laser operating at 980 nm

The DCHOF with the fundamental mode cut-off wavelength at ~1060 nm is first considered. The DCHOF, which consists of a ~ 5.4 μm Yb-doped alumino-silicate ring core (Δn_{co} ~ 0.0016, with respect to silica cladding) around an air hole of 10 μm diameter, and a depressed ring of Δn_{dip} ~ -0.0020 in the inner cladding of thickness 11 μm, as shown in figure 5-2 (a). Using these fiber parameters, the effective index in the core was obtained by numerically solving the characteristic equation 4-3, as in chapter 4. Figure 5-2 (b) shows the effective indices of two lowest-order modes (LP_{01} and LP_{11}). The fundamental (LP_{01}) mode cut-off wavelength was set at around 1060 nm, when the effective index became equal to the silica cladding index (1.45). Moreover, such a fiber would be single-

moded at 980 nm. The field distributions of LP_{01} mode both at 980 nm and 1060 nm, and for LP_{11} mode at 980 nm, are shown in figure 5-3. It is clear that no other mode except LP_{01} will be guided in the core at 980nm and that this mode remains guided up to wavelengths shorter than 1060 nm, which is basically the LP_{01} mode cut-off, and beyond that light will escape out of the core.

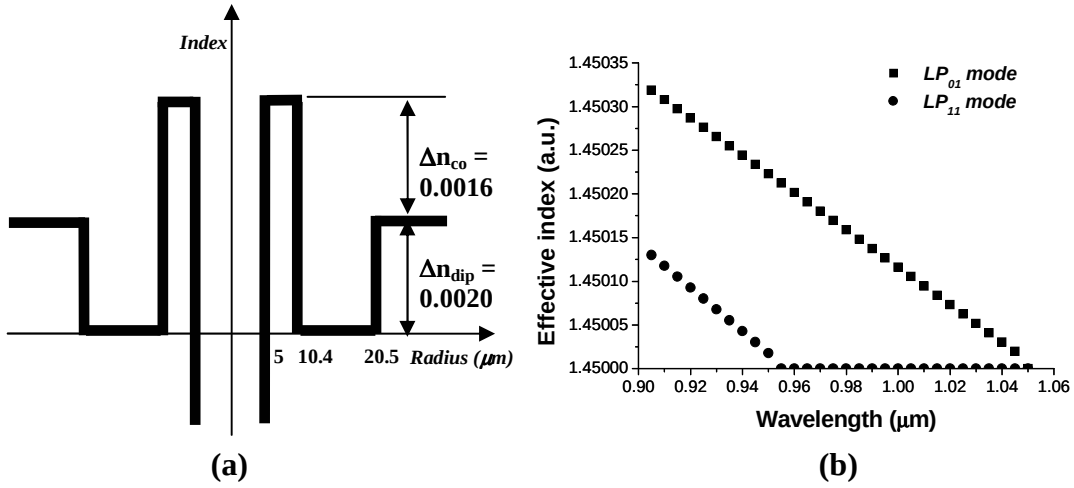

(a) **(b)**

Figure 5-2. (a): Schematic refractive index structure of the depressed clad hollow optical fiber (b). The effective index changes as a function of the wavelength.

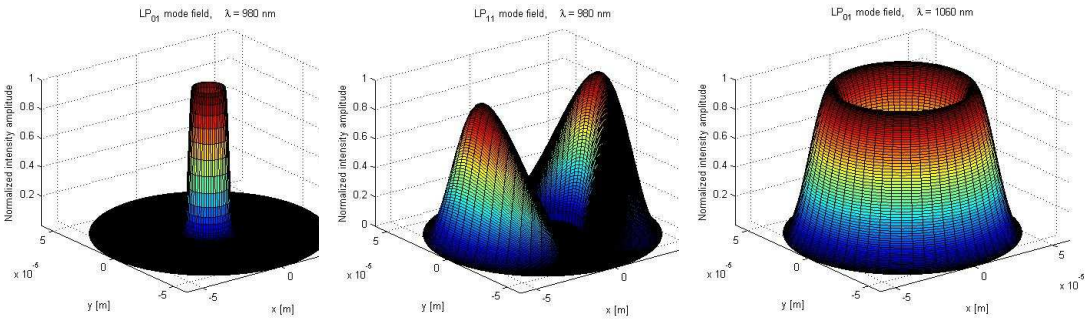

Figure 5-3. Modam field distributions in the designed DCHOF ; Fiber parameters : hole diameter : 10 μm, Core thickness : 5.4 μm, the width of depressed clad : 11 μm, and cladding diameter : 120 μm.

However, in such a design, the bending loss at 980 nm was not considered. The bending loss induced by the fundamental mode cut-off might cause a significant reduction of the gain at 980 nm, because the wavelength spacing between 980 nm and 1060 nm is too narrow and thus the effective index at 980 nm is significantly low. This was verified through the bending loss calculation. As shown in figure 5-4, the bending loss at 980 nm in this fiber is ~ 11 dB/m, which is significantly high even though the bending radius is as large as 30 cm. It is practically impossible to strictly straighten the fiber in the fiber system although the induced loss by bending can be removed in this way. In order to avoid the high loss at 980 nm, the very sharp filtering between two emissions will be required. Moreover, the suppression of the stimulated emission at 1030 nm should be considered because 1030 nm has a very high gain at the large pump absorption, which causes the significant degradation of the efficiency at 980 nm, as shown in the previous section 5-1-1. This makes it much more difficult to generate the efficient YDFL operating at 980 nm.

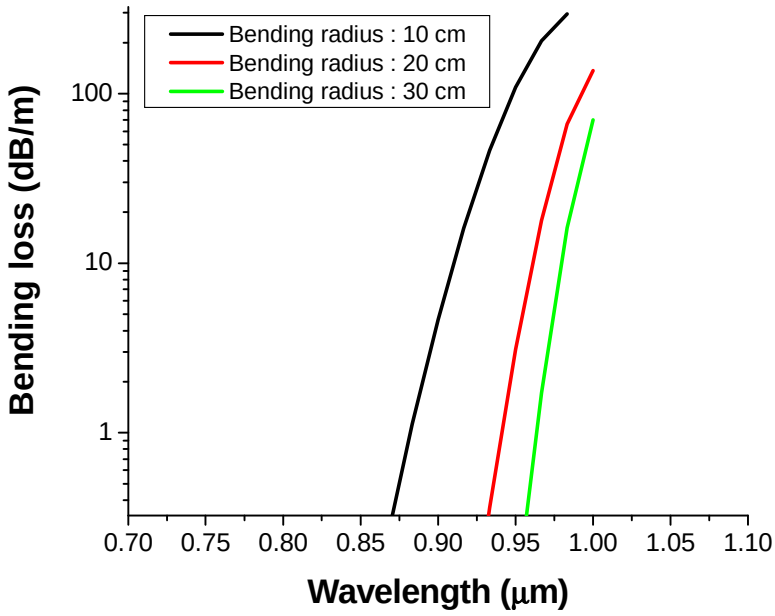

Figure 5-4. Theoretical bending loss as a function of the wavelength, of the designed fibr when fiber was coiled with a bending radius of 10 cm, 20 cm, and 30 cm.

For lasing at 980 nm in Yb-doped DCHOF, the gain at both 1030 nm and 1060 nm should be suppressed until the gain at 980 nm overcomes the total loss of the laser cavity. Therefore, it is essential to maintain a low loss at 980 nm, while increase the loss at undesired emissions at the longer wavelength. Ideally, in order to filtering out emissions from 1030 nm to 1100 nm, it is the best to set the fundamental mode cut-off wavelength between 980 nm and 1030 nm. However, although the fundamental mode cut-off was set at 1060 nm, the bending loss at 980 nm was significant as shown in figure 5-4. In order to solve this problem, an alternative approach can be made. It is that, initially, the fundamental mode cut-off is set at the slightly longer wavelength and then the bending loss at such wavelengths is controlled by adjusting the coiling radius of the fiber. In practice, the cut-off wavelength is effectively shifted to shorter wavelengths as the bending radius decreases. In this section, the DCHOF with the fundamental mode cut-off at 1150 nm is considered. For this, the key issue for the Yb-doped DCHOF operating at 980 nm is how sharply the bending loss is increased between 980 nm and 1030 nm.

There are five parameters which affects the cut-off wavelength, so there are four independent variables when the cut-off wavelength is fixed to 1150 nm. For simplicity, the whole parameters will not be considered here, but only use the numerical aperture of the core, $NA_{co} = \sqrt{n_{co}^2 - n_{clad}^2}$ as a single independent variable. The hole radius is fixed to 5 μm and the numerical aperture of the depression $NA_{dip} = \sqrt{n_{clad}^2 - n_{dip}^2}$ is fixed to 0.08. This hole size and index depression allows for reliable fabrication and handling of DCHOFs. The thickness of the ring-core was adjusted to yield a cut-off wavelength of ~ 1150 nm. The thickness of the depressed clad was set to twice the thickness of the ring. Table 5-1 presents the fiber parameters and the LP_{01} mode cut-off wavelength of specific fiber designs of different core-NAs. The fabrication tolerance of the core thickness and the depressed clad is 2%, which cause a deviation of ±30 nm at the fundamental mode cut-off

wavelength depending on the core structure. Here, the variation of the hole size is not considered. However, it can be varied when the fiber is drawn depending on several parameters such as drawing temperature and the hole size at the preform stage. As even relatively small variations in core thickness give rise to large variations of the fundamental mode cut-off wavelength, it is important to control accurately the fiber diameter in the fiber drawing process. The fiber diameter can also affect the bending loss, here a fiber diameter of 120 μm is considered.

Table 5-1. Fiber parameters of selected fiber designs for YDFL at 980 nm

No.	Core		Depressed clad		Hole radius [μm]	Core area (μm^2)	LP_{01} mode cut-off wavelength [nm]
	Thickness ($r_{co} - r_{air}$) [μm]	NA	Thickness ($r_{dip} - r_{co}$) [μm]	NA			
S1	9.10 (±0.18)	0.05	18.2 (±0.36)	0.08	5	546	1150 (± 30)
S2	7.30 (± 0.15)	0.06	14.6 (±0.29)	0.08	5	396	1150 (± 30)
S3	6.05 (± 0.12)	0.07	11.1 (±0.23)	0.08	5	305	1150 (± 30)
S4	5.15. (± 0.10)	0.08	10.3 (±0.20)	0.08	5	245	1150 (± 30)
S5	4.45 (± 0.09)	0.09	8.9 (±0.17)	0.08	5	202	1150 (± 30)

In all these fibers, the LP_{01} mode at 1150 nm has completely escaped from the core. However, the unwanted light from 1030 nm to 1100 nm is still guided by the core. For filtering these wavelengths, the fundamental mode cut-off needs to be effectively shifted by bending the fiber. As already stated, the bending loss characteristics will, to a large degree, decide the filter characteristics. The bending loss can be large also at wavelengths for which the LP_{01}-mode is guided, and it is required that the bending loss varies sufficiently quickly with wavelength for efficient 980 nm laser operation. Figure 5-5 shows the macroscopic bending loss as function of wavelength at different fiber parameters as presented in Table 5-1, where the fiber was coiled with bending radii of 20 cm (solid curves) and 7 cm (dashed curves). Even though the theoretical cut-off wavelength is 1150

nm, the effective cut-off is shifted to shorter wavelengths. Smaller bending radii and lower core NAs result in shorter effective cut-off wavelengths. At 20 cm bending radius, a fiber with 0.05 or 0.06 core-NA, or somewhere in between, may provide appropriate effective cut-off wavelength according to these theoretical calculations. At 7 cm bending radius, the 0.09 core-NA fiber appears more suitable. The other fibers would provide appropriate effective cut-off wavelengths at intermediate bend radii. However it is also important that the fiber sharpness is sufficient. Figure 5-5 shows that the higher-NA fibers result in sharper cut-offs. On the other hand, higher-NA fibers have smaller cores, which according to figure 5-1 escalates the filter requirements.

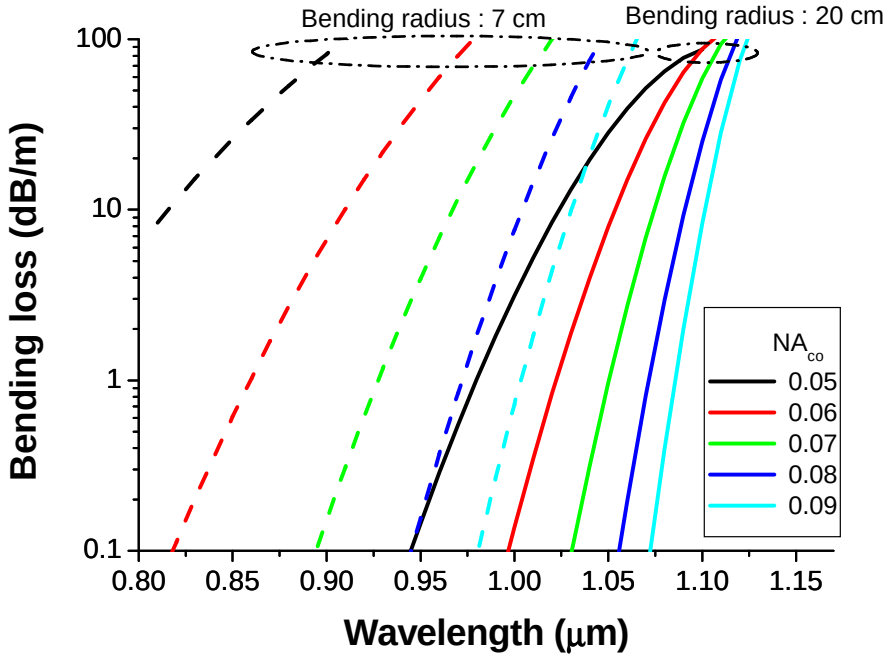

Figure 5-5. Bending loss as the function of the wavelength for different NA_{co} fibers at 7 cm and 20 cm bending radius according to Table 5-1.

Given these counteracting effects of a change in the core NA, it is necessary to analyze, and compare, the effects of the NA on filter requirements and filter sharpness in more detail in order to arrive at the optimum value. Figure 5-6 plots the required filtering loss at 1030 nm for a 0 dB net gain together with the bending loss at the two key

wavelengths, 980 nm and 1030 nm, vs. core NA. The other core parameters were varied as well, when the core NA changed, as presented in Table 5-1. The bending loss curves are plotted for a bending radius of 7 cm. For laser operation at 980 nm, the 1030 nm bending loss should be higher than the required 1030 nm filtering loss. This is the case for low NAs. However, if the NA is lower than necessary, then the 980 nm bending loss becomes higher than necessary. Therefore, the intersections between the curves for the 1030 nm bending loss and the required filtering loss correspond to the optimum fiber designs, for this particular fiber length and bending radius.

The loss at 980 nm corresponding to these intersections can then be determined from figure 5-6. For a more thorough optimization of the core NA, also other bending radii (4, 7, and 15 cm) and fiber lengths (3, 6, and 12 m) were considered. In all cases 7 cm gave the lowest, or close to the lowest, total loss at 980 nm. The total 980 nm bending losses are summarized in Table 5-2 for the different fiber lengths and operating pump absorptions, at 7 cm bending radius. We see that a fiber length of 12 m provide the lowest total loss at 980 nm for the three studied lengths, especially for low values (4 dB) of the total operating pump absorption. For higher values, the difference is smaller. Table 5-2 also specifies the optimum core NAs and Yb-concentrations for the different fiber lengths and pump absorption. In order to keep the 980 nm loss at an acceptable value, the operating pump absorption of 4 dB or 60% is targeted.

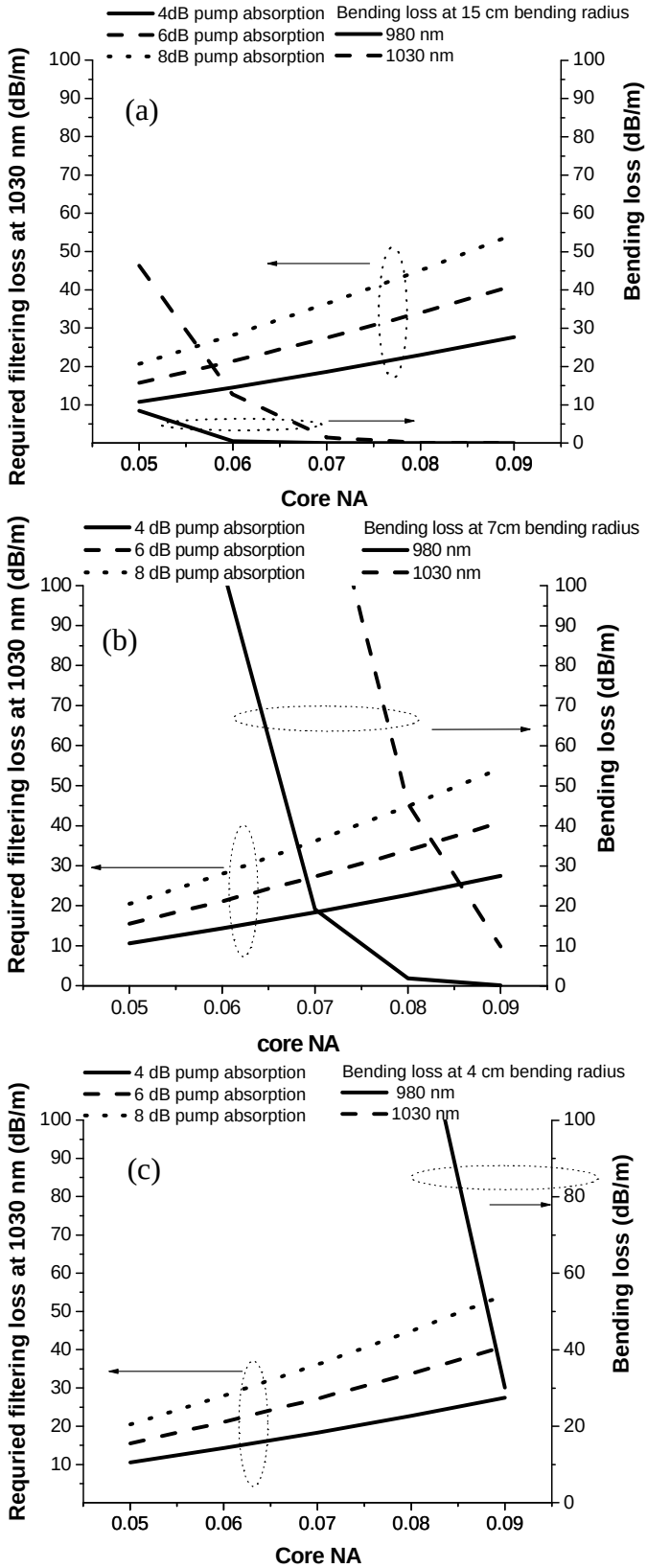

Figure 5-6. The required filtering loss at 1030 nm and bending loss at two different wavelengths (980 nm and 1030 nm) for different pump absorptions and the core NA according to Table 5-1. (a) bending radius : 15 cm, (b) bending radius : 7 cm, (c) bending radius : 4 cm

Table 5-3. Total loss at 980 nm, core NA and Yb concentration for different pump absorptions and fiber lengrths when the bending radius is 7 cm

σp : pump absorption, $\alpha 980$: total loss at 980 nm, NA_{co} : NA of the core, N_0 : Yb concentration

	Fiber length (m)								
	3			6			12		
σp	$\alpha 980$ (dB)	NA_{co}	N_0 (ppm)	$\alpha 980$ (dB)	NA_{co}	N_0 (ppm)	$\alpha 980$ (dB)	NA_{co}	N_0 (ppm)
4	5.4	0.081	4010	6	0.080	1960	1.2	0.089	1170
6	16.2	0.078	5640	7.2	0.082	3060	6	0.087	1690
8	26.1	0.075	7010	9.6	0.084	4280	8.4	0.085	2160

The optimum core design is derived, within the parameter space which is examined. There are however several points to be noted. This design gives us the minimum 980 nm loss, but the output power of a 980 nm YDFL will depend on the threshold. Futhermore the pump absorption is on the low side. This can be increased by reducing the inner-cladding area, at the expense of a more challenging pump launch. An important point is indeed that even though a 120 μm inner cladding diameter has been assumed, this assumption only affects the operating pump absorption. The same optimum core designs would be obtained with a different inner cladding size, but with different pump absorption.

In addition, a target of 0 dB total gain at 1030 nm is only approximately correct. With wavelength-selective cavity mirrors, (e.g., fiber Bragg gratings), a gain of at least 30 dB can be tolerated before strong ASE and even spurious lasing become unavoidable. On the other hand, in order to avoid strong ASE, the 1030 nm gain must be sufficiently suppressed everywhere in the fiber, not just on average. Thus, strong unwanted ASE could possibly occur even with a 0 dB average gain. Finally, bending loss depends strongly on fiber parameters and is difficult to calculate accurately. A slight deviation in the shape of

the core refractive index profile, for example, may well result in a significant difference in the spectral characteristics of the bending loss.

In fact, the fiber (F645-LF239) for 980 nm YDFL used in the next, deviates somewhat from the optimum design find above. The fabricated fber has a ring-shaped 5.7 μm thick Yb-doped alumino-silicate core with NA of 0.073 with respect to the silica cladding around an air hole of 10 μm diameter, and a 11 μm thick depressed ring of NA_{dip} = 0.08 immediately outside the core. The depressed ring is surrounded by a pure-silica region, which dominates the inner cladding. The core area in DCHOF becomes 281 μm^2. The low-power pump absorption is 1.3 dB/m in a 120 μm diameter inner cladding, corresponding to an Yb concentration of 1500 ppm by weight. Theoretically, the pump absorption becomes 0.6 dB/m at 50% Yb-excitation.

Given the deviations between the optimum fiber design and the fabricated fiber, some additional calculated characteristics will be described in the next section. Here, it is focused on whether the bending loss can provide sufficiently sharp spectral filtering. Using fiber parameters of the fabricated fiber, the effective indices of the LP_{01} mode (or equivalently, their propagation constants) and the bending loss at three different radii, 4 cm, 7 cm, and 15 cm were calculated. Figure 5-7(a) shows the effective index as a function of wavelength, showing that the DCHOF has a theoretical fundamental mode cut-off at ~1150 nm. This behavior is important, as rapid change of the effective index with wavelength is needed to get spectrally sharp bending loss characteristics. In order to effectively shift the fundamental mode cut-off to the shorter wavelength, as required for 980 nm laser operation, an additional bending in fibers is introduced. It introduces a high loss for long wavelengths, which gradually shifts to shorter wavelengths as the bend radius decreases. Experimentally, fibers are bent to a radius that provides the best output characteristics (typically the highest 980 nm output power). A good way to assess how well the fiber suppresses unwanted 1030

nm is therefore to calculate the bend loss. Figure 5-7(b) shows the calculated bending losses in the DCHOF at different bending radii, and suggests that ~ 7 cm is an appropriate bending radius. The large core is also important in terms of the pump absorption in cladding-pumped fibers, especially in the case of a 980 nm YDFL in which a small inner-cladding / core area ratio helps to reduce the gain at 1030 nm relative to that at 980 nm.

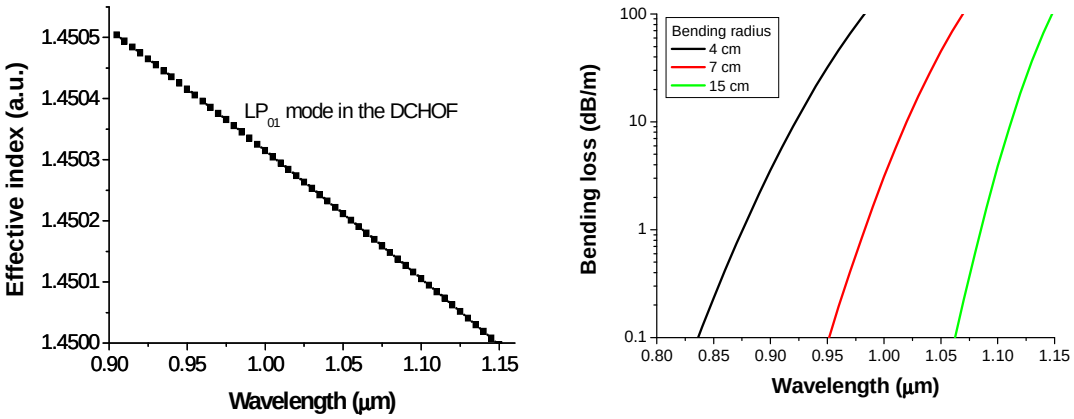

Figure 5-7 (a) Calculated effective index of the fundamental LP_{01} mode vs. wavelength for the designed DCHOF (b) Bending loss vs. wavelength at different bending radii of the DCHOF. Fiber parameters : Core thickness = 5.7 μm, Core NA = 0.073 with respect to the silica cladding, air hole diameter : 10 μm, Depressed clad thickness = 11 μm, and Depressed clad NA_{dip} = 0.08.

Using the designed DCHOF, the bending loss as a function of the bending radius at three different wavelengths, 980 nm, 1030 nm, and 1060 nm respectively was also calculated as shown in figure 5-8. The dotted rectangle indicates the available bending radius for 980 nm operation, where the bending loss at 980 nm is maintained as low value. Otherwise, above 10 dB/m of bending loss at both 1030 nm and 1060 nm can be induced. The tolerance in bending radii is small but seemingly sufficient. However tolerances in the fiber parameters must be considered. It was found that the fundamental mode cut-off is highly sensitive to the core thickness, more so than in a conventional fiber where the cut-off is proportional to the thickness. A change in cut-off may cause a significant variation in the bending loss. To investigate this, a ±2% tolerance of the core thickness was applied at a

central value of 5.7 μm thickness and then the bending loss was calculated at bending radius of 7 cm. Table 5-3 shows the bending loss changes depending on the variation of the core thickness. Here, A 2% variation of core thickness causes a relatively big change in the bending loss at 980 nm, 1030 nm and 1060 nm due to the variation of the fundamental mode cut-off. However, it is possible to compensate variations in the core thickness and other core parameters by changing the bending radius. Then the sharpness of the filter remains almost unaffected by a small change in core thickness.

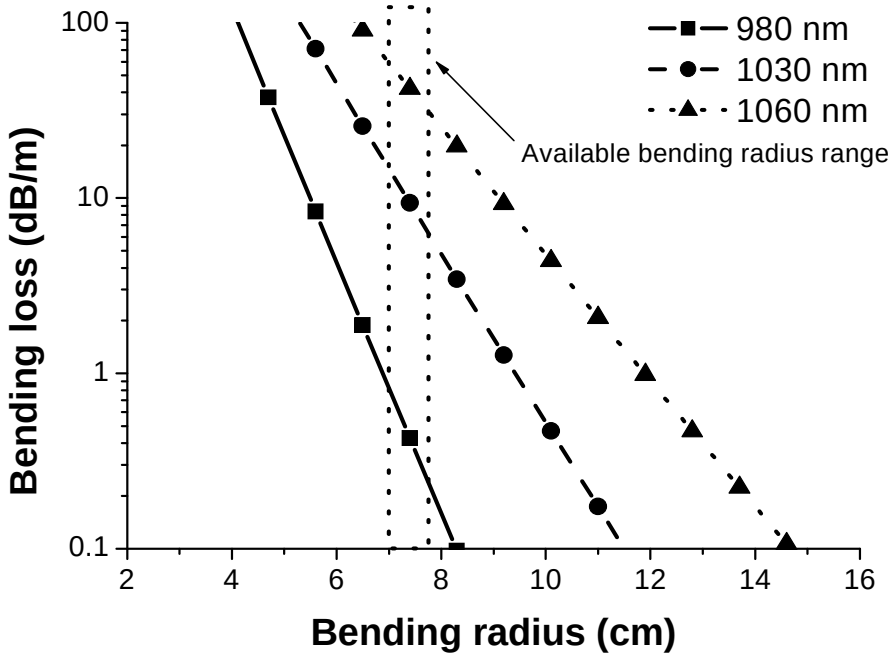

Figure 5-8. Bending loss vs. bending radius at three different wavelengths, 980 nm, 1030 nm, and 1060 nm

Table 5-3. The bending loss variation dependence on the 2% tolerance of the core thickness.

Core		Depressed clad		Hole radius (μm)	Bending loss (dB/m) at bending radius : 7 cm		
Thickness (μm)	NA	Thickness (μm)	NA		980 nm	1030 nm	1060 nm
5.7+0.114	0.073	11.4	0.080	5	0.14	3.19	14.80
5.7					0.82	14.70	59.10
5.7-0.114					2.33	33.74	117.23

5-1-3. Experimental investigation of the Yb:Al-doped DCHOF laser at 980 nm

A Yb-doped DCHOF preform (LF239) using the MCVD and solution doping technique was fabricated. The solution was composed of 1g $YbCl_3 \cdot 6H_2O$ and 2g $AlCl_3 \cdot 6H_2O$ in 200cc methanol (99.9999 % purity), which provides ~1500 ppm of Yb ion concentration in the aluminosilicate glass host. At the final collapsing stage, a hole of 0.5 mm diameter was left in the preform. The preform diameter was 12 mm. It was etched externally to 6 mm diameter in the concentrated HF bath in order to obtain the expected fiber structure. The etched preform was then milled to a double D-shape to improve the pump absorption by breaking the circular symmetry. The flat sides of the D-shape fiber were located around the fiber asymmetrically. The preform was then drawn to a fiber (F645-LF239), with 120 μm diameter inner cladding, and coated with a low-index polymer (UV curable) outer cladding, which provided a nominal inner-cladding NA of 0.48. The fiber has a central air hole diameter of ~10 μm, with a ring shaped Yb-doped alumino-silicate core and a depressed inner cladding section of thicknesses ~5.7 and ~11 μm respectively, as shown in figure 5-9. The core and the depressed cladding index differences were 0.0016 (NA_{co} ~ 0.073) and -0.002 (NA_{dip} ~ 0.080) respectively, both with respect to

the silica inner cladding. Thus the parameters of the fabricated fiber are the same as those used for our modal calculations in the previous section. The low-power pump absorption was 1.3 dB/m.

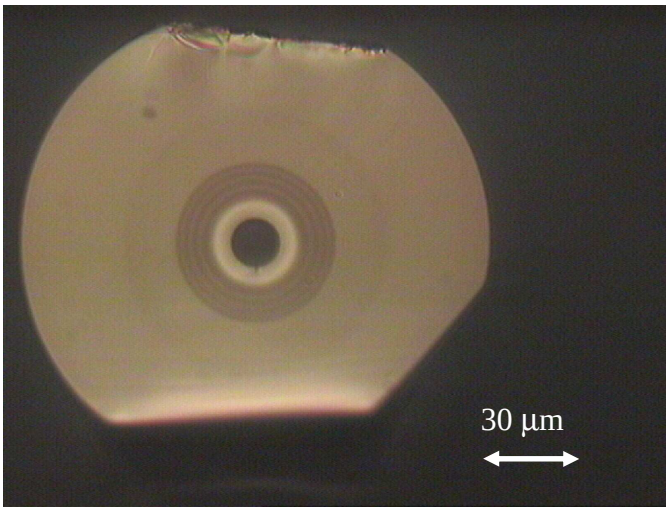

Figure 5-9. Microscope cross section image of the Yb:Al-doped DCHOF (F645-LF239).

.

The LP_{01} mode cut-off behavior of the fabricated DCHOF was verified by measurements of transmission spectra. A spectrally flat white light source was used for the transmission measurement. Both ends of the DCHOF were collapsed and then spliced to single mode fiber (SMF), in order to remove the cladding modes guided in the inner cladding. Figure 5-10 shows the transmission spectra in a 50 cm long Yb-doped DCHOF for bend radii of 15, 7 and 4 cm. Based on the calculated results, it can be assumed that the bending loss can be so low as to be ignored at the bending radius of 15 cm for wavelengths shorter than 1030 nm. Although the DCHOF does have a well defined fundamental mode cut-off in theory, the practical cut-off is less well defined. In a double clad fiber, the mode remains guided by the inner cladding even beyond the fundamental mode cut-off and can be captured back by the single mode fiber. This may cause the discrepancy between the

measured and calculated data of the bending loss. Moreover, in Yb-doped fibers, Yb absorption at 980 nm is significantly high, which prevents us from measuring the bending loss around 980 nm. As shown in figure 5-10, the bending loss at 980 nm cannot be experimentally estimated, while the bending loss at 1030 nm was measured as 9.2 dB/m at the bending radius of 7 cm and 15.2 dB/m at the bending radius of 4 cm. Comparing it with the calculated results in figure 5-8, at the small bending radius (4 cm), the difference between the measured and calculated loss is quite large. Otherwise, the calculated bending loss at the relatively large bending radius (7 cm) agrees reasonably well with the measured data. Discrepancies might be due to fiber uncertainties such as the tolerance of core index structure and mode coupling. In particular, any back-captured light would influence the result more at small bend radii with theoretically very high bending loss and it would reduce the sharpness of the filter. However, it is also found with non-double-clad fibers that the experimental bending loss spectrum is less sharp than the theoretical one. The 1030 nm measured and calculated bending losses at 7 cm bending radius can be used to more reliably predict the bending loss at 980 nm than the theoretical calculations of figures 5-7 and 5-8. A value of 0.82 dB/m is thus predicted, which is high enough to significantly degrade the efficiency. It is not clear that if the measured filter characteristics are sufficiently sharp for efficient high-power 980 nm operation. Rather, this has to be determined by laser experiments. The bending of the fiber should then be adjusted during laser operation to obtain the best combination of loss at 980 nm and 1030 nm.

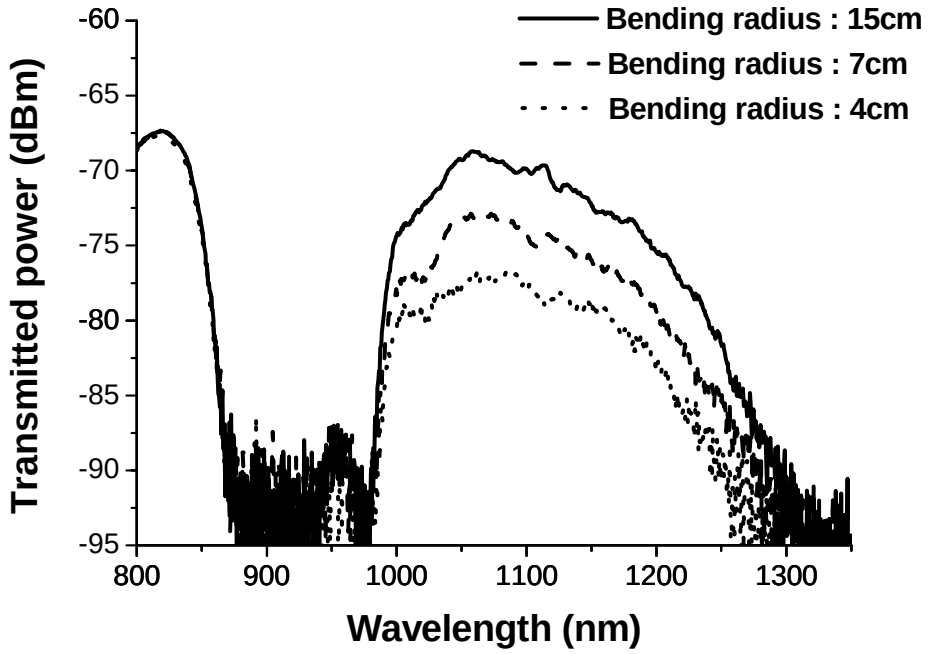

Figure 5-10. Transmitted spectra of the fabricated Yb:Al-doped DCHOF at different bending radii measured with a spectrally flat white light source. (Fiber number : F645-LF239)

The laser performance at 980 nm in a conventional laser configuration, as shown in figure 5-11, was assessed. A 6 m long fiber was pumped by two multimode laser diode sources of relatively low brightness, with 200 μm 0.2 NA fiber pigtails. Up to a total pump power of 19 W was launched into the Yb-doped fiber through both of its ends via a combination of lenses and dichroic mirrors (DMs). A laser cavity was formed between a perpendicularly cleaved fiber end facet (4% Fresnel reflection) at the outcoupling end of the fiber and a DM, highly reflective (HR) at 980 nm and highly transmissive (HT) at 1030 nm, at the other end of the fiber. The bending radius of the DCHOF was varied between 7 cm and 4 cm in order to find the maximum output at 980 nm and then the bending radius was fixed at 6 cm, which yielded the maximum output power at 980 nm. The single-pass pump absorption was 8 dB, which was calculated using the measured data of the input and output pump power in a single-pass of the pump light through the fiber.

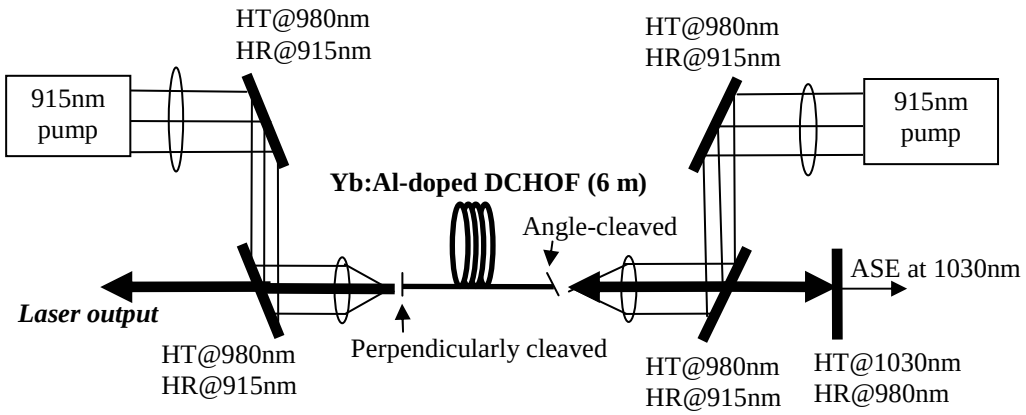

Figure 5-11. Laser configuration for Yb:Al-doped DCHOF operating at 980 nm. HT: High transmission, HR : High reflectivity, ASE : Amplified stimulated emission.

The 980 nm laser characteristics are shown in figure 5-12. The maximum output power was 3.1 W with 34% slope efficiency (η) and 9.2 W threshold power, both with respect to the launched pump power. According to the previous section, with the cross-sections of reference [15], such a high pump absorption requires a suppression at 1030 nm as high as 250 dB. It appears difficult to get such high suppression at 1030 nm without inducing significant bending loss at 980 nm, which may explain the relatively low slope efficiency. A bending loss of ~3.5 dB/m at 980 nm would lead to a slope efficiency of 34%. Moreover, Yb ion quenching can be significant. This will be discussed later in detail. On the other hand, the measured threshold is in good agreement with the theoretical value. However it is still relatively high, which further degrades the overall efficiency.

At this stage, the output was ring-shaped. The out-coupling end of the fiber was then collapsed and the beam quality measured. The power penalty from collapsing the fiber was less than 5%. An M^2 value of 1.09 was obtained, implying that the output beam was single-moded and nearly diffraction limited. Compared to the earlier results using JAC fiber structures [55], this fiber has an order of magnitude larger inner-cladding area.

Although the large inner-cladding results in a much higher 980 nm laser threshold, it does allow for pumping with standard pig-tailed multimode single-emitter laser diodes of relatively low brightness. The use of higher-power pump sources of higher brightness, including commercially available pigtailed diode bars and multi-emitter sources, as well as single- or even multi-emitter sources combined in commercially available tapered fiber bundles, should allow our fiber to be power-scaled well beyond the 10 W level.

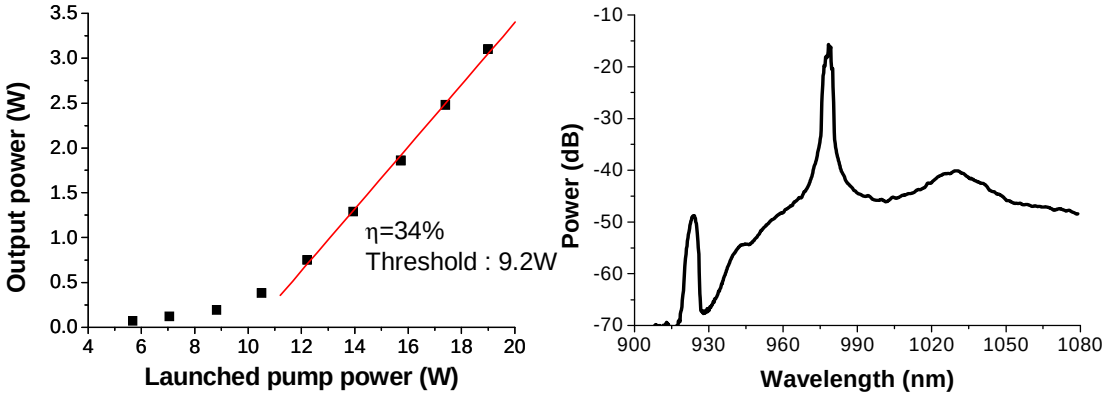

(a) (b)

Figure 5-12. (a) DCHOF laser 980 nm output power *vs*. launched pump power, (b) optical spectrum (res. 1 nm).

5-1-4. Power-scaling of the Yb:Al-doped DCHOF laser at 980 nm

In order to increase the 980 nm output power, the use of a smaller inner-cladding fiber was investigated. This reduces the laser threshold at 980 nm. The same preform (LF239) as the previous one was etched in a bath of HF acid to reduce the outer diameter only. The preform was then milled to a double D-shape as before and drawn to a 90 µm and 80 µm diameter fiber, to match the core parameters of the 120 µm diameter fiber, but with an inner cladding area that is ~44% and ~55% smaller. Figure 5-13 shows the laser

configuration used for the 90 μm and 80 μm fiber. The increased cladding-to-core area ratio led to an increased pump absorption. The fiber was therefore shortened to 3 m. This was pumped from one end using a 915 nm multimode diode, which delivers a maximum power of 32 W from a 100 μm, 0.4 NA, fiber. The maximum launched pump power was 19 W. As before, a laser cavity was formed between a perpendicularly cleaved end facet (4% Fresnel reflection) of the fiber and a 980 nm HR, 1030 nm HT dichroic mirror. This also reflects back the residual pump into the fiber, so that the pump was double-passed through the fiber. The fiber was coiled to an optimum radius of ~7 cm, which again resulted in the highest output power.

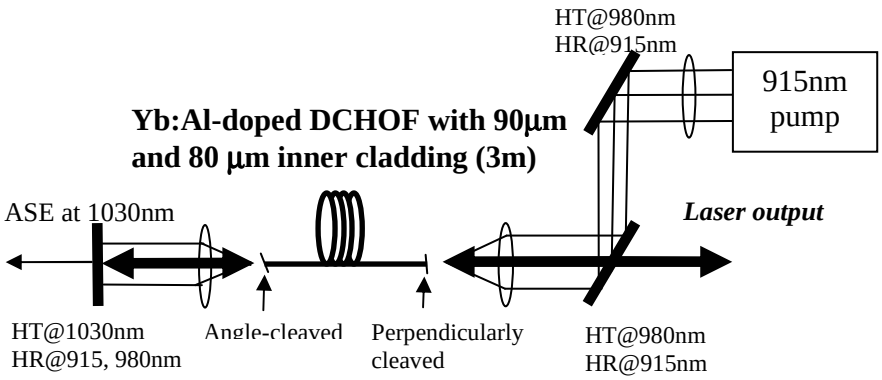

Figure 5-13. Laser configuration for 980nm Yb:Al-doped DCHOF with small inner cladding diameter. HT: High transmission, HR : High reflectivity ASE : amplified stimulated emission

The maximum 980 nm power obtained was 7.5 W, with 49% slope efficiency with respect to launched pump power (Figure 5-14), i.e., higher than in the larger (120 μm) inner cladding fiber. Moreover, in the 80 μm fiber, the efficiency (61% with respect to the launched pump power) was much better and also, the maximum output power was 9.2 W. The threshold for 90 μm and 80 μm fibers reduced to 4.2 W and 3.5 W of the launched pump power, i.e., 54% and 62% lower than the value for the thicker fiber. The beam quality was measured, after collapsing the pump launched end of the fiber, and an M^2 of 2.7 for 90 μm fiber and M^2 of 27 for 80 μm fiber were obtained. Contrary to the 120 μm

diameter fiber result, the beam quality in this case was degraded, even though the core size and NA in both fibers remain the same.

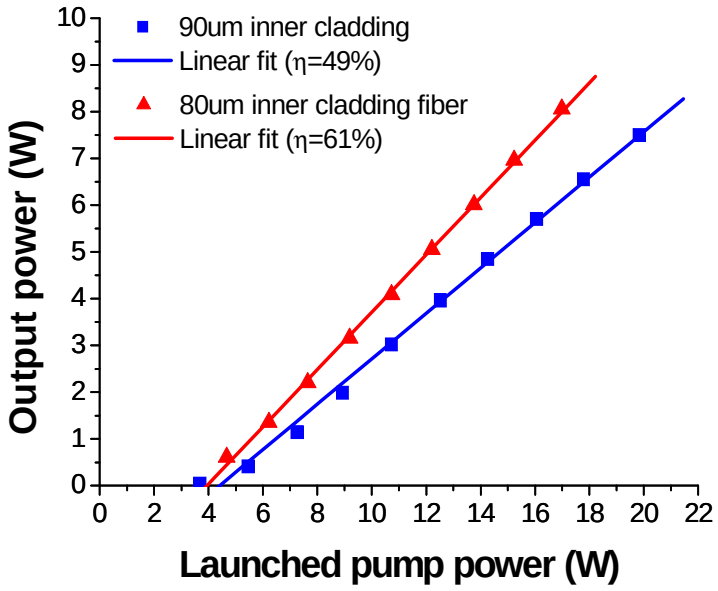

(a)

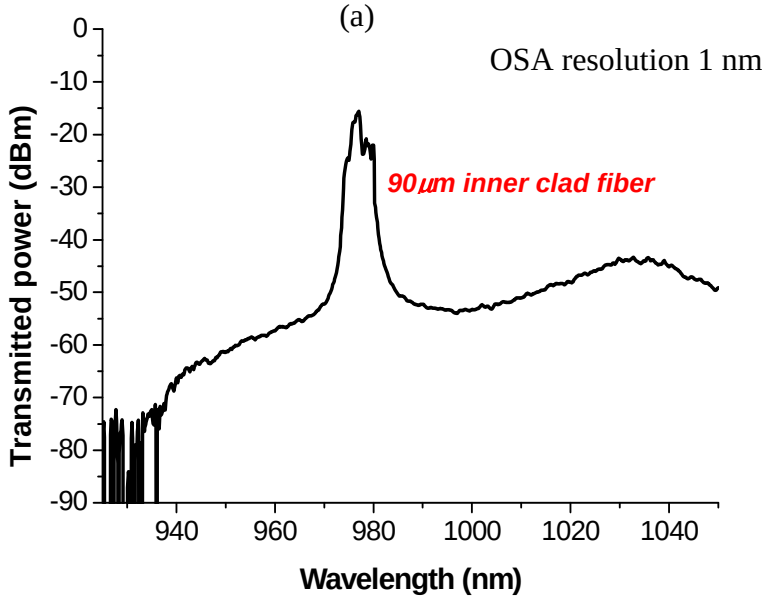

(b)

Figure 5-14, (a) Laser output characteristics of 980nm Yb:Al-doped DCHOF with 90 μm and 80 μm of the inner cladding diameter. (b) Output spectrum for Yb:Al-doped DCHOF laser with 90 μm inner cladding diameter.

The reasons for these differences in power characteristics and beam quality between the 90 and 120 μm diameter fibers is next discussed. The degraded beam quality can either be a result from lasing on cladding-modes or because of 980 nm laser radiation propagating in the core leaks out into the inner cladding. Such leakage can result from bending, since with a double-clad fiber, light lost from the core through bending would actually remain guided by the inner cladding. Even though the core parameters are similar for the 90 and 120 μm diameter fibers, the increased micro-bending of a thinner fiber could explain such differences in core-mode losses between the two fibers.

5-1-5. Analysis of beam quality degradation and low efficiency in the Yb:Al-doped DCHOF laser at 980 nm

In order to further investigate the reasons for the degraded beam quality, additional laser experiments were performed. A pinhole was used to separate the light guided in the core and in the inner cladding. In this case, the laser cavity was formed between a perpendicularly cleaved end facet of the DCHOF fiber and a bulk grating with 60% first-order diffraction efficiency in a Littrow configuration. Both fiber ends were collapsed. Here, the residual pump was not re-launched back into the fiber. The fiber length used was 1.5 m and the fiber with 90 μm inner cladding diameter was used. A similar behavior of the beam quality is expected for the different laser configurations used, despite the differences between them. The output powers were measured before and after the pinhole. The results are shown in figure 5-15. The maximum output power was 3.2 W before the pinhole, with a slope efficiency η of 49% with respect to the absorbed pump power. The beam propagation parameter M^2 was 2.7. After the pinhole the maximum power obtained was 1.95 W, with $\eta \sim 27\%$, and M^2 1.28. Significantly, at low power level (0.5 W output at

980 nm), there is no difference in output power between the two cases at low power, which shows that the laser is (nearly) diffraction-limited then. It can be concluded that bend-induced light leakage from the core into the cladding alone does not explain the degradation in beam quality, since this would be a largely power-independent process. Rather, there must be direct amplification of, and power transfer to, light propagating in cladding-modes, as a result of high gain in areas of the core that are not saturated by the lasing core-mode under high-power pumping. Some of the cladding-modes must have a significant overlap with such high-gain regions. The power-transfer can either be in the form of cladding-mode lasing, or through amplification of light that is leaking out from the lasing core-mode. Since there is a significant feedback at 980 nm, the gain required for cladding-mode lasing is expected to be lower than that required to amplify light leaked from the core mode. This would indicate that cladding-mode lasing is the cause of the degraded beam quality. However, if the leakage from the core mode is sufficiently high into high-gain cladding-modes, this need not be the case. Further experiments, e.g., with mode-selective feedback, would be needed to more definitely clarify this. In any case, the significantly lower confinement of the cladding-modes would explain why the cladding-modes of the 120 μm diameter fiber are not excited. It is also noted that the lack of excited cladding-modes in the 120 μm fiber implies that the leakage of light from the core to the cladding at 980 nm, i.e. the 980 nm bending-loss, is small.

The relatively low slope efficiency obtained in 120 μm inner cladding fiber, and the higher efficiency of the 90 μm fiber is considered. There are few possible explanations to this. As bending only couples light from the core to the inner cladding, bending-loss cannot explain the low efficiency. Furthermore, if bending-loss was anyway a significant loss mechanism, it would lead to large amounts of light emitted from the sides of the fiber. This was not observed. Another possibility would be that pump power absorbed in regions of

the core where the modal field of the core mode is weak cannot be transferred efficiently to the 980 nm laser field. However the low saturation intensity of Yb at 980 nm rules out this explanation. See, e.g., [15]. (Note that by contrast, despite the low saturation intensity, it is still possible for the gain to reach high values in such regions.) The most likely explanation seems to be quenching of Yb-ions, which can severely impact the efficiency of cladding-pumped 980 nm YDFLs [15], [113].

The efficiency of the core-mode lasing of the 90 μm fiber (27% in figure 5-15) is similar to that obtained with the 120 μm mode fiber, emitting only from the core-mode (34% in figure 5-12). Note that while the 34% refers to launched power, the pump absorption is ~90% so the value for the efficiency with respect to the absorbed power is similar, (approximately 37%). The lower efficiency of the core-mode of the 90 μm fiber may be due to pump power transfer to competing cladding modes, when they start to lase. If so, this indicates that a fraction, (37% – 27%) / 37% = 27%, of the absorbed pump power is used for stimulated emission of the cladding-modes rather than the core-modes. From figure 5-15, a slope efficiency for cladding-modes of 22% with respect to all of the absorbed pump power can be inferred. This would correspond to a slope efficiency of 22% / 27% = 81%, with respect to the 27% of the pump power that is available for cladding-pump lasing. Although this is only a rough estimate, a much higher slope efficiency for cladding-mode lasing is in agreement with the quenching hypothesis, as cladding-modes with a much smaller overlap with the Yb-doped core would be much less impacted by Yb-quenching than the core-mode is [15]. Further characterization, e.g. of unsaturable absorption [113], would be needed to firmly establish the impact of quenching in this fiber.

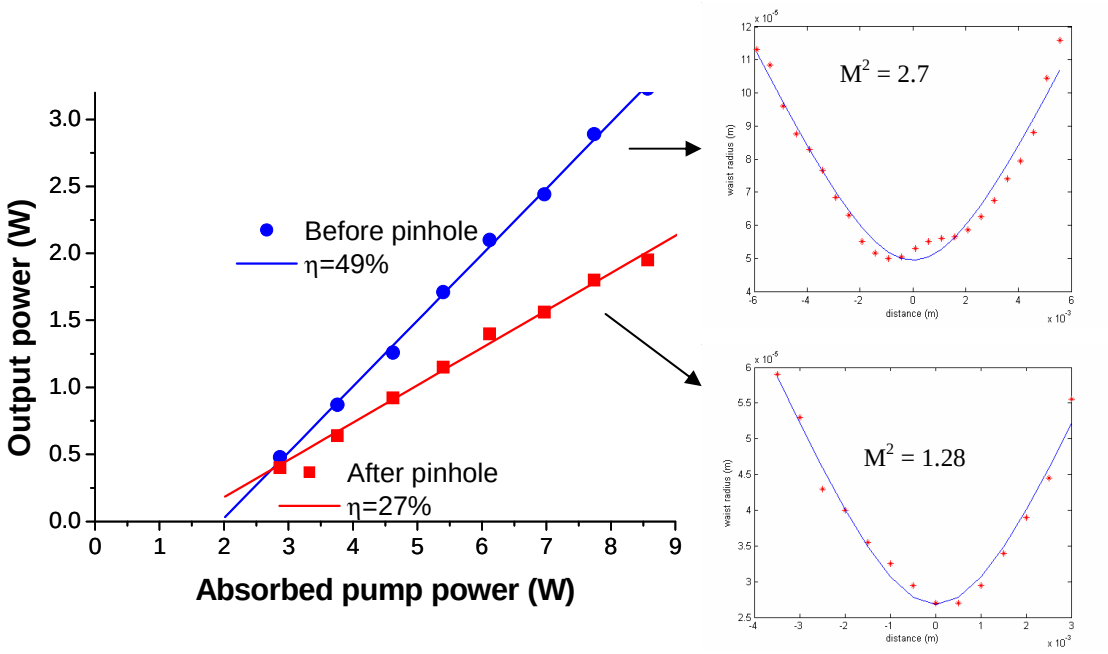

Figure 5-15. The laser characteristics of 980 nm Yb doped DCHOF laser (90 μm diameter) before pinhole and after pinhole. Inset : beam quality measurement data.

5-1-6. Summary of the Yb:Al-doped DCHOF laser at 980 nm

It is still challenging to scale up the output power at 980 nm with the cladding-pump YDFL maintaining a single-mode beam quality due to the problem of cladding-mode lasing. However, based on these results, a solution for suppressing the cladding-mode lasing can be chosen, and it would be the best way to reduce the gain of cladding-mode by adding absorbers for 980 nm in the inner cladding. Furthermore, more sophisticated control of the refractive index will be required for the sharp separation between 980 nm and 1030 nm.

5-2. Yb:Al-doped DCHOF laser operating at ~1040 nm

Generally, Yb-doped fiber lasers have a broad tunable range from 1.0 μm to 1.1 μm [92]. However, it is not power scalable at all wavelengths. While the output power at the longer wavelength side (1.1 μm) can reach above kW levels due to the four-level laser characteristics, the output power at the shorter wavelength side (< 1.06 μm) has still not reached to the kW level because of the three- (quasi three) level laser characteristic [114]. The difficulties of the YDFL operating at 980 nm have already been shown in the previous section. In this section, the power-scaling of the laser at the shorter wavelength side of the 1030-1080 nm emission band of a Yb-doped fiber laser, using the DCHOF structure, will be investigated. The operation at the shorter wavelength in the YDFL theoretically allows a higher quantum efficiency than at the longer wavelength, which could be advantageous in terms of the thermal management in very high output power levels (~kW).

The output power at the shorter wavelength is limited by the relatively high GSA. Fortunately, it is easier to generate the shorter wavelength lasing (~ 1040 nm) than to generate the laser at 980 nm because of the relatively low GSA and high gain at the shorter wavelength. In order to suppress the gain at the longer wavelength (~1.1 μm), the distributed wavelength fiber filter can be used. The DCHOF used in this thesis will be a good solution because it can obtain a single-mode and a relatively large core, whilst maintaining the fundamental mode cut-off wavelength at the proper location. As mentioned in the previous section, the fundamental mode cut-off wavelength effectively shifts to the shorter wavelength side by bending the fiber. If the bending loss is properly controlled, the gain at the longer wavelength will be reduced.

The large core is preferred for scaling up the output power in the YDFL because it allows the improvement of the pump absorption, as well as avoids an optical and thermal

damage and any nonlinear scatterings, such as stimulated Raman scattering (SRS) at the significant power level. However, the large core eventually leads to the multimode output beam. In practice, it is an obvious choice to use a single-mode core in order to obtain a robust single mode output, but it causes the significant fiber nonlinearities, especially, SRS. This is the main obstacle to scale up the output power in a single-mode core. The relatively large core of the DCHOF will mitigate SRS and provide a robust single mode output beam quality.

In this section, using a DCHOF structure, the operation at the shorter wavelength in the Yb:Al-doped DCHOF, is first investigated..

5-2-1. Experimental investigation of the Yb:Al-doped DCHOF laser operating at 1046 nm

In most Yb-doped alumino-silicate fiber lasers, the output wavelength is ~1.1 μm with the lowest threshold, as mentioned before, whilst the Yb-doped phospho-silicate fiber laser can produce the laser output at a relatively shorter wavelength, which is not as efficient as aluminosilicate host due to the limited solubility of Yb ions in the phosposilicate host. However, the DCHOF is available to generate a laser output at the shorter wavelength, $\leq$ 1.06μm by suppressing the amplified stimulated emission (ASE) at 1.1 μm using the fundamental mode cut-off. Even Raman gain at the 1st Stokes wavelength can be reduced due to the induced loss by the fundamental mode cut-off when the cut-off wavelength is located properly between the signal and 1st order stoke wavelength [39] and the power scaling up to multi kW using single mode doped core is possible without the limitation imposed by SRS in fiber-based systems [93].

The same preform as used in the previous section (LF239) was drawn to a fiber with 170 μm inner-cladding diameter (F643-LF239) in order to move the fundamental mode cut-off to a slightly longer wavelength, and coated with a low-index polymer outer cladding which provided a nominal inner-cladding NA of 0.48. The core comprised a 6.2 μm Yb-doped ring (NA ~ 0.07) around an air hole of 18μm diameter, and a depressed ring in the inner cladding of thickness 14 μm (NA ~ 0.08). From these fiber parameters, the modal characteristics, using the equation (4-3) in the previous chapter 4, were numerically analyzed. Figure 5-16 (a) shows the effective indexes changes of LP_{01} mode depending on the wavelength of such a fiber. The fundamental, LP_{01}, mode cut-off is ~1.15 μm. Thus the guided core mode does not exist beyond this wavelength. Experimentally, the cut-off wavelength was measured with a white light transmission measurement, as shown in figure 5-16 (b), and the result is in good agreement with our modeling.

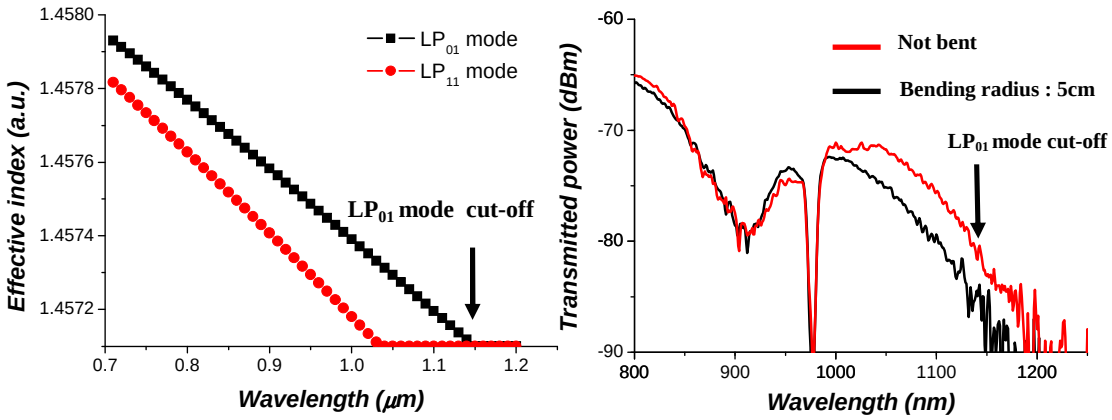

(a) (b)

Figure 5-16. (a) Effective indexes changes of each guided mode in DCHOF (b) Spectrum of transmitted light from a tungsten filament lamp (fiber length : 1 m)

Based on the transmission spectrum, the induced loss by the fundamental mode cut-off is around 10 dB/m, while the loss at 1040 nm was not significantly affected by the fundamental mode cut-off. Although the bending radius was as small as 5 cm, the induced

bending loss was 1 dB/m, which is much smaller than before. The Yb-doped DCHOF was pumped by 975 nm multimode diode stack lasers (Laserline source with 500 W output) through a combination of collimating lenses and dichroic mirrors. Figure 5-17 shows the laser configuration for Yb:Al-doped DCHOF. 5 m long fiber was used and a simple laser cavity was formed between perpendicularly cleaved end facets of the fiber, providing 4% Fresnel reflections. Dichroic mirrors (high reflection at 980 nm, high transmission at 1030 nm) were used to separate signal and pump beams. The output power was monitored at both sides with power meters. The operational pump absorption was 2 dB/m.

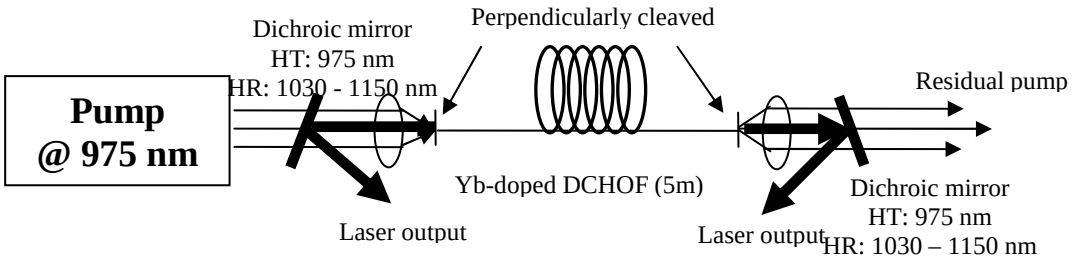

Figure 5-17. Laser configuration for Yb-doped DCHOF . HR: high reflectivity, HT: high transmission.

Figure 5-18 shows the laser output characteristics. The output power reached 59.1 W with a slope efficiency of 81% with respect to the launched pump power and 85% with respect to the absorbed pump power, with a central lasing wavelength of 1046nm. The emission at longer wavelength with low threshold was suppressed by the LP_{01} mode cut-off, instead, the shorter wavelength of 1046 nm was lased in this cavity. The mode field at the longer wavelength is not confined to the doped core and exists as the cladding mode, which is caused to significantly reduce the overlap with the doped core significantly and thus the gain at longer wavelengths is not enough to generate a laser. In practice, the overlap factor at 1046nm was 61%, while it is 3% at 1080 nm according to the calculation. In a narrow wavelength range of 34 nm, the overlap factor is reduced by a factor of 20,

which means that the gain at longer wavelengths can be suppressed by a factor of 20 and it was possible due to the steep LP_{01} cut-off characteristic of DCHOF. In this case, the laser wavelength of 1046nm is quite near the fundamental mode cut-off. It can be expected that a high loss is employed at the signal wavelength due to the fundamental mode cut-off. However, the laser at the shorter wavelength can be achievable with such high efficiency without any additional loss by the LP_{01} mode-cut-off. In addition, only the LP_{01} mode is guided in this ring core at the laser wavelength of 1046nm, where the LP_{11} mode is cut-off based on the modal calculation in figure 5-16 and thus, the output beam quality is expected to be a diffraction-limited single mode, as shown in the previous results [94]. Moreover, as the emission at longer wavelength is filtered out from the core, SRS, the main constraint on power scaling, can be suppressed by the induced loss of the fundamental mode cut-off. In practice, the suppression of SRS was demonstrated using W-type fiber, which has a similar cut-off characteristic and will be discussed in details in chapter 6.

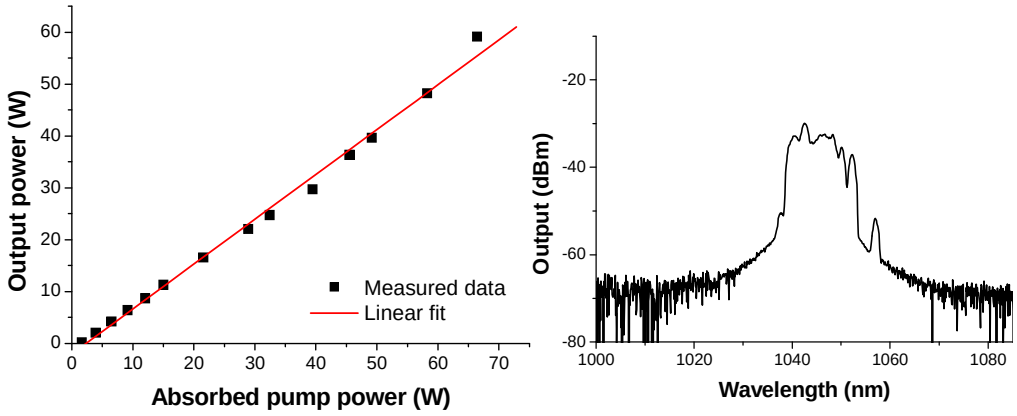

(a) (b)

Figure 5-18. (a) Laser output characteristics of Yb-doped DCHOF at 1046nm, (b) Laser output spectrum (OSA resolution : 2 nm)

The Yb:Al-doped DCHOF thus looks promising to generate lasers over all the emission bands of Yb ions in a silicate glass host.

5-3. Summary

In this chapter, an Yb:Al-doped silica DCHOF, designed with non-zero fundamental mode cut-off, for high-power cladding-pumped 980 nm laser operation was demonstrated. In addition, laser operation at the other shorter wavelength (1046 nm) in the Yb:Al-doped silica DCHOF was also presented. Such fibers act as short-pass filters that allow unwanted longer wavelengths to be suppressed.

Firstly, the requirements of a cladding-pumped 980 nm fiber laser were analyzed, in particular the need to suppress competing emission at 1030 nm and longer wavelengths. Then the ability of DCHOFs of different designs to satisfy these requirements was investigated. It was found that even though the 980 nm emission in the Yb-system is quite close to the competing emission, which normally dominates in a cladding-pumped fiber, it is still possible to design the DCHOF to efficiently suppress the competing emission at the longer wavelength. Experimentally, 3.1 W of output power was obtained in a nearly diffraction limited beam (M^2 1.09) in a fiber with a 120 μm inner cladding diameter, with a laser threshold of 9.2 W and a slope efficiency of 34%. Although, the large inner cladding facilitates pumping with a low brightness pump diodes, but it leads to a high 980 nm laser threshold. The output power increased to 7.5 W when the inner cladding diameter was reduced to 90 μm, while keeping the core parameters constant, as a result of a lower threshold. However, at the same time, the beam quality degraded to an M^2-value of 2.7. This is due to cladding-mode lasing in the thinner fiber with its larger overlap between the cladding-modes and the core. In an improved fiber design, cladding-modes can be suppressed by a 980 nm absorber in the cladding. The relatively low slope efficiency is attributed to Yb-quenching, which can be avoided with improved fabrication [113].

A cladding-diameter of 90 – 100 μm is still compatible with standard low-cost diode sources. Our initial result suggests that the DCHOF approach can be used for low-cost single-mode 980 nm laser sources, with a few watts of output power, pumped by single-emitter multimode diodes with ~ 10 W of output power. It would allow for scaling up the power beyond 10 W with commercially available multi-diode and multi-emitter diode sources including diode bars.

Secondly, through a simple laser characterization of the Yb:Al-doped DCHOF, the suppression of the gain at the longer wavelength side in Yb emission bands was verified. The DCHOF structure was useful to suppress the undesired emission at the longer wavelength when the fiber was properly designed. 59.1W of the output power with 85% slope efficiency with respect to the absorbed pump power at a shorter wavelength, 1046nm, was demonstrated, by filtering out the emission at the longer wavelength (~ 1100 nm). In addition, the high pump absorption in DCHOF was achieved due to the ring core. The output beam is expected to be single-mode based on our modal calculation. Therefore, the Yb-doped DCHOF shows promising prospects to scale up the output power in a single mode core fiber as well as for the generation of output at a shorter wavelength.

PART IV.

THE SUPPRESSION OF THE STIMULATED RAMAN SCATTERING

Chapter 6. The suppression of the stimulated Raman scattering in Yb-doped, W-type fiber.

6-1. The stimulated Raman scattering in the Yb-doped fiber amplifier

6-1-1. SRS in a high power fiber laser and amplifier

Cladding-pumping enables fiber lasers to reach output power levels where they can compete with conventional bulk solid state lasers in many applications such as micro-machining, welding and materials processing. The continuous wave (CW) output power of high brightness cladding-pumped ytterbium (Yb) doped fiber lasers has already reached the kW-level [5, 6]. Moreover, fiber-based master oscillator – power amplifier (MOPA) sources show the potential to scale up the average output power of more sophisticated waveforms, such as picosecond pulses [10]. For those, fiber nonlinearities become an important issue. Stimulated Raman scattering (SRS) is a main obstacle for power scaling of pulsed or CW fiber systems. It can occur in the laser or amplifier itself as well as in any delivery fiber. To date, most high power pulsed fiber sources use a large low-NA core and a relatively short fiber. The resulting reduction of the power density and the interaction length mitigate SRS and other nonlinear effects. This has enabled pulsed fiber amplifiers to be scaled to the MW level and beyond [11, 12]. While large cores eventually lead to a multimode output beam and so a degraded beam quality, the beam quality obtained with a multimode core can be improved by filtering out the higher order modes, e.g., by tapering the fiber or by coiling a low-NA fiber [56, 57]. However, these methods have their

limitations and may be difficult to implement in a robust and reliable manner. In practice, the acceptance of mode-filtered and short fiber devices has been slow in commercial products. Furthermore, those methods designed to achieve high peak powers and diffraction-limited output are difficult to implement in high power delivery fibers, which is another important application.

Hence, a single-mode core still remains an obvious choice for high beam quality. However, a single-mode (i.e., small) core requires a long fiber in the cladding-pumped configuration, because of the relatively low pump absorption due to the large area ratio between the inner cladding (pump waveguide) and the Yb-doped core. The resulting strong interaction of the optical field with the small core over a long fiber will reduce the SRS threshold significantly [58]. The SRS threshold becomes proportional to the inverse of the fourth power of the core diameter. Therefore, the suppression of SRS is required in order to scale up the output power in a small-core robustly single-mode system. Recently, several groups have demonstrated SRS suppression through bending the single-mode fiber and thus by introducing wavelength dependent loss [64, 65]. However, such fibers with a normal step index structure will introduce a significant amount of loss at the signal wavelength too, because of the relatively slow dependence of bending loss on the wavelength. Recently, a dual hole assisted fiber with the fundamental mode cut-off has been suggested for the suppression of Raman gain [39]. This fiber can provide a sharper cut-off characteristic, but the fiber was passive rather than active, and no amplifier or laser results were presented.

In this chapter, a W-type fiber designed with a true fundamental mode cut-off is proposed for SRS suppression in a high power fiber-based source with a single-mode output. In several Yb-doped fiber-based sources, the SRS suppression will be demonstrated experimentally. The use of a small core fiber, readily compatible with existing fiber

technology, would allow for a compactly packaged, all-fiber high power source.

6-1-2. SRS suppression: approach and simulations

In a co-pumped YDFA, the power evolution of the pump (P_P), signal (P_S) and Raman Stokes (P_R) (the lower indices, P, S and R indicates the pump, the signal and Raman Stokes respectively) is determined by the following coupled differential equations in the steady state,

$$\frac{dP_P}{dz} = [(\sigma_P^a + \sigma_P^e)N_2 - \sigma_P^a]N\Gamma_P P_P, \tag{6-1}$$

$$\frac{dP_S}{dz} = [(\sigma_S^a + \sigma_S^e)N_2 - \sigma_S^a]N\Gamma_S P_S - \frac{\nu_S}{\nu_R}\frac{g_R}{A_{eff}}\Gamma_R P_R P_S, \tag{6-2}$$

$$\frac{dP_R}{dz} = [(\sigma_R^a + \sigma_R^e)N_2 - \sigma_R^a]N\Gamma_R P_R + \frac{g_R}{A_{eff}}P_S\Gamma_R(P_R + P_{spon}\kappa) - \alpha_R P_R. \tag{6-3}$$

Here, σ_i^a and σ_i^e ($i = P, S$ and R) are the absorption and emission cross sections of Yb-ions and N is total number of Yb-ions in the doped core. Γ_i is the mode overlap with the Yb-doped area, A_{eff} is the effective area for the Raman interaction, ν_S and ν_R are the signal and Raman Stokes frequencies, and g_R is the Raman gain coefficient of standard single-mode germanosilicate fiber at ~1 μm (~1x10^{-13} m/W in case of polarized light and reduced by a factor of 2 for unpolarized light). P_{spon} is the spontaneous Raman scattering power, which becomes ~177 nW when assuming an effective Raman Stokes bandwidth of ~1 THz and that one photon is generated per mode per unit time per unit frequency. κ is a polarization factor ($\kappa = 1$ for polarized light and $\kappa = 2$ for unpolarized light). Although, depending on the operating conditions, amplified spontaneous emission (ASE)

from the Yb-ions may be important in an amplifier system, a similar spontaneous emission term resulting from the Yb-ions is neglected in this calculation. Furthermore, α_R is the background attenuation coefficient of the Raman Stokes wave. The motivation for this work was to make α_R large enough to suppress the build-up of the Stokes wave. By contrast, the background attenuation coefficients for the pump and signal waves are small, and have been neglected. Finally, N_2 is the normalized excited-state population of the Yb-ions, which becomes

$$N_2 = \frac{\sigma_p^a P_P \Gamma_P / Ah\nu_P + \sigma_S^a P_S \Gamma_S / Ah\nu_S + \sigma_R^a P_R \Gamma_R / Ah\nu_R}{1/\tau + (\sigma_P^a + \sigma_P^e) P_P \Gamma_P / Ah\nu_P + (\sigma_S^a + \sigma_S^e) P_S \Gamma_S / Ah\nu_S + (\sigma_R^a + \sigma_R^e) P_R \Gamma_R / Ah\nu_R} . \quad (6\text{-}4)$$

Here, τ is the fluorescence lifetime of the Yb-ions and h is Planck's constant. , A is the Yb-doped area (typically the core area),

Though equations. (6-1) – (6-4) are for the steady state, they can also be used in the quasi-steady state. In our case the pulse energy will be on the μJ level, which is low compared to the intrinsic saturation energy of a typical single-mode YDFA (~ 10 μJ or more). In this situation, in the interaction with the Yb-ions, described by equation (6-4), the average power of the signal should be used. However, the Raman interaction is near-instantaneous so, for that, the peak powers must be used. The Yb-induced amplification described by equations (6-2) – (6-3) applies to both instantaneous and average power. Hence, the peak power, rather than the average powers, should be used in equations (6-2) – (6-3). The pump is cw, and its cw power should be used in equation (6-1).

The Raman Stokes power is generally dependent on the signal intensity and the fiber loss at the Stokes wavelength (α_R) from equation (6-3). Therefore, the design approach for SRS suppression is to either choose a larger core fiber, e.g., a low-NA large mode area (LMA) fiber [95, 96], which increases the effective area, or to enhance the loss

at the Stokes wavelength without any additional loss at the signal wavelength. In this chapter, the second option was selected, and the core structure was designed in such a way that the propagation loss at the Raman Stokes wavelength would be high while the loss at the signal wavelength would remain low. For this, a W-type fiber was used, which only guides light with wavelengths shorter than the cut-off wavelength of the fundamental LP_{01} mode [8, 14, 37]. Light above that wavelength escapes from the core. The interaction between the core, or light guided in the core, with any un-guided light is drastically reduced. W-type fibers have been used in the past few years for Nd-doped double-clad fiber lasers at around 930 nm [8, 46]. These require that emission from the competing unwanted 1060 nm transition is suppressed. Similarly, a W-type fiber designed for appropriate LP_{01} cut-off wavelength can effectively suppress SRS.

Although a W-type fiber does have a well-defined fundamental-mode cut-off in theory, the practical cut-off is less well defined. This is particularly so since the effective index of the mode, which becomes lower than the refractive index of the cladding for wavelengths beyond the cut-off, varies quite slowly with wavelength near the cut-off. Furthermore, in a double-clad fiber, the mode remains guided by the inner cladding even beyond the cut-off wavelength of the core structure. The overlap of the fundamental mode with the core decreases significantly even before the theoretical cut-off wavelength is reached due to an increasing mode field diameter. The gradual decrease is continuous beyond the cut-off. The details depend on the geometry of the inner cladding. In addition, as the mode field diameter increases near to cut-off, mode-coupling and micro-bend loss to cladding-modes becomes significant in double-clad fibers. This spreads the light out among modes of the inner cladding. This will be significant in a small inner cladding as mentioned in the previous chapter 5. However, in the case of W-type fiber in this chapter, the inner cladding area is over 1000 times larger than the core area, so further interaction

with the core becomes negligible. Thus the light is effectively lost from the core.

In practice, bending, including micro-bending, would shift the effective cut-off to a shorter wavelength, and increase the loss at a fixed wavelength, without any change of the qualitative behavior of the fiber. With or without bending there is a gradual increase, with wavelength, of loss from the core to the surrounding inner cladding, rather than a sharp cut-off. This justifies the use of a simple loss coefficient for the Stokes wave, on both sides of the cut-off wavelength, instead of a more complex, but probably not more accurate, analysis of the modal fields and mode-coupling. Experimentally, the performance of the amplifier will be optimized by bending the fiber, to induce as large as possible loss for the Stokes wave, but stopping before the loss-increase at the signal wavelength starts to degrade the performance.

In order to theoretically evaluate the maximum signal output power from an Yb-doped fiber amplifier, as limited by SRS without considering Yb ASE, the coupled equations (6-1) – (6-4) for the pump, signal and Raman Stokes, was numerically solved. The fiber had an effective area (A_{eff}) of 75 μm^2, and a pump absorption of 0.3 dB/m in the cladding-pump configuration. The Yb^{3+} ion concentration in the core is 1.65×10^{25} ions/m^3. The absorption cross section at the pump wavelength (980 nm) is 2.4 pm^2, the absorption and emission cross section at the signal wavelength (1060 nm) is 0.005 pm^2 and 0.3 pm^2 respectively and the lifetime of Yb^{3+} ions is 0.8 ms. An average signal power of 2 W is launched into the fiber, which is equivalent to ~600 W peak power for 103 ps 32 MHz repetition rate pulses in the experiment. The power of the cw pump was varied to evaluate the obtainable signal output power, limited by SRS. The pump and signal are co-propagating from $z = 0$ to $z = L$ (L = 23 m is the fiber length). The Raman Stokes wave also starts to evolve from the input end of the fiber. Since the physical length of the pulses in the fiber is only 2 cm, i.e., much shorter than the fiber, SRS will only be effective in the

forward-propagating direction. The pump and the signal wavelengths are 980 nm and 1060 nm respectively. The 1st order Raman Stokes appears at 1114 nm. Raman conversion to higher Stokes orders is neglected, as only the regime in which the power in the 1st order Stokes wave will be small is considered. The dispersion of the W-type fiber was calculated, which is considered to be –38 ps nm^{-1} km^{-1}. This leads to a walk-off between signal and Stokes waves of 47 ps over 23 m of fiber. However, the Raman amplification will be concentrated into a smaller length of the fiber, where the signal power is high. In particular, with high loss at the Stokes wavelength, the Raman gain will be too low to overcome the loss for low signal power. This reduces the actual fiber length over which the Stokes wave builds up and over which dispersion is important. Thus, though the walk-off may reduce the interaction between signal and pump pulses somewhat, the effect should be small, and is neglected in our steady-state analysis.

The intrinsic background attenuation coefficient at 1114 nm, induced by material scattering and impurity absorption, is taken to be 0.01 dB/m. This value is in line with losses measured in double-clad Yb-doped fiber, and is much lower than what will be required to suppress SRS. The mode overlap factors of the signal and Raman Stokes (Γ_S , Γ_R) are approximated to unity. Although for the signal, the overlap factor was estimated to be 0.77, the difference this makes will not be significant compared to the impact of other factors such as uncertainties in dopant concentrations and cross-sections. More interesting is the variation of the mode area of the Stokes wave near the cut-off wavelength. For such a fiber, at the theoretical cut-off of 1110 nm, the overlap with the Yb-doped raised-index core, is as low as 0.06. However, at the Stokes wavelength of 1114 nm, the calculated overlap becomes smaller than 0.03, which is approximated by unity. Note that because of uncertainties about the fiber parameters, it is unclear how close to the cut-off wavelength it actually is, and hence what the overlap would be in the actual fiber.

The effective area for the Raman interaction similarly depends on the wavelength, and indeed on the bending if this distorts the mode profile, but also these effects are neglected. Figure 6-1 shows a simulation of the power evolution of the signal and Stokes waves for α_R = 0.0023 m^{-1} (0.01 dB/km). The 1060 nm signal peak power reaches 5.56 kW but subsequent SRS leads to a complete depletion of the signal. In figure 6-1, the maximum signal power coincides with the initial rise of the Stokes wave. The maximum signal power is SRS-limited.. As this maximum is associated with the rapid growth of Stokes power, it is also defined to be the Raman threshold. However, there are many exceptions to this situation: If SRS is completely suppressed, the maximum signal power will be reached in the fiber output end, without reaching Raman threshold. In other cases, the loss at the Stokes wavelength can be so large that when the Stokes wave builds up and depletes the signal, the Raman gain and also the Stokes power drops back before the Stokes power reaches the signal power.

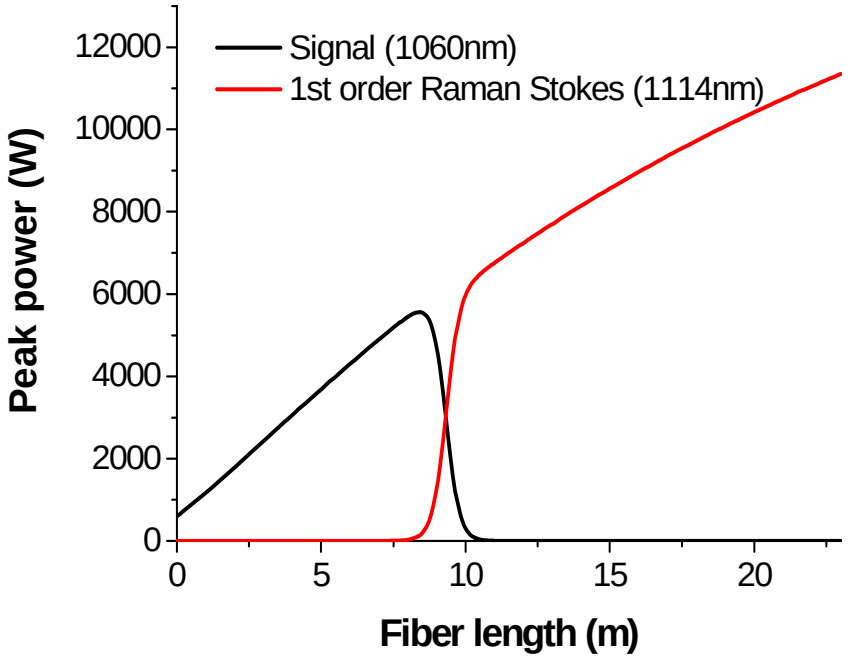

Figure 6-1. Simulated power evolution of the signal and the Raman Stokes wave in our Yb-doped fiber, in the absence of Raman suppression. Absorbed pump power: 40 W (launched pump power : 70 W), input signal: 2 W average power in 103 ps pulses at 32 MHz repetition rate.

In this case, this definition will be used for Raman threshold, whereas the conventional definition of Raman threshold (or critical power), where the Stokes and signal output powers are equal [72, 73], breaks down. It is noted though that with sufficiently high pump power, the Yb-gain would be high enough for the signal power to grow even after the Stokes power exceeds the signal power. In this regime, which is reached neither in experiments nor in simulations, another definition of the threshold power should be used.

It is also pointed out that in order to reach the maximum power of 5.56 kW in figure 6-1, the fiber length would have to be cut. This however would not represent a practical amplifier, as the pump absorption would be only 2 dB. For good pump absorption and efficient operation, this particular fiber should be at least 20 m, and preferably significantly longer. For such long fibers, the peak output power (i.e., Raman threshold with our definition) that could be reached in the absence of any SRS suppression would be significantly lower. In practice this regime would be reached by operating with a higher repetition rate or a lower pump power. The benefits of SRS suppression would be greater with the longer fiber length required for efficient, practical, operation of a strictly single-mode fiber amplifier, as the suppression would act over a longer length of fiber.

Figure 6-2 shows the maximum peak signal power (Raman threshold) and the fiber length at which the corresponding power is reached *vs*. loss at the Stokes wavelength in a Yb-doped fiber amplifier operating at 1060 nm. The maximum power increases linearly with the loss at the Stokes wavelength, as SRS is suppressed. A loss of 20 dB/m at the Stokes wavelength allows for a fiber length of 21 m and a peak output power of 11 kW, before SRS begins to deplete the signal. Note that whereas the simulations extended over 23 m of fiber, the fiber would have to be terminated at the maximum signal power to avoid severe SRS in the remaining fiber, as illustrated in figure 6-1.

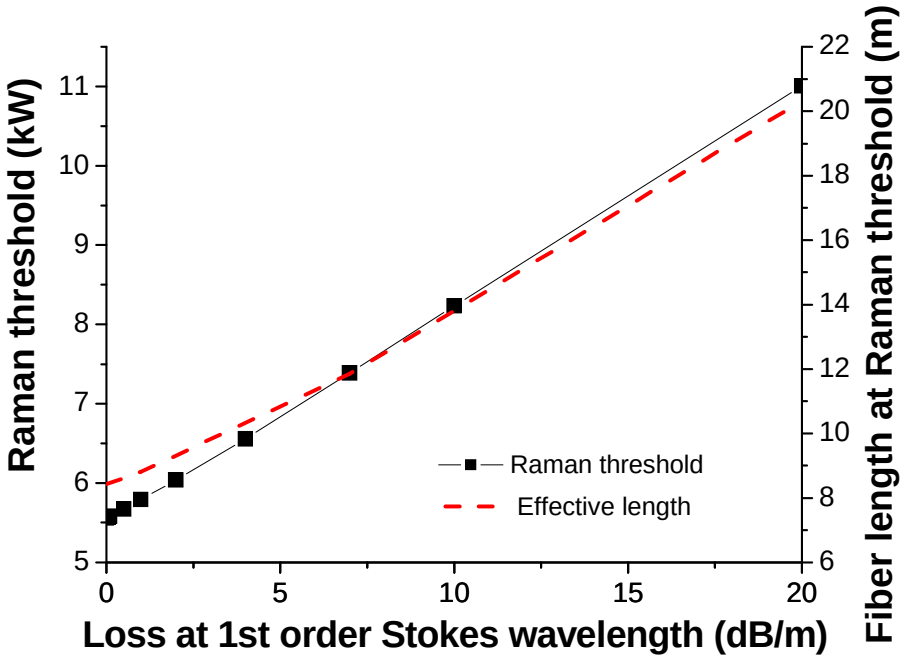

Figure 6-2. Calculated maximum signal power (Raman threshold) and the fiber length at corresponding power vs. loss at the Raman Stokes wavelength. Launched pump power 70 W, pump absorption 0.3 dB/m, input signal, 2 W average power in 103 ps pulses at 32 MHz repetition rate).

6-1-3. SRS-suppressing fiber design

A W-type fiber was designed for a fundamental mode (LP_{01}) cut-off between 1060 nm and 1114 nm. The core structure consists of a 7 μm diameter core, and a 7 μm thick depressed clad. The index difference (Δn) of the doped core and the depressed clad are 0.003 and -0.002 respectively, both with respect to the silica outer cladding (n_{silica} = 1.45). The effective indices of the two lowest-order modes (LP_{01} and LP_{11}) were calculated using the above fiber parameters based on a weakly guiding approximation and linearly polarized modes as presented in reference [8]. As shown in figure 6-3(a), the LP_{01} mode cut-off wavelength, where the effective index (n_{eff}) became equal to the silica cladding index (n_{silica}), will be around 1.1 μm. However, because of the subtle nature of the cut-off as mentioned before, and uncertainties of the fiber parameters, the exact theoretical value of

the cut-off wavelength is of little use and even quite difficult to determine exactly. Furthermore, the induced loss is really more interesting. Figure 6-3(b) shows the bending loss of our W-type fiber at different bending radii near the LP_{01} mode cut-off wavelength, calculated with both the matlab® (The Mathworks, Inc.) code made by myself based on the reference [81] and a commercial software package (Fiber_CAD 1.5, Optiwave Systems). The differences of simulated results between the methods were not significant as far as the loss and the fundamental mode cut-off are concerned. Here, an actual LP_{01} mode cut-off will be at ~ 1.16 μm for the bending radius of 30 cm, where the loss starts to increase significantly. Moreover, the effective LP_{01} mode cut-off shifts to shorter wavelengths by additional bending. At a bending radius of 10 cm, the bending loss becomes as high as 20 dB/m at 1114 nm, while the bending loss at 1060 nm remains below 1 dB/m. In a double-clad fiber, light at the Stokes wavelength would quickly leak out from the core into the inner cladding, while 1060 nm signal light is maintained as a well-confined single mode in the core.

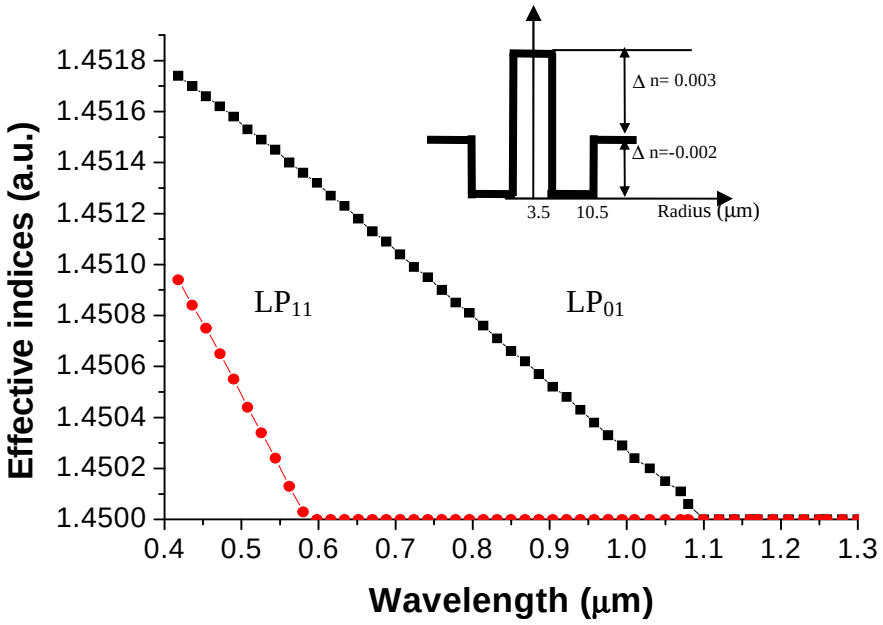

(a)

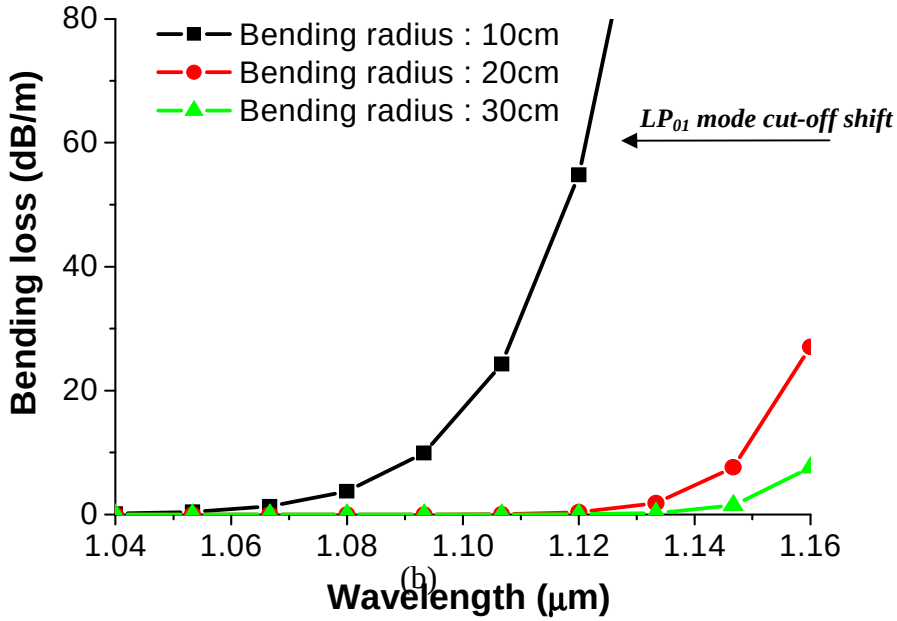

(b)

Figure 6-3. (a) Effective indices vs. wavelength of the W-type fiber we designed. Inset: W-type waveguide (b) Calculated LP_{01} mode bending loss of the designed W-type fiber *versus* wavelength at different bending radii.

6-2. Experimental investigation of the suppression of SRS in Yb-doped, W-type fiber, MOPA source

6-2-1. The fabrication of the W-type fiber

An Yb-doped W-type fiber preform (LF247) was fabricated in house using a standard MCVD and solution doping technique. The solution is composed of 2g $YbCl_3 \cdot 6H_2O$ and 4g of $AlCl_4 \cdot 6H_2O$ in 200cc methanol (purity : 99.9999%). This solution will provide around 2000 ppm of Yb ion concentration in an aluminosilicate host. The preform was further jacketed in order to increase the inner cladding size, for efficient pump coupling into the fiber from a highly multimode diode pump source, whilst maintaining single-mode core dimensions. The preform was milled to a D-shape in order to maintain a uniform pump absorption along the fiber. The preform was then drawn to a fiber (F750-LF247) of inner-cladding diameter 370 μm and coated with a low-index polymer outer cladding (UV curable), which provides a nominal inner-cladding NA of 0.48. The fiber has a core diameter of 7 μm, with a depressed ring in the inner cladding of thickness 7 μm. The core and the depressed cladding index differences are effectively 0.003 and -0.002 respectively, both with respect to the silica inner cladding. The fiber parameters match those of our modal calculations, described in the previous section. The small signal absorption at the pump wavelength, 975 nm, was ~0.3 dB/m. Figure 6-4 (a) shows core transmission spectra of this fiber, measured at different bend radii with a spectrally flat white light source. From this, the actual effective LP_{01} mode cut-off wavelength can be estimated at the wavelength where the loss in the fiber approaches 5 dB/m [82]. Figure 6-4 (b) shows the resulting cut-off wavelengths. It becomes 1157 nm for a straight 1 m long fiber. This value is slightly different from our calculation, which is attributed to imperfections in the refractive index profile and uncertainties in parameters. In general,

though, the fabricated fiber matched well with the expected LP_{01} mode cut-off characteristics and, with additional bending, the cut-off wavelength can be shifted further to shorter wavelengths, between the signal and Stokes wavelengths. However it is emphasized that it is really the loss spectrum rather than the cut-off wavelength that is of interest. Figure 6-4 (a) shows that when the fiber is coiled to a radius of 7 cm, the bend-loss at 1060 nm remains small while it becomes 5 dB/m at 1114 nm.

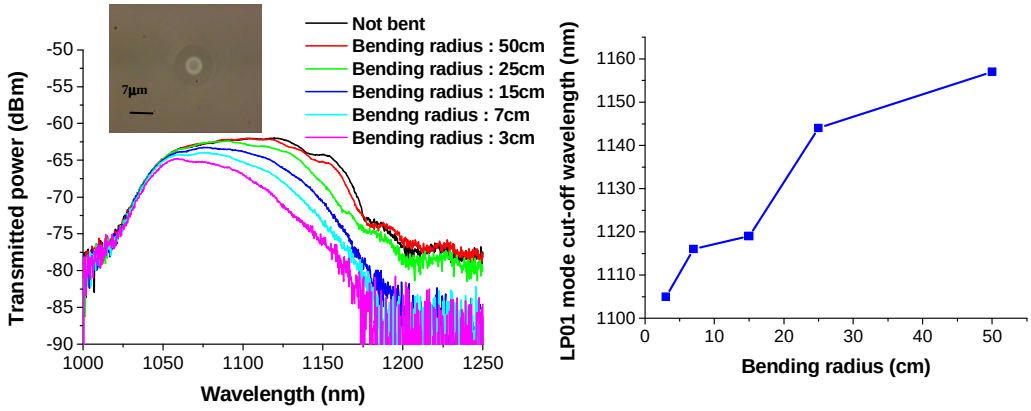

(a) (b)

Figure 6-4. (a) White light transmission spectra for different bend radii of the fabricated fiber measured with a tungsten-halogen lamp. Fiber length 1 m, spectral resolution 1 nm. Inset: back-lit image of our W-type fiber. (b) LP_{01} mode cut-off *vs*. bend radius.

6-2-2. Picosecond pulse, Yb:Al-doped, W-type fiber MOPA

The W-type fiber was incorporated into a pulsed MOPA system (Figure 6-5). Its peak output power would be sufficient to reach the SRS threshold, for low losses at the Raman Stokes wavelength. A 1060 nm fiber pigtailed Fabry Perot laser diode was used as a seed source. It was gain-switched at 32 MHz repetition rate and generated pulses of 103 ps duration. The average output power was 0.5 mW. The diode was first amplified to 3 W average power through three cascaded YDFAs. After transmission through a free-space isolator with 1.5 dB of insertion loss, the signal was free-space coupled into the final high-

power amplifier stage. It was made with a 23 m long piece of the W-type Yb-doped fiber, cladding-pumped in a co-propagating configuration by a diode stack at 975 nm. The Yb-doped W-type fiber, used only in the final amplifier, was angle-polished at both ends.

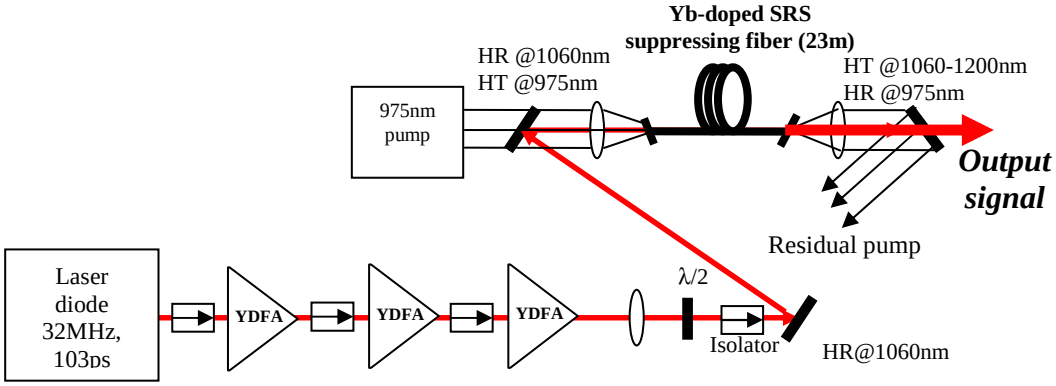

Figure 6-5. Experimental MOPA set-up. HR: high reflectivity, HT: high transmission

Figure 6-6 shows the average output power of the amplifier at different final-stage pump powers for fiber bending radii of 15 and 5 cm, at a constant signal input power. When the fiber was coiled to a 15 cm bending radius, the overall efficiency was 53% with respect to the absorbed pump power, while for a bending radius of 5 cm, the efficiency increased to 80%. For a 15 cm bending radius, a roll-over in the output is observed at 40 W of absorbed pump power, which indicates that the power has been transferred from the 1060 nm signal to the Raman Stokes beam. By contrast, when the fiber was coiled to a bending radius of 5 cm, the average output power increased linearly with the absorbed pump power. There was no roll-over, and the output power was limited by the available pump power.

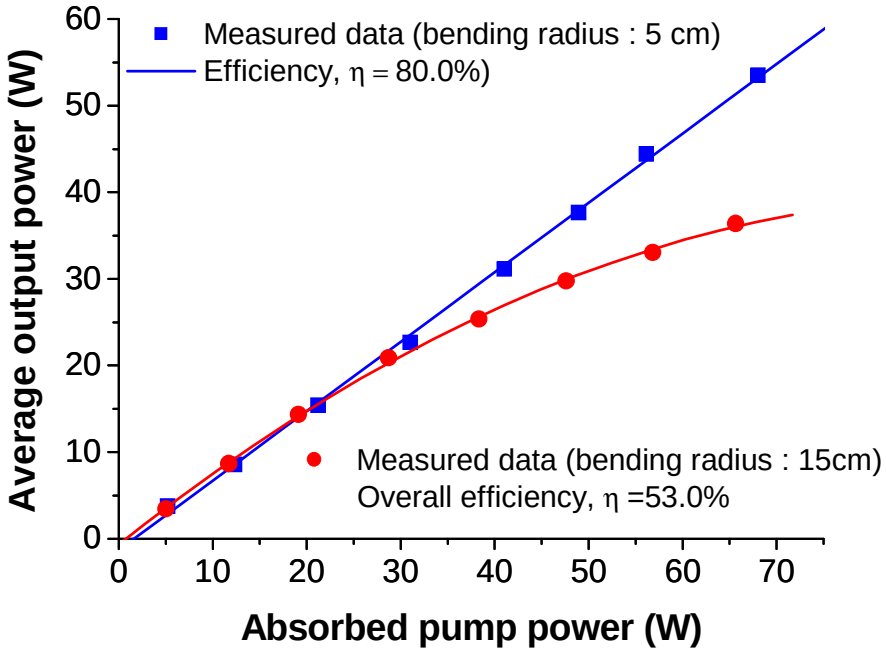

Figure 6-6. Output power characteristics of the MOPA system at different bending radii.

Figure 6-7 shows optical output spectra measured at different pump powers. For a 15 cm bend radius, the Raman Stokes becomes significant for 66 W even less of absorbed pump power. In this case, although the induced loss by the fundamental mode cut-off at 1114 nm was ~2.5 dB/m, estimated from figure 6-4(a), the suppression of SRS was not enough. By contrast, no power has been observed in the Raman Stokes for a bending radius of 5 cm, even at the maximum pump power. This is because of the higher loss at 1114 nm.

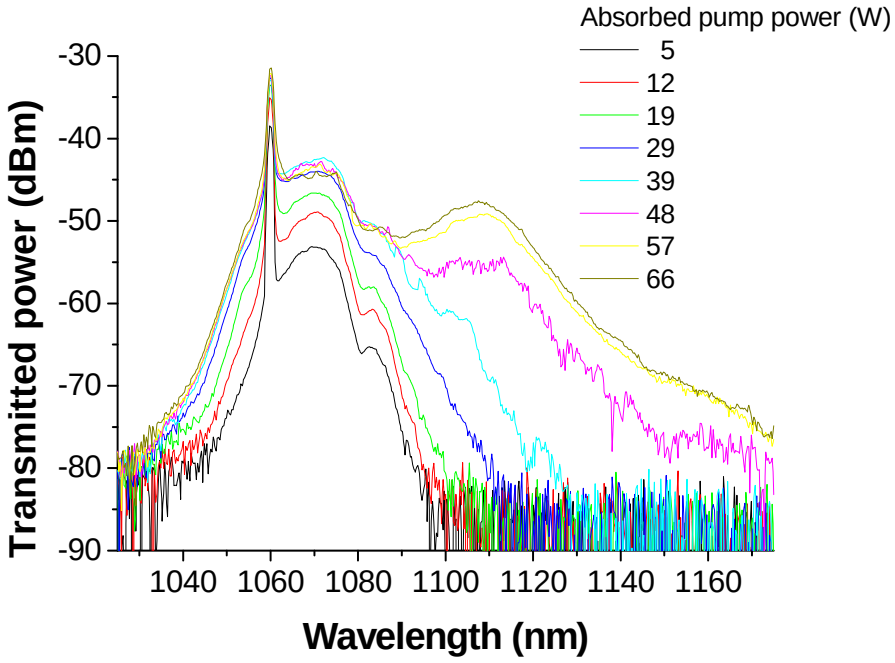

(a)

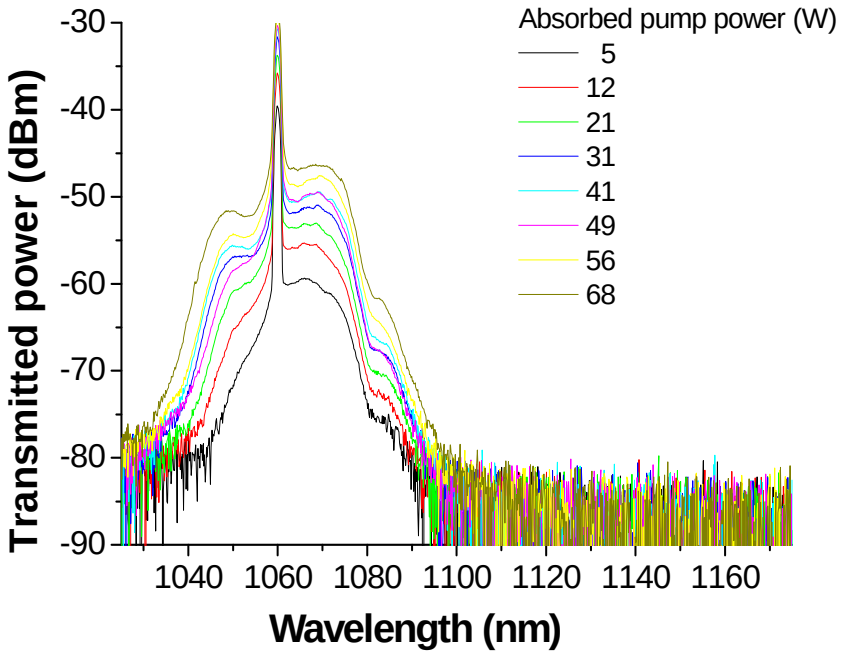

(b)

Figure 6-7. Optical output spectra of the MOPA system. (a) bending radius 15cm, (b) bending radius 5cm. OSA resolution 1 nm.

Figure 6-8 shows the fractions of the total power in the signal at 1060 nm, the Yb ASE, and the Raman Stokes beam, respectively. In order to see the fraction of each power component, the output spectra in figures 6-7(a) and 6-7(b), on a linear scale, were fitted by four Gaussian shaped function. Their center wavelengths, peak heights and widths were found through a least-square fitting procedure for each spectrum. Good fits were obtained. The integrated power, in the different peaks were calculated, and attributed to the signal (1060 nm peak), Yb ASE (1050 nm, 1070 nm peaks) and 1^{st} order Raman Stokes (1114 nm peak). The fiber with the bending radius of 15 cm suffered significantly from energy transfer to both Yb ASE at the longer wavelength (~1070 nm) and the Raman Stokes at 1114 nm. It can be seen from figure 6-8(a) that only 48% of the total power is at 1060 nm at the maximum pump power. On the other hand, when the fiber was coiled to 5 cm bending radius, the signal power increases linearly with respect to the pump power and 81% of the total power remains at 1060 nm at the maximum pump power, which corresponds to a peak power of 13 kW. Interestingly, the spectral filtering induced by the bending is sharp enough to also suppress ASE. This is important, since in this regime with our pulse parameters the dominant loss mechanism is ASE, according to figure 6-8 (a). It is noted that ASE is bi-directional, with most power normally emitted towards the pump launch, i.e., signal input end of the fiber. Here, the backward-propagating power was not monitered, but this could explain the reduction in forward output power seen in figure 6-6 with the 15 cm bend radius. In this case, however, SRS as well as ASE from the earlier amplifier stages would enhance the ASE in the forward direction, but not in the backward direction. Thus, the influence of the backward ASE remains uncertain. Finally, it is pointed out that at higher peak powers, SRS rather than ASE would become the dominant loss mechanism, but they can both be mitigated significantly using a W-type core structure with a fundamental mode cut-off.

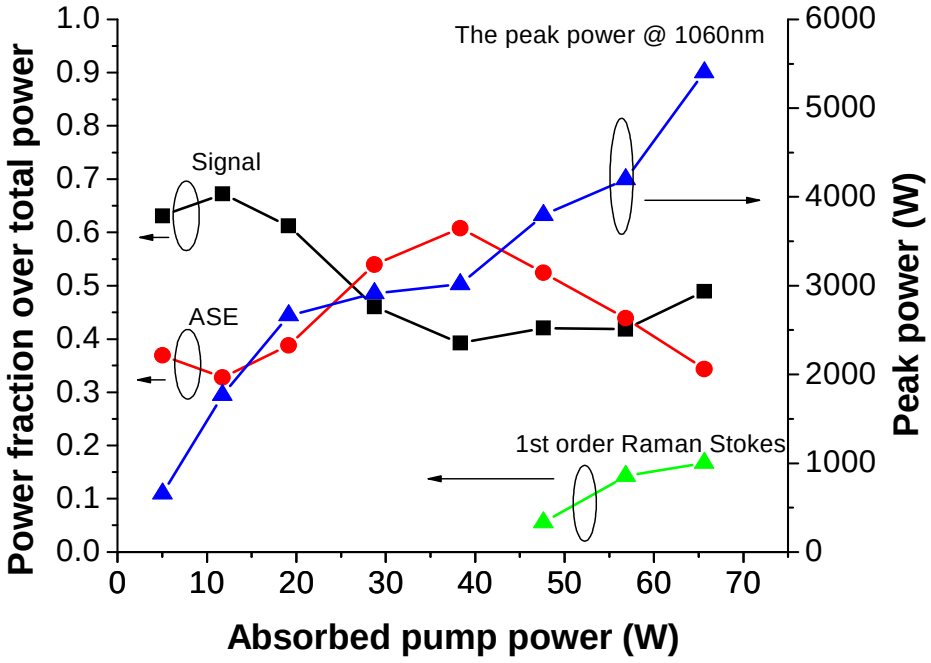

(a)

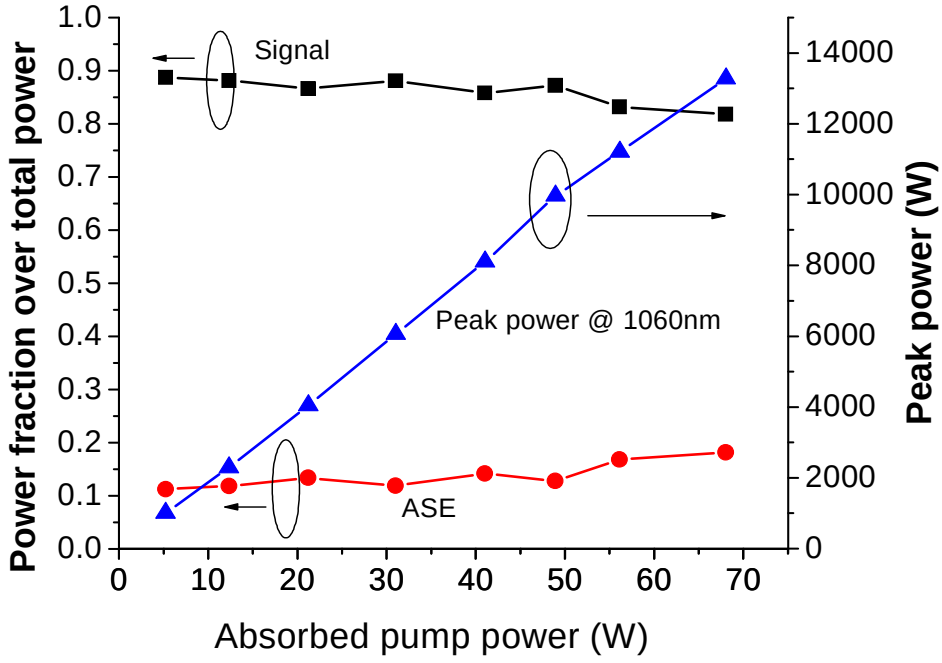

(b)

Figure 6-8. The ratio of the signal, the Yb ASE and the Raman Stokes power over the total output power in the forward direction and the corresponding signal peak power at 1060 nm. (a) bending radius 15 cm, (b) bending radius 5 cm.

6-2-3. Nanosecond pulse Yb:Al-doped, W-type fiber, MOPA

Using the same W-type fiber used in the previous section, the suppression of SRS in nano-second pulse fiber MOPA was experimentally investigated. Figure 6-9 shows the experimental setup for fiber MOPA of nanosecond pulses. As a master oscillator, the semi-conductor diode source was used, which provided 20 nsec pulse width and 100 mW average output power at 100 kHz. This signal was directly free-space coupled into the Yb-doped W-type fiber for SRS suppression after a free-space isolator with 1.5 dB of insertion loss. A 23 m long piece of the W-type Yb-doped fiber, cladding-pumped in a co-propagating configuration by a diode stack at 975 nm, was used in the same manner used in the previous section. The Yb-doped W-type fiber was also angle-polished at both ends.

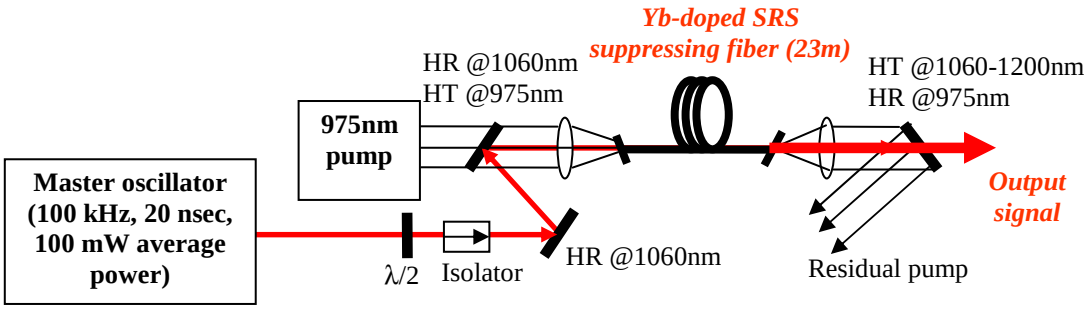

Figure 6-9. Experimental MOPA set-up for nanosecond pulses. HR: high reflectivity, HT: high transmission

Figure 6-10 presents the signal spectrum from the master oscillator used in this MOPA system. The spectral width is relatively broad, which might cause a significant spectral broadening after the final amplifier stage. However, here, the only interest is in the SRS suppression in W-type fiber. Therefore, for simplicity, this signal was just used without any ASE filter in this configuration.

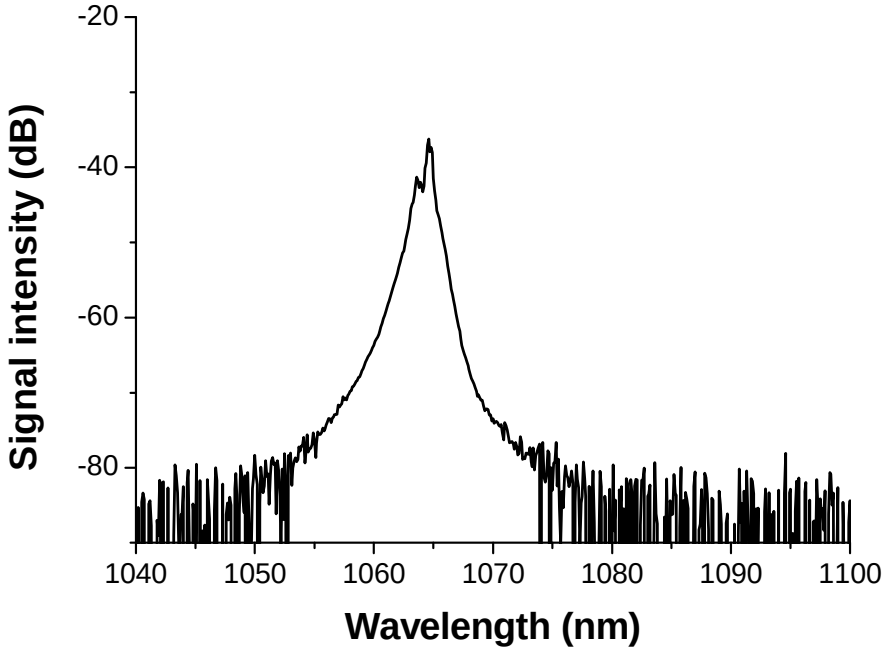

Figure 6-10. The spectrum of the signal source used in nanosecond pulse amplification in Yb-doped W-type fiber.

Figure 6-11 shows the output characteristics of such a MOPA system. Here, tow fibers are used. One is with the fundamental mode cut-off at ~1080 nm and the other is with the fundamental mode cut-off at ~2000 nm, which referred as without the fundamental mode cut-off in figure 6-11. With respect to the absorbed pump power, the slope efficiency was 79% when the fundamental mode cut-off is 1080 nm. In the case of the fiber without the fundamental mode cut-off, there was no roll-over in the output characteristic as well due to transfer of energy in 1st order Raman stokes, as shown in the amplification of pico-second pulses and the slope efficiency was also 73% with respect to the absorbed pump power, which is not so different. This is because the total power of the output beam was measured and the ASE portion of the output beam, whose contribution to SRS is relatively trivial, is significant in this MOPA set-up. However, in the analysis of the spectral purity analysis of the output beam, the SRS suppression in W-type fiber with the fundamental mode cut-off, was clearly observed.

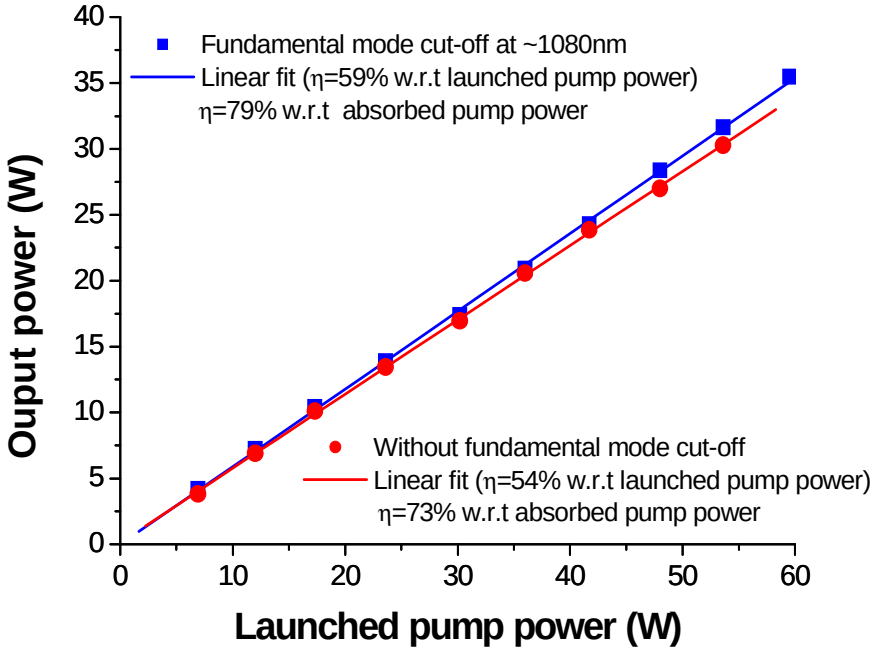

Figure 6-11. Output power characteristics of the MOPA system for nano-second pulse.

Figure 6-12 shows spectra of output beams at 10 W and 50W of pump power. Here, at 10 W of the launched pump power, the 1st order Raman Stokes was shown in the fiber without the fundamental mode cut-off. At 50 W of pump power, most of the power was transferred to the Stokes wave in this fiber.

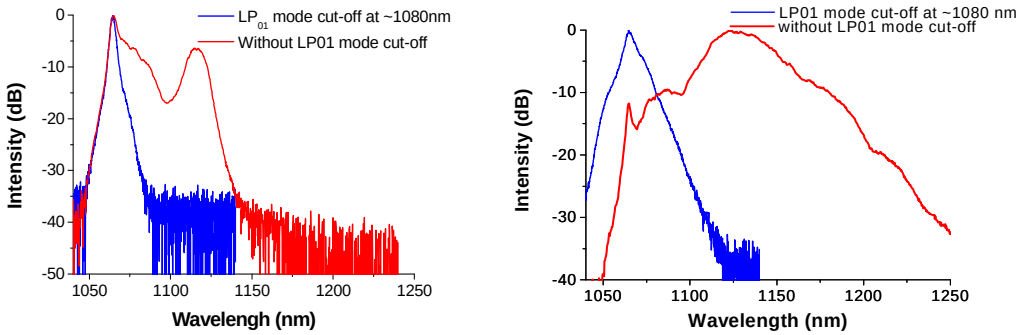

(a) (b)

Figure 6-12. Output spectra of nanosecond pulse fiber amplifier at (a) 10 W pump power and (b) 50 W pump power (Res. 1 nm).

On the other hand, in fiber with fundamental mode cut-off, Raman Stokes does not

appear. Even at 50 W of pump power, the SRS was not observed in the output beam.

On a linear scale, the output spectra at 50 W pump power, were fitted by a three and four Gaussian shaped functions with and without fundamental mode cut-off fibers respectively in order to see the fraction of the power component, as shown in figure 6-13. Their center wavelengths, peak heights and widths were found through a least-squares fitting procedure for each spectrum and each peak was attributed to the signal (1060 nm peak), Yb ASE (1050 nm, 1070 nm peaks) and 1^{st} and 2^{nd} order Raman Stokes (1114 nm and 1160 nm peak). In the case of the fiber with the fundamental mode cut-off, the signal portion in the output beam was 50%, where the spectral broadening due to the spectral phase modulation (SPM) (dot circle in figure 6-13 (a)) was shown to be significant. The other portions were ASE at 1050 nm and 1080 nm. There was no Raman Stokes. Here, the maximum output beam power was 8.8 kW, which is lower than before due to the loss by ASE. Contrary to this, in the fiber without the fundamental mode cut-off, the power was completely transferred to Raman Stokes and the signal (1060 nm) portion was less than 0.1 %. This clearly demonstrate that SRS was suppressed in a nanosecond pulse, high power, Yb-doped fiber MOPA system using a W-type fiber with the proper control of the fundamental (LP_{01}) mode cut-off.

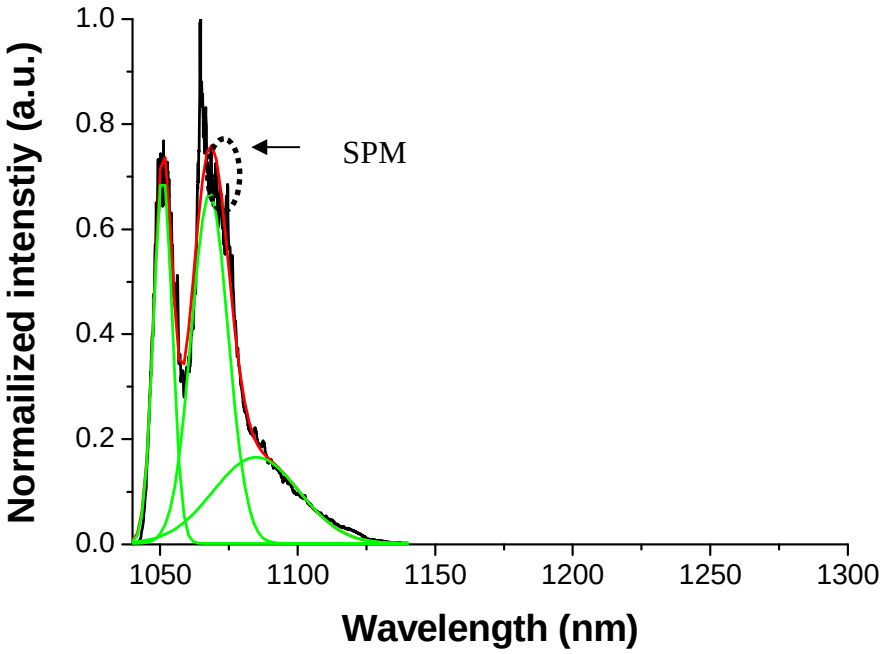

(a)

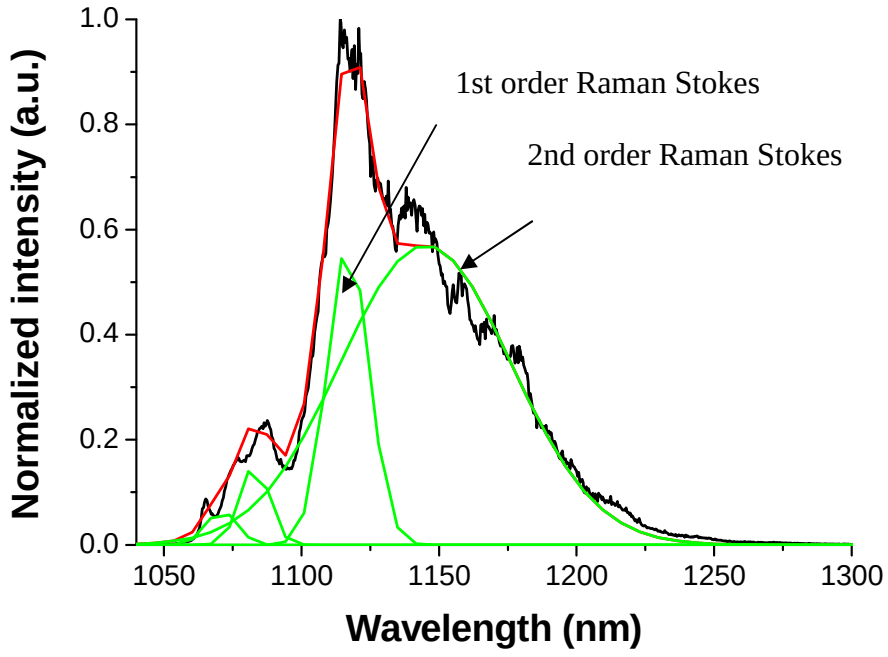

(b)

Figure 6-13. Output power characteristics of the MOPA system for nano-second pulse at 50 W pump power. (a) The fundamental mode cut-off at 1080 nm; SPM : Spectral phase modulation (b) Without the fundamental mode cut-off

6-3. CW characteristics of the Yb:Al-doped W-type fiber

For CW, high power, Yb-doped, single-mode fiber sources, a single-mode core is preferred for a robust waveguide. In order to do this, SRS should be suppressed for power-scaling to kW levels in such a single mode core [58]. In the previous sections, the SRS suppression was demonstrated in a pulsed MOPA system using W-type, Yb-doped fiber with the fundamental mode cut-off. Such a fiber was also employed in a CW configuration to demonstrate SRS suppression. Figure 6-14 shows the experimental setup for CW laser generation. Here, the Yb-doped W-type fiber was cladding pumped by a 975 nm diode stack source through a combination of collimating lenses. The maximum pump power launched into the fiber was 472 W. A simple laser cavity was formed between perpendicularly polished end facets of the fiber, providing 4% Fresnel reflection, and a lens coupled 100% dichroic mirror with a high broadband reflection from 1030 to 1150nm. A 37 m length of the fiber length was used, which is longer than that used in the pulsed MOPA configuration, in order to increase the Raman gain in the CW system.

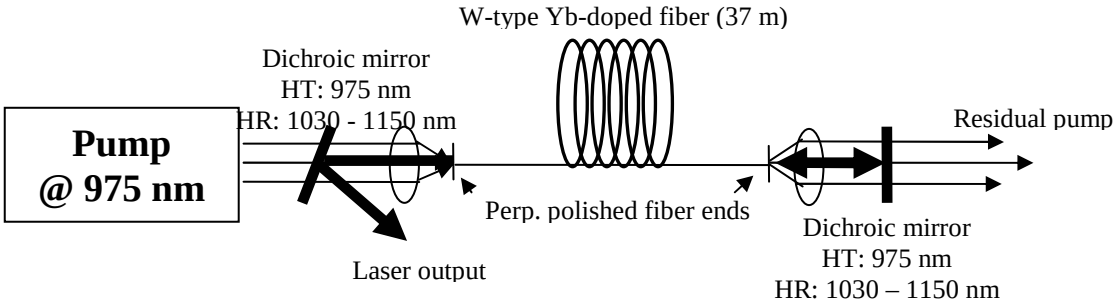

Figure 6-14. Experimental setup. HR: high reflectivity, HT: high transmission.

Figure 6-15 shows the laser output characteristics. The output power reached 314 W with a slope efficiency of 65% with respect to the absorbed pump power at 1077 nm. Based on the Raman threshold calculation, using the equation from the reference [73], the Raman oscillation threshold of a fiber with such a core size (~ 7 μm core diameter) is

around 140 W. However, the Yb-doped, W-type fiber with the fundamental (LP_{01}) mode cut-off at ~1100 nm helped in Raman suppression in a small core fiber. There is no roll-off due to SRS when the output power reached 314 W.

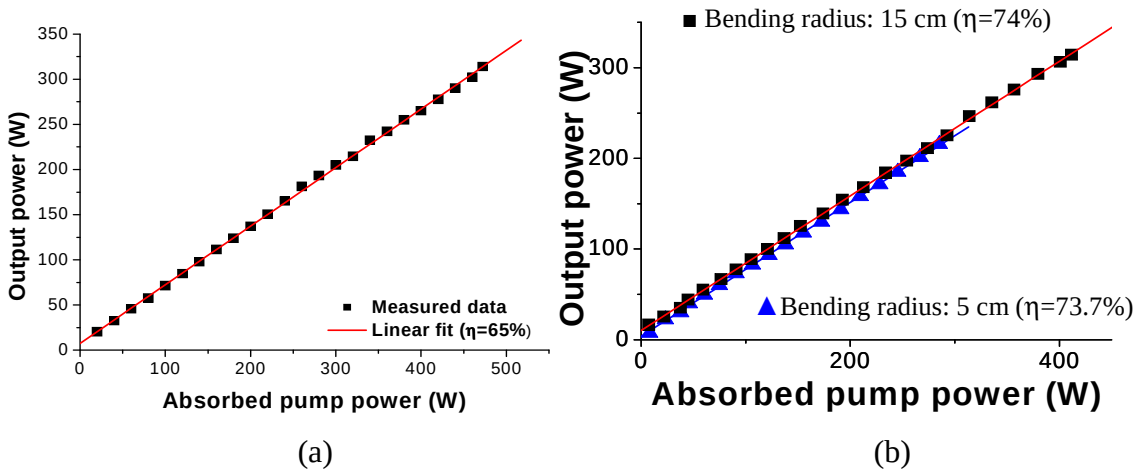

(a) (b)

Figure 6-15. Laser output characteristics of Yb-doped W-type fiber laser, (a) 37 m long fiber, (b) 23 m long fiber with bending radius 15 cm and 5 cm.

It was observed in figure 6-4 (a) that there is a large loss (leakage) of ~5dB/m, for light generated in the core at the 1st order Stokes wavelength (1120 nm). With an effective area of 75 μm^2 when core diameter is 7 μm at 1077 nm, this indicates that loss at 1st order Stokes leakage exceeds the Raman gain at 1120 nm when the signal power at 1077 nm reaches 1.2 kW. This is quite close to the CW damage threshold [122]. In this experiment, even though the output power (314 W) is high enough to generate SRS in a similar step index core fiber [13], the suppression of SRS in W-type fiber was possible because of the proper selection of LP_{01} mode cut-off. The relatively low slope efficiency is due to high background loss caused by the long length of the fiber. When a 23 m long fiber (bending radius : 15 cm) was used, the slope efficiency was 74% with respect to the absorbed pump power and over 300 W of output power at 1077 nm was obtained (figure 6-15 (b)).

The laser wavelength can be tuned to shorter wavelengths, as shown in figure 6-16, by bending the fiber. When the bending radius was changed from 15 cm to 5 cm, the central wavelength moved from 1077 nm to 1058 nm. In this case, the slope efficiency was 73.7% with respect to the absorbed pump power (figure 6-16).

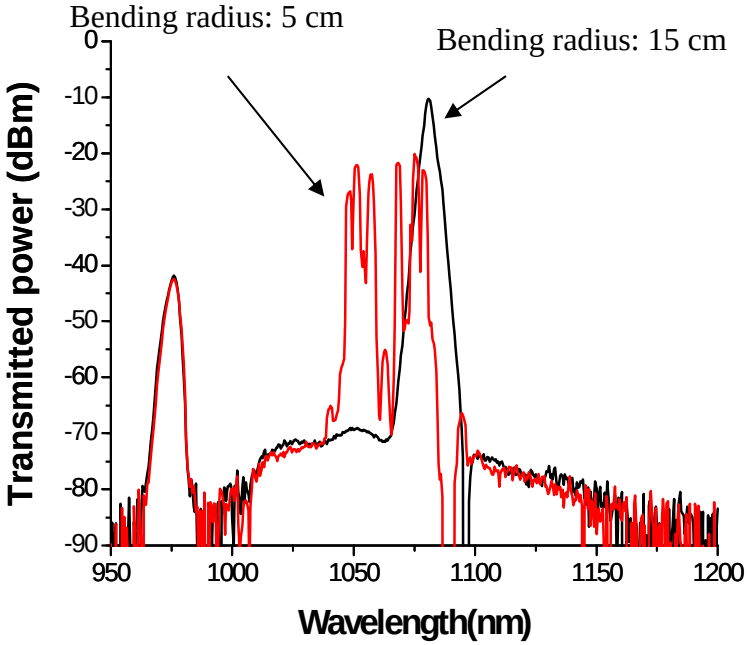

Figure 6-16. Optical spectra of Yb-doped W-type fiber laser when fiber bending radius is 15 cm and 7 cm at maximum pump power. (Resolution 2 nm, fiber length: 23m.)

6-4. Summary

In this chapter, the ASE and SRS suppression in a pulsed high power, Yb-doped, single-mode fiber MOPA system was experimentally demonstrated using a W-type fiber with fundamental (LP_{01}) mode cut-off. A combination of LP_{01} mode cut-off in W-type fiber and additional bending in the fiber can create a significant loss in Stokes wavelength. This suppressed the build-up of the Stokes wave and even the ASE quite close to the signal

wavelength (1060 nm). SRS suppressing W-type fiber used in the final amplifier stage provided 53 W of average output power with 103 ps pulse width at 32 MHz repetition rate was generated, which corresponds to 13 kW peak power. There was no power at the Raman Stokes wavelength in the output beam. Moreover, Yb ASE at longer wavelength (~ 1080 nm) was also significantly reduced. By contrast, when the fiber was bent with 15 cm bending radius, the loss at the Raman Stokes wavelength was not enough to suppress both SRS and Yb ASE, and the peak power dropped to only 5.4 kW. Furthermore, in a ns pulse, Yb:Al-doped fiber MOPA system, the suppression of SRS was also experimentally verified. Here, the maximum peak power was 8.8 kW at 100 kHz repetition rate and 20 nsec pulse width. The output was limited by the Yb-ASE at the shorter wavelength (~1030 nm). The efficiency of this power amplifier was 79% with respect to the absorbed pump power.

In a CW configuration, using a small-core Yb-doped fiber laser, a 314 W output power with 65% slope efficiency with respect to the absorbed pump power with a true single mode output was also demonstrated using W-type fiber. The output power was only limited by the available pump power. The SRS in the W-type fiber was suppressed efficiently even though a small core (7 μm core diameter) and long length (37 m) of the fiber used here.

This result shows that it is indeed possible to suppress the SRS, which is the main obstacle for power-scaling in a high-power fiber system. This can be obtained by using the bending loss created by the fundamental mode cut-off. Therefore, it shows the prospects to scale up the output power in a single mode core fiber to multi kW level in both CW and pulsed fiber based system. Furthermore, the use of a small core fiber, readily compatible with existing fiber technology, would allow for a compactly packaged, all-fiber high power source.

Chapter 7. Conclusion and future prospects

In this thesis, the study on the fiber design and fabrication for high power three level fiber lasers and amplifiers was presented. In recent years, the output power at ~1 μm using YDFL was significantly increased via the cladding-pump technology and competes with bulk-type solid-state lasers in many applications such as material processing. However, various applications require lasers operating at different wavelengths and their power-scaling using the cladding-pump configuration and the realization are still challenging. To overcome this challenge, a novel fiber structure is required at some points.

Rare-earth doped fibers have multiple emission bands but, in practice, it is not possible to obtain the laser output at all emission bands. In order to realize a laser output at a specific desired wavelength, the other competing unwanted stimulated emissions need to be suppressed. The unwanted stimulated emission can build up to a significant power level and prevents laser emission at the desired wavelengths. Although the gain can reach a level which is enough to cause lasing, the simultaneous significant emission at the undesired wavelengths such as ASE and SRS, degrades the gain and efficiency at the wanted wavelength. This is particularly relevant in the cladding-pumping configuration due to the relatively low pump absorption, which requires a long device length. Therefore, a wavelength-selective filter is used to suppress unwanted emissions. In particular, the distributed wavelength fiber waveguide filter should be used, rather than the free-space external filter, because the gain in the fiber is distributed along the fiber and the filtering of the unwanted gain should take place along the fiber. For this, I proposed the step hollow optical fiber (HOF) (chapter 3) and depressed clad hollow optical fiber (DCHOF) (chapter 4 and chapter 5).

As a fiber filter, W-type fiber, with the fundamental (LP_{01}) mode cut-off, is widely used. For the cladding-pumped Nd^{3+}-doped aluminosilicate fiber laser operating at 930 nm, a W-type fiber structure was used. It shows efficient operation of the single mode NDFL at 930 nm. However, W-type fiber is difficult to scale to large core areas because the fundamental mode cut-off cannot be set at the proper wavelength maintaining a large core area. In order to maintain the cut-off wavelength between 930 and 1060 nm as the core size is increased, the numerical aperture (NA) must be reduced. Unfortunately, this makes the cut-off less distinct. A large core area allows more extractable energy in the pulsed system, low fiber nonlinearities, and a large threshold for optical damage. Therefore, the hollow fiber structure was suggested in this thesis. I theoretically and experimentally demonstrated the HOF as the distributed fiber waveguide filter. In chapter 3, I initially presented the modal characteristic of step HOF and have shown the laser output characteristic of Er:Yb co-doped step HOF. Later, I modified the refractive index structure of step HOF and suggested the DCHOF in order to obtain sharp fundamental mode cut-off over the step HOF. In chapter 4, I theoretically analyzed modal properties of the DCHOF. Based on this analysis, I demonstrated a single-mode, Nd:Al-doped DCHOF, operating at 930 nm and through Q-switched pulsed configuration. The larger core area in the DCHOF contrary to W-type fiber, made it possible to extract a much higher pulse energy at 930 nm from Nd:Al-doped DCHOF. In chapter 5, using the Yb:Al-doped DCHOF, I experimentally demonstrated the operation at 980 nm. I carried out a more specific analysis of DHOCF in terms of the fundamental mode cut-off and induced bending loss.

In chapter 6, I utilised the W-type fiber waveguide filter with a single mode core in high power fiber systems. Particularly, it might be used in CW and pulsed fiber systems in order to achieve a robust single-mode output for practical use. For this, the suppression of the stimulated Raman scattering (SRS) is essential. I theoretically and experimentally

demonstrated the suppression of the stimulated Raman scattering (SRS) in a high power Yb:Al-doped MOPA system using the W-type fiber with the fundamental mode cut-off. The high induced loss, caused by the fundamental mode cut-off, reduced the Raman gain at the Stokes wave. Because of that, it prohibited power transition from the desired signal to its Stokes wave. It opens up the possibility of power-scaling up to kW levels in a small and single-mode core, which is an obvious choice for generation of the robust single-mode output.

7-1. Summary of the contribution

The summary of the results I achieved is presented in this section.

- **Step hollow optical fibers** : Chapter 3 presented the feasibility of step HOF for high power fiber sources. The step HOF consists of the ring-core around the air hole in the center. It has the fundamental mode cut-off at a finite wavelength due to the negative dielectric volume provided by the air hole. It thus acts as a distributed fiber waveguide filter. However, its fundamental mode cut-off sharpness is not good enough to suppress unwanted stimulated emission because of the slow dependency of effective indices on wavelength. It provides the large bending loss at a broad wavelength range near the fundamental mode cut-off. In spite of this, the ring-core structure of the step HOF provides the relatively large ratio of core and cladding, which can improve the pump absorption in the cladding pumping configuration. An Er:Yb-doped step HOF laser was first demonstrated. The maximum output power was 2.5 W at 1544 nm when the pump power of 12.6 W was launched. The slope efficiency was 26% with respect to the launched pump power. These efficiency was highly

dependent on the core thickness, which also determines the fundamental mode cut-off wavelength. In the small core thickness regime, the efficiency at 1550 nm was quite low (~ 8% w.r.t the launched pump power for a 125 μm inner cladding fiber) and Yb co-lasing at 1060 nm became significant because of the low gain at the Er emission band. This was due to the induced loss at 1550 nm and low signal modal overlap factor near the fundamental mode cut-off wavelength. Otherwise, in the large core thickness, the efficiency was improved (η=29% w.r.t the absorbed pump power at 250 μm outer cladding diameter fiber). Contrary to the improved efficiency, the large hole and step core HOF degrades the beam quality (M^2 value = 5.2) because the higher order mode can easily be excited in the large hole and large core fiber. Otherwise, in the small core fiber, the beam quality factor was improved (M^2 value for 125 μm inner cladding fiber = 1.5 and M^2 value for 150 μm inner cladding fiber = 2.4). In this experiment, the operation at the shorter wavelength (<1530 nm) was not realized because the Yb gain reached a high enough level to lase before Er gain at a shorter wavelength did. For the operation of the shorter wavelength (S-band) in Er^{3+}-doped fiber, Yb gain should be suppressed if Er:Yb-doped fiber is used. In order to avoid this, the pure erbium doped fiber is a better choice because no suppression of the Yb-gain at the shorter wavelength is required.

- **Nd:Al-doped depressed clad hollow optical fiber** : The DCHOF consists of an air hole at the center of the fiber, a ring-shaped core surrounding the central air hole, a depressed refractive index of first cladding and a second cladding. In the first section, the modal characteristics and bending loss properties of the DCHOF were investigated. Based on these results, the fiber was designed for the laser operation at 930 nm in Nd:Al-doped DCHOF and it was demonstrated

experimentally. It provided the maximum output power of 3.3 W with the 41% slope efficiency with respect to the launched pump power. The laser was tunable from 917 nm to 936 nm. The beam quality factor was M^2 value of 1.05 when the hole at the fiber output end was collapsed. Although aluminosilicate host enhances the solubility limit of Nd-ions, but at the same time, favours 1060 nm emission. However, this showed the efficient suppression of the stimulated emission at 1060 nm. It produced similar results as with the Nd:Al-doped W-type fiber presented in reference [8]. However, in the Q-switched configuration, the DCHOF generated a much higher energy than the W-type fiber. This is due to the large core area of the DCHOF. Nd:Al-doped DCHOF produced 133 μJ pulse energy at 5 kHz repetition rate. The pulse width was 172 ns and the average output power was 647 mW. This corresponds to ~750 W of peak power. Then, using the Q-switched Nd:Al-doped DCHOF sources, the blue light was generated by frequency doubling. The average output power of the beam at 927 nm was 902 mW at a 5 kHz repetition rate and the pulse energy was 176 μJ, where the pulse width was 140 ns. The corresponding peak power was 1.3 kW. The SHG crystal used for this was bismuth borate (BiB_3O_6). The maximum blue power was 50 mW at 463.5 nm. The conversion efficiency of the crystal was 10.8%, which was low due to the un-polarized characteristic of the output beam, at 927 nm, from the DCHOF. However, through a simple frequency doubling process, the relatively high blue power was achieved due to the high peak power of the laser output at 927 nm. This shows the possibility of the power-scaling of the blue. In reference [24], the elliptical HOF provided high birefringence due to the large refractive index difference between air hole and

core. It will be useful for polarization-maintaining fiber. Thus, for the second harmonic high conversion efficiency, the elliptical DCHOF can be considered.

- **Yb:Al-doped depressed clad hollow optical fiber :** In chapter 5, the DCHOF structure was used for generating high power 980 nm laser sources in Yb:Al-doped DCHOF. It is much more challenging to generate 980 nm fiber souces because of the very high GSA in Yb^{3+}-doped fibers at 980 nm. In order to overcome the GSA, the very high pump absorption is required. Furthermore, the wavelength space between 980 nm and ~1030 nm, where it should be suppressed, is too narrow to be sharply separated. Eventually, the induced bending loss affects the 980 nm loss. In order to solve this, more sophisticated fiber control is required. In this chapter, the bending loss effect on 980 nm, depending on the fiber parameter, were presented and then using a Yb:Al-doped DCHOFs, the 980 nm operation was demonstrated. The inner cladding diameter was 120 μm. It provided 3.1 W output power with an M^2 value of 1.09. The slope efficiency was 34% with respect to the launched pump power. In order to scale up the output power by reducing the laser threshold, the relatively small inner cladding (90 μm and 80 μm diameter) Yb:Al-doped DCHOFs was used. They have nearly the same core structure as the 120 μm inner cladding diameter fiber. The output power was increased to 7.5 W for 90 μm and 9.2 W for 80 μm because of the reduction of the laser threshold. However, the beam quality was significantly degraded due to the cladding mode lasing. The power leaked out from the core to the inner cladding by relatively high bending loss. Because of that, the significant power in the inner cladding causes lasing at 980 nm. In particular, this cladding mode lasing became significant in the small inner cladding fiber due to the relatively large intensity and the large overlap with the

Yb-doped core of the cladding modes. Therefore, in order to increase the output power at 980 nm, whilst maintaining a single-mode beam quality, the suppression of higher order modes is required. For this, much more distinct cut-off filtering is essential. Alternatively, by using absorbers such as erbium in the inner cladding, the power of cladding modes can be reduced.

- **Suppression of stimulated Raman scattering using W-type fiber structure :** In chapter 6, I experimentally demonstrated SRS suppression in a pulsed high power, Yb-doped single-mode fiber MOPA system using a W-type fiber with the fundamental mode cut-off with a small core. The cut-off filtering induces the loss at the unwanted Raman stokes wave in high power fiber systems and thus increases the Raman threshold. The power from the signal to Stokes waves is not transferred. It is quite useful to scale up the output power in a small and single-mode core. In practice, for a robust generation of the single mode output, the single mode core is an obvious choice. W-type fiber is useful for that because it has a single mode core and the fundamental mode cut-off. In picosecond pulse (103 ps pulses at 32 MHz repetition rate) amplification, 13 kW peak power was achieved without of any sign of the SRS. However, without SRS suppression, the maximum peak power achieved was only 5.4 kW. The loss at the Stokes wave was controlled by bending W-type fiber, which effectively shifted the fundamental mode cut-off wavelength. In nanosecond pulse (20 nsec pulses width at 100 kHz repetition rate) amplification, the W-type fiber was also tested. When SRS was suppressed by the induced loss at the Stokes wavelengh due to the fundamental mode cut-off, the maximum peak power was 8.8 kW. Otherwise, for the fiber without the fundamental mode cut-off at the Stokes wavelength, most of power was transferred to Raman Stokes.

In addition, the Yb-doped W-type fiber provided 314 W cw output power without any roll-off in the output due to the Raman effect. Although the W-type fiber could not reach the peak power that has been achieved from a large core and low NA fiber, it has shown the practical advantage of the robust single-mode output that results from the use of a strictly single-mode core. It looks promising for scaling up the output power of both CW and pulsed fiber sources while maintaining a robust single mode output beam.

7-2 Future prospects

There are issues to improve the performances of fiber lasers presented in this thesis and also further scientific investigations are required. These are summarized below

- **Refractive index control of HOF in the fabrication process :** The fundamental mode cut-off is sensitive to the core thickness and NA. A small change of the fiber structure causes a significant shift of the fundamental mode cut-off wavelength. Sophisticated control of these prameters is required to obtain better control of the cut-off. Moreover, in the DCHOF, the higher order mode can be easily excited depending on the hole size. In order to make sure of a single-mode operation, the careful control of the hole size is required. In general, the hole size is varied at the preform collapsing stage in the MCVD process as well as during the fiber drawing stage. In the MCVD stage, the internal tube pressure should be carefully controlled during the collapsing stage. In the drawing process, the temperature and the pulling speed should be controlled carefully in order to obtain the right hole size in the fiber.

- **The development of the polarization maintained DCHOF :** The Nd:Al-doped DCHOF provided high pulse energy and peak power at 927 nm, which is quite useful for blue light generation (463.6 nm) by frequency doubling. However, its output beam is un-polarized light, which degrades the conversion efficiency. Therefore, the polarization-maintained DCHOF is required. For this, the elliptical DCHOF can be considered. The large index difference between the air hole and core will help to create the large birefringence. Furthermore, their fabrication process is very different to other polarization maintaining fibers such as PANDA [97] or bow-tie fiber [98]. In addition, the polarization-maintaining DCHOF may enhance the amplification of sophisticated waveforms such as picoseond and femtosecond pulses.
- **SRS suppression using DCHOF :** In this thesis, for SRS suppression, the W-type fiber was used. However, the scaling of their core area in W-type fiber is limited, as mentioned in chapter 4. In many practical applications, the large core is necessary, while maintaining the fundamental mode cut-off characteristic and single mode guiding at the desired wavelength. One option is to use DCHOF. DCHOF has a similar (or better) cut-off characteristic and can provide a 4~5 times larger core area than the W-type fiber, depending on the hole size. It allows more extractable energy and peak power without SRS and can also generate a single mode output in a robust way.
- **Yb-doped Modified DCHOF for 980 nm laser output :** In chapter 5, the problem for power-scaling of Yb-doped DCHOF at 980 nm is the cladding mode lasing. In order to avoid this, a much sharper fundamental mode cut-off is required to reduce the bending loss at 980 nm. In addition, the cladding mode lasing can be generated due to the relatively high gain at 980 nm in Yb-doped

fibers, even though their overlap with the doped core is small. Therefore, it is necessary to suppress the gain of the cladding mode actively. To suppress the 980 nm cladding modes, the absorber (eg. erbium or samarium) for 980 nm could be employed in the inner cladding.

Bibliography

[1] S. B. Poole, D. N. Payne and M. E. Fermann, "Fabrication of low loss optical fibres containing rare earth ions", Electonics Letters **21**, p737-738 (1985)

[2] S. Sudo, *Optical fibre amplifiers: materials, devices and applications* Artech house, (1997)

[3] Y. Wang, "Thermal effects in kilowatt fiber lasers," IEEE Photonics Technology Letters, **16,** p63-65 (2004)

[4] Y. Jeong, J. K. Sahu, D. N. Payne, and J. Nilsson, "Ytterbium-doped large-core fibre laser with 1 kW of continuous-wave output power," Electronics Letters **40**, p470- 471 (2004)

[5] Y. Jeong, J. K. Sahu, D. N. Payne, and J. Nilsson, "Ytterbium-doped large-core fiber laser with 1.36 kW continuous-wave output power", Optics Express **12**, p6088-6092 (2004)

[6] V. Gapontsev, "2kW single mode output from the fiber laser" presented at Photonic West 2005, San Jose, USA, Jan 21- 26 (2005)

[7] C. H. Yeh, C. C. Lee, and S. Chi, "A tunable S-band erbium-doped fiber ring laser," IEEE Photonics Technology Letters **15** p1053-1055 (2003)

[8] D. B. S. Soh, S. Yoo, J. Nilsson, J. K. Sahu, K. Oh, S. Baek, Y. Jeong, C. Codemard, P. Dupriez, J. Kim, and V. Philippov, " Neodymium-doped cladding-pumped aluminosilicate fiber laser tunable in the 0.9 μm wavelength range," IEEE Journal of Quantum Electronics **40** p1275-1282 (2004)

[9] P. D. Dragic, L. M. Little, and G. C. Papen, "Fiber amplification in the 940-nm water vapor absorption band using the $^4F_{3/2} \rightarrow {}^4I_{9/2}$ transition in Nd," IEEE Photonics Technology Letters. **11**, p1478-1479 (1997)

[10] P. Dupriez, A. Piper, A. Malinowski, J. K. Sahu, M. Ibsen, Y. Jeong, L. M. B. Hickey, M. N. Zervas, J. Nilsson, and D. J. Richardson, "321 W average power 1 GHz, 20 ps 1060 nm pulsed fiber MOPA source," presented at OFC 2005, Anaheim, USA 6-11 Mar 2005 (Post deadline)

[11] C. D. Brooks and F. D. Teodoro, "1-mJ energy, 1-MW peak-power, 10-W average-power, spectrally naroow, diffraction-limited pulses from a photonic-crystal fiber amplifier," Optics Express **13,** p8999-9002 (2005)

[12] F. D. Teodoro, J. P. Koplow, S. W. Moore, and D. A. V. Kliner, “Diffraction-limited, 300-kW-peak-power pulses from a Yb-doped fiber amplifier,” in Proc.CLEO 2002, Long Beach, USA, 19-24 May 2002 Technical Digest vol.1 p592-593.

[13] N. S. Platonov, D. V. Gapontsev, V. P. Gapontsev, and V. Shumilin, “ 135 W CW fiber laser with perfect single mode output” in Proc. CLEO 2002, Long Beach, USA, 19-24 May 2002 (postdeadline paper CPDC3).

[14] V. Neves and F. S. C. Fernandes, “Modal characteristics for W-type and M-type dielectric profile fibres”, *Microwave & Optics Technology Letters* **22**, p398-405, (1999)

[15] J. Nilsson, J. D. Minelly, R. Paschotta, A. C. Tropper, and D. C. Hanna, “Ring-doped cladding-pumped single-mode three-level fiber laser,” Optics Letters **23**, p355-357 (1998)

[16] X. Wang and M. G. Littman, “Laser cavity for generation of variabl-radius rings of light,” Optics Letters **18**, p767-768 (1993)

[17] Y. W. Shi, K. Ito, Y. Matsuura, and M. Miyagi, “Low-loss pilot-beam delivery in hollow optical fiber for high-energy infrared laser light,” Proceedings of SPIE **5630** p122-129 (2005)

[18] J. Yin and Y. Zhu, “LP_{01}-mode output beam from a micro-sized hollow optical fiber:A simple theoretical model and its applications in atom optics,” Journal of Applied Physics **85,** p2473-2481 (1999)

[19] H. Ito, K. Sakaki, M. Ohtsu, and W. Jhe “Evanescent-light guiding of atoms through hollow optical fiber for optically controlled atomic deposition,” Applied Physics Letters **70**, p2496-2498 (1997)

[20] S. Choi, K. Oh, W. Shin, C. S. Park, U. C, Paek, K. J. Park, Y. C. Chung, G. Y. Kim, and Y. G. Lee, “ Novel mode conversion based on hollow optical fiber for gigabit LAN commumication,” IEEE Photonics Technology Letters **14**, p248-250 (2002)

[21] S. Choi and K. Oh, “A new LP_{02} mode dispersion compensation scheme based on mode converter using hollow optical fiber,” Optics communications **221**, p307-312 (2003)

[22] S. Choi, T. J. Eom, J. Yu, B. H. Lee, and K. Oh, “Novel all-fiber bandpass filter based on hollow optical fiber,” IEEE Photonics Technology Letters **14,** p1701-1703 (2002)

[23] S. Choi, Y. Jung, T. J. Eom, B. H. Lee, and K. Oh, "Broadband tunable all-fiber bandpass filter based on hollow optical fiber," IEEE Photonics Technology Letters **17**, p115-117 (2005)

[24] I. K. Hwang, Y. H. Lee, K. Oh, and D. N. Payne, "High birefringence in elliptical hollow optical fiber," Optics Express **12**, p1916-1923 (2004)

[25] J. A. Harrington et al., "Transmission properties of hollow glass waveguide for the delivery of CO2 surgical laser power," IEEE Journal of Selected Topics Quantum Electronics **5**, p948-953 (1999)

[26] B. Tmelkuran, S. D. Hart, G. Benoit, J. D. Joannopoulos, and Y. Fink, "Wavelength-scalable hollow optical fibres with large photonic bandgaps for CO_2 laser transmission," Nature **420**, p650-653 (2002)

[27] R. F. Cregan, B. J. Mangan, J. C. Knight, T. A. Birks, P. J. Russel, P. J. Roberts, and D. C. Allan, "Single-Mode Photonic Band Gap Guidance of Light in Air," Science **285,** p1537-1539 (1999)

[28] Y. Matsuura, G. Takada, T. Yamamoto, Y. W. Shi, and M. Miyagi, "Hollow fibers for delivery of harmonic pulses of Q-switched Nd:YAG lasers," Applied Optics **41,** p442-445 (2002)

[29] U. Kubo, Y. Hashishin, H. Nakano, and H. Tanaka, "Hollow light guide and optical fiber for UV laser transmission," Proceedings of SPIE **3199,** p75-80 (1998)

[30] Y. Matsuura and M. Miyagi, "Hollow optical fibers for ultraviolet and vacuum ultraviolet light," IEEE Journal of Selected Topics in Quantum Electronics **10**, p1430-1434 (2004)

[31] J. Nilsson, R. Paschotta, J. E. Caplen, and D. C. Hanna, "Yb^{3+}-ring-doped fiber for high-energy pulse amplification," Optics Letters **22**, p1092-1094 (1997)

[32] P. Glas, M. Naumann, A. Schirrmacher, and T. Pertsch, "Neodymium-doped hollow optical fiber laser for applications in laser-guided atoms," in proceeding of CLEO'98 San. Francisco, CA, USA CTh060 428-429 (1998)

[33] P. R. Chaudhuri, C. Lu, and W. Xiaoyan, "Scalar model and exact vectorial description for the design analysis of hollow optical fibre components " Optics Communications **141**, p285-293 (2003)

[34] B. Ortega and L. Dong, "Characteristics of mismatched twin-core fiber spectral filters," IEEE Photonics Technology Letters **10,** p991-993 (1998)

[35] Z. M. Mao and W. P. Huang, "An ARROW optical wavelength filter: design and analysis," IEEE photonics technology letters **11,** p1183-1188 (1993)

[36] K. Morishita, "Optical fiber devices using dispersive materials," IEEE Journal of Lightwave Technology, **15**, p294-298 (1989)

[37] M. Monerie, "Propagation in doubly clad single-mode fibres", IEEE Journal of Quantum Electronics **QE-18**, p535-542 (1982)

[38] S. Kawakami and S. Nishida, "Characterisics of a doubly clad optical fiber with a low-index inner cladding," IEEE Journal of Quantum Electronics **QE-10,** p535-542 (1982)

[39] L. Zenteno, J. Wang, D. Walton, B. Ruffin, M. Li, S. Gray, A. Crowley, and X. Chen, "Suppression of Raman gain in single-transverse-mode dual-hole-assisted fiber" Optics Express **13**, p8921-8926 (2005)

[40] E. Snitzer, "Optical maser action of Nd^{3+} in a Barium Crown Glass," Physics Review Letters **7**, p444-446 (1961)

[41] R. J. Mears, L. Reekie, S. B. Poole, and D. N. Payne, "Neodymium-doped silica single-mode fiber lasers," Electronics Letters, **21,** p738-740 (1985)

[42] J. D. Minelly, E. R. Taylor, K. P. Jedrzejewski, J. Wang, and D. N. Payne, "Laser-diode pumped neodymium-doped fiber laser with output power in excess of 1 Watt," presented at CLEO'92 Anaheim CA, May 1992, Paper CWE6.

[43] H. Po, J. D. Cao, B. M. Laliberte, R.A. Minns, R. F. Robinson, B. H. Rockney, R. R. Tricca, and Y. H. Zhang, "High power neodymium-doped single transverse mode fiber laser," Electronics Letters **29,** p1500-1501 (1993)

[44] H. Zellmer, A. Tünnermann, H. Welling, and V. Reichel, "Double-clad fiber laer with 30 W output power," in proceedings of Optical Amplifiers and their Applications 16, OSA Trends in Optics and Photonics (The Optical Society of America Washington DC, 1997) 137-140.

[45] M. A. Noginov, "Development of Nd-doped solid-state laser materials for 944 nm operation," IEEE Journal of Quantum Electronics **37**, p469-481 (2001)

[46] T. J. Kane, G. Keaton, M. A. Arbore, D. R. Balsley, J. F. Black, J. L. Brooks, M. Byer, L. A. Eyres, M. Leonardo, J. J. Morehead, C. Rich, D. J. Richard, L. A. Smoliar, and Y. Zhou, "3-Watt blue source based on 914-nm Nd:YVO_4 passively-Q-switched laser amplified in cladding-pumped Nd:fiber", presented at Adv. Solid-State Photonics Santa Fe, NM, USA, February 2-5, 2004, paper MD7.

[47] E. F. Wassermann, “Fabrication of large scale periodic magnetic nanostructures,” Journal of Applied Physics **83**, p1753-1757 (1998)

[48] L. Reekie, I. M. Jauncey, S. B. Poole, and D. N. Payne, “Diode-laser-pumped Nd^{3+}-doped fiber laser operating at 938 nm,” Electronics Letters **23,** p884-885 (1987)

[49] A. L. Cook and H. D. Hendricks, “Diode-laser-pumped tunable 896-939.5 nm neodymium-doped fiber laser with 43 mW output power,” Applied Optics 37(15) 3276-3281 (1998)

[50] P. D. Dragic and G. C. Papen, “Efficient amplification using $^4F_{3/2} \rightarrow {}^4I_{9/2}$ transition in Nd-doped silica fiber,” IEEE Photonics Technology Letters **11**, p1593-1595 (1999)

[51] J. Dawson, R. Beach, A. Drobshoff, Z. Liao, D. Pennington. S. Payne, L. Taylor, W. Hackenberg, and D. Bonaccini, “Scalable 11 W 938 nm Nd^{3+}-doped fiber laser,” in Proceedings of Advanced Solid-State Photonics, Santa Fe, NM, USA, February 2-5, 2004 paper MD8.

[52] L. B. Fu, R. Selvas, M. Ibsen, J. K. Sahu, J. N. Jang, S. U. Alam, J. Nilsson, D. J. Richardson, D. N. Payne, C. Codemard, S. Goncharov, I. Zalevsky, and A. B. Grudinin, “Fiber-DFB laser array pumped with a single 1W CW Yb-fiber laser,” IEEE Photonics Technology Letters **15**, p655-657 (2003)

[53] V. Prosentsov, E. Sherman, A. Patlakh, Y. Ariel and D. Eger, “Efficient Yb-doped air-clad fiber laser operating at 980 nm and its frequency doubling,” Proceedings of SPIE **4974**, p193-201 (2003)

[54] D. B. S. Soh, C. Codemard, S. Wang, J. Nilsson, J. K. Sahu, F. Laurell, V. Philippov, Y. Jeong, C. Alegria, S. Baek, “A 980 nm Yb-doped fiber MOPA source and its frequency doubling,” IEEE Photonics Technology Letters **16,** p1032-1034 (2004)

[55] K. H. Ylä-Jarkko R. Selvas, D. B. S. Soh, J. K. Sahu, C. A. Codemard, J. Nilsson, S. A. Alam, A. B. Grudinin, “A 3.5 W 977 nm cladding-pumped jacketed-air clad ytterbium-doped fiber laser,” OSA Trends in Optics and Photonics *v. 83,* Advanced Solid State Photonics 2003, John J. Zayhowski, ed., Postdeadline paper p 103-107.

[56] J. A. Alvarez-Chavez, A. B. Grudinin, J. Nilsson, P. W. Turner, and W. A. Clarkson, “Mode selection in high power cladding pumped fiber lasers with tapered section,” presented at CLOE/QELS 1999 Baltimore 23-28 May 1999 CWE7.

[57] J. Limpert, A. Liem, H. Zellmer, and A. Tünnermann, “500 W continuous-wave fiber laser with excellent beam quality” Electronics Letters **39**, p645-647 (2003)

[58] N. S. Platonov, D. V. Gapontsev, V. P. Gapontsev, and V. Shumilin, “ 135 W CW

fiber laser with perfect single mode output" in Proc. CLEO 2002, Long Beach, USA, 19-24 May 2002 (postdeadline paper CPDC3).

[59] S. Pitois, G. Millot, and P. T. Dinda, "Influence of parametric four-wave mixing effects on stimulated Raman scattering in bimodal optical fibers," Optics Letters **23**, p1456-1458 (1998)

[60] S. Trillo and S. Wabnitz, "Parametric and Raman amplification in birefringent fibers," Journal of Optical Society of America B **9**, p1061-1082 (1992)

[61] P. T. Dinda, G. Millot, and S. Wabnitz, "Polarization switching and suppression of stimulated Raman scattering in birefringent optical fibers," Journal of Optical Society of America B **15**, p1433-1441 (1998)

[62] T. Sylvestre, H. Maillotte, and E. Lantz, "Stimulated Raman scattering under dual-frequency pumping in single mode fibers," Electronics Letters **34** p1417-1418 (1998)

[63] P. T. Dinda, S. Wabnitz, E. Coquet, T. Sylvestre, H. Maillotte, and E. Lantz, " Demonstration of stimulated Raman scattering suppression in optical fibers in a multifrequency pumping configuration," Journal of Optical Society of America B **16**, p757-767 (1999)

[64] E. A. Kuzin, G. Beltran-Perez, M. A. Basurto-Pensado, R. Rojas-Laguna, J. A. Andrade-Lucio, M. Torres-Cisneros, and E. Alvarado-Mendez, "Stimulated Raman scattering in a fiber with bending loss" Optics Communications **169**, p87-91 (1999)

[65] P. D. Dragic, "Suppression of first order stimulated Raman scattering in erbium-doped fiber laser based LIDAR transmitters through induced bending loss" Optics Communications **250**, p403-410 (2005)

[66] T. Izawa, T. Miyashita, and F. Hanawa, "Continuous optical fiber perform fabrication method," U. S. Patent, 4,062,665 (Filed Apr. 5, 1977. Patented Dec. 13, 1977)

[67] W. G. Frnch, A. D. Pearson, G. W. Tasker, and J. B. MaChesney, "Low-loss fused Silica Optical waveguide with borosilicate cladding," Applied Physics Letters **23,** p338-339 (1973)

[68] S. Sudo, *Optical fiber amplifiers: materials, devices, and applications* (Artech House optoelectronics library, K. Fujiura, T. Kanamori, and S. Sudo, "Fiber materials and fabrications," Chapter 4, 1997)

[69] J. E. Townsend, S. B. Poole, and D. N. Payne, "Solution doping technique for fabrication of rare-earth doped optical fibers," Electronics Letters **23,** p329-331 (1987)

[70] F. D. Teodoro and C. D. Brooks, "Multistage Yb-doped fiber amplifier generating

megawatt peak-power, subnanosecond pulses," Optics Letters **30**, p3299-3301 (2005)

[71] B. A. E. Saleh and M. C. Teich, *Fundamental of photonics*, (A Willey-Interscience Pulication, John Wiley & Sons, Inc. 1991)

[72] G. P. Agrawal, *Nonlinear fiber optics*, (San Diego, Academic press 3rd edition 2001)

[73] R. G. Smith, "Optical power handling capacity of low loss optical fibers as determined by stimulated Raman and Brillouin scattering" Applied Optics **11,** p2489-2494 (1972)

[74] J. Yin and Y. Zhu, "LP_{01}-mode output beam from a micro-sized hollow optical fibre: A simple theoretical model and its applications in atom optics", Journal of Applied Physics **85**, p2473- 2481 (1999)

[75] G. L. Keaton, M. A. Arbore, and T. J. Kane, "Optical wavelength filtering apparatus with depressed-index claddings," U.S. Patent, 6,563,995 2003.

[76] H. Ito, K. Sakaki, T. Nakata, W. Jhe and M. Ohtus, "Optical potential for atom guidance in a cylindrical-core hollow fibre," Optics Communications **115**, p57-64 (1995)

[77] C. Barnard, P. Myslinski, J. Chrostowski and M. Kavehrad, "Analytical model for rare-earth-doped fiber amplifiers and lasers," IEEE Journal of Quantum Electronics **30**, p1817-1830 (1994)

[78] M. J. F. Digonnet, "Closed-form expressions for the gain in three- and four-level laser fibers," IEEE Journal of Quantum Electronics **26**, p1788-1796 (1990)

[79] A. W. Snyder and J. D. Love, *Optical Waveguide Theory*, (Kluwer Academic Publishers, 2000)

[80] D. Marcuse, "Curvature loss formula for optical fibers," Journal of Optical. Society America **66**, p216-220 (1976)

[81] J. Sakai and T. Kimura, "Bending loss of propagation modes in arbitrary-index profile optical fibers," Applied Optics **17**, p1499–1506 (1978)

[82] L. G. Cohen, D. Marcuse, and W. L. Mammel, "Radiating leak-mode losses in single-mode lightguides with depressed-index claddings" IEEE Journal of Quantum Electronics **QE-18**, p1467-1472 (1982).

[83] A. E. Siegman, "Defining, measuring, and optimizing laser beam quality," in Laser Resonators and Coherent Optics: Modeling, Technology, and Applications; Proceeding of SPIE **1868** (invited paper) pp2-12 (1993)

[84] D. B. S. Soh, “Advanced waveguides for high power optical fiber sources,” Ph.D. thesis, Optoelectronics Research Center, University of Southampton in 2005

[85] ISO 11146-2, “Lasers and laser-related equipment – Test methods for laser beam widths, divergence angles and beam propagation ratios – Part 2: General astigmatic beams,” International Organization for Standardization, 2005.

[86] J. K. Sahu, Y. Jeong, D. J. Richardson, J. Nilsson, ‘’ 103 W erbium/ytterbium co-doped fibre laser’’, Optics Communications **227**, p159-163 (2003)

[87] G. G. Vienne, J. E. Caplen, L. Dong, J. D. Minelly, J. Nilsson, and D. N. Payne, “Fabrication and characterization of Yb^{3+}:Er^{3+} phosphosilicate fibres for lasers”, Journal of Lightwave Technology **16**, p1990-2001 (1998)

[88] J. Dawson, R. Beach, A. Drobshoff, Z. Liao, D. Pennington, S. Payne, L. Taylor, W. Hackenberg, and D. Bonaccini, “930 nm Nd-doped high power cladding pumped fiber amplifier,” in ASSP, OSA Technical Digest, (Optical Soiciety of America, Washington, DC 2003), 115-121.

[89] D. J. Richardson, P. Britton, and D. Taverner, “Diode-pumed, high-energy, single transverse mode Q-switch fiber laser,” Electronics Letters **33**, p1955-1956 (1997)

[90] T. Lauterborn, S. Heinemann, and A. Galvanauskas, “Single transverse mode Yb-doped fiber laser generating up to 0.5 mJ / 11 W with flexible pulse parameters”, in Proceedings SPIE **5887**, p1-7 (2005)

[91] R. Paschotta, J. Nilsson, A. C. Tropper, and D. C. Hanna, “Ytterbium-doped fiber amplifiers,” IEEE Journal of Quantum Electronics **33,** p1049-1056 (1997)

[92] J. K. Sahu, C. C. Renaud, K. Furusawa, R. Selvas, J. A. Alvarez-Chavez, D. J. Richardson, and J. Nilsson “Jacketed air-clad pumped ytterbium-doped fiber laser with wide tuning range,” Electronics Letters **37**, p1116-1117 (2001)

[93] J. K. Sahu, P. Dupriez, J. Kim, C. Codemard, J. Nilsson, and D. N. Payne, “Suppression of stimulated Raman scattering in a high-peak-power pulsed 1060nm fiber MOPA source with purely single-mode output using W-type fiber,” OFC 2006 Anaheim 5-10 March 2006 OWD5.

[94] J. Kim, D. B. S. Soh, C. Codemard, S. Yoo, Y. Jeong, J. Nilsson, and J. K. Sahu “Yb:Al-doped depressed clad hollow optical fiber laser operating at 980nm,” CLEO/IQEC Pacific Rim Tokyo 11-15 July 2005 CTuI4-5.

[95] J. M. Fini, “Bend-resistant design of conventional and microstructure fibers with very large mode area,” Optics Express **14,** p69-81 (2006)

[96] J. Limpert, T. Schriber, S. Nolte, H. Zellmer, A. Tunnermann, R. Iliew, F. Lederer, J. Broeng, G. Vienne, A. Petersson, and C. Jakobsen, “High-power air-clad large-mode-area photonic crystal fiber laser,“ Optics Express **11**, p818-823 (2003)

[97] K. Okamoto, T. Hosaka, and J. Noda, “High-birefringence polarizing fiber with flat cladding,” Journal of Lightwave Technology **LT-3**, p758-762 (1985)

[98] M. P. Varnham, D. N. Payne, R. D. Birch, and E. J. Tarbox, “Single-polarization operation of highly birefringent bow-tie optical fibers,” Electronics Letters **19**, p247-247 (1983)

[99] X. Daxhelet and F. Conthier, “Optical properties of tapered fiber filters for telecommunications,” In proceeding SPIE **4216**, p67-77 (2001)

[100] W.G. French, A. D. Pearson, G. W. Tasker, and J. B. MacChesney, “Low-loss fiber fused silica optial waveguide with borosilicate cladding,” Applied Physics Letters **23**, p340-341 (1973)

[101] L. Tingye, *Optical fiber communications*, New York: Academic press inc. 1985.

[102] K. L. Walker, F. T. Geyling, and S. R. Nagel, “Thermophoretic deposition of small particles in the modified chemical vapour deposition (MCVD) process,” Journal of the American Ceramic Society **63**, p552-558 (1980)

[103] V. G. Plotnichenko, G. A. Ivanov, E. B. Kryukova, V. A. Aksenov, V. O. Sokolov, and V. A. Isaev, “Influence of molecular hydrogen diffusion on concentration and distribution of hydroxyl groups in silica fibers,” Journal of Lightwave Technology **23**, p341-347 (2005)

[104] D. Kouznetsov, J. V. Moloney, and E. M. Wright, "Efficiency of pump absorption in double-clad fiber amplifiers: I. Fiber with circular symmetry,” Journal of Optical Society of America B **18**, p743-749 (2001)

[105] D. Kouznetsov, J. V. Moloney, and E. M. Wright, "Efficiency of pump absorption in double-clad fiber amplifiers: II. Broken circular symmetry,” Journal of Optical Society of America B **19**, p1259-1263 (2002)

[106] V. Doya, O. Legrand, and F. Mortessagne, “Optimized absorption in a chaotic double-clad fiber amplifier,” Optics Letters **26,** p872-874 (2001)

[107] J. Xu, J. Lu, J. Lu, and K. Ueda, “Influence of cross-sectional shape on absorption characteristics of double-clad fiber lasers,” Optics Engineering, **42,** p2527-2533 (2003)

[108] S. Sakaguchi and T. Kimura, “High-speed drawing of optical fibers with pressurized coating,” Journal of Lightwave Technology **3**, p669-673 (1985)

[109] C. Y. Zhao and S. H. K. Lee, “Physical considerations of a pressurized optical fiber coating process, “ Journal of Material Processing and Manufacturing Science **8**, p53-73 (1999)

[110] P. W. France, P. L. Dunn, and M. H. Reeve, “Plastic coating of glass fibers and its influence on strength,” Fiber and Integrated Optics **2**, p267-286 (1979)

[111] P. S. Oh, J. J. Mcalarney, and D. K. Nath, “ Effects of fiber drawing tension on optical and mechanical properties of optical fiber,” Journal of the American Ceramic Society **66,** p84-85 (1983)

[112] K. Arai, H. Namikawa, K. Kumata, and T. Honda, “Aluminum or phosphorous co-doping effects on the fluorescence and structural properties of neodymium-doped silica glass,” Journal of Applied Physics **59**, p3430-3446 (1986)

[113] R. Pashotta, J. Nilsson, P. R. Barber, J. E. Caplen, A. C. Tropper, and D. C. Hanna, “Lifetime quenching in Yb-dped fibers,” Optics communications **136,** p375-378 (1997)

[114] L. Orsila and O. G. Okhotnikov, “Three- and four-level transition dynamics in Yb-fiber laser,” Optics Express **13**, p3218-3223 (2005)

[115] R.Selvas, K. H. Yla-Jarkko, J. K. Sahu, L. B. Fu, J. N. Jang, J. Nilsson, S. U. Alam, P. W. Turner, J. Moore, and A. B. Grudinin, “High power, low noise Yb-doped cladding-pumped three-level fiber sources at 980 nm,” Optics Letters **28**, p1093-1095 (2003)

[116] P. C. Schultz, “Fabrication of optical waveguide by the outside vapour deposition process,” Proceedings of IEEE, 68, p1187-1190 (1980)

[117] T. Izawa and S. Sudo, *Optical Fibers; Materials and Fabrication*, Dordrecht: D. Reidel, 1987

[118] P. D. Ritger and N. J. Rose, *Differential Equations with Applications*, International series in pure and applied mathematics copyright 1968

[119] M. Miyamoto, T. Sakai, R. Yamauchi, and K. Inada “Bending loss evaluation of single-mode fibers with arbitrary core index profile by far-field pattern,” IEEE Journal of Lightwave Technology **6**, p 673-677 (1990)

[120] J. W. Goodman, *Introduction to Fourier optics*. New York: McGraw-Hill, 1968.

[121] D. B. S. Soh, S. W. Yoo, J. Nilsson, J. K. Sahu, S. Baek, Y. Jeong, L. J. Cooper, C. Codemard, P. Dupriez, C. Alegria, V. Philippov, and K. Oh, “Cladding pumped Nd-doped fiber laser tunable from 908 to 938 nm,” CLEO/IQEC 2004 San Francisco 16-21 May 2004 CMK

[122] J. Nilsson, J. K. Sahu, Y. Jeong, W. A. Clarkson, R. Selvas, A. B. Grudinin, and S.-U. Alam. “High power fiber lasers: New developments,” SPIE : Advances in Fiber lasers. L. N. Durvasula Ed. 2003 4974 p 50-59 (2003)